TAILORING THE TOUGHNESS AND BIOLOGICAL RESPONSE OF PHOTOPOLYMERIZABLE NETWORKS FOR ORTHOPAEDIC APPLICATIONS

A Dissertation
Presented to
The Academic Faculty

by

Kathryn Elizabeth Smith

In Partial Fulfillment
of the Requirements for the Degree
Bioengineering in the
Woodruff School of Mechanical Engineering

Georgia Institute of Technology
December 2010

TAILORING THE TOUGHNESS AND BIOLOGICAL RESPONSE OF PHOTOPOLYMERIZABLE NETWORKS FOR ORTHOPAEDIC APPLICATIONS

Approved by:

Dr. Ken Gall, Advisor
School of Materials Science and Eng
Georgia Institute of Technology

Dr. Barbara Boyan, Co-advisor
School of Biomedical Engineering
Georgia Institute of Technology

Dr. Andres Garcia
School of Mechanical Engineering
Georgia Institute of Technology

Dr. Johnna Temenoff
School of Biomedical Engineering
Georgia Institute of Technology

Dr. Yonathan Thio
School of Polymer Textiles and Fiber Engineering
Georgia Institute of Technology

Date Approved: June 9, 2010

ACKNOWLEDGEMENTS

This work would not have been possible (and my sanity would not have remained intact) without having the support and encouragement from my family and friends. First and foremost, I want to thank my parents for their love and continuous support through all of my endeavors and for always telling me I can achieve whatever I want. I also have to especially thank my brother, Burns, for wanting to pursue a degree in engineering, and thus forcing me to sit through college recruitment visits, listening to talks on engineering programs as a high school senior. It was during this time that I stumbled upon the Biological Engineering program at Mississippi State, and the rest is history. I also have to thank my other two siblings, Drew and Caroline, for keeping me grounded and always findings ways to tease me about my "Kathryn"isms.

My progression over the past four years would not have been possible without the guidance from my graduate advisors. I would like to thank Ken Gall for taking on a young student who had never heard of a glass transition temperature and providing me with not only a plethora of knowledge on materials science but also instilling many invaluable skills I can apply in becoming an exciting, successful researcher. Whenever I would hit a road block or feel lost in my work, Ken's encouraging words and sage advice always put me back on track feeling ever the more motivated. I would like to thank Barbara Boyan for always lending her opinions on the convergence of materials science and biology, and for serving not only as an amazing mentor, but also as an outstanding role model to women trying to pave their own career paths in the science community. I would also like to acknowledge my other committee members, Andres Garcia, Johnna

Temenoff, and Yonathan Thio for giving their time and consideration towards my research.

This work would not have been possible without the strong relationships I have formed with my labmates. I have to particularly thank Matthew DiPrima for his patience in helping me whenever the Insight went down or for laser-cutting obscene amounts of material; Walter Voit for helping me work through those tough critical problems and introducing me to Siedtlers and Set; and Scott Kasprzak for his handy machine shop skills and shared love of Diet Coke. Also, I would like to give a special thank you to Sharon Hyzy for all of her work with assisting me with the cell culture and biochemical assays. In addition, this work would never have reached fruition without the numerous undergraduates who assisted with making material and running tests: Hillary Harris, Samantha Willis, Sara Downey, Michelle Hyjek, Paul Millard, Maya Uddin, Jessica Wyche, Suzanne Parks, Phillip Trusty, Evan Stone, Beatrice Wan, Kavonna Allen, and Scott Jossey.

Finally, a special thank you to David Safranski: polymer wizard and lab safety nazi. Thank you for always giving me the confidence when I started to doubt myself, for keeping me company when I was alone working late, for always lending an ear when I needed a second opinion and for always being my biggest cheerleader and champion.

TABLE OF CONTENTS

LIST OF TABLES

LIST OF FIGURES

LIST OF SYMBOLS AND ABBREVIATIONS

s	stress
e	strain
u	Poisson's ratio
PBS	phosphate buffered saline
2HEMA	2-hydroxyethyl methacrylate
PMMA	poly(methyl methacrylate)
DMPA	2,2-dimethoxy-2-phenyl acetophenone
PEG	poly(ethylene glycol)
PEGDMA	poly(ethylene glycol) dimethacrylate
Tg	glass transition temperature
ΔC_p	change in heat capacity
DSC	differential scanning calorimetry
DMA	dynamic mechanical analysis
E_r	rubbery modulus
M_c	molecular weight between crosslinks
E	elastic modulus
C_∞	Flory's characteristic ratio
PEEK	poly(ether ether ketone)
PC	polycarbonate
ECM	extracellular matrix
TGF-b1	transforming growth factor b-1
OCN	osteocalcin
OPN	osteopontin

BSP	bone-sialo protein
FGF-2	fibroblast growth factor-2
PGE_2	prostaglandin-2
ALP	alkaline phosphatase
RGD	arginine-glycine-aspartic acid
kPa	kilopascal
MPa	megaPascal
Gap	gigaPascal
K	Kelvin
^oC	degrees Celsius
DMEM	Dulbecco's modified eagle's medium
FBS	fetal bovine serum
MMA	methyl methacrylate
MA	methyl acrylate
M_n	average molecular weight
q	swelling ratio
W_w	wet weight
W_i	initial pre-swelling weight
MJ	megajoules
SPU	segmented polyurethane
CRNT	carbon fiber reinforced nanotubes
UHMWPE	ultra high molecular weight polyethylene
TGA	thermogravimetric analysis
BMA	benzyl methacrylate
FTIR-ATR	fourier transform infrared spectroscopy in attentuated reflectance mode

PDMS	polydimethylsiloxane
W_d	sample weight after drying
KBr	potassium bromide
ΔS^c	change in configurational entropy
VEGF	vascular endothelial growth factor
DDDA	dodecanediol dimethacrylate
DEGDMA	diethylene glycol dimethacrylate
DI	deionized
XPS	x-ray photoelectron spectroscopy
R_a	average roughness
TCPS	tissue culture polystyrene
ELISA	enzyme-linked immunosorbent assay
SEM	scanning electron microscopy
E_s	surface elastic modulus

SUMMARY

Novel surgical strategies are currently being developed to treat spinal disc degeneration. However, these strategies are limited by the lack of materials available that (1) possess the appropriate mechanical properties to mimic the tissue the material is replacing or repairing and (2) maintain their mechanical function for long durations *in vivo* without negatively affecting the tissue response of adjacent tissue (i.e. bone). One approach to improve the durability of materials is to enhance their toughness, particularly under physiological conditions in the presence of moisture. Polymers formed through photopolymerization have emerged as candidate biomaterials for applications where it is advantageous to have *in situ* formation, fast synthesis rates, and simple processing into diverse geometries. However, most photopolymerizable networks possess limited toughness *in vivo* due to the presence of water inherent in most biological tissues.

Therefore, the overall objective of this research was to develop photopolymerizable (meth)acrylate networks that are both mechanically and biologically compatible under physiological conditions to be implemented in spinal repair procedures. The fundamental approach was to determine structure-property relationships between toughness, network structure, and environmental conditions using several model copolymer networks in order to facilitate the design of photopolymerizable networks that are tough in physiological solution. In addition to characterizing the mechanical properties, the effect of changing the polymers' chemistry and stiffness on the osteoblast response was assessed in relation to how these material properties promote bone formation over resorption.

In the initial chapters of this work, the thermal, swelling, and mechanical properties of (meth)acrylate networks is detailed in an attempt to build an understanding of how intrinsic and extrinsic factors influence network toughness. Several model copolymer networks along with several common biomedical-grade polymers were subjected to tensile strain-to-failure testing at different temperatures and in the presence of phosphate buffered saline (PBS). It was demonstrated that networks toughness reached a maxima at a temperature close to the material's glass transition temperature (Tg), and the breadth and magnitude of this peak were dependent on the breadth of the glass transition behavior as well as copolymer chemistry and crosslinking density. When the materials were soaked in PBS, this toughness-temperature peak shifted to a lower temperature causing toughness to increase or decrease depending on the location of the testing temperature with Tg.

To test the hypothesis that toughness could be optimized in PBS by adjusting the toughness-temperature peak by tuning Tg, two ternary networks, MA-co-MMA-co-PEGDMA and 2HEMA-co-BMA-co-PEGDMA, were developed with varying weight ratios of MA to MMA or 2HEMA to BMA such that the Tg could be altered over a broad range of temperatures. Results showed that Tg decreased in PBS to an extent dependent upon the total water content and thermodynamic state of the water molecules absorbed within the network. For both networks, toughness peaked in the composition whose Tg was just below the testing temperature (37°C) in PBS with the MA-co-MMA-co-PEGDMA network exhibiting higher peak toughness compared with 2HEMA-co-BMA-co-PEGDMA. Compositions of both networks that displayed enhanced toughness also exhibited elastic moduli in the range of 10-500MPa.

Next, the effect of immersion time in PBS (up to 9 months) on toughness was examined for several MA-co-MMA-co-PEGDMA compositions that possessed a broad range of thermomechanical behavior from glassy to ductile to viscoelastic to rubbery in order to ascertain whether their toughness could be sustained for long time spans in a physiological environment. Those compositions that initially had higher Tg's were unable to maintain their toughness after several months in PBS while those compositions that were in their viscoelastic regime were able to maintain toughness after 9 months in PBS. To reduce the extent of water-polymer interactions that cause polymer degradation, an additional network crosslinked with DDDA, rather than PEGDMA, was designed. It was determined that MA-MMA-DDDA networks were further able to maintain toughness due to the restricted mobility of water molecules to interact with hydrophilic chemical groups in the network and thus, could serve as candidate materials for load-bearing biomedical applications including spinal repair.

In tandem with assessing the mechanical properties, the ability of (meth)acrylate networks to promote a favorable osteogenic response was investigated using an *in vitro* cell culture model with human MG63 osteoblast-like cells. Properties such as surface chemistry and stiffness were adjusted by varying the comonomer concentrations and/or crosslinking density. By testing two copolymer systems, PEGDMA-co-DEGDMA and 2HEMA-co-PEGDMA, the differentiation of MG63 cells was found to be primarily dependent on surface chemistry with PEG-based materials promoting a more mature osteoblast phenotype than 2HEMA surfaces. Amongst each copolymer group, copolymer stiffness was found to regulate osteoblast differentiation in a manner dependent upon the surface chemistry. Due to this strong relationship between cell response and copolymer

chemistry, the MG63 cell response on MA-co-MMA-co-PEGDMA networks was evaluated as a function of MA concentration. Because MA and MMA have similar chemical structures, the elastic modulus could be varied over several orders of magnitude without drastically changing chemistry. After performing several experiments, it was determined that the effect of copolymer stiffness on osteoblast differentiation on MA-co-MMA-co-PEGDMA networks was altered with each new set of copolymers. X-ray photoelectron spectroscopy analysis revealed that although the bulk material properties are not affected, the surface presentation of specific chemical groups in the network changed with each new experiment potentially affecting how cells function on the surface. In general, MA-co-MMA-co-PEGDMA and 50MA-co-MMA-co-DDDA networks promote a favorable osteoblast response in comparison to TCPS suggesting its use as a bone-interfacing load-bearing biomaterial.

In summary, the relationships between network structure, mechanical behavior, and biological response established in this work will facilitate the design of tough, biocompatible photopolymerizable networks for implementation with spinal repair procedures. In a broad sense, the results presented within will contribute to the growing field of biomaterials by better defining the interrelationships between polymer chemistry, mechanics, and biology.

CHAPTER 1

INTRODUCTION

1.1 Motivation

Lower back pain, usually related to disc degeneration, is the most common musculoskeletal ailment in the United States costing more than $15 billion per year in treatment and compensation [1-2]. Currently when a patient no longer benefits from conservative treatment methods, surgical approaches including spinal fusion, discectomy, and total disc replacement serve as the next step in the treatment continuum. However, these options are highly invasive, often restrict the patient's range of motion and decrease their level of activity, thus facilitating more pain and the need for further treatment [3-4]. New less-invasive therapeutic approaches are being investigated that involve the partial or total replacement of the inner disc nucleus and/or repair of the outer annulus [2, 5]. For instance, a torn annulus could be repaired by injecting an adhesive around the damaged tissue or using a readily deformable rod to connect adjacent vertebra around the disc to help with load transfer. However, these therapies require implant materials that exhibit the appropriate mechanical properties, are durable or tough, promote a favorable biological response, and can be inserted in a minimally invasive manner.

In order to not disrupt the biomechanical environment of the physiological region, it is critical that the mechanical properties of the synthetic material be able to mimic the surrounding tissue [2, 4]. If a replacement material is unable to match the mechanical properties, particularly stiffness, of the native tissue over acute and chronic timescales, pain, subsequent injury, and device failure can occur resulting in unwanted repeat surgeries. The human spine is subjected to a complex loading regime that includes

tensile, compressive, flexure, and shear loading that is repeated over various frequencies [3, 6]. Thus, a material must also exhibit excellent toughness, particularly in an *in vivo* hydrated environment, to ensure the implant maintains its function for long durations [2]. Besides having the appropriate inherent toughness, the material must also interact with surrounding tissue (i.e. bone) such that the biological functions of the tissue are not compromised. In this regard, the material should produce a favorable osteogenic response to ensure proper osseointegration and reduced the likelihood of bone resorption. In addition, it is highly desired that the surgical implantation of such materials/devices be performed in a minimally invasive manner due to the close proximity of vital organs including the spinal cord and the long recovery times associated with invasive surgeries [2]. Thus, a material that can be inserted in a minimally invasive manner and also possess the appropriate mechanical and biological properties would serve as an ideal candidate for implementation in spinal repair applications.

Polymers formed through photopolymerization have emerged as candidate biomaterials for applications where it is advantageous to have *in situ* formation, fast synthesis rates, and simple processing into diverse geometries [7]. Many existing photopolymerizable chemistries possess tailorable material properties allowing for their use in a broad range of material platforms from hydrogels [7-8] to biodegradable materials [9] to shape memory systems [10]. However to facilitate their use in orthopaedic applications, particularly in disc repair, an extensive investigation of structure-property relationships (both mechanical and biological) must be undertaken in order to identify novel methods to improve their mechanical properties without compromising the biological function of bone.

1.2 Research Objectives

The **overall objective** of this research was to develop photopolymerizable (meth)acrylate networks that are both mechanically and biologically compatible under physiological conditions to be implemented in spinal repair procedures. As seen in Figure 1.1, the fundamental approach was to establish structure-property relationships between toughness and network structure under different environmental conditions of several model copolymer networks in order to facilitate the design of several photopolymerizable networks that maintain their toughness under physiological conditions. In tandem to characterizing the mechanical properties, the *in vitro* response of immature pre-osteoblast cells due to changing the polymers' chemistry and stiffness was assessed in relation to how specific (meth)acrylate copolymer systems promote bone formation over resorption.

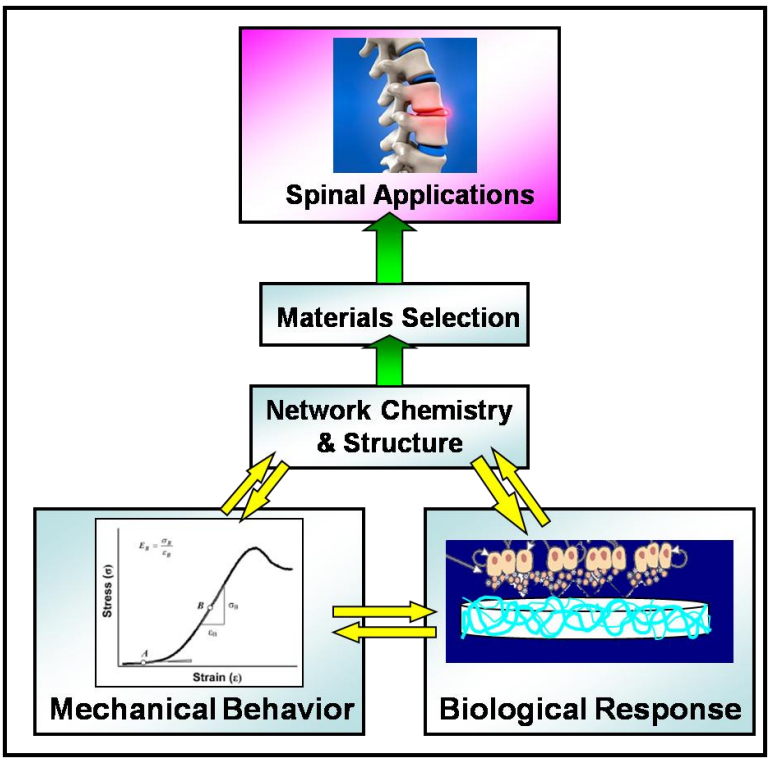

Figure 1.1. Schematic of experimental approach outlined in this research

These biological-mechanical interrelationships were used to select candidate networks that can be implemented as orthopaedic load-bearing implant materials. The innovation of this project stems from examining both biological and mechanical behaviors of photopolymerizable networks as they relate to network chemistry and structure, facilitating the design of several photocurable biomaterials with enhanced toughness that can be mechanically tuned to replace or repair native various bone-interfacing soft tissues. This research was performed through two specific aims as outlined below:

1. **Evaluate the relationship between the chemical structure and toughness of (meth)acrylate networks under different environmental conditions.**
   Networks that are highly biocompatible typically possess marginal toughness, making them poor candidate materials in orthopaedic devices. Previous studies had shown that polymer mechanical properties are highly dependent upon polymer chemistry as well as the material's testing environment, particularly the presence of moisture. Therefore, we aimed to characterize the structure-toughness relationships in several (meth)acrylate networks with variable chemistries by assessing their tensile stress-strain behavior at different temperatures and in the presence and absence of phosphate buffered saline (PBS). Using these relationships, several networks with tailorable chemistries were designed to establish relationships with polymer hydrophilicity, glass transition temperature and toughness. Subsequently, several initially tough candidate networks were

identified to study how network toughness is affected by long term exposure to PBS.

2. **Assess the osteogenic response on candidate polymer networks and determine the relationship between cell response and polymer material properties.**

   In order to remain a viable implant in the spine, the local chemistry of the biomaterial must not have an adverse effect on bone growth. Studies have shown that osteoblast proliferation and differentiation are highly dependent on the cell's mechanical and chemical environment [11-12], but a thorough evaluation on the mechanical and chemical effects on the osteogenic response have not been performed with most acrylate-based chemistries that show potential for significant toughening. In order to better identify photopolymers that will interact favorably with bone, the *in vitro* response of an immature osteoblast-like cell line was evaluated on several model (meth)acrylate networks with tunable stiffness and chemistry using a series of assays that quantify cell viability, proliferation, and differentiation. In addition, the osteogenic potential of these cells on tough (meth)acrylate networks, identified in Aim 1, was assessed and compared with the responses on other model copolymer systems.

To date, no studies have attempted to understand how to improve toughness of these materials by studying water-polymer interactions. Due to the high water content inherent to many physiological regions including disc tissue, these findings could

improve the durability of polymer networks such that their use can successfully be extended to other load-bearing biomedical applications. Because the material is photopolymerizable, it also has the potential to be injected into the body and then cured into the annular space or other regions that have limited surgical access. Another option would be to utilize the shape memory capabilities of these networks to create a material that can be inserted in a compact shape and then deployed by a thermal or mechanical stimulus upon entering the body.

The significance of this work stems from understanding the interrelationships between network structure, mechanical behavior, and biological response to facilitate the design of biocompatible photopolymerizable materials with the appropriate stiffness and toughness for use in load bearing orthopaedic applications such as spinal repair. By considering how physiological conditions, particularly the presence of water, influence these relationships, polymeric biomaterials can be created for not only novel implant devices, but for a plethora of applications such as more durable tissue engineering scaffolds and drug delivery vehicles.

In the chapters that follow, a rigorous characterization of the mechanical properties of copolymer (meth)acrylate networks is reported and discussed in terms of how chemistry, network structure, temperature, and solution affect toughness. Several fundamental relationships are established that will guide the future development of tough polymer networks. In particular, the glass transition temperature will be identified as the critical property associated with tailoring the mechanical properties. In later chapters, the effect of varying these same material properties on the osteogenic response is examined.

Finally, the significance of the findings on network toughness combined with the biological response is discussed.

CHAPTER 2

BACKGROUND

2.1 Photopolymerizable Networks

2.1.1 Current Use in Biomedical Applications

Photopolymerizable networks are materials that can be formed from liquid monomer or a combination of liquid monomers into a solid network upon exposure to visible or ultraviolet (UV) light. To facilitate the polymerization process, a photoinitiator must be present that will cleave and form a free radical upon exposure to UV light and subsequently, interact with certain reactive bonds on the monomers to initiate the polymerization reaction. These materials offer many advantages as biomedical materials including their ability to be formed *in situ* and into complex geometries rendering them useful for minimally invasive procedures. Photopolymerization is also an advantageous technique due to the large spatial and temporal control of the synthesis process, allowing for a variety of polymerization times from seconds to several hours [7] as well as the ability to create specific topographical features using an array of lithography techniques [13-15]. In addition, the reaction can take place at either ambient or physiological temperatures with minimal heat production [16].

Photopolymerizable materials can also be modified chemically to form biodegradable [17-19], injectable [8, 20], thermally activated (shape memory effect) polymer systems [21-22], facilitating their use in a diverse range of biomedical applications. Some current clinical uses of photopolymerizable networks include dental resins and contact lenses, but these materials are also being investigated as sensor

coatings, tissue barriers to improve wound healing [23] or prevent thrombosis [24], drug delivery vehicles [25], cell encapsulation materials [8], tissue engineering scaffolds [19, 26] and shape memory tissue fixation devices [22].

2.1.2 (Meth)Acrylate Copolymers: Structure and Synthesis

Acrylate copolymers are some of the most widely-used polymers synthesized through photopolymerization as their network formation is highly efficient due to the high reactivity of their vinyl functional groups. The polymerization kinetics and their effect on various material properties have been well-studied [27-29], and many acrylate chemistries have also been shown to be biocompatible [7, 30-32]. For example, 2-hydroxyethyl methacrylate (2HEMA) is the primary component of many contact lenses due its extreme hydrophilicity while poly(methyl methacrylate) (PMMA) is used as bone cement because of its incredible mechanical strength. In addition, many acrylate monomers that can be formed into copolymer networks are commercially available at relatively cheap costs improving the capability to mass produce these materials.

The chemical structure of a representative acrylate monomer, methyl acrylate (MA), is shown in Figure 2.2. Acrylate networks are formed through a free radical polymerization by incorporating at least one monofunctional monomer (one vinyl bond) and a difunctional crosslinker (2 vinyl bonds). During photopolymerization (Figure 2.2), the UV light interacts with the photoinitiator, in a process called photocleaving, to form free radicals on each remaining portion that cleave the carbon-carbon double bonds located on the monomers (“1” in Figure 2.1). Subsequently, these reacted monomers form their own free radicals on the same C-C bond that then, interact with other adjacent carbon-carbon double bonds allowing for propagation of the reaction and chain growth

("2" in Figure 2.1). Termination occurs when two radicals bind together ("3" in Figure 2.1). When choosing a photoinitiator, it is important to consider its biocompatibility, solubility, and stability. 2,2-dimethoxy-2-phenyl acetophenone (DMPA) (seen in Figure 2.1) is advantageous for biological purposes, because its side pendant group has been shown to reduce the number of unreacted photoinitiators and its products are biocompatible [16]. As one of the more commonly used photoinitiators, DMPA has already been extensively studied to form gels from PEG-based acrylates [23].

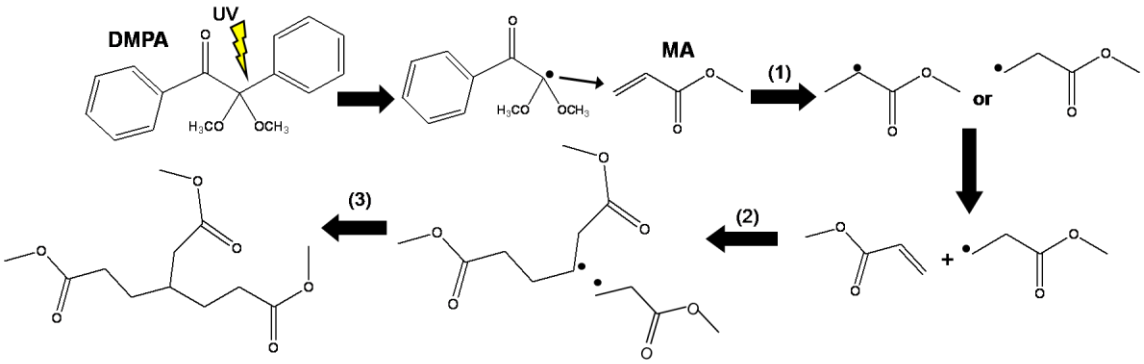

Figure 2.1. Diagram illustrating the free radical polymerization of acrylates initiated by the cleaving of DMPA by UV light and forming a free radical resulting in the subsequent reaction steps: (1) initiation, (2) propagation, and (3) termination.

If only monofunctional or linear monomers are present, long entangled polymer chains will be synthesized forming a thermoplastic that is capable of melting and plastic flow. Conversely, if a difunctional acrylate, or crosslinker, is mixed with a linear monomer, the dual functionality leads to the formation of crosslinks amongst the linear chains resulting in a tight thermoset network that possesses unique thermal, mechanical, and swelling properties that can be modulated by changing monomer chemistry, crosslinker concentration, and molecular weight [10, 33-34]. Because each acrylate monomer possesses its own individual chemical structure, combining multiple linear monomers and/or crosslinkers to form networks can allow for precise tailoring of a

variety of properties. For example the inclusion of a monomer that has a highly polar pendant, such as 2HEMA, increases the overall swellability of the network in water [35]. Understanding these structure-property relationships is a central theme that will be investigated in detail to determine how (meth)acrylate networks can be used as load-bearing biomaterials.

Besides the influence of monomer chemistry, the kinetics of the polymerization reaction will also determine the microstructure of the network. Several factors have been shown to control the photopolymerization process and resultant network structure formed. Sample thickness is one important variable that affects photopolymerization. As light from the UV source penetrates the sample, the rays are absorbed by the photoinitiator causing a decrease in light intensity the further the light must penetrate or the greater the sample thickness (Figure 2.2). Changing the UV intensity will alter the rate by which free radicals are formed and vinyl bonds are converted in the mixture [27, 36]. Oftentimes if the sample is thick enough, the surface closest to the UV source will have a higher polymerization rate compared with the converse side leading to inhomogeneous regions in the sample. In addition, if the intensity is mitigated too much deep in a thick sample, the conversion of reactive bonds could be low leaving many unreacted monomers in the sample that could alter the mechanical properties or potentially leach out over time.

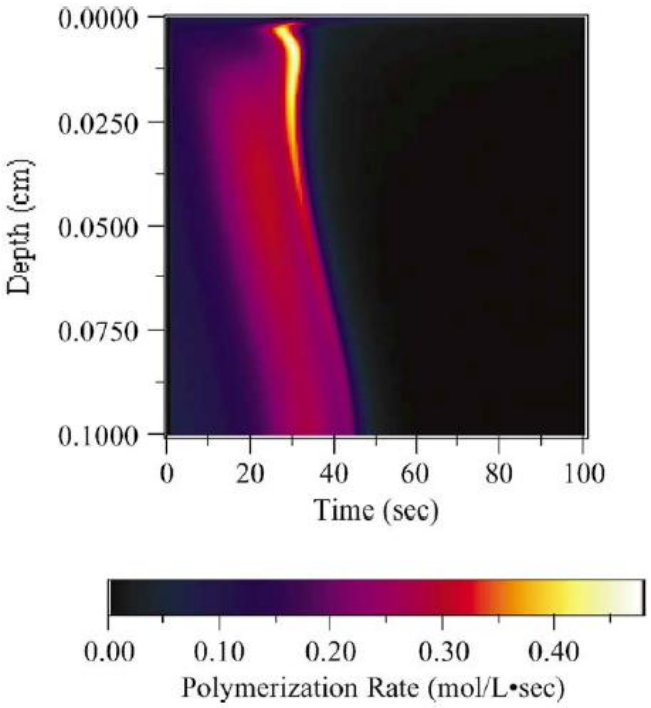

Figure 2.2. Polymerization rate as a function of depth and time into a sample during a typical photopolymerization. The sample thickness was 1mm and UV intensity was 10mW/cm^2. 2[36].

2.2 Thermomechanical Behavior of Polymers

2.2.1 Glass Transition Temperature

Polymer networks, including acrylates, exhibit a unique thermomechanical behavior that can be easily tailored by varying network chemistry and structure. In particular, the glass transition temperature (Tg) of polymers, including acrylates, is a critical property that dictates a material's mechanical, swelling, electrical, and thermal behavior [37-41]. In a broad sense, a polymer's Tg is the temperature where the polymer chains undergo a relaxation related to rapid vibrational movements and increased chain flexibility and mobility. From a mechanical standpoint, Tg represents the temperature span to which a polymer transitions from a brittle glassy material to a soft elastomer decreasing in modulus as the environmental temperature increases above Tg.

Network Tg is dependent upon the chemistry and structure of the polymer network. From the perspective of individual monomer chemistries, polymers with additional side groups hanging off the backbone often exhibit higher Tg's because higher temperatures are required to increase the molecular vibrations. For example, (meth)acrylate monomers exhibit higher Tg's compared with acrylates containing the same pendant group due to the extra methyl group present near the vinyl bond [34, 42]. However, if the length of the pendant group increases to a certain extent, the increased steric hindrance allows for more segmental motion in the backbone thus reducing Tg. In addition, polymers that contain high intermolecular bonding, such as 2HEMA typically also exhibit higher Tg's as they require higher temperatures to break secondary hydrogen or Van der Waals bonds [42-43]. With respect to multifunctional monomers, Tg will also increase with a decrease in the molecular weight of the crosslinker or increase in functionality due to higher restrictions in mobility imparted by a consequential increase in crosslink density [33, 38]. Increasing crosslink density also causes the breadth of the glass transition to increase as network heterogeneity increases causing micro-phase regions to relax at different temperatures [33, 44].

When two or more monomers are combined to form a copolymer network, the Tg of that copolymer network relies upon the Tg's and concentrations of the individual monomers incorporated into the network [39, 45-46]. Many theoretical models have been suggested to predict a copolymer's Tg. For instance, the most simplistic model relates monomer composition and Tg by:

$$Tg = w_1 Tg_1 + w_2 Tg_2 + w_3 Tg_3 \ldots\ldots$$

Where Tg_i and w_i are the individual Tg's and weight fractions of monomer i=1,2,3,….

However, studies have shown that copolymer Tg cannot be fully determined using a simple additive property, but that other intrinsic factors must be considered when predicting Tg based off of comonomer composition [45-48]. One of the most general forms, the Couchman-Karaz equation, takes into account changes in heat capacity (ΔC_p) of the different monomers, assuming ΔC_p does not depend on temperature, such that:

$$\ln T_g = \frac{(w_1 \Delta C_{p1} \ln T_{g1}) + (w_2 \Delta C_{p2} \ln T_{g2})}{w_1 \Delta C_{p1} + w_2 \Delta C_{p2}}$$

where w_i= the weight fraction of monomer i with i=1,2,3, etc [45]. This equation can be simplified further to the Fox equation by assuming that ΔC_p is nearly equivalent for all of the monomers [48]:

$$\frac{1}{Tg} = \frac{w_1}{Tg_1} + \frac{w_2}{Tg_2} + ...$$

The Gordon-Taylor Equation represents another simplified version of the Couchman-Karaz equation that also takes into account intermolecular interactions within the network by including an additional parameter k:

$$T_g = \frac{w_1 T_{g1} + k(w_2 T_{g2})}{w_1 + k w_2}$$

$$k = \frac{\Delta C_{p2}}{\Delta C_{p1}} \approx \frac{\Delta \alpha_2}{\Delta \alpha_1}$$

Where $\Delta \alpha_i$ is the coefficient of expansion for monomer i=1,2 and density of the two monomers is assumed equal [46]. If the intermolecular interactions between the polymer chains are weak, then the Fox and Gordon-Taylor equations usually hold [47]. Thus using the appropriate model equation, the glass transition behavior of a copolymer network can

be better predicted. A primary focus of this work details using this relationship between monomer concentrations and Tg to achieve specific desired mechanical properties.

Several techniques have been adopted to characterize a polymer's glass transition behavior. Differential scanning calorimetry (DSC) is one technique that takes a thermodynamic approach in determining a polymer's Tg by measuring changes in heat flow relative to the heat flow of air as temperature is increased or decreased [49-50]. A representative DSC curve showing the differential heat flow as a function of temperature is shown in Figure 2.3.

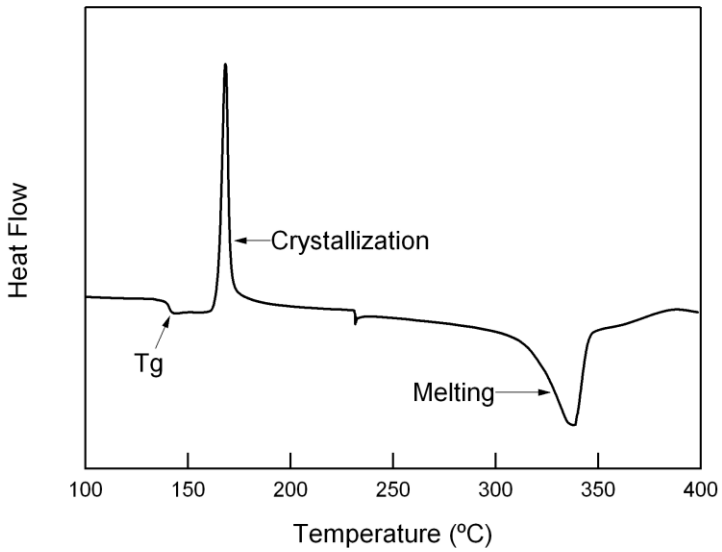

Figure 2.3. Representative DSC curve of polymer that undergoes a glass transition, crystallization, and melting as temperature is increased from 100°C to 400°C.

First order transitions in heat flow are measured as melting or crystallization peaks depending upon whether the polymer is undergoing heating or cooling. A polymer's Tg is denoted as a second order step change in the heat flow [49]. DSC is particularly useful when wanting to determine the Tg of water-sorbed polymers as the airtight pans used to hold the sample during the temperature scans keeps moisture from

evaporating too quickly [51]. Because water has its own thermal properties, information such as water content and state can also be extracted from DSC thermograms by evaluating the area of peaks occurring around 0°C and 100°C associated with melting and vaporizing of water molecules, respectively [52-53]. Water hydrogen bonded to polar groups in the polymer, an effect that subsequently alters the polymer chain dynamics, can also be determined through DSC. Because bound water molecules require higher temperatures than free water to vaporize, bound water concentrations are often assessed by measuring the temperature that the peak associated with water vaporization occurs [54].

Dynamic mechanical analysis (DMA) is another technique that assesses a polymer's thermomechanical properties by applying a sinusoidal force on a material to attain a specified strain over a sweep of temperatures at a given frequency. Properties such as modulus are determined from the measured stress and input specimen dimensions at each temperature point. A representative DMA curve plotting storage modulus and tan delta as a function of temperature is shown in Figure 2.4. The tan delta represents the ratio of the loss modulus (energy dissipated or viscous portion) to the storage modulus (elastic portion) and supplies information on the dampening capacity of the material. Tg occurs in the temperature region where modulus drops several orders of magnitude, specifically at the temperature of the tan delta curve peak. Besides identifying Tg, DMA can also be used to attain other information pertaining to the thermomechanical behavior and structure of a polymer. For example, by measuring the rubbery modulus (E_r) (modulus above Tg) through DMA, the crosslinking density of the network can be ascertained using the theory of rubber elasticity:

$$E_r = \frac{rRT}{M_C}$$

Where r is the mass density, R is the universal gas constant, T is temperature, and M_c is the molecular weight between crosslinks [55]. Thus from this equation, a higher rubbery modulus signifies less length between crosslinks in the network and a higher crosslink density.

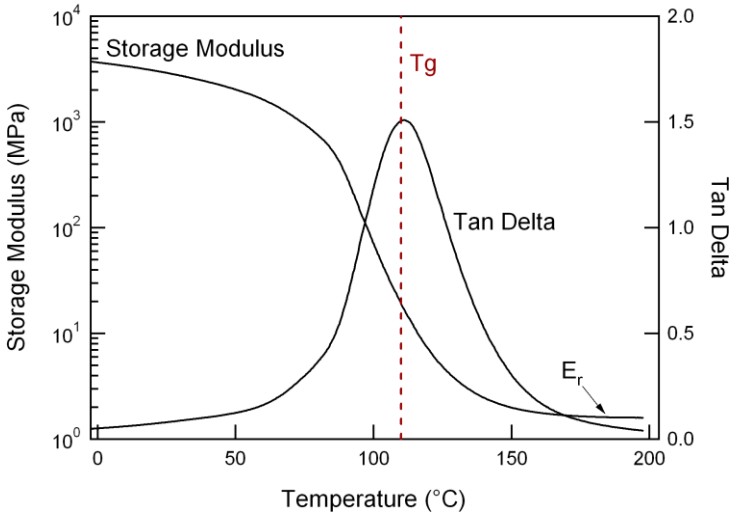

Figure 2.4. Characteristic DMA curve of a polymer network with Tg defined as the peak of the tan delta.

2.2.2 Role of Temperature on Mechanical Properties

An advantage of acrylate-based networks for load-bearing applications is their easily tailorable of mechanical properties by varying network chemistry and structure. Because Tg affects the mobility and rigidity of polymer chains, the mechanical behavior of polymers is highly temperature dependent. In general, a polymer's mechanical properties can be broadly classified into three categories related to the environmental temperature in relation to the material's Tg: glassy, viscoelastic, and rubbery (Figure 2.5). In the glassy regime (below Tg), chain mobility is restricted causing the polymer to

exhibit brittle behavior characterized by high elastic modulus and usually failure stresses, an absence of yielding behavior, and low strain capacity. As a polymer approaches its Tg, the polymer acts in its viscoelastic regime characterized by a moderate modulus, some yielding behavior and increased strain capacity compared with glassy polymers. It is within this regime that slight fluctuations in extrinsic factors such as temperature and strain rate can have a large impact on mechanical properties. At temperatures above Tg, polymer networks exhibit rubbery elastomeric behavior characterized by a low modulus and moderate strain capacity, but no yielding behavior. Unlike their thermoplastic counterparts, polymer networks do not melt above Tg thus making them useful materials for high temperature applications.

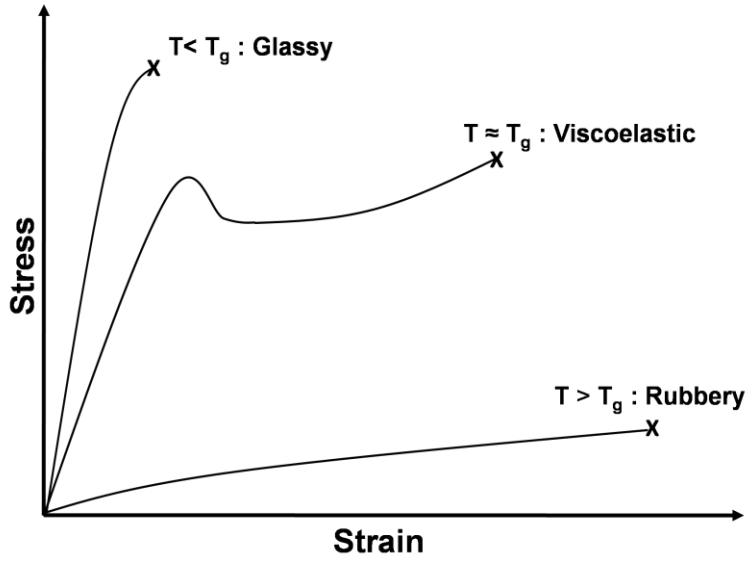

Figure 2.5. Example stress-strain curves under tension for polymers exhibiting glassy, viscoelastic, and rubbery behaviors.

The mechanical behavior of polymer networks is strongly influenced by the network chemistry and structure. For instance, increasing the concentration of crosslinker, and thus the crosslink density, will increase the elastic modulus as well as ultimate strength of the network [56], but decrease the ultimate failure strains the material

can attain [33]. Ultimate strength and elastic modulus can also be increased by increasing the amount of photoinitiator or light intensity allowing for more double bond conversions to occur and a denser, more-crosslinked network to form [56]. Several studies have attempted to experimentally compare the mechanical strength of different acrylate monomers to evaluate their overall mechanical contribution to the network. For example, Lustig et al. report that methyl methacrylate (MMA) and 2HEMA have comparable levels of mechanical strength when incorporated into a copolymer system under dry conditions [57]. The high strength of 2HEMA is attributed to the presence of intermolecular hydrogen bonds between hydroxyl groups located on the pendant chains. Another systematic study on the influence of monomer chemistry on the mechanical properties revealed that within a certain range of crosslinking density, networks that contain phenyl rings exhibit increased strength and extensibility compared with other monomers such as PMMA and poly(ethylene glycol) phenyl ether acrylate (PEGPEA) [34]. These findings were taken into consideration within this current work when selecting monomers to incorporate into the model copolymer networks.

2.2.3 Toughness

Although much work in the literature has been devoted to understanding structure-property relationships in regards to modulus, strength, deformability, less is known on how to tailor network toughness [34, 58]. Toughness is a material property that can be measured by the amount of energy required to break a material and broadly reflects upon the overall stresses and strains the material can withstand. With respect to polymers, key mechanical parameters that correspond to enhanced toughness include

increased strength, ductility, and/or extensibility since these properties all correspond to additional energy requirements to initiate failure. In addition to sustaining large loads and strains, tough materials are relatively flaw insensitive since their toughening mechanisms can accommodate local strains at geometrical or material discontinuities.

Materials that are used in a load-carrying capacity must exhibit not only a similar compliance, as often measured by elastic modulus, but also have a similar level of toughness as the tissue it is replacing or repairing . Biological tissues have unique hierarchical structures that provide the tissue with specific mechanical properties to allow the tissue to serve its physiological function under complex loading regimes. Many biological tissues are hailed in the literature for having "high" toughness, particularly fibrillar or ceramic-based biological tissues. Figure 2.6 illustrates the relationship between the elastic modulus and toughness of many biological tissues in comparison with materials that are already used clinically. Calcified tissues such as bone and tooth enamel exhibit high moduli but moderate toughness due to their inherent brittleness. Collagen-rich fibrillar tissues such as tendon, skin, and disc annulus have moderate compliance, but improved toughness due to their maintenance of strength at higher strains [59-61]. At the lower end of the spectrum, high water content tissues such as articular cartilage and nucleus pulposus have both low moduli and toughness. Interestingly though, their physiological functions are partially mechanical requiring them to be subjected to continuous loading cycles, and in some cases over large stress and strain ranges.

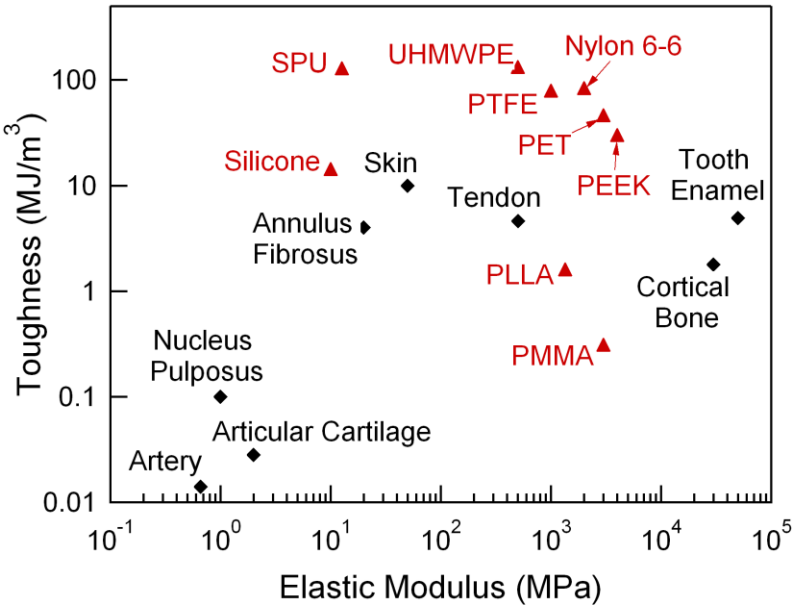

Figure 2.6. Toughness vs. elastic modulus for several load-bearing biological tissues (black) and polymers currently used clinically (red). If toughness was not specifically given in the study, a value was determined by calculating the area under the reported stress strain curve. SPU = segmented polyurethane; UHMWPE = ultra-high molecular weight polyethylene; PET = poly(ethylene terephthalate); PTFE = poly(tetrafluorethylene); PLLA = poly(L-lactide); PEEK = poly(ether ether ketone) [62-70] [71-74].

In general the toughness of successful clinical implant materials is relatively high in comparison to biological tissues. Over a similar range of elastic moduli, the toughness of the majority of synthetic polymers in use today (10 to 100 MJ/m^3) is larger than the majority of living tissues (0.01 to 10 MJ/m^3). The only exceptions in clinical use are PMMA and PLLA. PMMA was grandfathered into use in 1976 and is used predominately as bone cement in restricted loading environments (for example in a bone crevice or a medullary canal). In addition, PMMA is typically polymerized into solid form inside the body, providing versatility not provided by the other materials. The PLLA polymer has relatively low toughness but also provides secondary function inside

the body through degradation. However, researchers are attempting to toughen PLLA-based implant materials as well as design other tough degradable materials [75-76].

Similar to biological tissues, a material's toughness is directly related to its chemical and macroscopic structure. Several theoretical models have been developed to understand how chemical structure affects toughness in linear polymers. For example, Wu predicted that toughness is dependent upon the chemical composition and chain structure quantified through two interrelated variables in thermoplastic polymers, the entanglement density (υ_e) and Flory's characteristic ratio (C_∞) [58], a theory that has later been validated through experimental observations [77-79]. Using Wu's theory, the inherent toughness in polymers such as poly(ether ether ketone) (PEEK) and polycarbonate is predicted as these two polymers have relatively low C_∞ values while PMMA, a brittle polymer has a much higher C_∞ value. The low characteristic ratios and thus high toughness of PC and PEEK are attributed to the presence of phenyl ring-oxygen group in the backbone that allows for both rigidity and flexibility of the chains. Taking these structural features of PEEK and PC into consideration, one study reported that incorporating phenyl rings into the backbone of thiol-ene-acrylates provides enhanced toughness when impact testing was performed [80].

Although Wu's theory accounts for the relative toughness of linear polymers, as it pertains to the chemistry of the backbone, the models do not consider other distinct structural characteristics such as side group chemistry and crosslinking density that are inherent in copolymer networks. For instance, another study found that the toughness of acrylate-based networks was dependent upon the chemistry of the linear monomers at low crosslinking densities (E_r<10MPa), but then becomes dependent solely on the

crosslink density above this specific crosslink concentration. Within this low crosslinking range, it was determined that Wu's characteristic ratio was not a good predictive parameter of network toughness but rather a monomer's cohesive energy density provided a better predictive assessment of network toughness. Specifically, meth(acrylate) monomers possessed higher toughness over their acrylate counterparts while monomers containing bulky phenyl rings in their side group provided increased toughness over longer linear side chains [34]. For this current research, these relationships served as initial design tools to specifically the tailor mechanical properties of photopolymerizable (meth)acrylate networks

2.2.4 Effect of Water Absorption

Since intervertebral disc tissue contains a large amount of water, it is imperative to understand how polymer chemistry dictates water-polymer interactions, and how these interactions subsequently affect mechanical properties. For instance, previous studies have shown that immersing a polymer in water will result in a precipitous change in mechanical properties. For example at room temperature, linear acrylates such as PMMA will decrease in strength when soaked in water for long durations [81]. This loss of "mechanical integrity" is the result of water molecules penetrating into the polymer and disrupting the intermolecular bonding between chains to form their own hydrogen bonds with polar groups within the polymer. This effect, generally termed "plasticization", results in increased chain mobility and reduced backbone rigidity, in some cases corresponding to a reduction in Tg [35, 54, 82].

The extent to which Tg decreases in water is governed by the immersion time and total water content within the network as well as the state of the absorbed water molecules [54, 83-84]. In general, the Tg will continuously decrease as the water content or immersion time increases, an effect driven by the initial water-polymer hydrogen bonds formed within the network [37, 54, 83]. In hydrogels where the water content can be greater than polymer content, the polymer will swell several times its original size in order to optimize the number of water-polymer hydrogen bonds that can be formed.

From a thermodynamic perspective, the effect of water on polymer properties, including Tg, is related to the state of the absorbed water molecules. In simplistic terms, water molecules can be found in one of two states within the network, each of which plays its own role in affecting the glass transition behavior of polymers. As displayed in Figure 2.7, water molecules that form hydrogen bonds with polymer chains are termed "bound water" while those water molecules that remain distant from the polymer chains and form hydrogen-bonds with other water molecules are called "free water" [37, 83, 85-86]. Tg is affected by bound water in that the hydrogen bonding of water molecules to the polymer chains will result in the formation of a one-phase thermodynamic system that will exhibit a Tg that is dependent upon the Tg's and concentrations of the polymer network and water molecules in a manner that can be determined using the principles discussed in Section 2.3 [51]. It is believed that the increased binding of water drives the initial absorption process into the network resulting in the largest initial decrease in Tg. Despite not directly bonding with the network, free water also affects the Tg of polymer networks, particularly more hydrophobic polymers, by increasing the intermolecular distance between the polymer chains, thus disrupting the interchain secondary bonding,

including both hydrogen bonding and secondary hydrophobic interactions, and increasing chain mobility [37, 83].

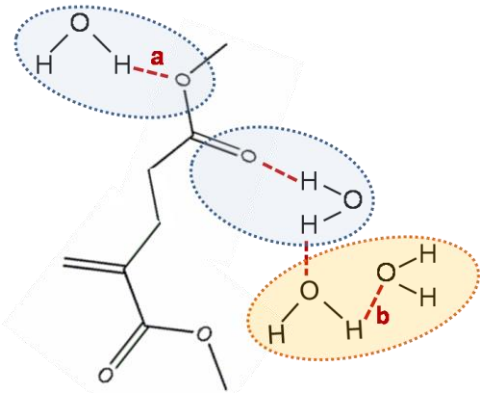

Figure 2.7. Thermodynamic states of water when absorbed into a polymer network. Water molecules can either form hydrogen bonds with polar groups, such as the esters found in acrylates ("a" in figure) or with other adjacent water molecules ("b").

As might be expected, the water state and concentrations of each state will be dependent upon the network chemistry and structure. For instance, the extent of bound water is closely proportional to the number of polar groups such as such as hydroxyl or amine groups, present in the network [87]. In general, acrylate polymers will have some bound water present due to the characteristic ester bond (O-C=O) found in the chemical structure. Bulky side groups, such as a phenyl ring or long side chains, can prevent water binding by acting act as steric barriers [37, 83]. Similarly, the extent of free water present is also limited by any bulky groups because the amount of free volume present is reduced in the network. Independent of chemistry, changing the crosslinking density of the network will also affect total water content by limiting the mobility of water molecules and reducing the availability of hydrophilic binding sites due to steric hindrance [83, 87]. In the case of hydrophobic glassy polymers, water penetration is driven more by diffusion-related forces than thermodynamic factors. Although no binding sites might be present, over long periods of time, water diffuses into the matrix to

fill any micropores present [88]. Similar to the free water discussed above, these molecules over time disrupt the intermolecular bonding and cause conformational rearrangements such that the chains will be in their most energetically favorable state by limiting interactions with the water molecules and maximizing their own secondary interactions. Other external factors including temperature will affect the total water content and water state. Increasing temperature to above Tg allows for more water to penetrate the network due to the increased free volume and chain mobility. These factors must all be considered when understanding the relationship between network chemistry and T_g under aqueous conditions.

Based off of these observations, it is possible that water content can also determine the extent to which toughness is altered in solution and thus, can be one mechanism utilized to enhance toughness under physiological conditions. Developing tougher hydrogels for orthopaedic applications has been particularly challenging since, by definition, hydrogels typically contain at least 50% their weight in water resulting in large alterations in mechanical properties. Several groups are currently working on developing mechanically enhanced hydrogels by changing network structure or type of crosslinking [89-90].

2.3 Osteogenesis and its Regulation by Biomaterials

2.3.1 Bone Development and Remodeling

The effectiveness of implant materials is heavily dependent upon the interaction between the material and the surrounding biological environment. Eliciting an appropriate biological response requires understanding the biological mechanisms involved in bone remodeling and how the material surface affects the biological function of bone.

Bone is a complex hierarchial tissue that is composed of a collagen-rich organic phase and an inorganic mineral phase. During the initial stages of bone development, mesenchymal stem cells migrate from the bone marrow to the defect or implant site. As the cells adhere to their environment, they begin to synthesize and deposit the organic phase of the extracellular matrix (ECM). Collagen is the main constituent of this soft matrix, also called osteoid, but other matrix proteins including osteopontin, osteocalcin, bone sialoprotein, and fibronectin are also produced during this stage and serve their own individual purpose in directing bone maturation. As the cells further differentiate, they then begin to mineralize the ECM by depositing crystals of calcium phosphate before finally transforming into osteocytes or mature bone cells. On the other hand, bone resorption is initiated when osteoclasts, macrophage-like cells, are recruited to break down the deposted bone matrix. This remodeling process, formation vs. resorption, is highly regulated in an attempt to prevent the over or under production of bone tissue, either of which can lead to severe physiological disorders. With regards to bone-interfacing implants, the under-production or increased resorption of bone can lead to the implant loosening over time and thus, is considered an undesired response [91].

Osteoblasts are the primary bone-forming cell and must attach to a pre-existing surface to produce osteoid and calcify their extracellular matrix. These cells undergo a complex sequence of events to reach a mature osteoblast phenotype that can be broken down into three distinct periods associated with the increased and decreased expression of specific osteogenic factors: (1) proliferation, (2) matrix formation, and (3) mineralization (Figure 2.8) [92]. It is not the purpose here to detail the regulation of all phenotypic markers but to highlight key proteins associated with each stage that provide a basis for assessing the differentiation state and function of cells in question.

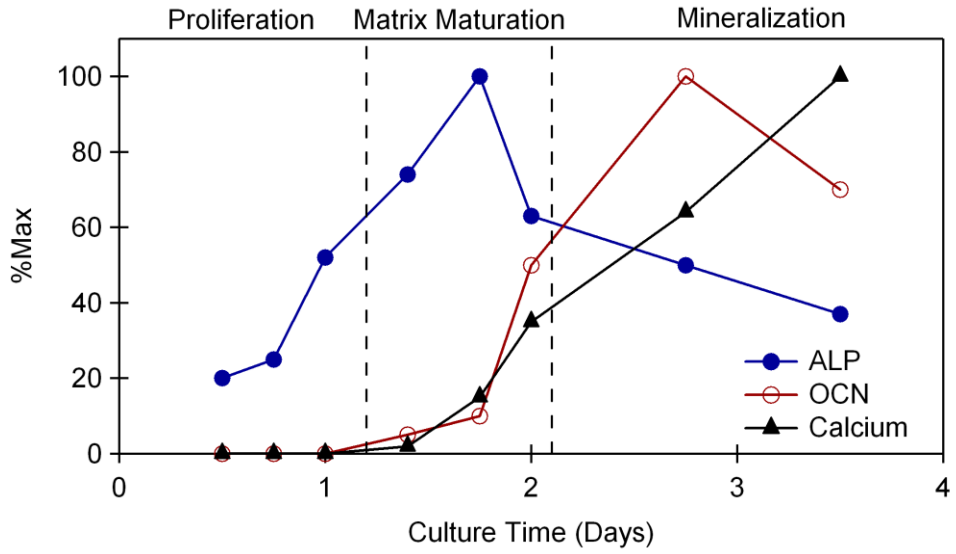

Figure 2.8. Schematic of the temporal sequences of gene expression and synthesis of markers related to the maturation of osteoblasts and tissue development (adapted from [92].

During the proliferative stage, DNA synthesis is increased while ECM proteins including collagen and fibronectin and transforming growth factor beta-1 (TGF-b1), a regulator of matrix synthesis, are up-regulated in culture. As the proliferation declines, the beginning of differentiation is associated with elevated alkaline phosphatase specific activity. Alkaline phosphatase specific activity is believed to be involved with the onset

of matrix protein secretion and organization, making its increased activity a primary marker of early stage differentiation [93]. A decrease in alkaline specific activity signifies the onset of the mineralization stage that is marked by the increased expression of several matrix proteins including osteocalcin (OCN), osteopontin (OPN), and bone sialo-protein (BSP). Because osteocalcin is produced at the onset of mineral nodule formation, its increased production is a well-accepted marker of late-stage osteoblast differentiation. TGF-β1 is believed to be another osteogenic regulator by acting to stimulate proliferation, promote ECM production, and down-regulate osteoclast activity [94]. Osteoclastogenesis can also be mediated by osteoprotegerin (OPG), a decoy receptor that binds to RANK ligand on osteoblasts preventing their interaction with RANK on osteoclasts [95]. Thus, increased expression of OPG would favor osteogenesis.[96] Additionally, other markers including FGF-2, $PGE_{2,}$ BSP are believed to be regulatory markers of osteogenesis expressed at different points during maturation [96-97]. This temporally regulated sequence of gene expression and subseuent protein synthesis is closely associated with ECM development and osteoblast maturations and have been observed *in vivo* through histochemical staining and *in vitro* by observing the gene expression of the osteogenic markers [92].

The differentiation state of osteoblasts is also associated with their morphology. Upon attachment, osteoblasts will exhibit a flattened morphology that evolves as differentiation progresses with cells becoming more columnar in shape. These changes in cell shape are associated with matrix and mineral accumulation around the cell and contribute to intracellular signaling pathways that regulate the expression of osteogenic genes. Osteoblasts primarily attach and respond to their extracellular environment

through integrins, a class of transmembrane heterodimeric proteins that consist of two subunits (alpha and beta). Integrins serve to transmit signals from the extracellular environment to the cytoplasm causing activation of various downstream signaling pathways that lead to changes in cytoskeleton organization, gene expression, and protein translocation. These extracellular cues can be chemical, topographical, or mechanical in nature with certain characteristics of each signal able to produce a similar cell response [12]. For instance with regards to chemical cues, integrins will recognize and bind to specific peptide sequences on extracellular matrix proteins such as the arginine-glycine-aspartic acid (RGD) motif found on fibronectin. Similarly, mechanical stimulation will induce the expression of osteogenic markers through a pathway mediated by the alpha 2 beta 1 integrin [98-100]. As might be expected, cell attachment and function is mediated through integrin binding in a similar fashion on synthetic materials [101-102].

2.3.2 Cell-Material Interactions

Because osteoblasts must attach to a surface to differentiate and produce new matrix, their morphology, differentiation and function are affected by the surface properties of synthetic materials including the surface wettability, topography, and stiffness in a manner that mimics the physiological response of osteoblasts to their native extracellular environment. Surface energy, or wettability, as measured by the contact angle between water droplets and the surface, affects both cell attachment and proliferation [103] by changing the surface presentation of extracellular matrix proteins to which cells bind. In particular, it has been shown that a contact angle above 45 degrees is necessary for adequate cell adhesion and proliferation on polymer films [104], but

osteoblast differentiation is promoted on more hydrophilic surfaces. On hydrophilic metal oxide surfaces, human osteoblast-like MG63 cells exhibit a differentiated phenotype and also secrete factors that create an osteogenic microenvironment [105]. With polymers, wettability is affected by both network chemistry and crosslink density, thus enabling the cell response to surface energy to be tailored on polymer surfaces by varying copolymer composition [106] or functionalizing the surface with specific chemical groups [102].

Besides surface chemistry, surface roughness or topography can also regulate osteoblast function by either controlling the protein adsorption or by inducing cells to alter their morphology due to specific spatial boundaries. Consequently, cell binding and function is affected in a manner that is dependent on the size scale of the topographical features. [91, 107-110]. For instance, MG63 cells become more differentiated on titanium with micron-scale roughness in comparison to smooth or sub-micron scale rough surfaces [111]. Similarly, rough surfaces containing pits or pores with a peak-to-peak distance less than the size of the cell will cause cells to form a cuboidal or rounded morphology as the cells anchor themselves around the pit translating into altered intracellular signaling [112]. Thus, many implants, in particularly titanium dental implants, have been developed with specific topographical features to enhance matrix production and bone growth around the implant.

More recently, much interest has been generated on whether cells, including osteoblasts, can mechano-sense their extracellular environment. Several studies have reported that cell attachment, proliferation, and differentiation are all modulated by the substrate rigidity to a degree dependent upon the substrate stiffness in relation to the stiffness of the native tissue [11, 113-117]. In other words, cells will mimic their *in vivo*

behavior more when they are cultured on substrates whose rigidity matches that of that cell type's native tissue matrix. Thus, considering the relatively stiff nature of bone, it is expected that osteoblasts will attach more, increase their proliferation rate, and exhibit a more mature phenotype on stiffer surfaces, greater than 100kPa [114-115]. Kong et al. have proposed that this modulated osteoblast response relates to the cells' ability to more efficiently generate force through their cytoskeleton in response to the larger resistance induced by the rigid substrate [113], and that these generated traction forces will alter the assembly of intracellular machinery that drives its ability to enter the cell cycle or differentiate [115]. The most reported substrate model utilized to study these stiffness effects is to use a polyacrylamide gel and changing its crosslinking density to achieve variable levels of stiffness. To mitigate any chemistry effects and to promote cell binding, these surfaces are sometimes coated with collagen or RGD peptides. More recently, stiffness effects on osteoblast differentiation are being investigated on PEG-based gels that have stiffnesses that can be modified by crosslinking concentrations or water content. In all of these studies, a trend of increased osteoblast maturation with increasing stiffness is observed with a more pronounced effect being observed in stem cell lines versus more committed cell lines such as MC3T3-E1 cells. These findings suggest that the mechanical microenvironment can have implications on developing therapies to promote bone formation and osseointegration. Figure 2.9 summarizes the cell response to the material surface.

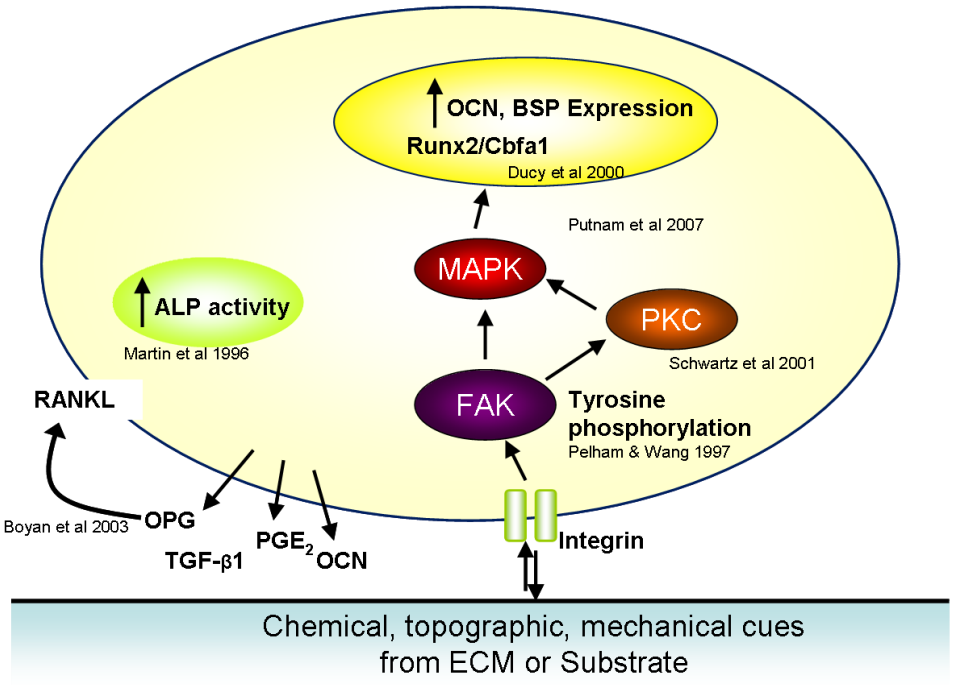

Figure 2.9 Illustration of intracellular signaling pathways associated with osteoblast binding to its ECM or synthetic surface.

2.3.3 Biocompatibility of Photopolymerizable Materials

The biocompatibility of photopolymerizable materials has been studied extensively in the literature [7-8, 19-20, 26, 29, 31, 104, 118-119]. A primary concern of photocurable polymers is the potential cytotoxicity related to any residual monomer residing in the network that could leach out. The level of toxicity has been correlated to the chemical structure, concentration, and water solubility of the monomers [32, 120]. For example, acrylates exhibit higher cytotoxic effects compared with their methyl acrylate counterparts in terms of cell viability [32]. Monomers that have bulky side groups such as phenyl rings or long chains have also been linked with lower cell viability compared with smaller molecules such as MMA. Monomers that are more water soluble, and thus can easily be degraded through hydrolysis, have also been correlated to higher cytotoxicity [120]. Cell death due to monomer leaching can be mitigated though by

improving the conversion efficiency of the polymerization reaction, removing any residual monomer prior to implantation, or reducing water absorption. Due to the toxicity of certain low molecular weight monomers, their use as injectable systems is limited, and so instead, injectable photopolymerizable materials are formed from macromolecular precursors, such as PEG acrylate derivates [7], polypropylene fumarate derivatives [121], and poly(beta-amino ester) acrylates [9] and have some demonstrated success in supporting cell growth, including osteoblast growth. With regards to this present research, any networks containing potential toxic monomers (i.e. BMA and MA) that are developed and characterized were not considered for possible injectable applications, but rather as pre-formed materials that can be delivered in an alternative manner.

Photopolymerizable materials have also been shown to support osteoblast growth and differentiation. An *in vitro* study screening the growth potential of osteoblasts on specific photografted polymers, including some acrylates, reported that osteoblast proliferation and differentiation were both dependent on the chemical structure of side groups in a manner independent of surface wettability [122]. Furthermore, those photopolymers that exhibited excellent *in vitro* compatibility corresponded to increased osseointegration when implanted in an animal model [123]. In many cases, the cells are photoencapsulated in a hydrogel that serves as a delivery vehicle or if functionalized with bioactive molecules, as a biomimetic ECM to promote a specific cellular response [7, 20, 26, 118, 124-125]. In particular, photocured PEGDA hydrogels have been shown to guide the differentiation of MSCs or immature osteoblasts [97, 124] verifying their use as bone tissue engineering scaffolds.

2.3.4 MG63 Pre-osteoblast Cell Culture Model

In order to reliably establish relationships between the material surface and cellular response, a well-defined cell culture model must be adopted. Human MG63 pre-osteoblast cells, an osteoblast-like osteosarcoma cell line have been used extensively to determine what factors are related to the expression of the osteoblast phenotype and what signaling pathways involve the regulation of genes that encode osteogenic marker proteins [92]. These cells initially exhibit an immature osteoblast phenotype, but can differentiate into mature osteoblasts over a several day culture period when exposed to certain stimuli [96]. For each experiment, MG63 cells are plated directly on the material surface in 24-well culture plates and grown to confluency in Dulbecco's Modified Eagle's Medium (DMEM) plus 10% fetal bovine serum (FBS). 24 hours prior to harvesting, the media is changed and then collected at harvest to determine the amount of certain osteogenic factors that were produced during that 24 hour period.

Previous studies have used this model to determine the osseointegrative potential of implant surfaces with various chemistries and topographies showing that MG63 cells cultured in this manner will exhibit an osteoblast phenotype more on hydrophilic sand-blasted, acid-etched titanium surfaces than on smooth pure titanium [96, 101, 108, 126]. These results further correlated to better bone to implant contact *in vivo* leading to higher pull-out strengths and less implant loosening [91, 127-128], validating the use of this cell culture model to study the osteogenic potential of different material surfaces. This MG63 cell culture model was adapted to evaluate the *in vitro* osteogenic response on photopolymerizable (meth)acrylate networks and slightly modified for use with polymer discs. The entire culture setup is show in Figure 2.10.

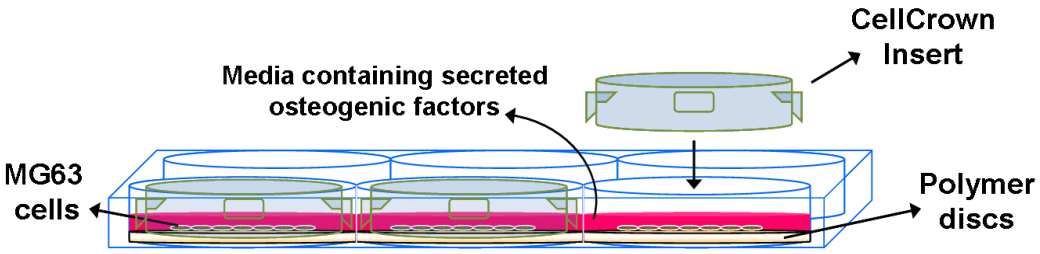

Figure 2.10. *In vitro* culture model implemented to evaluate the osteogenic response of MG63 osteoblast-like cells to (meth)acrylate networks.

CHAPTER 3

CHARACTERIZATION OF TOUGHNESS IN PHOTOPOLYMERIZABLE (METH)ACRYLATE NETWORKS UNDER VARIOUS ENVIRONMENTAL CONDITIONS

3.1 Introduction

Polymer networks formed through photopolymerization have emerged as candidate biomaterials for applications where it is advantageous to have *in situ* formation, fast synthesis rates, and simple processing into diverse geometries. As a subset of photopolymers, (meth)acrylate-based networks are advantageous because their material properties can be easily tuned by control of chemistry and crosslinking density.

Depending on the application, polymer networks must possess a certain range of mechanical properties. The elastic modulus is an important property because it governs the deformation of the material and is critical in managing stress transfer to surrounding tissue. For instance, polymers used in a shape memory fixation device must possess a relatively high modulus (10-50MPa) to allow for high-strength deployment into a stiff tissue such as bone [22] while a soft tissue replacement material must have a modulus that matches the native tissue it is replacing (0.1-100MPa depending on the tissue) [129-130].

*Modified from
Smith KE, Temenoff JS, Gall K. On the Toughness of Photopolymerizable (Meth)Acrylate Networks for Biomedical Applications. *Journal of Applied Polymer Science*, 2009; 114(5): 2711-2722.

Additionally in applications involving implantation into readily deformable regions (i.e. intervertebral disc, tendon, etc), a material that can sustain high failure strains (greater than 100%) is often necessary [59, 131]. Although it is relatively easy to tailor the stiffness or deformability of polymer networks to match that of host biological materials [132-134], maintaining toughness, another key mechanical property, in line with biological tissues is elusive, especially in polymer networks. Toughness broadly measures the capacity of a material to absorb strain energy and resist cracking under applied stress. Photopolymerizable (meth)acrylate networks possess a broad range of thermomechanical properties allowing them to serve as various material platforms ranging from hydrogels[7] to shape memory polymers[22]. However, photopolymerizable (meth)acrylate networks sometimes lack the toughness, for implementation in high-loading environments or in applications where mechanical function must be maintained for long durations.

In order to develop tougher, more durable photocurable (meth)acrylate networks, a fundamental understanding of the toughening mechanisms within such materials must be established. Several theoretical models have been developed to understand the structure-toughness relationship in linear polymers where high toughness is attributed to the presence of certain chemical groups and their associated intermolecular interactions [58]. For example, the high inherent toughness of PEEK is attributed to the phenyl ring-oxygen-phenyl ring group in the backbone as well as the ability to crystallize [58, 135-136]. However, these relationships between monomer structure and toughness are further complicated with copolymer networks that contain crosslinks and multiple monomer components [34].

To date, there has been minimal work focusing on the toughness of biomedical grade (meth)acrylate networks particularly under physiological conditions [137]. The objective of this study is to build an understanding of how intrinsic and extrinsic factors influence network toughness in photopolymerizable (meth)acrylate networks. The approach consisted of performing stress-strain measurements on a series of "benchmark" tough polymers and several model (meth)acrylate networks to understand how chemistry and polymer structure influence toughness. To further understand how the thermal transition behavior influences network toughness, the stress-strain response at multiple temperatures spanning the glassy to viscoelastic to rubbery regime was evaluated. Lastly, this study also aimed to identify how the relationships between toughness, chemical structure, and temperature are influenced by immersion in phosphate buffered saline (PBS). The results provide the fundamental knowledge required to guide the development and implementation of tough photopolymerizable polymers for load-bearing orthopaedic applications.

3.2 Materials and Methods

3.2.1 Materials

Poly(methyl methacrylate) (PMMA), polycarbonate (PC), and poly(ether ether ketone) (PEEK) were obtained from McMaster-Carr Inc as sheets of thickness 1.6mm, 1.0mm, and 0.2mm, respectively, and used as reference materials due to their well-studied mechanical behavior and common use as biomedical materials. Methyl methacrylate (MMA), methyl acrylate (MA), and 2-hydroxyethyl methacrylate (2HEMA) monomers, and a poly(ethylene glycol) dimethacrylate (PEGDMA) crosslinker with a

molecular weight of M_n=750 were chosen as the photopolymerizable acrylates. The chemical structures for each monomer are shown in Figure 1. The monomer solutions and photoinitiator, 2,2 dimethoxy 2-phenylacetophenone (DMPA), were purchased from Sigma-Aldrich and used as received.

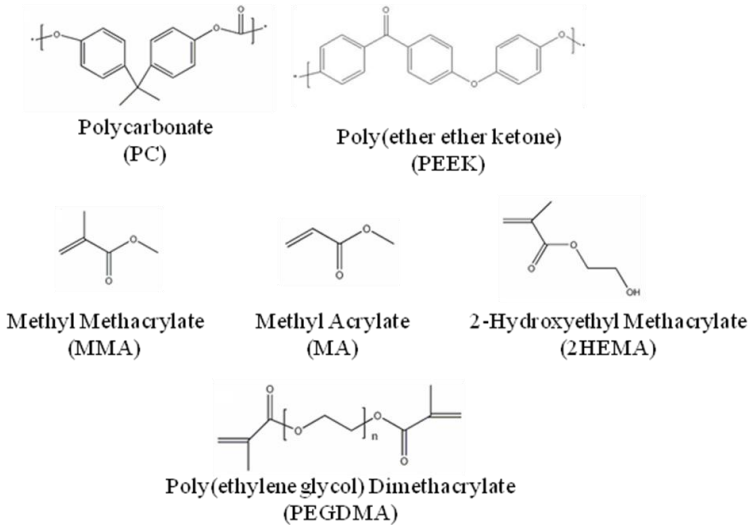

Figure 3.1. Chemical structures of selected thermoplastic polymers, PC and PEEK, and the (meth)acrylate monomers incorporated into copolymer networks.

3.2.2 Network Synthesis

Monomer solutions were formulated by combining a monofunctional (meth)acrylate (linear chain builder) and a difunctional methacrylate (crosslinker) in a ratio determined by weight and 0.5 wt.% photoinitiator. Table 1 shows the monomer components and their chemical structures. The weight ratios of the monomers in each copolymer network are displayed in Table 2. Each of the networks was carefully designed to screen for various chemical and structural effects. The 2HEMA-co-2%PEGDMA is a lightly crosslinked, hydrophilic hydrogel network, similar to that used in soft contact lens applications. The MMA-co-45%PEGDMA is a moderately

crosslinked material that demonstrates excellent shape memory properties in high force applications[22] and is moderately hydrophilic. The MA-co-MMA-co-2%PEGDMA is a lightly crosslinked, relatively hydrophobic shape memory polymer that would operate best in large-deformation, low-stress biomedical applications.

Each solution was mixed manually in a glass vial and injected in between two glass slides using a glass pipette. The glass slides were separated with two 1mm glass spacers and coated with Rain-X to enhance release. The samples were then placed under a 365nm UV lamp (Blak Ray Model B 100AP) for 10 to 30 minutes depending on the network.

Table 3.1: Networks created using a monofunctional (meth)acrylate and crosslinker (PEGDMA) and their corresponding average T_g, rubbery moduli (E), and swelling ratios (q).

Name	Monomer Ratio Wt%	T_g (°C)	E (MPa)	q
MMA-co-45%PEGDMA	55% MMA 45% PEGDMA	66.8 ± 2.2	12.4 ± 0.3	1.14 ± 0.01
2HEMA-co-2%PEGDMA	98% 2HEMA 2% PEGDMA	111.7 ± 1.3	1.43 ± 0.2	1.58 ± 0.05
MA-co-MMA-co-2%PEGDMA	52% MA 46%MMA 2%PEGDMA	57.1 ± 1.2	0.270 ± 0.2	1.02 ± 0.01
100%PEGDMA	100% PEGDMA	-20.3 ± 0.3	30.9 ± 0.6	1.46 ± 0.02

3.2.3 Dynamic Mechanical Analysis

Thermomechanical properties were determined using a dynamic mechanical analyzer (TA Instruments DMA Q800). All copolymers were cut into 20mm x 5mm rectangular samples, and the edges were sanded to remove any microdefects. Samples were cooled to -75°C, equilibrated at -75°C for 2 minutes, and subsequently heated to 200°C at a constant rate of 5°C/min. Tests were performed in tension mode at a frequency

of 1Hz with a 0.1kN preload force, 0.2% strain rate, and 150% force track. The glass transition temperature (T_g) was defined as the peak of the tan δ (ratio of loss modulus to storage modulus) curve produced by plotting tan δ versus temperature.[138] The Universal Analysis software package was used to determine the exact temperature corresponding to the maxima on the curve. The rubbery modulus (E_r) was determined as the value of the storage modulus above T_g where the tan δ does not change. DMA was repeated once for each composition. T_g and E_r values for each composition were averaged and standard deviation calculated.

3.2.4 Tensile Strain-to-Failure Testing

Tensile strain-to-failure tests were performed on a universal testing machine (MTS Systems, Insight 2) using a 2kN load cell and a crosshead speed of 1 mm/min. Dogbone samples were laser-cut according to dimensions specified in ASTM D 638-03 Type IV or Type V (see below). The edges were sanded to remove any defects from the laser and the width and thickness in the gauge section were measured using digital calipers. Samples were loaded into tensile grips, heated in a thermal chamber, and held at the testing temperature for 10 minutes to allow for thermal equilibration. Each polymer system was tested in tension at temperatures below and above its Tg. Only samples that broke in their gauge length were used for further calculations. Elastic modulus was denoted as the slope of the initial linear region of the stress-strain curve while toughness was calculated as the area under the stress-strain curve in units of MJ/m^3. The failure strain and consequently, toughness of PMMA and PEEK could not be captured for temperatures near their T_g (120°C and 140°C, respectively) due to the height limits of the thermal chamber that prevented the samples from stretching to strains past 500%.

However, since samples of both PMMA and PEEK were able to break at all other temperatures, it was assumed that the peak failure strain and toughness would occur at that temperature closest to their individual T_g.

For all polymers except MA-co-MMA-co-2%PEGDMA, the type IV specimen geometry was adopted with a 20mm gauge length and 2.8mm gauge width. Due to the characteristic ability of MA-co-MMA-co-2%PEGDMA to sustain large deformations, a specimen geometry (ASTM D 638 Type V) with a smaller gauge length was used for this material. During initial testing, a large amount of deformation was observed outside the Type IV designated gauge length (7.62mm) in the MA-co-MMA-co-2%PEGDMA specimens. To account for this large deformation, an effective gauge length at each temperature was determined by placing laser tape at the ends of the prescribed gauge section and using a laser extensometer to measure the displacement. Although these networks stretched outside the region distinguishable by the laser, the initial strains recorded from the laser and the grip-to-grip displacement measured from the crosshead were used to calculate the effective gauge length at each temperature. This average gauge length (25mm) was used to calculate the engineering strains sustained by the MA-co-MMA-co-2%PEGDMA samples.

Network toughness under aqueous conditions was assessed by performing the same tensile strain to failure tests in a heated phosphate buffered saline (PBS) bath. PBS was formulated by mixing one phosphate buffered saline tablet (Sigma Aldrich; #P4417) with 200 ml of distilled water until dissolved. Prior to soaking, the mass and sample dimensions (gauge length, width, and thickness) were measured. Each sample was

soaked for 24 hours in PBS, and remeasured. Swelling ratio was calculated according to the formula [139]:

$$q=W_w/W_i$$

Where W_w is the weight mass of the sample and W_i is the initial pre-swelling mass (n=4). Samples were immediately loaded on the MTS Insight 2 and allowed to equilibrate in a heated PBS bath for 10 minutes. Due to the limitations of the PBS freezing near 0°C and boiling near 100°C, tests were only performed at temperatures between 20°C to 80°C.

Given the large number of temperatures and materials, tests under each condition were repeated only once (n=2). In these instances, the stress strain curves after two tests visually demonstrated clear repeatability in behavior as indicated by the magnitudes of the elastic modulus, ultimate stresses, and failure strains as well as the repeated presence of other observable behaviors (i.e. yielding or strain hardening). For the MA-co-MMA-co-2%PEGDMA networks, this defined repeatability in stress strain behavior at certain temperatures was not observed after two tests, mostly due to large variability in failure strain, at certain temperatures (20°C and 30°C). As will be highlighted in the results and discussion, at these temperatures the network is entering its viscoelastic state where it is beginning to transition from glassy to rubbery. Thus within this region, it is expected for there to be large sample to sample variability in certain properties (i.e. failure strain). Therefore for MA-co-MMA-co-2%PEGDMA tested at 20°C and 30°C in air, a sample size of 4 was used to better identify the characteristic stress strain behavior under those testing conditions. All toughness and failure strain values for each testing condition were averaged and presented as means $\pm$ standard deviation in the results. Although one cannot reliably use this data to perform an extensive statistical analysis for comparing

values at one temperature to the next, the trends with increasing or decreasing temperature are very clear, as will be discussed below.

3.3 Results

3.3.1 Dynamic Mechanical Analysis

Representative plots of storage modulus as a function of temperature for each material is shown in Figures 3.2 and 3.3. The glass transition region was identified as the range of temperatures where the storage modulus drops several orders of magnitude. As shown in Figure 3.2 PEEK, PMMA, and PC have T_g's between 130^{o}C and 150^{o}C, but possess different behaviors past their glass transition region. A complete loss of modulus in PC following the glass transition indicates thermoplastic flow. The modulus of PMMA reaches a temporary plateau with a more gradual flow behavior while the modulus of PEEK significantly increases above T_g marking thermally-induced crystallization. By design, the photopolymerized acrylate systems exhibit a wide range of T_g's and rubbery moduli (Figure 3.3) ranging from -230^{o}C to 110^{o}C and 0.1MPa to 30MPa, respectively (Table 3.1). The transition behavior of the designed (meth)acrylate systems most closely resemble PMMA, with exception to the distinct rubbery plateau in the more heavily crosslinked (meth)acrylate networks.

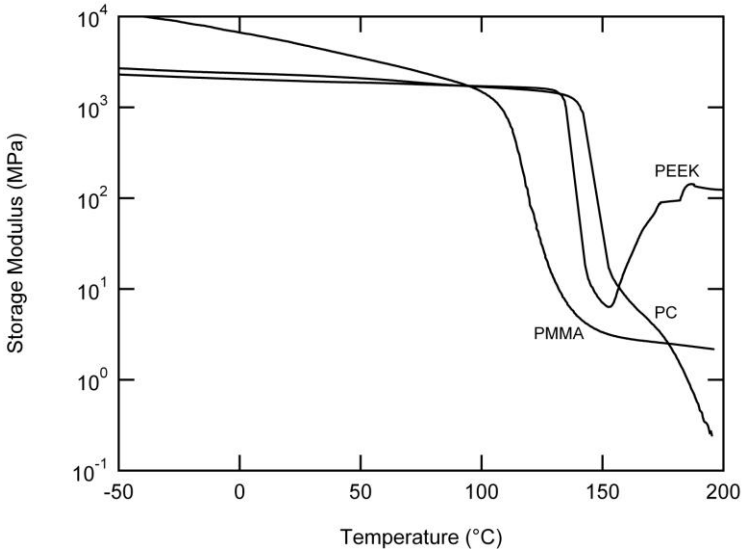

Figure 3.2. Representative DMA plots of the storage modulus versus temperature for some common thermoplastic polymers.

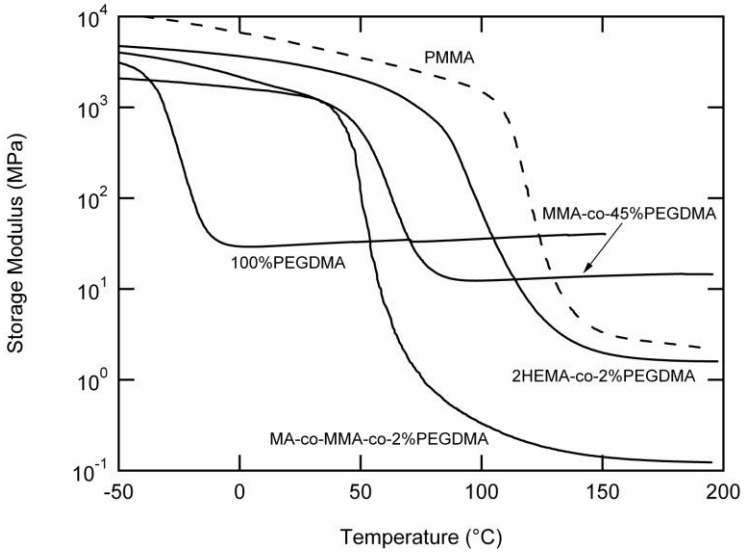

Figure 3.3 Representative DMA plots of the storage modulus versus temperature for several photopolymerized (meth)acrylate networks.

3.3.2 Stress-Strain Behavior

The influence of polymer chemistry and testing temperature on stress-strain behavior was examined by performing tensile strain-to-failure tests at different temperatures. Representative stress strain curves at select temperatures are displayed in

Figure 3.4. At temperatures below 80°C, PMMA (Figure 3.4) exhibits brittle behavior reaching high stresses around 55MPa and failing without any noticeable yielding. As the temperature increases towards the T_g, PMMA begins to yield and plasticize exhibiting more rubber-like behavior at and above the T_g. On the other hand, PEEK exhibits a ductile deformation response throughout the range of testing temperatures and maintains both high stresses (>60MPa) and high strains (>500%) as the testing temperature approaches and surpasses T_g. An increase in strength around 100% strain is observed in PEEK at testing temperatures below its T_g. PC is not included in Figure 2 for clarity, but its stress-strain behavior demonstrated a similar trend with temperature as PMMA.

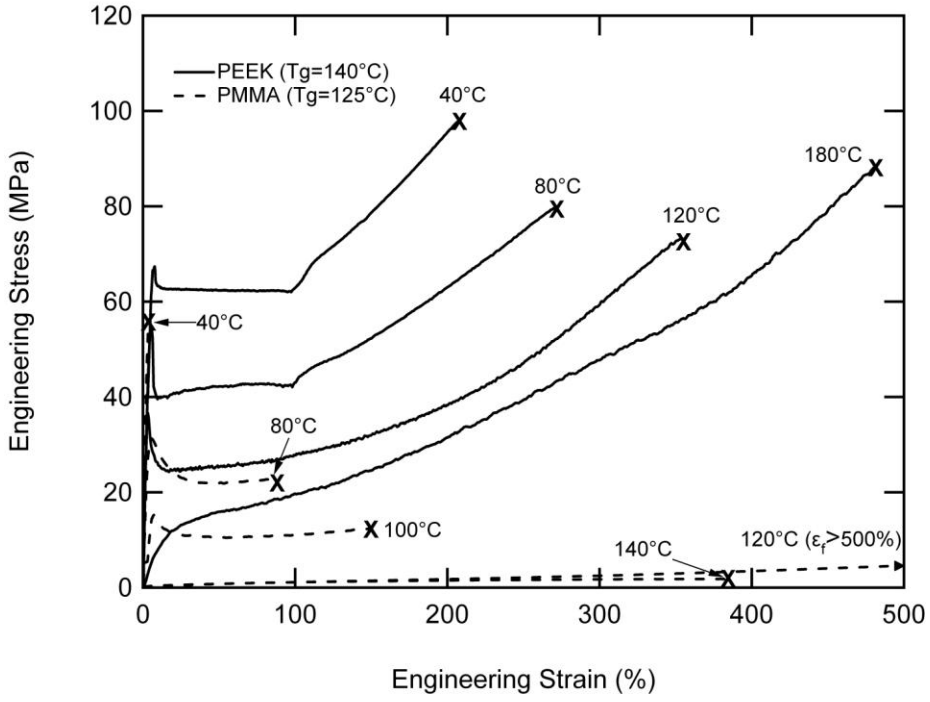

Figure 3.4. Representative tensile stress-strain behavior for PMMA and PEEK at select temperatures.

The (meth)acrylate networks, 2HEMA-co-2%PEGDMA, MA-co-MMA-co-2%PEGDMA, and MMA-co-45%PEGDMA, follow very similar trends with temperature as PMMA (Figures 3.5 and 3.6). A drop in modulus and increase in failure strain is

observed as the testing temperature approaches the material's T_g. Above T_g, the networks show a drop in failure strain and plateau in modulus (a slight increase is seen with increasing temperature as would be expected based on the theory of rubbery elasticity). The addition of a significant amount of crosslinker (PEGDMA) to MMA results in a decrease in extensibility of the system but an increase in modulus and strain hardening (Figure 3.5 versus 3.4, PMMA). The (meth)acrylates with lower crosslinker concentration, MA-co-MMA-co-2%PEGDMA (Figure 3.5) and 2HEMA-co-2%PEGDMA (Figure 3.6) reach higher failure strains with little strain hardening. When comparing the stress strain behavior amongst the networks and thermoplastics near body temperature (40 ^{o}C), the elastic modulus falls within the same range for all the polymers, but the failure strain and yield behavior vary considerably from material to material.

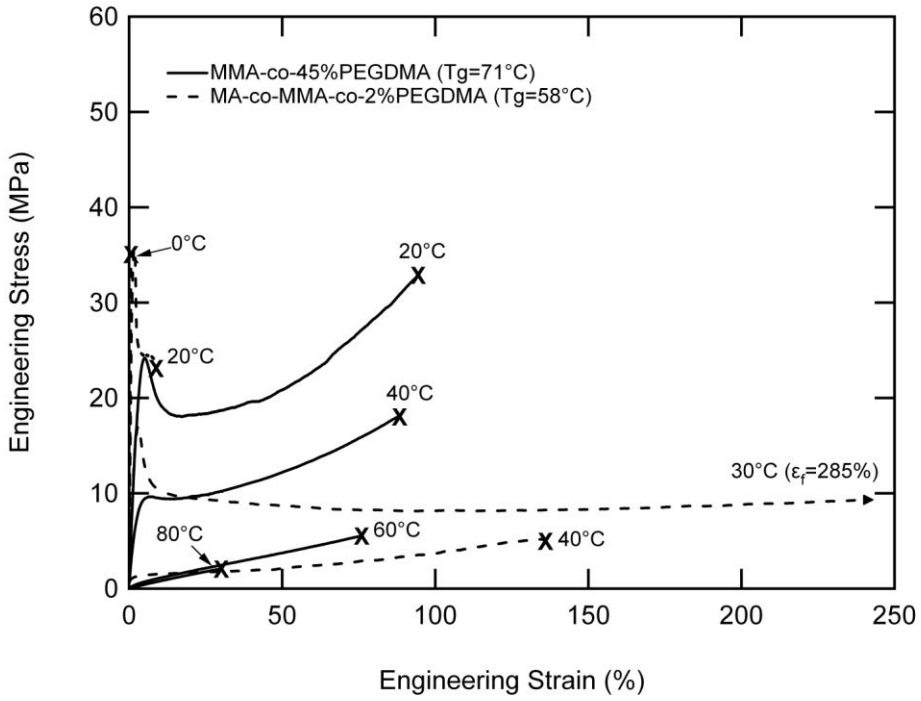

Figure 3.5. Representative tensile stress-strain behavior for MMA-co-PEGDMA and MMA-co-MA-co-PEGDMA.at select temperatures.

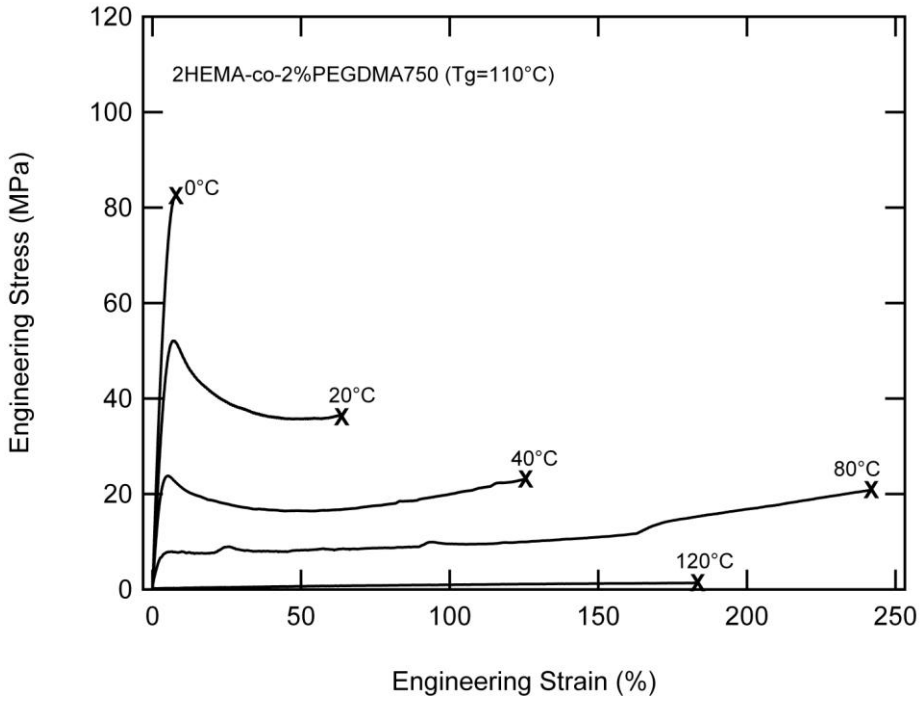

Figure 3.6. Representative tensile stress-strain behavior for 2HEMA-co-PEGDMA at select temperatures.

3.3.3 Toughness in Relation to Temperature

Using the stress-strain curves in Figure 3.4-6, failure strains and toughness as a function of temperature were averaged for each material and superimposed with representative temperature-dependent tan delta curves obtained from DMA in order to identify any significant correlations with the thermal transition behavior. The tan delta curve reaches a maximum at a material's T_g and is an indicator of increased dampening and energy loss, key components of suppressing material damage and enhancing material toughness. Both PMMA (Figure 3.7) and PEEK (Figure 3.8) experience maximum failure strains near their T_g. PMMA peaks in toughness slightly below its T_g and maintains relatively low toughness at all other testing temperatures above and below T_g. This peak in toughness is significant, as the peak value is typically an order of magnitude higher

than toughness values at other temperatures for all of the networks considered. Conversely, in PEEK, the failure strain continues to increase as temperature increases while toughness remains relatively constant, and is nearly an order of magnitude higher or more than PMMA at all temperatures.

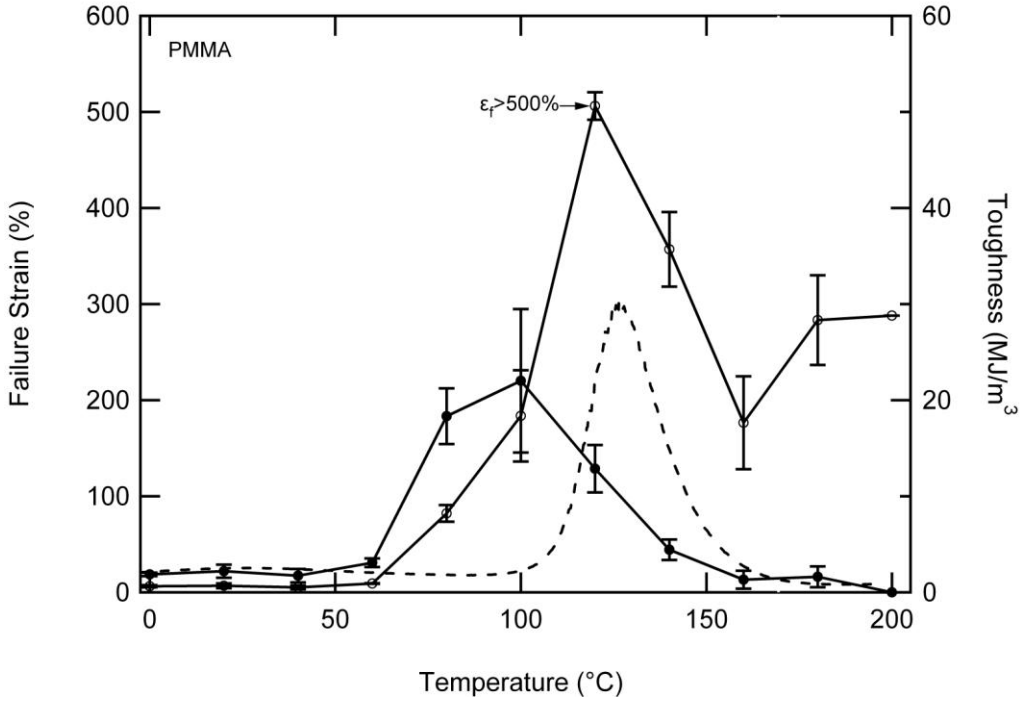

Figure 3.7. The effect of temperature on the failure strain (open circles) and toughness (closed circles) of PMMA. Dotted line denotes the tan delta curve obtained from DMA.

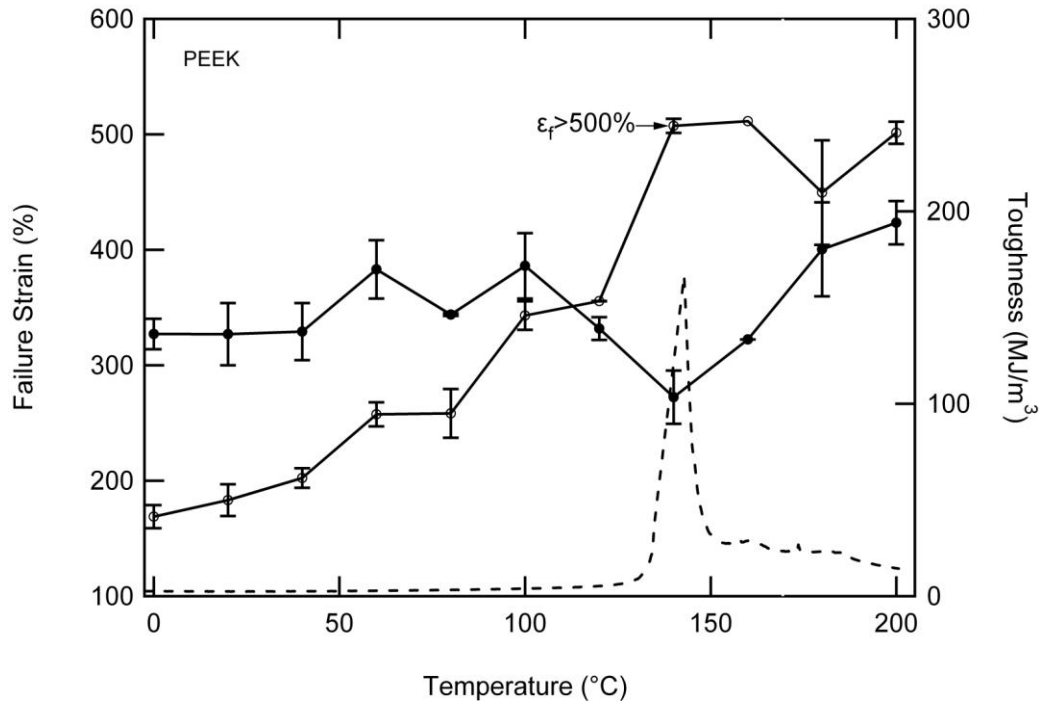

Figure 3.8. The effect of temperature on the failure strain (open circles) and toughness (closed circles) of PEEK. Dotted line denotes the tan delta curve obtained from DMA.

For the crosslinked (meth)acrylate networks, peaks in both toughness and failure strain also occur below their T_g. However, the distance between the toughness and tan delta peaks as well as the breadth of each peak differs significantly between each system. Prior to further examining the results, it is important to note that the location of both the toughness and tan delta peak will vary with applied strain rate, a variable held constant here. The width of both the tan delta and toughness peaks of MMA-co-45%PEGDMA are very broad (50°C and at least 40°C temperature spans, respectively) with about 70°C separation between the peak of the tan delta and maximal toughness peak (Figure 3.9). In addition, another smaller tan delta peak occurs at 10°C above the toughness peak. Thus, both the tan delta peak around T_g and this smaller peak could contribute to the enhanced toughness of MMA-co-45%PEGDMA at lower temperatures. From Figure 3.11,

2HEMA-co-2%PEGDMA shows a similar trend as MMA-co-45%PEGDMA with broad tan delta and toughness peaks (60°C temperature spans each) with the two peaks occurring 60°C apart. Conversely, for MA-co-MMA-co-2%PEGDMA, the tan delta and toughness peaks cover a much narrower temperature range compared to the other networks (20°C and 10°C) and occur 30°C apart from each other (Figure 3.10).

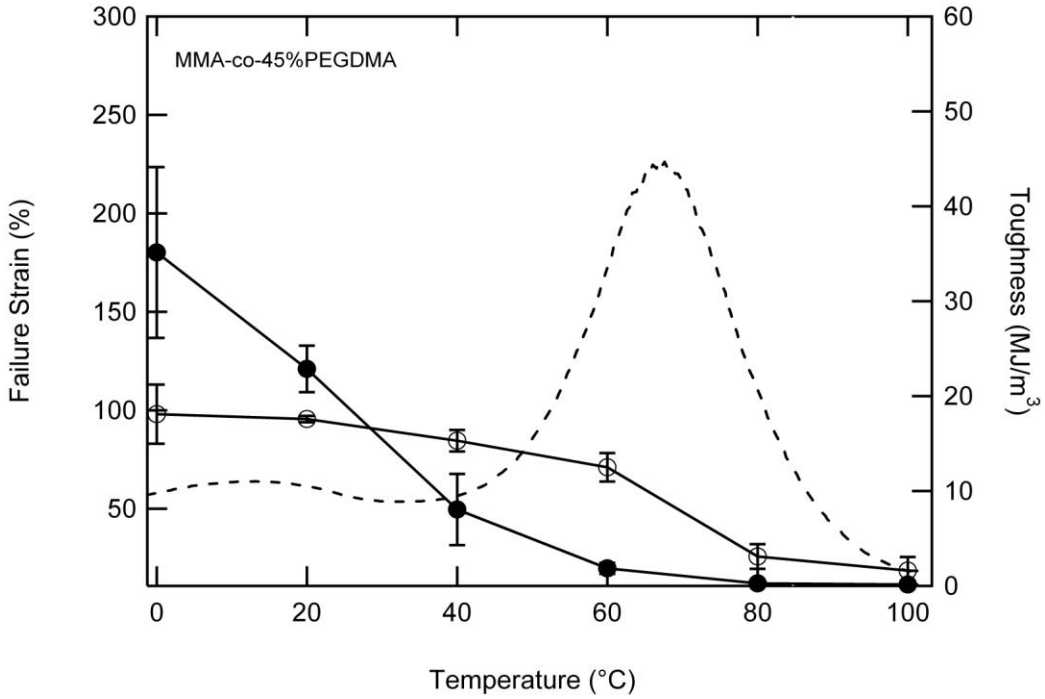

Figure 3.9. The effect of temperature on the failure strain (open circles) and toughness (closed circles) of MMA-co-45%PEGDMA. Dotted line denotes the tan delta curve obtained from DMA.

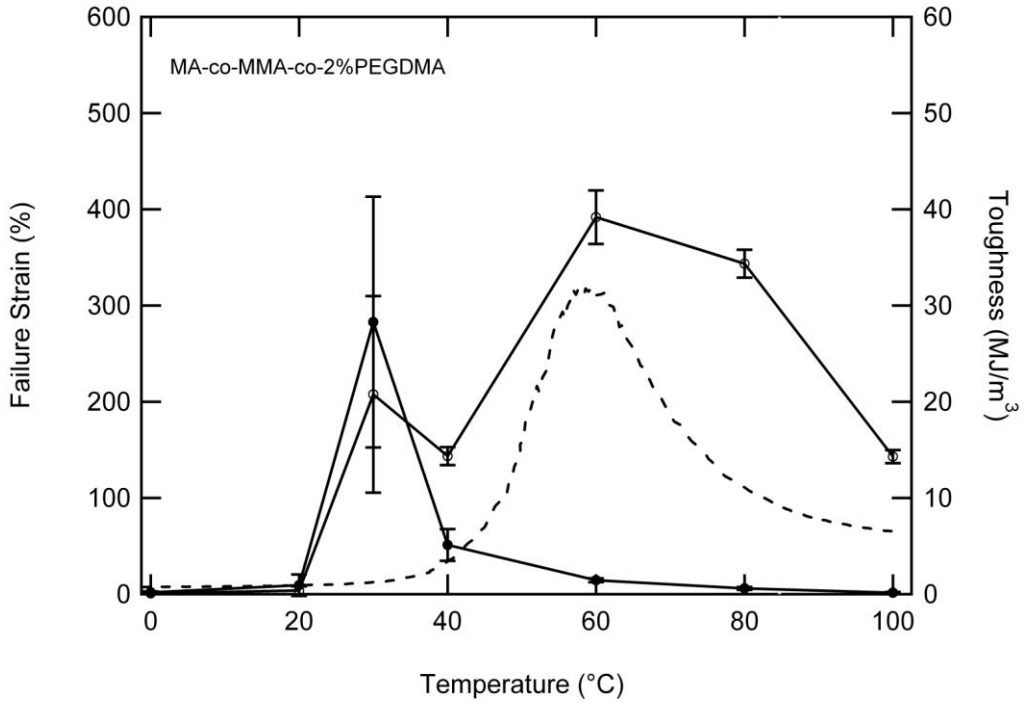

Figure 3.10 The effect of temperature on the failure strain (open circles) and toughness (closed circles) of MA-co-MMA-co-2%PEGDMA. Dotted line denotes the tan delta curve obtained from DMA.

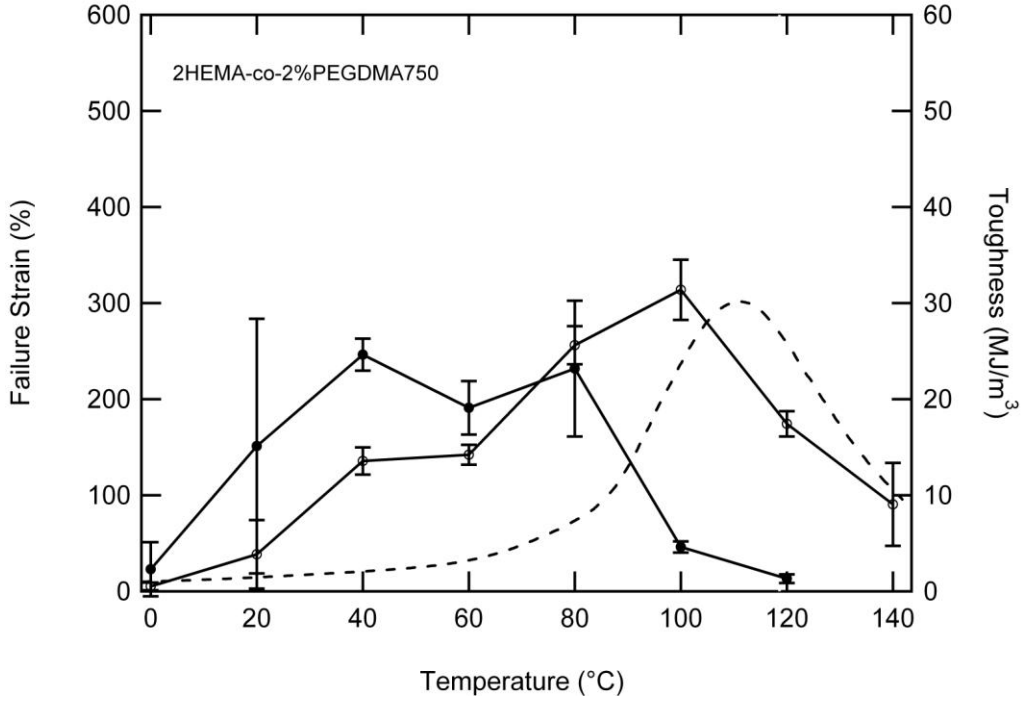

Figure 3.11. The effect of temperature on the failure strain (open circles) and toughness (closed circles) of 2HEMA-co-2%PEGDMA. Dotted line denotes the tan delta curve obtained from DMA.

3.3.4 Effect of PBS on Toughness

Figures 3.12 and 3.13 highlight the change in stress-strain behavior in the presence of PBS for the (meth)acrylate networks. The stress strain curves shown represent one test of two performed at each testing condition. For MMA-co-45%PEGDMA and 2HEMA-co-2%PEGDMA, the stress-strain behavior in PBS below T_g matches the behavior of the same system tested at temperatures above the T_g in air. Thus at 40 °C in PBS, the (meth)acrylate systems are effectively above their glass transition and are acting in their rubbery state in terms of failure strain and toughness. When tested at 20°C, MA-co-MMA-co-2%PEGDMA experiences a large increase in failure strains with soaking which is also consistent with the network deformed in the dry state at slightly elevated temperatures (Figure 3.13). In addition, failure strains still remain greater than 200% at temperatures above 40°C while at lower temperatures (around 20°C), yielding behavior still occurs. It is important to highlight that depending on the system and testing temperature the toughness can appear to increase (MA-co-MMA-co-2%PEGDMA, T = 20 °C) or decrease (2HEMA-co-2%PEGDMA, T = 40 °C) with exposure to PBS. This difference is related to the relative position of the testing temperature on the toughness peak in temperature space, and will be further explored in the discussion.

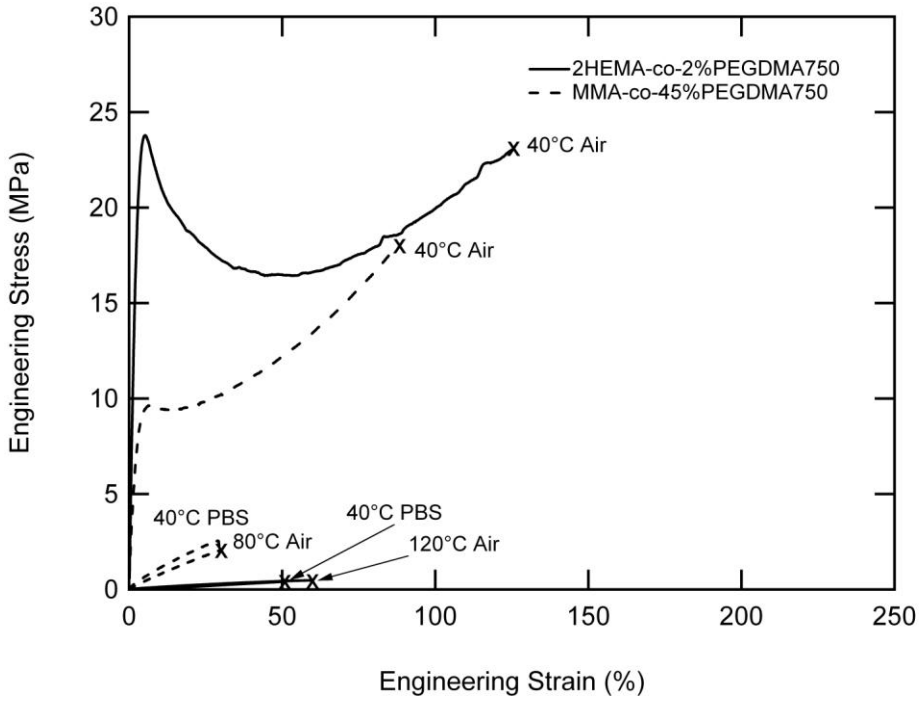

Figure 3.12. Representative stress-strain curves for 2HEMA-co-2%PEGDMA and MMA-co-45%PEGDMA.

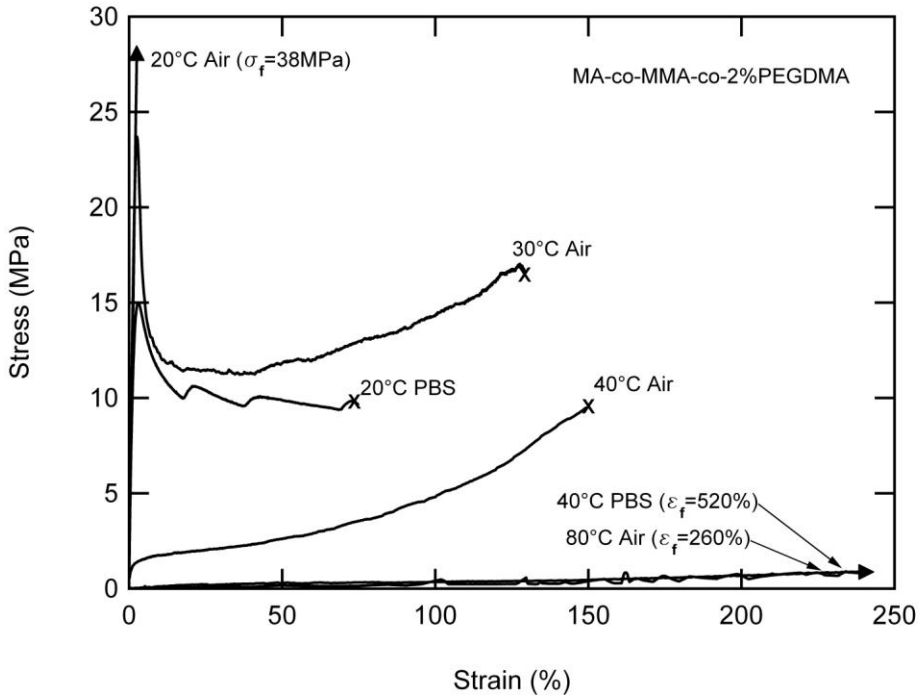

Figure 3.13. Representative stress-strain curves for MA-co-MMA-co-2%PEGDMA.

3.3.5 Toughness versus Elastic Modulus

When designing synthetic biomaterials that must function under rigorous loading environments, two key properties to consider are the elastic modulus and toughness of the material. In Figure 3.14, average toughness values are plotted against average elastic modulus values for all (meth)acrylate networks tested in air and PBS at 40°C and compared with several common biomedical grade polymers studied in the literature[140-142]. For the sake of clarity in the figure, error bars have been removed and thus the indicated points can be considered a range of toughness and modulus values indicative of that composition. Looking at this plot, several important trends can be identified. First, both (meth)acrylate networks and linear polymers with similar moduli at 40°C show a broad range of toughness values ranging three orders of magnitude from over 100 MJ/m^3 to approximately 0.1 MJ/m^3. Secondly, the photopolymerized (meth)acrylate networks possess less toughness than other polymers such as PC, PEEK, UHMWPE, and segmented polyurethane (SPU). Finally, PBS decreases the modulus and toughness of the networks significantly with exception to MA-co-MMA-co-2%PEGDMA. The decrease in modulus and toughness of the 2HEMA-co-2%PEGDMA polymer is extreme, dropping three orders of magnitude in both quantities while MMA-co-45%PEGDMA only decreases about one order of magnitude for both properties.

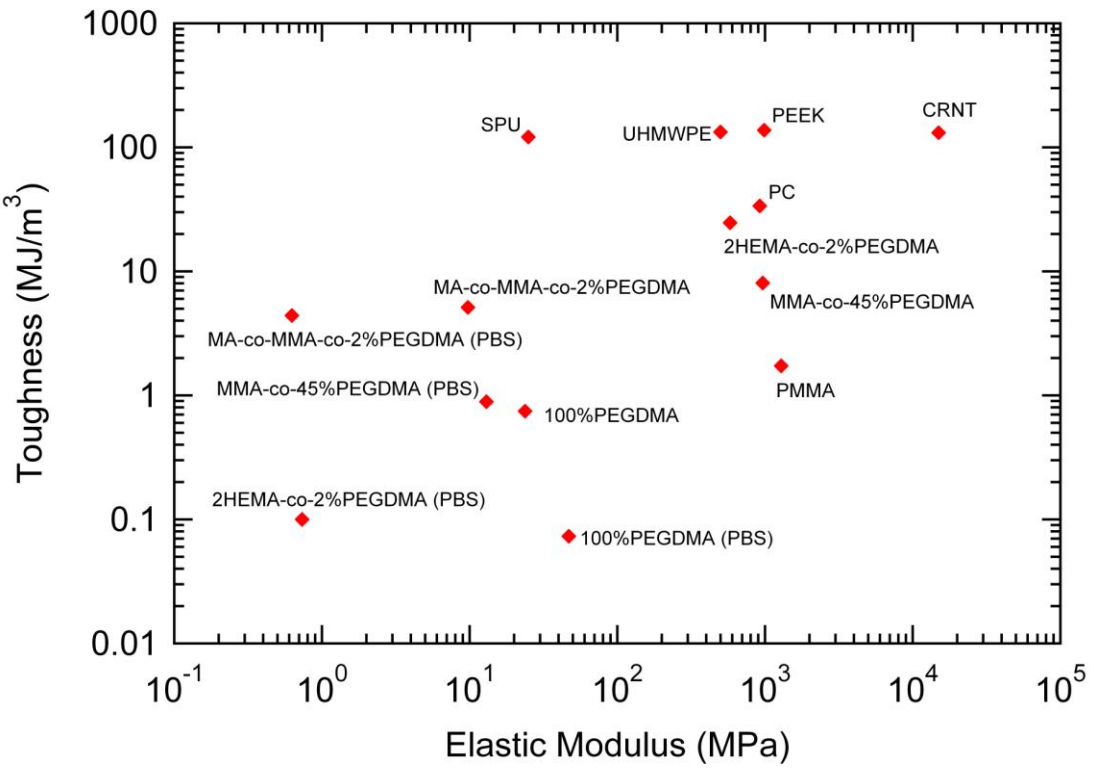

Figure 3.14. Average toughness plotted as a function of elastic modulus for acrylate networks and the thermoplastic polymers tested in this study at 40°C at a strain rate of 5%/min as well as some other common biomedical polymers. Toughness values of CRNT, UHMWPE, and SPU were calculated as the area under the stress-strain curves found in the literature [140-142]. The elastic modulus values were provided in the literature. CRNT=carbon reinforced nanotubes, UHMWPE= ultra-high molecular weight polyethylene, SPU=segmented polyurethane.

3.4 Discussion

Inherent toughness of a material dictates the ultimate stress and strain the material can withstand and is an important mechanical consideration when designing biomaterials for long-term implantation. For example, a tough contact lens would prevent frequent tearing and ripping from daily insertion and removal. A tough cardiovascular stent would enable implantation in remote locations in the leg where large bending forces are exerted on the blood vessel wall. Additionally, a tough replacement disk for spinal applications

would improve the longevity of the device and allow it to sustain the rigorous loading regime imparted on the spine. The purpose of this study was to characterize toughness in photopolymerized (meth)acrylate networks by performing uniaxial tension experiments under various environmental conditions. Although many factors are known to influence the mechanical properties of polymer systems, especially thermoplastics, this is the first comprehensive study on the toughness of photopolymerized (meth)acrylate networks. In the remainder of this discussion, various toughening mechanisms in photopolymerized (meth)acrylate networks, elucidated by the presented results, will be explored focusing on their relevance towards designing potential biomaterial platforms.

The temperature dependence of network toughness is strongly dependent on the T_g as revealed in earlier work on thermoplastics[143] and rubber networks [132-134]. Similar to previous studies involving linear polymers [133, 137, 143-144], the (meth)acrylate networks demonstrate a transition from brittle to ductile to rubbery behavior as temperature is increased, correlating to peaks in both toughness and failure strain at temperatures slightly below the T_g. This temperature-dependent toughness maximum can be attributed to the viscoelastic nature of the chains that occurs at the onset of the glass transition [132-134]. Within this temperature region, molecular vibrations are beginning to increase allowing the chains to cooperatively disentangle and stretch without substantial loss in load carrying capacity [143]. Thus, one way to enhance toughness within a particular (meth)acrylate network could involve tailoring the T_g of the system to create a toughness peak at a particular temperature (i.e. body temperature). The drawback with this monolithic (single material) approach is that the elastic modulus of the material is fixed in the viscoelastic regime and will be extremely rate dependent.

Another method to enhance network toughness involves altering the crosslinking density. In this study, slightly higher toughness values are observed in the lightly crosslinked networks (MMA-co-MA-co-2%PEGDMA) compared to the highly crosslinked network (MMA-co-45%PEGDMA) (Figure 3e vs. 3c and Figure 5). In general, toughness remains constant in a network despite changing crosslinker concentrations [145], with exception of lightly crosslinked networks [137], which can show enhanced toughness. Unfortunately, there are several inherent trade-offs with adjusting the crosslinking density [121, 146] or molecular weight [147] to control network toughness. A high crosslink density inhibits global chain movement during deformation, thus increasing strength (higher yield strength), limiting strains (lower strain to failure), and increasing stresses at equivalent deformation levels (higher rubbery modulus) [137, 143]. Another drawback of maximizing toughness through network crosslinking density is that other important material features such as swelling capacity and rubbery modulus also depend strongly on crosslinking density.

Aside from toughening with temperature-dependent viscous effects and network crosslinking, enhancement of toughness through monomer chemistry is another possibility. The influence of the network chemistry can be observed by comparing the toughness of uncrosslinked polymers such as PMMA, PC, and PEEK (Figure 3 & 5) which all have similar T_g's, but contain unique chemical features. From Figures 2 and 3, the vast difference in the stress-strain behaviors of these polymers at similar testing temperatures indicates that polymer chemistry can greatly impact the toughness of polymers. The high levels of toughness of PEEK and PC can be explained by the phenyl ring-oxygen bonds located in the backbone of the polymer chains. Phenyl rings consist

of tight chemical bonds that provide rigidity and strength to a chain while their intermittent bonding with oxygen atoms along the backbone allow them to flip rapidly and rotate around the backbone, thus adding flexibility during deformation [135]. The significantly larger toughness values of PEEK compared to PC suggest there is another toughening mechanism driven by polymer structure. In the case of PEEK, this mechanism is the semicrystalline nature of the polymer induced by strain hardening increasing the energy required to break [77, 143]. Thus, provided the chemistries are biocompatible, the incorporation of unique chemical structures, such as phenyl rings, into the backbone to provide enhanced toughness in photopolymerizable (meth)acrylates is an important avenue for future research.

When comparing toughness in thermoplastics to the (meth)acrylate networks at 40^{o}C, 2HEMA-co-2%PEGDMA and MA-co-MMA-co-2%PEGDMA (under dry conditions) exhibit toughness levels in the same range as some common tough polymers such as PC (Figure 5) near body temperature. The chemical structures of the individual monomers, would suggest these backbones would have limited toughness based on the theory of Wu [58], but the macromolecular structure of the crosslinked network and the interactions between side groups imparts toughness beyond predictions based on chain backbone flexibility. For example, hydrogen bonding between hydroxyl side groups can be a contributing factor to the toughness of the 2HEMA-based network. Similarly, the toughness of MA-co-MMA-co-2%PEGDMA can be attributed to hydrophobic bonding between methyl groups in adjacent chains. Therefore, network chemistry can not only influences the toughness of individual polymer chains, but can also enhance the macromolecular toughness through the formation of intermolecular bonds. Using this

knowledge in combination with the observed dependence on temperature and crosslinking density, a polymer network can potentially be designed that has the appropriate modulus and deformability AND possess enhanced toughness.

An overarching concern in developing new polymer biomaterials, especially hydrogels and shape memory polymers with T_g's close to body temperature, is the toughness in the presence of water or saline. A material that cannot maintain toughness in solution may be unable to function properly in the body potentially leading to device failure or injury to the surrounding tissue. The results of this study demonstrate that the toughness mechanisms discussed thus far in (meth)acrylate networks are significantly altered when the polymer is soaked in solution. The drop in elastic modulus observed in this study corresponds to findings of previous studies and is attributed to water "plasticizing" the polymer resulting in a decrease in Tg [54, 148]. Comparing the stress-strain behavior in air and PBS, no obvious trend in toughness is observed amongst the networks. Both 2HEMA-co-2%PEGDMA and MMA-co-45%PEGDMA have decreased toughness in PBS at all temperatures while the toughness of MA-co-MMA-co-2%PEGDMA actually improves at 20 ^{o}C in PBS compared with air conditions (Figure 5b).

This apparent anomaly of both decreasing and increasing toughness with water uptake is explained if one considers a shift in the toughness-temperature peak with hydration. The interrelationship between toughness, temperature, and capacity to absorb water is illustrated in Figure 3.15. Water absorption changes the effective location of the toughness peak by lowering the T_g. Depending on where the testing temperature intersects the original toughness peak and how far the peak shifts by the amount of water,

toughness could increase or decrease under aqueous conditions. Specifically, if the test temperature is to the left of the toughness peak in air, moderate water uptake may increase toughness ("a" in Figure 3.15). An example of this would be the MA-co-MMA-co-2%PEGDMA system where 20 °C is to the left of the air toughness peak (Figure 3.10), and water exposure increases toughness at 20 °C due to a moderate shift of the toughness peak toward a lower temperature (Figure 3.13). On the other hand, if the testing temperature is located at the toughness peak or to the right of the peak in air, water exposure can decrease toughness ("b" in Figure 3.15). An example of this would be the 2HEMA-co-2%PEGDMA network which sits at the middle of its toughness "peak" in air at 40°C (Figure 3.11), however, a large leftward shift of this peak with water uptake leaves the material with low toughness at 40°C (Figure 3.12). Based on this paradigm, one way to control a polymer's toughness under aqueous conditions is to tailor the monomer components so that the Tg and consequently, the maximal toughness of the polymer system will occur around body temperature in the presence of water. This approach would require knowledge on the shift in toughness with temperature (strain rate) and water absorption (time) to assure the toughness peak in water was at equilibrium.

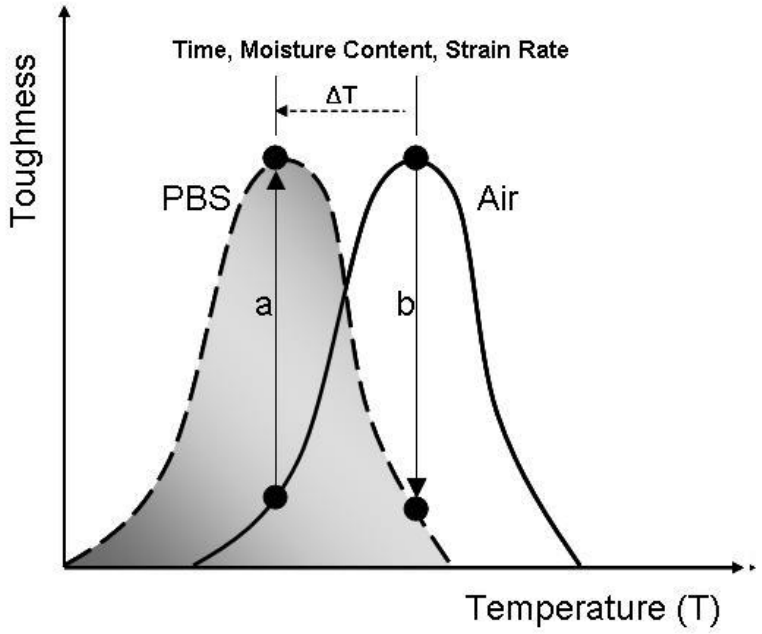

Figure 3.15. Schematic illustrating how the temperature-dependent toughness maxima shifts to lower temperatures in PBS. The temperature difference between the toughness peak in air and PBS (ΔT) is governed by several factors including soak time, strain rate, and swellability of the network. As discussed, "a" and "b" represent two scenarios explaining how the toughness of acrylate networks can either increase or decrease in PBS.

As mentioned above, the degree of the toughness shift in PBS is partially dictated by the hydrophilicity of the network components. When comparing the toughness loss in PBS, 2HEMA-co-2%PEGDMA exhibits a larger change in toughness compared to MMA-co-45%PEGDMA and MA-co-MMA-co-2%PEGDMA. Due to the hydroxyl groups located in the pendant group, the 2HEMA network will contain large water-chain interactions that drive increased water absorption as indicated by the higher swelling ratio (q=1.58). It is interesting to note that if the high toughness of the 2HEMA system was partially driven by chain interactions due to hydrogen bonding, the PBS effectively eliminates this toughening mechanism by forming new bonds with the hydroxyl side groups. Although MMA-co-45%PEGDMA and MA-co-MMA-co-2%PEGDMA have low swelling ratios, their change in mechanical properties in PBS indicates that the PBS

still alters the network structure, mostly by interacting with the glycol groups in the PEGDMA crosslinker. Even in the absence of PEGDMA, pure PMMA [149-150], thiolene acrylates [148], and polyurethane acrylates [54, 148, 151] have previously exhibited this water effect over much longer time scales. Based off of these observations between toughness and swelling, it can be suggested that the more water the network can absorb, the more water molecules are present to interact with the polymer chains, and the larger the shift the toughness peak will shift with exposure to water. However, further work is needed to understand if the magnitude of the toughness-temperature peak changes or if it only experiences a shift to lower temperatures. Thus, this hypothesis will be explored extensively in the next chapter.

3.5 Conclusions

The results presented in this study provide several key mechanisms of the toughness-structure relationships exhibited within photopolymerizable (meth)acrylate networks. Specifically, the study demonstrates that toughness in photopolymerizable networks is controlled by:

(1) *Test temperature relative to T_g.* All of the networks demonstrate a peak in toughness at a temperature below the glass transition temperature. The location and breadth of the toughness peak depends strongly on the nature of the glass transition in the network (i.e. breadth, number of peaks).

(2) *Network structure, in particular crosslinking density*. At "equivalent" test temperatures relative to Tg, networks with different crosslink densities demonstrate varying toughness, with low crosslink concentration offering better

toughness relative to highly crosslinked systems, even though less crosslinking results in lower rubbery moduli values.

(3) *Network Chemistry*. For equivalent Tg and crosslink density, the presence of certain chemical groups is shown to impact toughness.

(4) *Water content*. Since water lowers the glass transition temperature of polymers, apparent toughness is significantly altered in water driven by changes in the test temperature relative to the glass transition temperature discussed in item (1).

Optimizing toughness in (meth)acrylate networks can only be achieved by considering these relationships between mechanical properties, chemical structure, and environmental conditions. By selecting "toughening" chemical components and using the appropriate amount of crosslinker, the ability to tune the toughness of these systems under physiological conditions will render them useful in the design of implant materials or for load-bearing applications such as spinal disc repair.

CHAPTER 4

EFFECT OF GLASS TRANSITION TEMPERATURE ON TOUGHNESS OF (METH)ACRYLATE NETWORKS UNDER PHYSIOLOGICAL CONDITIONS

4.1 Introduction

A key characteristic of a viable orthopedic biomaterial is its ability to withstand harsh mechanical environments, such as those found in the knee, hip, and spinal regions by exhibiting appropriate mechanical behavior. First, the mechanical properties of the material (specifically, its modulus) must mimic the mechanical behavior of native orthopedic tissue (i.e. tendon, cartilage, or ligament) in order to avoid a mechanical mismatch between the synthetic material and biological tissue resulting in device failure and injury to adjacent tissue [152]. Second, the material must have excellent toughness to be able to sustain large repeated loading regimes. By enhancing toughness of polymer networks, wear and fatigue failures can be minimized [153], and the mechanical properties can be better aligned with naturally tough orthopedic soft tissues. Even synthetic degradable polymers, that are intended to dissolve in the body, can benefit from enhanced toughness since premature fracture, wear, or fatigue can greatly affect degradation rate and device performance prior to complete dissolution.

*Modified from
Smith KE, Parks SS, Hyjek ME, Downey SE, and Gall K. The effect of the glass transition temperature on the toughness of photopolymerizable (meth)acrylate networks under physiological conditions. *Polymer*, 2009; 50(9): 5112-5123.

Designing tough, chemically crosslinked polymer networks first requires understanding what chemical characteristics influence the mechanical properties as well as how these structure-property relationships change under physiological conditions. In the previous chapter, the mechanical properties were found to be highly dependent on temperature and the presence of PBS in a manner dependent upon the location of Tg with the testing temperature. Specifically, the elastic modulus will decrease and failure strains will increase as the testing temperature approaches T_g [5]. Above T_g, the elastic modulus will plateau or increase slightly and failure strains will decrease [5, 6]. Based off of this trend from a brittle to ductile to rubbery state, maximal toughness typically occurs at a testing temperature slightly below or at the polymer's T_g where the chains are becoming more mobile allowing the network to sustain larger strains without losing much strength [7]. Because of this relationship between toughness and temperature, the mechanical properties at body temperature rather than room temperature must be considered for implantation into the body.

Results discussed in the previous chapter elucidated the importance of considering how saline solution or water influences the mechanical properties of polymer networks [8, 9]. Several studies have identified the role of water in altering the mechanical properties of polymer networks [10-12]. Similar to increasing temperature, immersing a polymer in water leads to a decrease in elastic modulus and an increase in failure strains [13]. This change in stress strain behavior from a brittle to more ductile or rubbery state suggests that T_g is decreasing in solution [12, 14, 15]. Based off of these observations, it has been suggested that water content can also determine the extent to which toughness is

altered in solution and thus, can be one mechanism to which toughness can be enhanced under physiological conditions.

The effect of water on the network T_g is governed by the total water content within the network as well as the state of the sorbed water molecules [12, 14, 16]. In general, the T_g of a polymer network will continuously decrease as water absorption into the network increases, an effect driven by the water-polymer interactions created within the network [10, 12, 14]. In simplistic terms, water molecules can be found in one of two states within the network, each of which plays its own role in the glass transition behavior of polymers. For water molecules that form hydrogen bonds with polymer chains, the term, "bound water", is used while those water molecules that remain distant from the chains and maintain their mobility to form their own hydrogen-bonded clusters are called "free water" [10, 14, 17, 18]. The total water content and proportions of free versus bound water in the networks are dictated by the presence of polar groups or steric barriers and the crosslinking density. These factors must all be considered when understanding the relationship between network chemistry and T_g under aqueous conditions.

Because the mechanical properties of polymers are temperature-dependent and altered under aqueous conditions, it has been suggested that the toughness of polymer networks will be dependent on this relationship between T_g and water content. In this study, the effect of water content and T_g on toughness is examined in photopolymerizable (meth)acrylate networks. Photopolymerizable networks offer additional advantages as polymeric biomaterials due to their ability to be formed *in situ*, and into complex geometries, rendering them useful for minimally invasive procedures [21, 22]. In particular, (meth)acrylate-based networks formed through photopolymerization possess

material properties that can be easily tuned by control of chemistry and crosslinking density. The broad range of thermomechanical properties in these networks enables the development of various material platforms ranging from hydrogels [21, 23] to biodegradable networks [23] to shape memory polymers [3, 24]. However, the toughness of photopolymerized (meth)acrylate networks is limited for long term use in high loading environments, especially under aqueous conditions.

Therefore, the objective of this study is to understand the role of the glass transition behavior and water content on network toughness under physiological conditions. The approach involves performing stress-strain measurements in parallel with differential scanning calorimetry (DSC) and thermogravimetric analysis (TGA) on two model ternary (meth)acrylate networks, MMA-co-MA-co-PEGDMA and 2HEMA-co-BMA-co-PEGDMA. Different compositions of each network are formulated by varying the weight ratios of the two linear monomers (MMA:MA or BMA:2HEMA). The first aim is to identify how the T_g of each network changes as the composition changes in both air and PBS. Secondly, the swelling behavior as a function of composition is evaluated and related to the T_g of each network immersed in PBS. Finally, toughness is determined in air and PBS at 37°C to identify relationships between chemistry and toughness. From this study, two materials with enhanced toughness are identified and it is shown that network toughening is achieved through different mechanisms in each network.

4.2 Materials and Methods

4.2.1 Materials

Methyl methacrylate (MMA), methyl acrylate (MA), benzyl methacrylate (BMA) and 2-hydroxyethyl methacrylate (2HEMA) monomers, and poly(ethylene glycol) dimethacrylate (PEGDMA) crosslinker with a molecular weight of M_n~750 were obtained from Sigma-Aldrich and used as received. 2,2 dimethoxy 2-phenylacetophenone (DMPA) was used as the photoinitiator and was purchased from Sigma-Aldrich as well. The chemical structures of monomers used are presented in Figure 4.1.

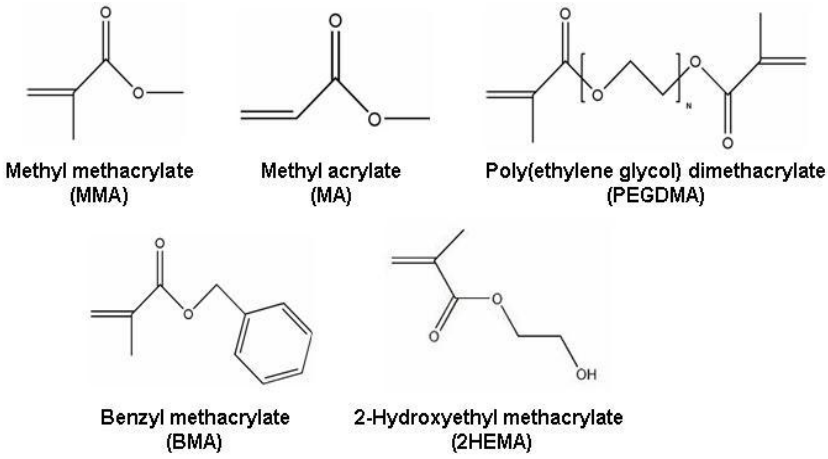

Figure 4.1 Chemical structures of monomers incorporated into networks.

4.2.2 Synthesis

Monomer solutions were formulated by combining two monofunctional acrylates or (meth)acrylates (MA and MMA or BMA and 2HEMA) and a difunctional (meth)acrylate (PEGDMA). MA-co-MMA-co-PEGDMA solutions were prepared by combining ratios of MA and MMA determined by weight percentage with 10% PEGDMA and 1% DMPA. The weight percentages of MA and MMA used for each

composition are listed in Table 4.1. 2HEMA-co-BMA-co-PEGDMA solutions were prepared by combining different ratios of BMA and 2HEMA determined by weight percentage with 2% PEGDMA and 0.5% DMPA. The weight percentages of BMA and 2HEMA used for each composition are listed in Table 4.2.

Each solution was mixed manually in a glass vial and injected between two glass slides using a glass pipette. Slides were separated with two 1mm glass spacers. To prevent leakage of the MA-co-MMA-co-PEGDMA solution, all four sides of the slides were taped. Slides were coated with Rain-X to enhance release. Due to the strong adhesiveness of 2HEMA, slides used for the 2HEMA-co-BMA-co-PEGDMA solutions were coated with poly(dimethylsiloxane) (PDMS; Dow Corning Sylgard 184), instead of Rain-X, to prevent adhesion and to enhance release. The samples were placed in a UV chamber (Model CL-1000L Ultraviolet Crosslinker; λ=365nm; energy=2000x100$\mu J/cm^2$) for the minimal amount of time needed to fully polymerize (approximately 30 minutes and 10 minutes for MA-co-MMA-co-PEGDMA and 2HEMA-co-BMA-co-PEGDMA, respectively).

Table 4.1. Formulated compositions of MA-co-MMA-co-PEGDMA consisting of 10wt.% PEGDMA (Mn~750) and MA and MMA with weight ratios listed (by weight) of MA:MMA. The T_g in air and PBS measured through DSC are listed as well as the swelling ratio (q) determined after immersion in PBS for 1 week.

Name	Wt.% MA:MMA	T_g (°C)		q
		Air	PBS	
18%MA-co-MMA-co-PEGDMA	20:80	49.5 ± 0.5	48.9 ± 3.1	1.01 ± 0.010
27%MA-co-MMA-co-PEGDMA	30:70	46.3 ± 2.3	41.0 ± 0.8	1.03 ± 0.002
29%MA-co-MMA-co-PEGDMA	32:58	46.7 ± 2.8	41.4 ± 1.2	1.02 ± 0.005
31%MA-co-MMA-co-PEGDMA	34:56	45.6 ± 8.5	39.0 ± 0.2	1.03 ± 0.003
34%MA-co-MMA-co-PEGDMA	38:52	43.8 ± 2.2	34.3 ± 3.3	1.03 ± 0.008
36%MA-co-MMA-co-PEGDMA	40:60	43.8 ± 1.6	34.2 ± 3.1	1.03 ± 0.008
40%MA-co-MMA-co-PEGDMA	45:55	35.4 ± 3.0	18.5 ± 4.7	1.04 ± 0.010
54%MA-co-MMA-co-PEGDMA	60:40	28.1 ± 0.9	13.1 ± 2.4	1.03 ± 0.003
63%MA-co-MMA-co-PEGDMA	70:30	20.4 ± 0.7	9.3 ± 0.4	1.03 ± 0.004
72%MA-co-MMA-co-PEGDMA	80:20	21.5 ± 4.3	5.3 ± 2.8	1.04 ± 0.004

Table 4.2. Formulated compositions of BMA-co-2HEMA-co-PEGDMA consisting of 2wt.% PEGDMA (Mn~750) and BMA and 2HEMA with weight ratios listed (by weight) of BMA:2HEMA. The T_g in air and PBS measured through DSC are listed as well as the swelling ratio (q) determined after immersion in PBS for 1 week.

Name	Wt.% 2HEMA:BMA	T_g (°C)		q
		Air	PBS	
98%BMA-co-PEGDMA	0:100	56.7 ± 1.6	52.8 ± 1.1	1.00 ± 0.001
19%2HEMA -co-BMA-co-PEGDMA	20:80	57.5 ± 1.3	50.4 ± 2.2	1.01 ± 0.002
39%2HEMA-co-BMA-co-PEGDMA	40:60	57.7 ± 2.7	41.7 ± 1.7	1.02 ± 0.002
49%2HEMA-co-BMA-co-PEGDMA	50:50	55.7 ± 0.9	41.9 ± 0.5	1.03 ± 0.004
54%2HEMA-co-BMA-co-PEGDMA	55:45	54.6 ± 1.8	38.8 ± 3.5	1.05 ± 0.008
59%2HEMA-co-BMA-co-PEGDMA	60:40	55.6 ± 1.0	35.7 ± 1.5	1.06 ± 0.008
64%2HEMA-co-BMA-co-PEGDMA	65:35	57.7 ± 0.9	33.8 ± 2.3	1.11 ± 0.006
69%2HEMA-co-BMA-co-PEGDMA	70:30	57.7 ± 0.3	28.9 ± 1.1	1.14 ± .006
73%2HEMA-co-BMA-co-PEGDMA	75:25	57.1 ± 0.5	21.8 ± 2.1	1.16 ± .007
78%2HEMA-co-BMA-co-PEGDMA	80:20	56.2 ± 0.8	18.9 ± 0.3	1.21 ± 0.007
98%2HEMA-co-PEGDMA	100:0	58.1 ± 0.3	19.8 ± 0.5	1.65 ± 0.030

4.2.3 Differential Scanning Calorimetry

The glass transition temperature (Tg) of each network was determined by performing differential scanning calorimetry (DSC; TA Instruments Q100, Newcastle, DE) under a nitrogen environment. Samples were weighed on a balance (average sample mass between 10-15mg) and then cooled to -80°C and subsequently heated to 200°C at a constant rate of 5°C/min. Tg was denoted as the mid-point of the second order transition on the heating scan. Samples of each composition were soaked in phosphate buffered saline (PBS; Sigma Aldrich) for 1 week and run on the DSC using the same procedure. Before testing, each sample was removed from the solution and patted dry with a paper towel to remove excess moisture. Average Tg and standard deviation were calculated for each composition under each condition (n=3).

4.2.4 Swelling Study

To evaluate the equilibrium swelling behavior of each network, samples were soaked in PBS for 1 week. Each sample was laser-cut into a rectangular piece with a width of 5mm and a length of 20mm. Sample mass was measured after 1 week of soaking (W_W). Each sample was dried in a vacuum at 40°C for 24 hours and the mass was measured again (W_D). The swelling ratio (q) was calculated according to the formula:

$$q = W_w/W_D \qquad (1)$$

Average q values and standard deviation were calculated for each composition (n=4).

4.2.5 Thermogravimetric Analysis

Mass loss as a function of temperature was determined using a thermogravimetric analyzer (TA instruments; New Castle, DE). Samples were tested under dry conditions and after soaking in PBS for 1 week. Those samples immersed in PBS were patted to remove excess surface moisture and then quickly loaded into the pan to avoid evaporation of PBS within the sample. Samples were heated from room temperature to 400°C at a rate of 5°C/min under a nitrogen environment. Sample mass (W_T) as a function of temperature was recorded for each sample, and total, free, and bound water contents were calculated according to previous studies. [12, 15, 25] Mean values and standard deviation of total water content and bound water content were calculated for each composition (n=3).

4.2.6 Fourier Transform Infrared Spectroscopy

Chemical structure for select networks was evaluated by performing fourier transform infrared spectroscopy (FTIR) in total attenuated reflectance (ATR) mode using a Bruker Optics Tensor Spectrometer with a KBr crystal. Ten scans were obtained at 1Hz on dry samples and samples immersed in PBS for one week. Prior to obtaining spectra, wet samples were patted lightly to remove bulk water on the surface and then immediately placed on the crystal. Peak wavenumbers were identified using the OMNIC software. 3 samples were scanned per condition.

4.2.7 Tensile Strain-to-Failure Testing

Tensile strain-to-failure tests were performed on a universal testing machine (MTS Insight 2) using a 2kN load cell. Dogbone samples were laser-cut according to dimensions specified in ASTM D 638-03 Type IV with a 20mm gauge length and a 2.8mm gauge width. Before testing, the edges were sanded to remove any defects from the laser, and the width and thickness in the gauge section were measured using digital calipers. The samples tested in air were loaded in tensile grips, heated to 37°C in a thermal chamber, and held at 37°C for 10 minutes to allow for thermal equilibration. For testing under aqueous conditions, samples were soaked in PBS for 1 week. Prior to testing, the sample was removed from the PBS, patted with a paper towel to remove excess PBS, and its dimensions were measured using digital calipers. The soaked samples were loaded in tensile grips, submerged in a PBS bath at 37°C, and held at 37°C for 10 minutes to allow for thermal equilibration. All tests for these compositions were conducted at a strain rate of 5%/sec. Only samples that broke in their gauge length were used for property calculations. Toughness was calculated as the area under the stress-strain curve in units of MJ/m^3. Elastic modulus was calculated as the slope of the initial linear portion of the stress strain curve for each test.

Based on the results of the initial tests, one composition each of MA-co-MMA-co-PEGDMA and 2HEMA-co-BMA-co-PEGDMA underwent further tensile testing in PBS using the same procedure, but at different strain rates of 0.05%/sec, 0.5%/sec, and 50%/sec. Average toughness values and standard deviation were calculated for each composition. Compositions were tested four times at each strain rate under each condition (dry or wet).

4.3 Results

4.3.1 Differential Scanning Calorimetry

Representative DSC heat flow curves normalized by the sample mass are shown in Figures 4.2 and 4.3 for various compositions of MA-co-MMA-co-PEGDMA and 2HEMA-co-BMA-co-PEGDMA networks under dry and aqueous conditions. Tg is denoted on a sample curve as the second order change in heat flow. Looking at the thermograms of 98%2HEMA-co-PEGDMA, peaks are observed at 0°C and 100°C corresponding to water in the network undergoing a phase change from solid to liquid and liquid and gas. PBS evaporation can be observed in the thermograms of other compositions as minima in the heating curve that occurs around 100°C. In the 2HEMA-co-BMA-co-PEGDMA system, the area of these minima increases as more 2HEMA is added to the network. A similar minimum is observed in the MA-co-MMA-co-PEGDMA networks although there is no observable difference in area with changing composition.

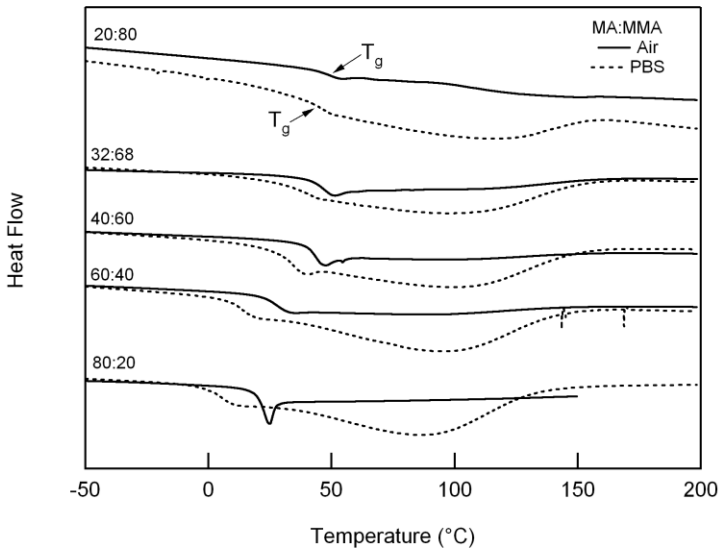

Figure 4.2. Representative DSC scans of MA-co-MMA-co-PEGDMA for select compositions (MA:MMA) under dry (solid line) and wet (dashed line) conditions.

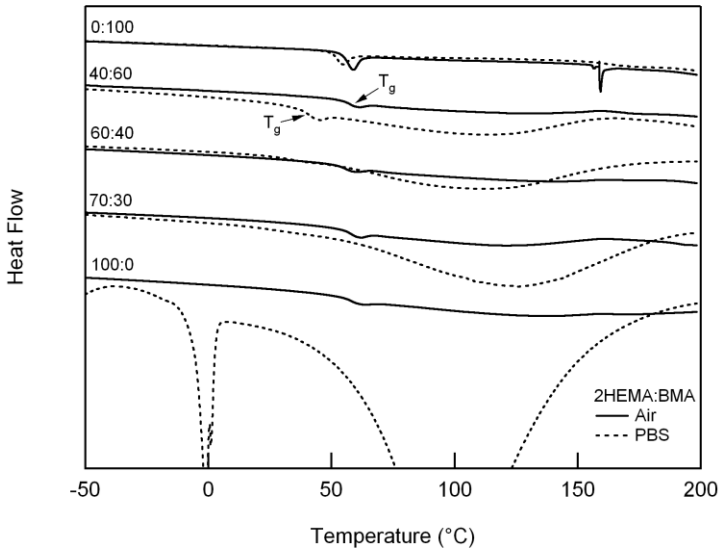

Figure 4.3. Representative DSC scans of 2HEMA-co-BMA-co-PEGDMA for select compositions (2HEMA:BMA) under dry (solid line) and wet (dashed line) conditions.

Average Tg's measured from the DSC are listed in Tables 4.1 and 4.2 and graphed in Figures 4.4 and 4.5 as a function of MA or 2HEMA percent weight fractions for MA-co-MMA-co-PEGDMA and 2HEMA-co-BMA-co-PEGDMA, respectively. For the MA-co-MMA-co-PEGDMA network, Tg decreases in both air and in PBS as the MA concentration increases with average values ranging from 49.47°C to 21.47°C and 48.90°C to 5.2°C, respectively. For each composition, the average Tg value in PBS is lower than the average Tg value in air. By comparing the change in Tg with composition, the Tg of 29%MA-co-MMA-co-PEGDMA decreases by 5°C; whereas, 72%MA-co-MMA-co-PEGDMA experiences a 15°C reduction in Tg when immersed in PBS. Similarly, Tg linearly depends on the weight fraction of MA under both dry and wet conditions, but this linear relationship between Tg and MA concentration in PBS has a larger slope compared with dry conditions indicating that Tg is decreased to a greater

extent in PBS as more MA is added to the network. Similarly, increasing the 2HEMA concentration in the 2HEMA-co-BMA-co-PEGDMA networks results in an incremental decrease in Tg in PBS with values ranging from 52.84°C to 19.79°C, but under dry conditions, the Tg is independent of relative BMA and 2HEMA concentrations. The decrease in Tg with PBS exhibits a nonlinear behavior converse to the relationship in MA-co-MMA-co-PEGDMA.

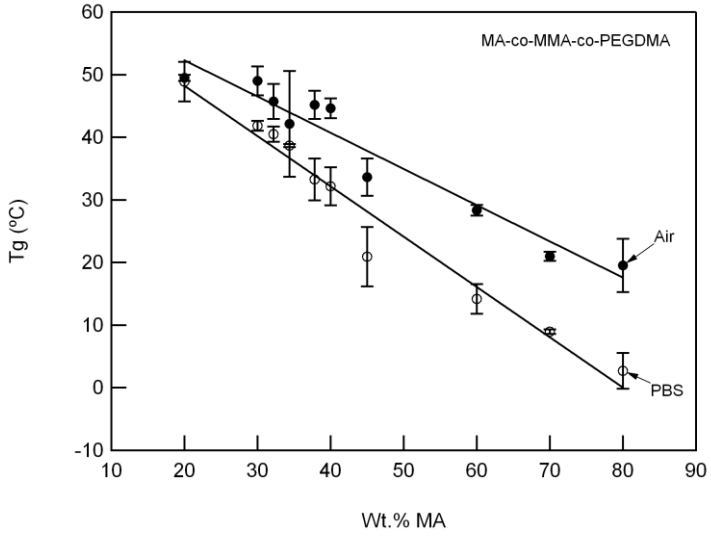

Figure 4.4. Effect of varying the MA concentration on Tg under both dry and wet conditions for MA-co-MMA-co-PEGDMA. A curve was fit to the experimental data showing the linear dependence of Tg on MA concentration.

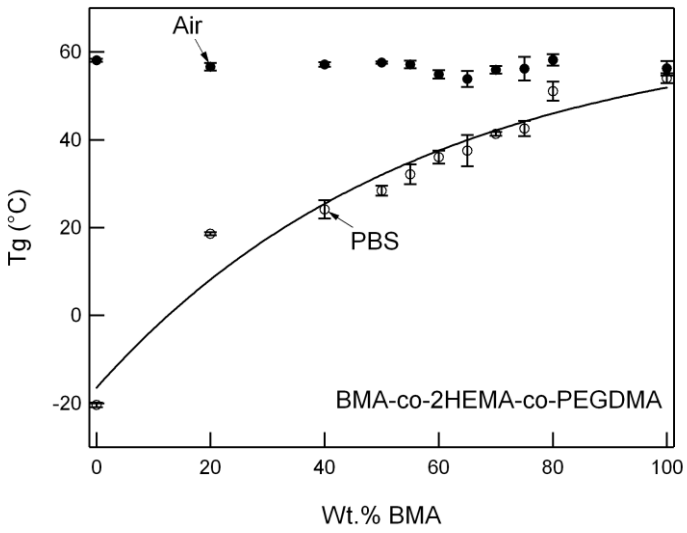

Figure 4.5. Effect of varying the BMA concentration on Tg under both dry and wet conditions for BMA-co-2HEMA-co-PEGDMA networks. A curve was fit to the experimental data showing the nonlinear dependence of Tg on BMA concentration.

Although these measured Tg values might be considered low, especially for the 98%2HEMA-co-PEGDMA material, it has been previously shown that Tg will vary depending on the analysis technique adopted (i.e. DSC vs. dynamic mechanical analysis).[26] In this study, DMA was initially performed on all compositions with Tg defined as the temperature where the tan delta reaches a maximum. It was determined that the Tg measured by DSC coincided with the onset temperature of the thermomechanical glass transition observed on the DMA (data not shown). Due to this difference, the Tg's determined by DSC will be coincidentally lower than expected to an extent determined by the breadth of the network's glass transition behavior [26].

4.3.2 Equilibrium Swelling Behavior

Average swelling ratios (q) for each composition of MA-co-MMA-co-PEGDMA and 2HEMA-co-BMA-co-PEGDMA are displayed in Tables 4.1 and 4.2, respectively.

Tg as a function of water absorption is shown for the two networks in Figure 4.6. In the MA-co-MMA-co-PEGDMA network, changing the MA concentration has no effect on water absorption with all networks exhibiting similar swelling ratios (q≈1.03-1.04). Conversely, water content in 2HEMA-co-BMA-co-PEGDMA increases as the concentration of 2HEMA increases with the swelling ratio reaching a maximum of 1.65 in the 98%2HEMA-co-PEGDMA network.

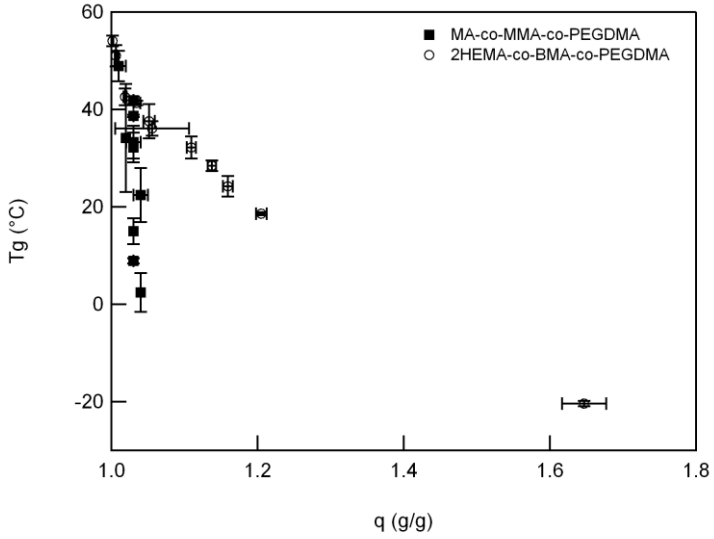

Figure 4.6. Effect of water absorption (as measured by the swelling ratio "q") on the Tg of each network.

4.3.3 Thermogravimetric Analysis

The total water content and fraction of bound water in select compositions of each network were determined through TGA. Representative DT/TGA plots of 29%MA-co-MMA-co-PEGDMA and 59%2HEMA-co-BMA-co-PEGDMA are shown in Figure 4.7. Sample mass (M_T) at each temperature point was used to calculate the percent of the initial sample mass remaining ($\%M_o$) by:

$$\%M_o = \frac{M_T}{M_o} \times 100$$

where M_o is the initial sample mass (10-15mg). $\%M_o$ was plotted as a function of temperature along with the derivative change in weight with temperature (DTG). Initial decomposition temperature was defined as the temperature where the DTG began to increase rapidly above 100°C. TGA profiles of other tested compositions were not included for clarity purposes, but exhibited similar behavior in comparison to the mass loss of dry and soaked samples. The presence of free water can be observed by the decrease in mass and rapid increase in DTG below 100°C compared with the thermograms for dry samples. Above 100°C, a greater mass loss also occurs in the PBS-soaked samples due to bound water eventually evaporating at a higher temperature. In the 32:68 MA network, this maxima is very broad and shallow; whereas, the 60:40 2HEMA network exhibits a higher and broader maxima in DTG with the rate peaking around 120°C. The effect of PBS on the thermal stability of the 2HEMA network is also evident by the increased decomposition temperature compared with dry samples.

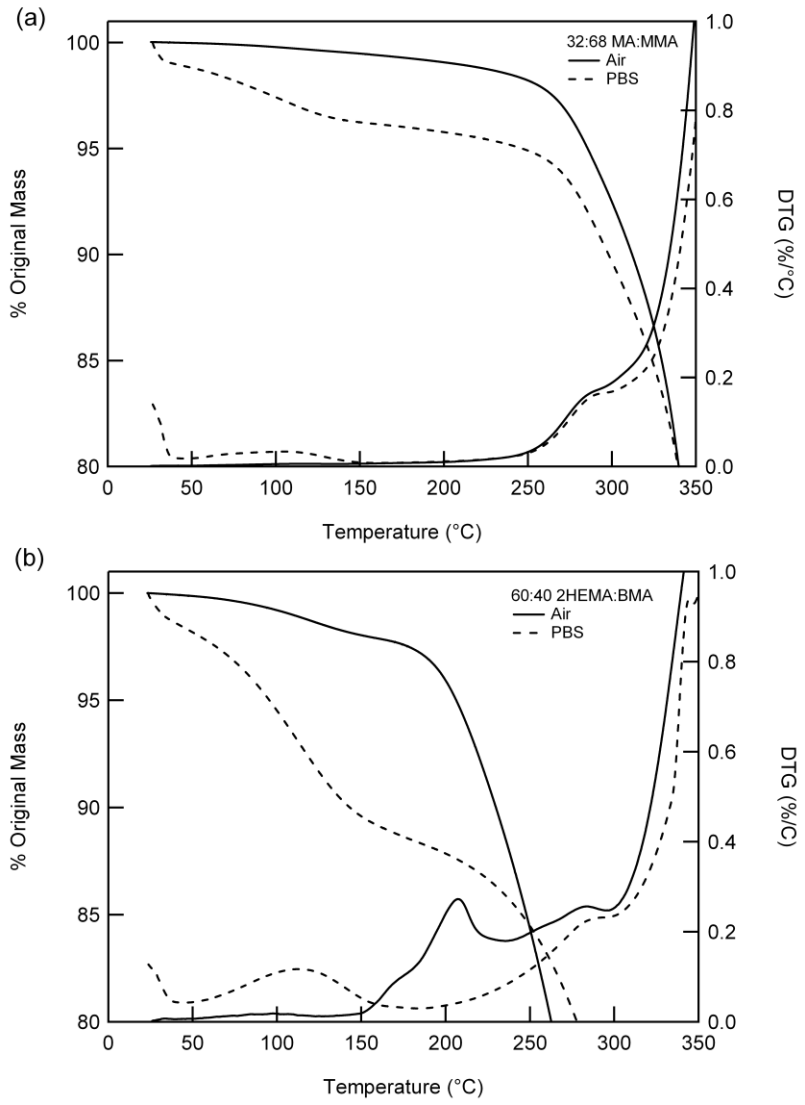

Figure 4.7. Representative TGA results of (a) 29%MA-co-MMA-co-PEGDMA (32:68) and (b) 59%2HEMA-co-BMA-co-PEGDMA (60:40) in air and after 1 week immersion in PBS.

Following the methods of previous studies [12, 18], the total water content (W_t) was defined as

$$W_t = 100 - \%M_D$$

where the $\%M_D$ is defined as the percent sample weight at a temperature slightly below the decomposition temperature for the network. Because BMA decomposes at a low

temperature (around 180°C), this was the temperature commonly adopted for the different compositions of BMA-co-2HEMA-co-PEGDMA network while the initial decomposition temperatures for various formulations of MA-co-MMA-co-PEGDMA ranged from 180°C to 200°C. The amount of free water was defined as:

$$W_f = 100 - \%M_T$$

where $\%M_T$ is the percent sample mass at 100°C. Although it would be expected that PBS evaporates at higher temperatures compared with pure water, thermograms from TGA showed complete evaporation of PBS by 100°C suggesting that the salt content, in this case, did not affect the overall phase transitions of the solution. Thus, it was assumed that PBS not directly hydrogen bonded with the network (the termed, "free water") will evaporate in a manner similar to its bulk state at 100°C. Thus, this temperature was adopted to determine the weight fraction of free water. Because bound water is in phase with the polymer network, these molecules will boil at a much higher temperature, oftentimes when the polymer begins to decompose. By assuming water can only be found in one of two states, the difference between the total water content and free water content was defined as the bound water within the network.[18] The total water and bound water content calculated from these plots for all compositions are shown in Figures 4.8 and 4.9 for MA-co-MMA-co-PEGDMA and . To determine if water state changes in the network independently of changes in total water content, the ratio of bound water to total water content are included for comparison.

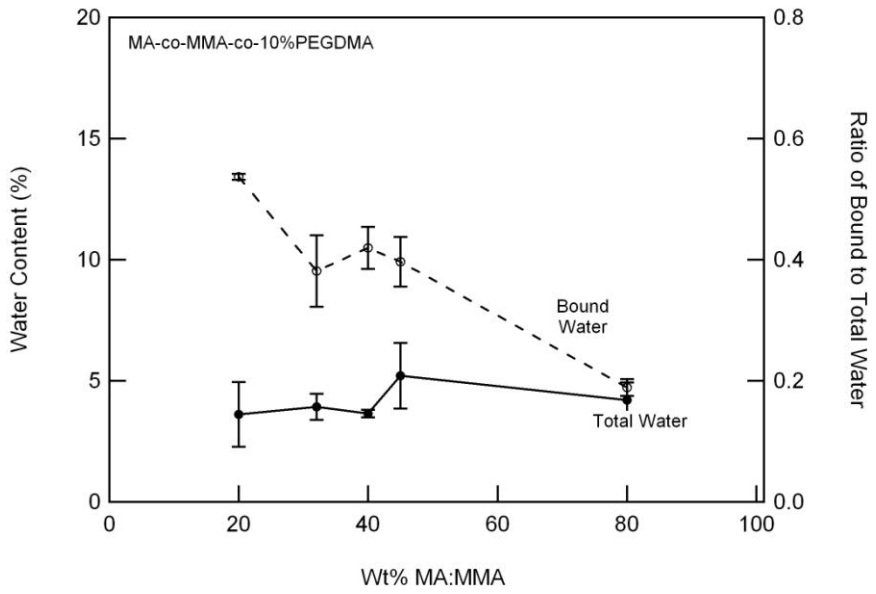

Figure 4.8. Total and bound water content as a function of MA concentration. The ratio of the bound to total water content is shown and represents average values calculated from several samples (n=4).

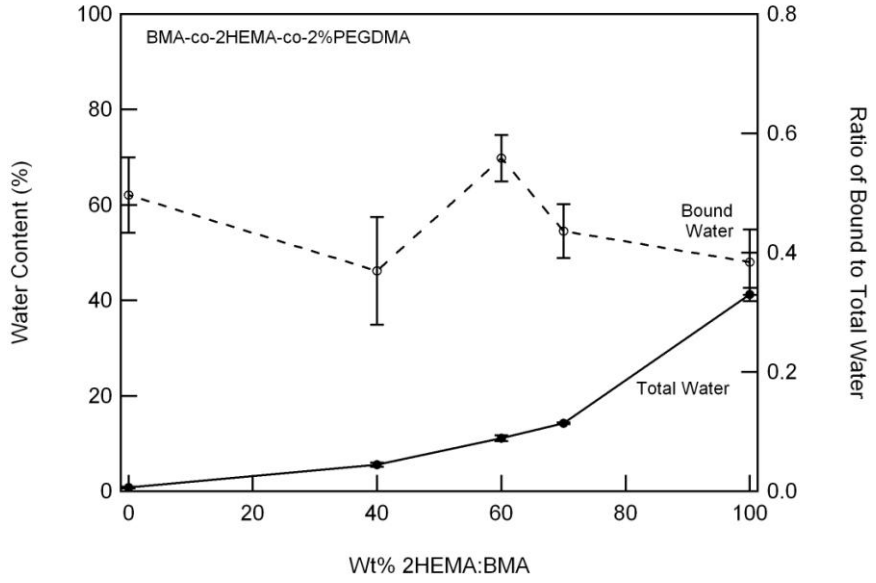

Figure 4.9. Total and bound water content as a function of 2HEMA concentration. The ratio of the bound to total water content is shown and represents average values calculated from several samples (n=4).

Consistent with swelling measurements, average total water content and bound water content remain relatively constant in the MA-co-MMA-co-PEGDMA network

despite changing the MA concentration (3.5-5.2% and 0.8-2.0%, respectively). The total water contents measured from TGA were consistent with the swelling ratios for the different compositions of MA-co-MMA-co-PEGDMA network. Interestingly, the ratio of bound water to total water content is higher for networks containing more MMA versus MA indicating that water behavior is dependent on the copolymer composition. In the 2HEMA-co-BMA-co-PEGDMA network, both total water content and bound water content (1% to 41.2% and less than 1% to 15.8%, respectively) increase as the concentration of 2HEMA increases, but there is no significant change in the ratio of bound to total water content. For formulations of the 2HEMA-co-BMA-co-PEGDMA networks containing more than 60% of 2HEMA, the water contents as measured through TGA were lower compared to the fraction of absorbed water extracted from the calculated swelling ratio. It is possible that some PBS evaporated during loading the sample into the TGA resulting in less mass loss due to water evaporation during heating. This effect was mitigated as best as possible by keeping samples hydrated prior to testing and quickly loading the samples before testing. It is also important to recognize that the two states of water described above are the extremes in a continuum of water states that exist within a polymer. More extensive studies of the thermal transitions of water in polymers have been detailed elsewhere and were beyond the scope of this study.[19, 27, 28]

4.3.4 Fourier Transform Infrared Spectroscopy

To better understand the water-polymer interactions in the MA-co-MMA-co-PEGDMA network, FTIR-ATR was performed on select compositions. Representative

FTIR spectra of 29%MA-co-MMA-co-PEGDMA, 40%MA-co-MMA-co-PEGDMA, and 63%MA-co-MMA-co-PEGDMA under both dry and wet conditions are shown in Figures 4.10 and 4.11. The peaks at 1160cm^{-1}, 1730 cm^{-1}, and 2950cm^{-1} correspond to the C-O-C stretching vibrations, C=O stretching vibration, and C-H stretching vibrations (for the methyl groups), respectively. A slight change in intensity in the C-O-C and C=O vibrational bands under wet conditions is observed, particularly in the 45:55 and 32:68 compositions, due to the formation of hydrogen bonds with surrounding water molecules (Figure 4.10). After immersion in PBS, peaks appear around 1650-1700cm^{-1} and 3400-3600cm^{-1} corresponding to O-H bending and stretching vibrations of the water molecules, respectively. The shifts in the O-H stretching and O-H bending bands to higher frequencies are indicative of the hydrophobicity of the network due to less hydrogen bond formations between adjacent water molecules and/or water molecules with polymer chains.[29] Comparing the frequencies amongst the three compositions in Figure 4.11, a right shift in the peak frequency for O-H stretching occurs in the 32:68 formulation compared to the other two compositions suggesting that hydrogen bonding is stronger in networks with lower MA concentration.

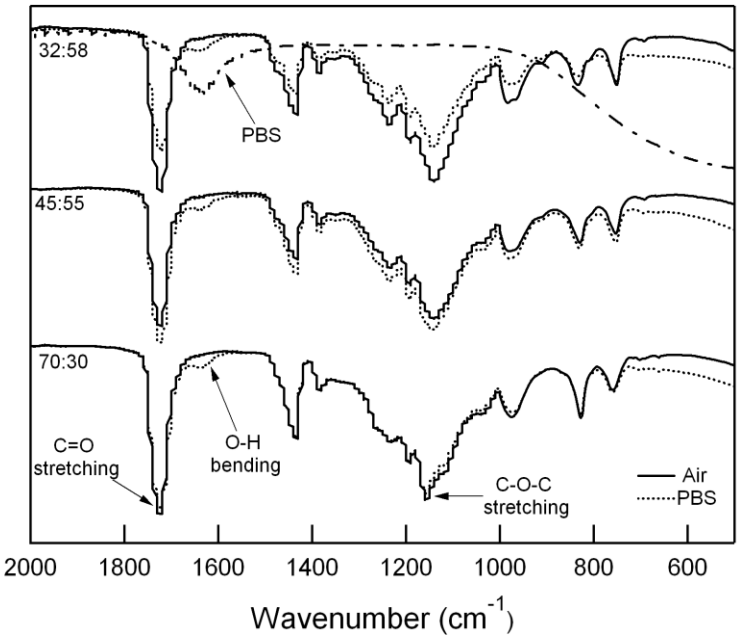

Figure 4.10. Representative FTIR-ATR spectra in the low frequency range frequency range for select MA-co-MMA-co-PEGDMA compositions (MA:MMA) under dry conditions and after 1 week immersion in PBS.

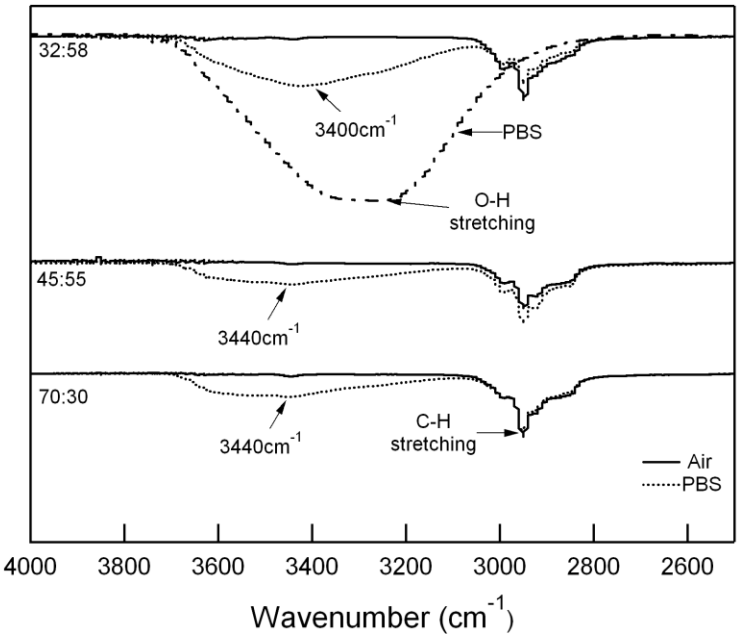

Figure 4.11. Representative FTIR-ATR spectra in the high frequency range for select MA-co-MMA-co-PEGDMA compositions (MA:MMA) under dry conditions and after 1 week immersion in PBS.

4.3.5 Stress-Strain Behavior

Representative stress-strain behaviors of MA-co-MMA-co-PEGDMA and 2HEMA-co-BMA-co-PEGDMA at different compositions under both dry and wet conditions at 37°C are shown in Figure 4.12, 4.13, and 4.14, respectively. For each composition, the stress-strain behavior is altered in PBS exhibiting a decreased modulus, reduced strength and increased failure strain compared to dry conditions. Under both dry and wet conditions, the MA-co-MMA-co-PEGDMA network exhibits a transition from brittle to ductile to rubbery behavior as MA concentration is systematically increased as indicated by a gradual decrease in modulus, the appearance and waning of yielding behavior, and increase in failure strain. Comparing Figure 4.12 and 4.13, the stress-strain behavior at each composition in air does not match the behavior of that same composition when soaked in PBS, but instead exhibits more ductile (i.e. 30:70) or rubbery (i.e. 45:55) mechanical behavior. In air, the stress-strain behavior of 2HEMA-co-BMA-co-PEGDMA was not affected by changing the 2HEMA concentration, but maintained brittle behavior independent of composition (data not shown). In PBS, 2HEMA-co-BMA-co-PEGDMA showed a similar relationship between composition and stress strain behavior as MA-co-MMA-co-PEGDMA with a glassy to rubbery transition occurring with increasing 2HEMA content (Figure 4.14).

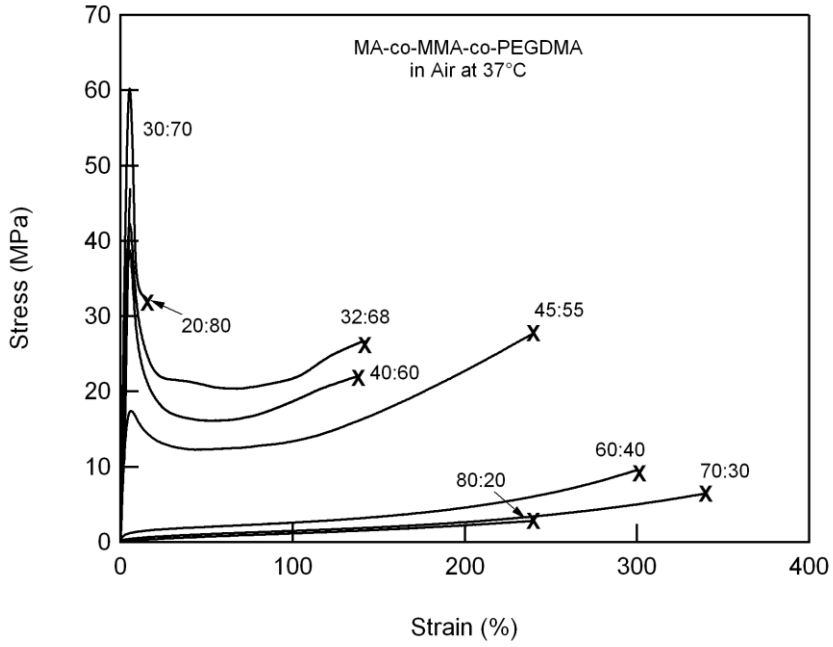

Figure 4.12. Stress-strain behavior of MA-co-MMA-co-10%PEGDMA at different ratios of MA:MMA tested in air at 37 °C.

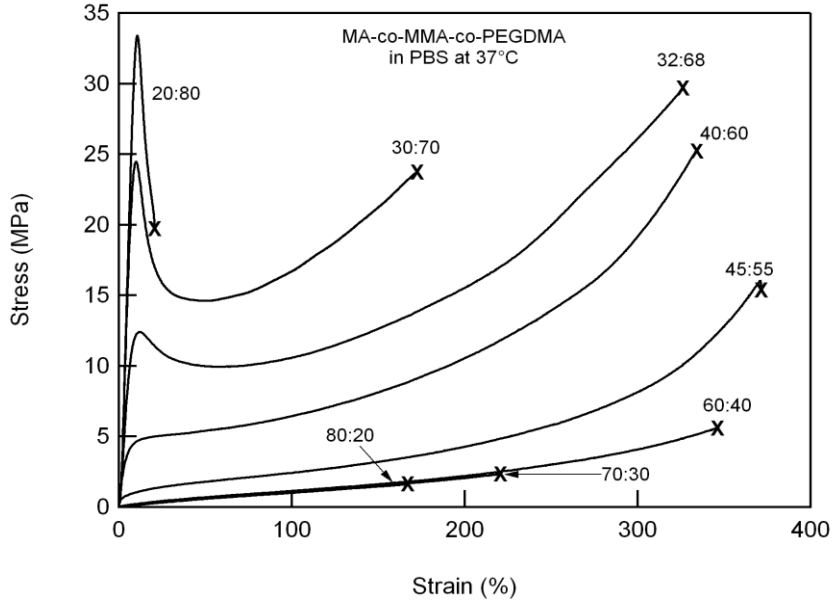

Figure 4.13. Stress-strain behavior of MA-co-MMA-co-10%PEGDMA at different ratios of MA:MMA tested in PBS at 37 °C.

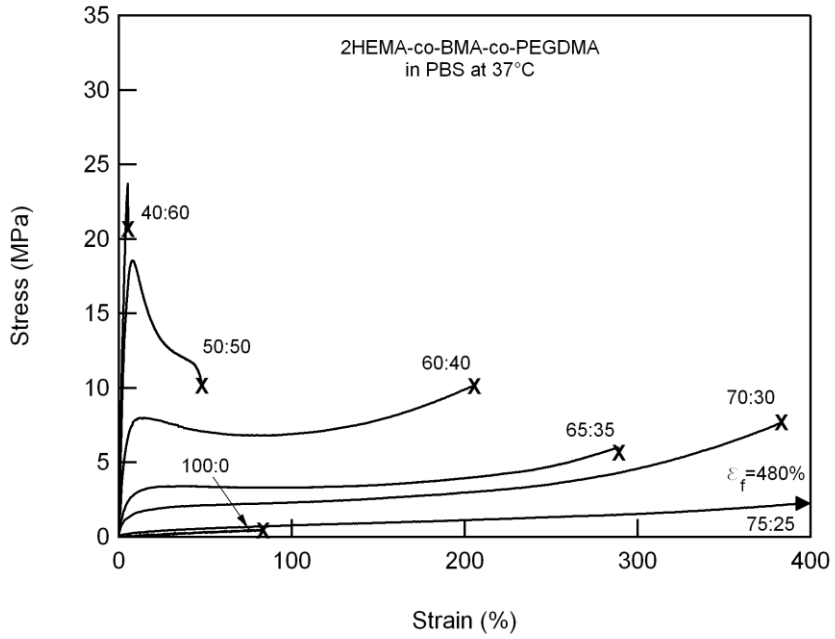

Figure 4.14. Stress-strain behavior of 2HEMA-co-BMA-co-2%PEGDMA at different ratios of 2HEMA:BMA tested in PBS at 37 °C.

4.3.6 Effect of Composition on Toughness

Using the area under the stress-strain curves, toughness is plotted as a function of MA or 2HEMA concentration as shown in Figures 4.15 and 4.16, respectively. In the MA-co-MMA-co-PEGDMA network, a peak in toughness in air and PBS occurs at the composition with 32%MA while an additional peak is also observed in air at the 45%MA composition. These peak compositions are easily identified as their toughness values are several orders of magnitude higher compared with other MA concentrations within the network. In comparison to MA-co-MMA-co-PEGDMA, the toughness of 2HEMA-co-BMA-co-PEGDMA in air is low and does not vary with changing 2HEMA concentration. In PBS, toughness is the highest for 59%2HEMA-co-BMA-co-PEGDMA and then decreases with increasing or decreasing 2HEMA concentration.

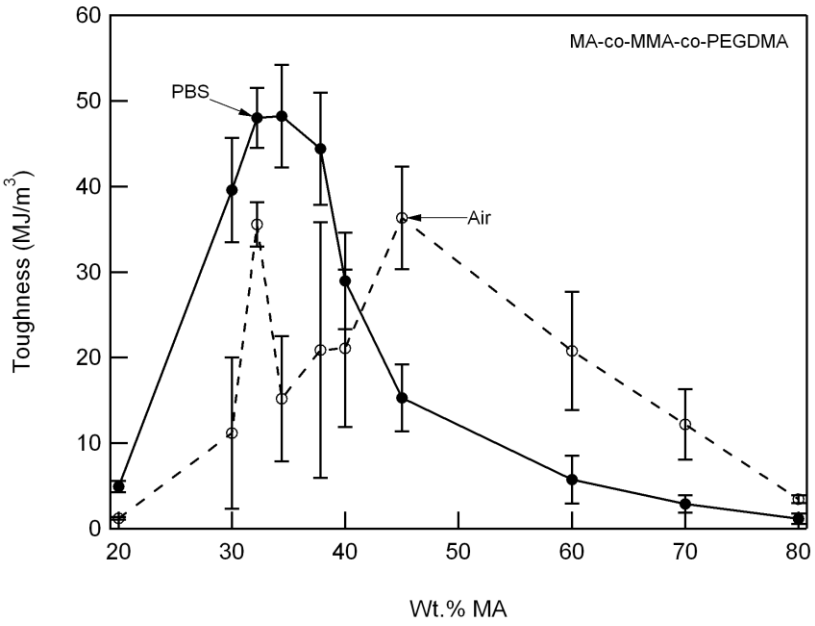

Figure 4.15. Toughness plotted as a function of composition for MA-co-MMA-co-10%PEGDMA. The toughness under both dry (dotted line) and wet (solid line) are compared for each network.

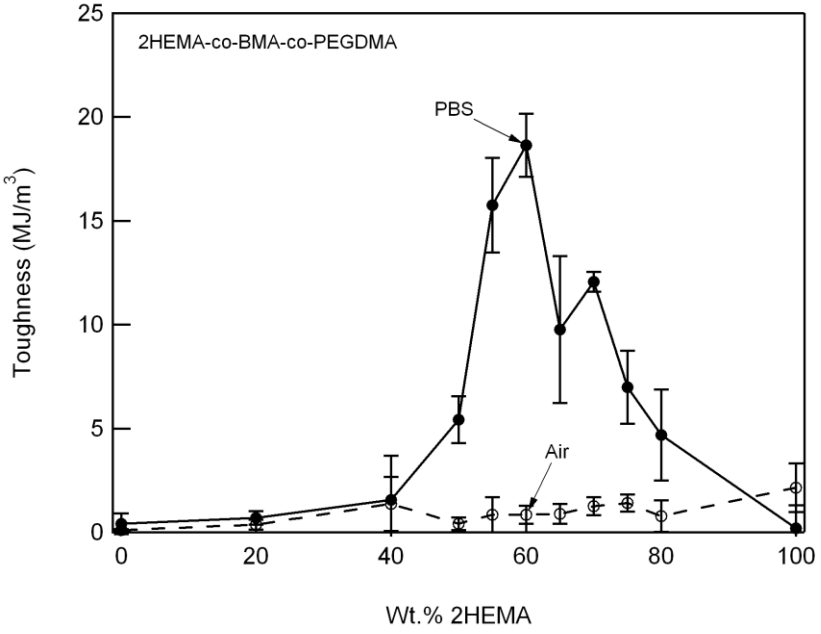

Figure 4.16. Toughness plotted as a function of composition for BMA-co-2HEMA-co-10%PEGDMA. The toughness under both dry (dotted line) and wet (solid line) are compared for each network.

4.3.7 Effect of Strain Rate on Network Toughness

The effect of strain rate on the toughness of 59%2HEMA-co-BMA-co-PEGDMA and 29%MA-co-MMA-co-PEGDMA is displayed in Figure 4.17. In both networks, toughness is altered when the strain rate changes over several orders of magnitude. At 5%/sec, the toughness of both MA-co-MMA-co-PEGDMA and 2HEMA-co-BMA-co-PEGDMA is highest. As the strain rate decreases from 5%/sec to 0.5%/sec to 0.05%/sec, network toughness gradually decreases with the MA-co-MMA-co-PEGDMA network exhibiting the larger change in toughness compared with 2HEMA-co-BMA-co-PEGDMA networks. The toughness of 59%2HEMA-co-BMA-co-PEGDMA does not change when tested between rates of 0.5-50%/sec but declines slightly when tested at 0.05%/sec.

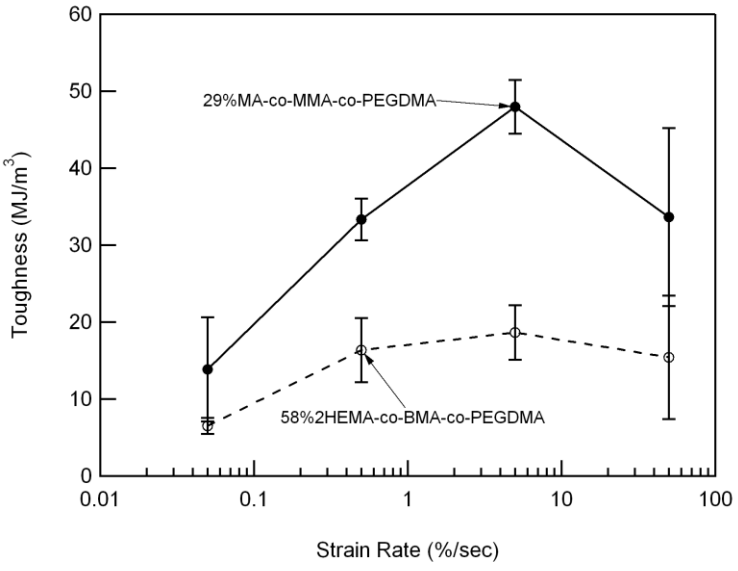

Figure 4.17. The effect of strain rate on the toughness of 29%MA-co-MMA-co-PEGDMA and 59%2HEMA-co-BMA-co-PEGDMA networks tested in PBS at 37°C.

4.4 Discussion

Because the spinal disc region contains a large amount of water, a material implanted into this region must be able to have the appropriate mechanical properties in the presence of solution. However, increased moisture content as a result of implantation into hydrated areas of the body is a common cause of mechanical failure for polymeric biomaterials. In many instances, it is necessary that the material be able to absorb a large amount of water (for example, in hydrogels) to serve its desired function in the body as well as maintain suitable mechanical properties to ensure durability and long-term functionality. A polymer biomaterial that is tough in solution would serve a variety of applications including a shape memory fixation device, compliant soft tissue replacement, hydrogel and/or tissue engineering scaffold. Although the materials studied here are non-degradable, the concepts discussed herein may also be extended to certain degradable polymer networks.

In this study, the influence of an aqueous environment on the toughness of photopolymerizable (meth)acrylate networks was examined using two ternary copolymer networks. Three component networks allow for the systematic control of various materials properties, such as Tg, by varying the weight ratio of the two linear monomers without changing the crosslinker concentration. Maintaining a constant crosslinker concentration is important as it has been shown that crosslinking density will affect water absorption and the mechanical properties independent of monomer chemistry. The combinations of linear monomers incorporated into each network were chosen for several reasons. In one network, MA and MMA were selected because they have different Tg's (-10°C and 130°C, respectively), but their structures provide a similar level of

hydrophobicity based on polarity (Figure 1). Previous studies also revealed that MA-co-MMA-co-PEGDMA (with 2% PEGDMA) has inherently high toughness with an elastic modulus in the range of many tough biological tissues [7]. Conversely, the two linear monomers selected for the second network, BMA and 2HEMA, both have high Tg's in relation to body temperature (80°C and 110°C, respectively), but have side groups with opposing degrees of hydrophilicity (Figure 1). In addition, 2HEMA is a monomer that is extensively used in contact lenses and hydrogels [30, 31] while BMA has been shown to have enhanced toughness at its glass transition temperature [32]. From the results presented here, it can be suggested that network toughness under physiological conditions is dependent on Tg, water absorption, and strain rate, in a manner related to network composition. In the following discussion, the individual role of each property on enhancing toughness, with respect to each network, will be examined as well as how these properties are interrelated in affecting toughness.

In the MA-co-MMA-co-PEGDMA system, Tg is dependent on MA concentration under both dry and wet conditions. The observed decrease in Tg with increasing MA concentration (Figure 4.4) can be explained by considering that the Tg of a copolymer network is dependent on the individual Tg's and concentrations of the monomer components [33, 34]. Because MA has a lower Tg compared to MMA and the PEGDMA concentration is constant in all network formulations, the Tg of the MA-co-MMA-co-PEGDMA network effectively decreases as more MA is added to the network. After immersion in PBS for 1 week, the Tg of each composition in PBS decreases indicating that water molecules are being absorbed and changing the thermodynamic state of the network. Due to the low water content in the network, the absorbed water molecules are

effectively acting as a plasticizer by increasing the configurational entropy accessible to the network in a manner related by the following expression derived from the Couchman equation:

$$\Delta S^c = -C_p \ln(\frac{T_{gPBS}}{T_{gAir}})$$

where ΔS^c is the change in the configurational entropy of mixing and C_p is the heat capacity of the network [33]. If it is assumed that heat capacity is not affected by the plasticizer, the larger increase in Tg with networks with higher MA concentration suggests that ΔS^c due to the introduction of PBS is composition-dependent. Several theories have been developed to predict the effect of water and copolymer composition on Tg including the Gordon-Taylor [35] and Couchman-Karaz equations [33, 36]. Because the total water content of MA-co-MMA-co-PEGDMA is low, it is difficult to apply these equations in predicting Tg as the concentration of the liquid diluent, PBS, is small enough such that it is difficult to ascertain if the diluent Tg would remain the same as in the bulk. The linear relationship between Tg and MA concentration suggests that this copolymer network follows simple additive properties related to the ideal volume of mixing, even in the presence of PBS [33, 34]. However, it is also important to note that these theories are simplistic in that they only take into account two-component systems and thus cannot be fully utilized to account for change in both the copolymer concentration and changes in water content.

Besides considering the change in thermodynamics associated with mixing the PBS and polymer chains, it is important to consider how the specific water state is changing within the different compositions. It has previously been reported that the state of water molecules within the polymer can directly attribute to its glass transition

behavior [12, 28]. Considering that water content of the network is not affected by MA concentration (Figure 4.6), the larger Tg reduction with increasing MA concentration in PBS (Figure 4.4) suggests that the weight ratio of MA to MMA in the network could be affecting the state of the sorbed water molecules resulting in differential decreases in Tg [12, 37]. Due to the difficulty in discerning the relative bound and free water contents, several different experimental techniques including DSC, TGA, and FTIR are usually employed to determine specific water-polymer interactions [12, 14, 27, 29, 38]. Because all MA-co-MMA-co-PEGDMA formulations have low water contents, the free water and bound water contents were undetectable through DSC. By considering that bound water will evaporate at a higher temperature due to its formation of a one-phase system with the network in comparison with free water which evaporates at 100°C similar to bulk water, the free and bound water fractions can be determined through thermogravimetric analysis[12, 25]. The observed 1-2% weight fraction of bound water, independent of MA concentration, (Figure 4.8) compares with other reported findings on polyurethanes that possess similar chemistry and hydrophobicity [12].

It might be expected that polymer networks with very low water content would not contain any unbound or free water, but rather all sorbed molecules would bind to any available hydrophilic chemical groups. However, the absence of potential binding sites in hydrophobic networks such as MA-co-MMA-co-PEGDMA causes sorbed water molecules to remain in an unbound state and arrange themselves into clusters in order to optimize the number of hydrogen bond interactions as well as minimize their interaction with the less energetically favorable hydrophobic components of the network [39]. These clusters will be located within the micropores of the network and exhibit a phase

transition behavior characteristic of bulk water [28, 29, 40, 41]. Although MA-co-MMA-co-PEGDMA is mostly hydrophobic, it is also evident from the FTIR spectra (Figure 4.11) that some water is still present in a bound state, forming hydrogen bonds with ethylene glycol on PEGDMA and the ester groups located in the acrylate subunits.

Interestingly by comparing the ratio of bound water to total water content in the network, it is observed that the bound water content relative to total water content decreases with increasing MA concentration suggesting that water prefers to remain in an unbound state as MA concentration increases (Figure 4.7). The lower O-H stretching frequency in the FTIR spectra of 29%MA-co-MMA-co-PEGDMA compared with the 63%MA and 40%MA formulations provides further evidence that more hydrogen bonding is occurring in formulations with less MA incorporated (Figure 4.11). Taking into consideration that free water content increases and Tg decreases to a greater extent with MA concentration (Figure 4.2), it can be suggested that the extent of Tg reduction in PBS is dependent upon the free water content within the network. To follow up on this theory, DSC was performed using a heat-cool-heat scanning procedure on select MA-MMA compositions after 1 week immersion in PBS (data not shown). Samples were heated to a certain temperature, T_1= 100°C, 120°C, or 140°C, then cooled to 0°C, held isothermal for 5 minutes, and reheated once again to 200°C. An increase in Tg after heating to only 100°C indicates that the removal of free water is causing the Tg of the network to return to its original state for the dry network. Although Tg was further increased upon heating to higher temperatures, the greatest increase in Tg occurred in the heating scans ramping to 100°C providing further evidence that the effect of PBS

immersion on the Tg of MA-co-MMA-co-PEGDMA is governed by the presence of free water in the network.

By comparing the results for the two copolymer networks, it is evident that the Tg of 2HEMA-co-BMA-co-PEGDMA is affected by PBS in a different manner compared with MA-co-MMA-co-PEGDMA. Unlike MA-co-MMA-co-PEGDMA, the 2HEMA concentration of 2HEMA-co-BMA-co-PEGDMA does not impact the Tg of the network under dry conditions (Figure 4.3). Because BMA and 2HEMA have similar reported Tg's [32, 42], the Tg of the copolymer network will not be affected by changing the concentration ratio of 2HEMA to BMA, according to theories on the effect of copolymer mixing on Tg [33-35]. However after 1 week immersion in PBS, Tg becomes strongly dependent on 2HEMA concentration, an effect driven by the increased water content with increasing 2HEMA concentration (Figure 4.3 and 4.4). In compositions with low water contents and little swellability (less than 60%2HEMA), the PBS is acting as a plasticizer, similar to the MA-co-MMA-co-PEGDMA network, to lower Tg by increasing the configurational entropy accessible to the network [33]. In this regime, the Tg experiences a few degrees reduction with an increase in 2HEMA (Table 4.1). In compositions containing more than 60%2HEMA, the 2-fold increase in network swellability (Table 4.1) indicates the polymer chains are being extended allowing for more PBS absorption, but less configurational entropy available to the network. In addition, the increased free volume allows the water molecules to act in a more stable state by forming hydrogen bonds with either the polymer chains or each other. The combination of these two mechanisms results in the Tg's of these compositions to

decrease to a greater extent compared with the low 2HEMA compositions effectively leaving the networks in a relaxed, rubbery state.

When examining water state within the network, bound water content increases as more 2HEMA is added to the network as would be expected as more potential sites become available for water binding to occur (Figure 4.9). Considering the polarity of the side groups of each monomer, it would be expected that the hydroxyl group in 2HEMA would readily form hydrogen bonds with adjacent water molecules. On the other hand, BMA contains a bulky, nonpolar phenyl ring in its side chain that limits the diffusion of water molecules and provides an energetically unfavorable environment for hydrogen bond formation to any hydrophilic components [14]. Unlike MA-co-MMA-co-PEGDMA, despite the change in water content with 2HEMA concentration, no trend is identified with the ratio of bound water to total water content indicating that the change in bound water with copolymer composition mirrors the change in total water content. This result in combination with the relationship between water state and Tg established in the MA-co-MMA-co-PEGDMA suggests that the individual influences of bound versus free water on Tg depends on the total amount of water absorption into the network. However, further evidence would be needed to verify this theory and is beyond the scope of this study.

Considering these relationships between Tg and network chemistry, trends between toughness and Tg under both dry and wet conditions are identified in both networks. For MA-co-MMA-co-PEGDMA in air, toughness is affected by varying the MA concentration, reaching a maximum in 29%MA-co-MMA-co-PEGDMA and 40%MA-co-MMA-co-PEGDMA. By comparing the stress strain behavior in air and

after immersion in PBS (Figures 4.12 and 4.13), it is evident that the mechanical behavior of MA-co-MMA-co-PEGDMA is influenced by the presence of PBS in a manner that is dependent on network composition. Since the Tg of each composition is reduced when the network is immersed in PBS, the stress strain behavior is transitioning in a manner similar to increasing temperature. Similar to dry conditions, toughness in PBS varies with composition with a peak in toughness occurring in 29%MA-co-MMA-co-PEGDMA. Interestingly, this composition also exhibited enhanced toughness in air despite having a Tg well above testing temperature (47°C). Looking at its stress strain behavior in Figure 8, 29%MA-co-MMA-co-PEGDMA (32:68) exhibits higher failure strains and ultimate stresses compared to compositions with slightly more or less MA (i.e. 30:70 and 40:60 compositions). This unique behavior would enable the use of this material for an application where excellent mechanical properties were required under varying degrees of hydration.

In 2HEMA-co-BMA-co-PEGDMA, toughness in air is not affected by 2HEMA concentration, but rather remains low in all compositions. Because the T_g of this network is more than 25°C above testing temperature, the material is acting in its glassy, brittle state. Like MA-co-MMA-co-PEGDMA, toughness of 2HEMA-co-BMA-co-PEGDMA is affected by immersion in PBS in a manner related to the concentration of 2HEMA incorporated into the network. Interestingly, toughness is enhanced in all formulations of the network indicating that water absorption can indeed act as a toughening mechanism in polymer networks under appropriate conditions. The toughness as a function of 2HEMA concentration displays a profile similar to the relationship between toughness and composition in MA-co-MMA-co-PEGDMA with toughness peaking in

59%2HEMA-co-BMA-co-PEGDMA (Figure 15 vs. 16). This composition exhibits slight yielding behavior, large failure strains (>200%) and some strain-induced hardening around 150% strain that all explain its enhanced toughness. When the BMA concentration reaches a certain amount (greater than 60%), both Tg and the stress strain behavior are affected little by immersion in PBS (Figure 4.4 and Figure 4.14). Despite having several hydrophilic components in the network, the bulkiness of BMA prevents few water molecules from binding and absorbing into the network as noted by the low water content present in these networks (Table 4.2 and Figure 4.6).

Comparing the calculated toughness values between the two "peak" compositions, the average toughness is higher in 29%MA-co-MMA-co-PEGDMA network versus 59%HEMA-co-BMA-co-MA-co-PEGDMA by more than 20 MJ/m^3. Because toughness is dependent on the magnitude of other mechanical properties including elastic modulus, failure strain, and ultimate strength, potential toughening mechanisms can be identified by examining the stress strain behavior. For example, 29%MA-co-MMA-co-PEGDMA possesses higher ultimate stresses and failure strains compared with 59%2HEMA-BMA-co-PEGDMA and also exhibits a strain-induced hardening effect (Figure 4.13 vs. Figure 4.14). The increased modulus and strength could be the result of the MA-co-MMA-co-PEGDMA network having a higher crosslinking concentration compared with 2HEMA-co-BMA-PEGDMA[3]. It has previously been proposed that strain hardening is induced by strong secondary bonding between the polymer chains [1] which will act to prevent chain displacement over larger ranges of loading. Although the formation of hydrogen bonds are unlikely between MA and MMA, hydrophobic bonding [43] between the side chains on the two monomers will enhance the strength of the polymer chains, an effect

that would not be inhibited, but actually enhanced by the presence of water or PBS [14]. Since BMA and 2HEMA possess opposite polarities on their side chains, the secondary intermolecular bonding is weak within this network and even further weakened in solution, causing chains to be easily misaligned especially at higher strains.

Previous studies have proposed that toughness in acrylate-based networks will reach a peak at a certain temperature, and that when immersed in PBS, this toughness maximum in the same network will shift to a lower temperature [7]. Considering this relationship between testing temperature and toughness in PBS, it can be suggested that optimal toughness occurs in PBS in the network whose Tg is reduced by PBS absorption in a manner that better aligns the temperature of optimal toughness with the testing temperature. For both the MA-co-MMA-co-PEGDMA and 2HEMA-co-BMA-co-PEGDMA networks, the compositions that possessed maximal toughness within each network (29%MA and 598.8%2HEMA, respectively) did in fact exhibit a Tg in PBS that was close to 37°C (Tables 4.1 and 4.2 and Figure 4.18). Therefore, a possible approach to attaining enhanced toughness under physiological conditions is creating a network whose Tg in PBS aligns with body temperature.

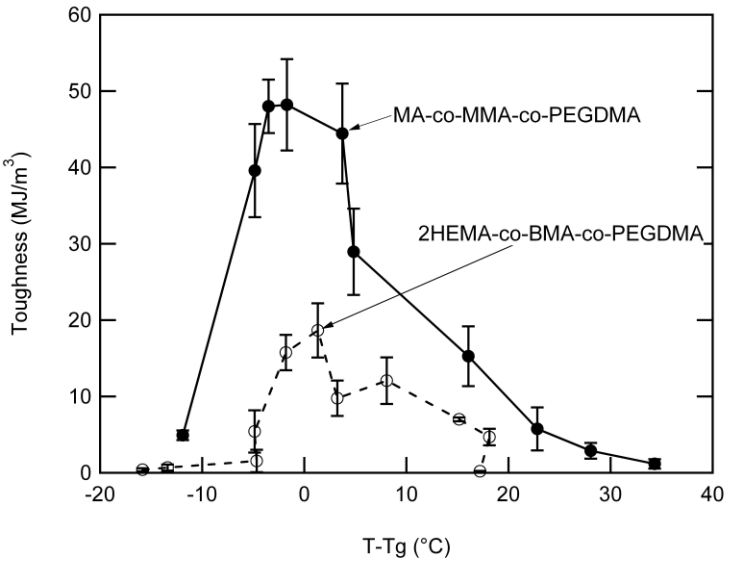

Figure 4.18. Network toughness as a function of the temperature difference between the testing temperature (T), 37°C, and the Tg determined in PBS for each composition.

It is also important to note that enhanced toughness is only achieved within a certain range of moduli (5-600MPa) for both networks (Figure 4.19). This three order of magnitude range indicates the limits in regards to network stiffness available in designing a tough polymer biomaterial using a shift in Tg approach. Because a compliance mismatch between the biomaterial and surrounding tissue could warrant possible device failure and further injury, it is important to align the modulus of the polymeric biomaterial with the native tissue. Considering the possible load-bearing types of biological tissues for which photopolymerizable networks could be utilized towards (i.e. tendon E=100-600MPa; intervertebral disc E=1-10MPa), several compositions from each network with enhanced toughness could be selected that possess similar moduli to native tissue.

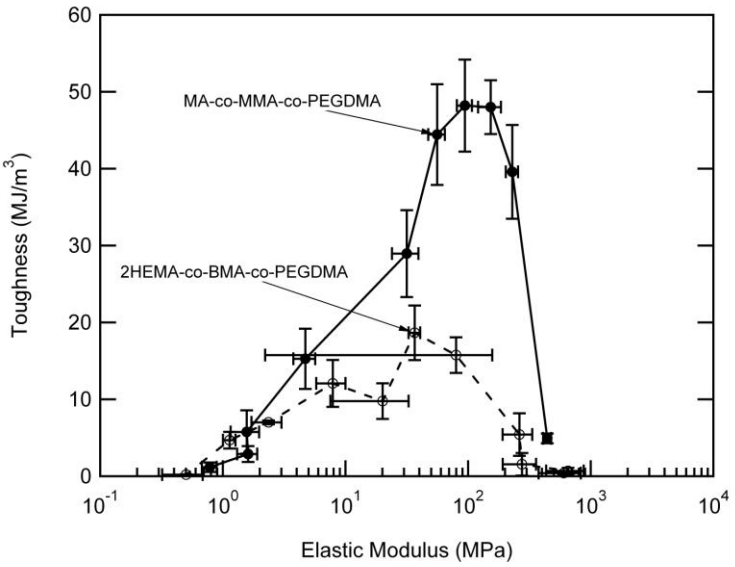

Figure 4.19. Network toughness as a function of elastic modulus for both meth(acrylate) networks tested in PBS. Values in figure are averages of several tests run for each composition.

It is well understood that temperature and time effects on the deformation of polymers can be superimposed [42]. In this study, the two compositions for each network identified as having maximal toughness (29%MA-co-MMA-co-PEGDMA and 58.8%2HEMA-co-BMA-co-PEGDMA) were deformed under tension in PBS at various strain rates to determine the sensitivity of toughness to varying the time scale. In both networks, toughness changes when the strain rate changes over several orders of magnitude with a maximum in toughness occurring at 5% strain/sec. This maximum is similar to the peak shown to occur in relation to the Tg of the network (Figure 4.17), but occurs more broadly over the range of strain rates tested. In addition, changing the strain rate affects the toughness more in MA-co-MMA-co-PEGDMA compared with 2HEMA-co-BMA-co-PEGDMA. The acute glass transition behavior of this network as observed through dynamic mechanical analysis suggests that the mechanical behavior would be highly dependent on strain rate while the broad transition of BMA-co-2HEMA-co-

PEGDMA networks makes this copolymer less affected by the magnitudes of relevant time scales. From these results, it is important to consider the loading rate of the mechanical environment to which the (meth)acrylate network would be utilized in the body. For the purposes of this study, the rates chosen represent loading rate that occur in the knee or spine under resting, normal, and high levels of activity [44].

Because the intended use of these networks is in an implantable biomaterial, PBS as a solvent was chosen to better mimic the physiological fluid and pH of the body. Although it is possible that salt could influence some of the above mentioned relationships, the chemical structures of the networks suggest they would not form interactions with the salt components. It is also important to note that the enhanced toughness in solution observed in this study is only representative of the polymer properties at a particular immersion time. In this study, immersion time in PBS was held constant (at 1 week) to allow each network to reach its swelling equilibrium, but this time point does not necessarily correspond to the complete stabilization of water-polymer interactions. Studies with PMMA have shown that plasticization will continuously occur well over a month [45]. Therefore because long term mechanical stability is important in many biomedical applications, future studies will examine the effect of varying immersion time over longer durations (i.e. months).

4.5 Conclusions

Three component (meth)acrylate networks were created to identify relationships between the glass transition region, water behavior, and tensile mechanical properties. One composition within each network was identified as possessing enhanced toughness.

Both compositions possessed T_g's close to body temperature, had average elastic moduli values between 50-100MPa in PBS, and exhibited slight PBS absorption (2-3%). The tailoring of T_g to achieve enhanced toughness in the two networks was achieved by two different mechanisms. In the MA-co-MMA-co-PEGDMA network, T_g was adjusted through a co-polymer mixing effect and the amount of free water found within the network. The T_g of the 2HEMA-co-BMA-co-PEGDMA network was adjusted by changing the hydrophilicity and subsequently, the total water content of the network. These relationships may be utilized to design photopolymerizable (meth)acrylate networks that will maintain the needed mechanical properties under aqueous conditions found within the body.

CHAPTER 5

EFFECT OF LONG TERM EXPOSURE TO PHYSIOLOGICAL CONDITIONS ON THE TOUGHNESS OF (METH)ACRYLATE NETWORKS

5.1. Introduction

In recent years, polymer-based biomaterials have been adopted for many orthopaedic implant applications over metal or ceramic-based implants because their compliance aligns better with native biological tissues, thus reducing stress shielding effects and potential tissue degeneration [154]. In particular, photopolymerizable polymers offer additional advantages in that they can be formed *in situ* and into complex geometries rendering them useful for minimally invasive procedures [26]. Many photopolymerizable material platforms, such as acrylate networks, also possess readily tailorable material properties through changes in network chemistry and structure [155-156]. These materials have been proposed as cartilage tissue replacements [157], bone cement [158], and shape memory fixation devices [156]. Although acrylate materials are very versatile from a processing and surgical methods standpoint, their "durability" based mechanical properties are considerably less than alternative implant materials such as PE or PEEK. In this work we aim to better understand the toughness of a model acrylate system as a function of longer-term exposure to aqueous solutions.

Besides having the appropriate elastic modulus, a key characteristic of a viable orthopedic biomaterial is its ability to withstand large mechanical loads and deformations for extended periods of time, requiring the material to be tough. Inherent toughness can be measured as the energy required to break a material and broadly reflects upon the

ultimate stress and strain the material can withstand. Inherent toughness has also been correlated to other important properties of implant materials including wear resistance, suggesting that toughness maybe an indicator of "overall" material durability [159]. Moreover, although acrylate-based materials have good wear resistance for dental applications, they achieve this through extremely high degrees of crosslinking [160-161], a mode of strengthening not available to applications that require open networks with elastic modulus in the MPa to kPa range. Material durability or toughness is crucial in that premature mechanical failure of implants can lead to further tissue injury, pain, and additional surgical procedures. Polymer-based biomaterials are particularly plagued with unsuitable toughness due to the inherent trade-off between low modulus and toughness [162].

Another prevalent issue with polymers implemented in biomedical load-bearing applications is the loss of their mechanical properties, including toughness, after implantation due to the exposure to physiological conditions, particularly moisture [163-164]. This effect, termed plasticization, is typically driven by the presence of polar chemical groups in the network structure that thermodynamically drive water molecules into the network resulting in increased chain mobility that reduces the strength and modulus but increases ductility [54, 82]. This change in mechanical properties is associated with a reduction in the glass transition temperature (Tg) of the polymer. If the network is able to uptake enough water, its mechanical behavior will transition swiftly from glassy to rubbery indicating that the amount of water absorption dictates the degree of change in Tg and thus, mechanical properties [82, 164].

In Chapter 4, the toughness of a (meth)acrylate-based network containing methyl acrylate (MA) and methyl methacrylate (MMA) crosslinked with poly(ethylene glycol dimethacrylate) (PEGDMA) was shown to increase significantly at 37°C after one week immersion in phosphate buffered saline (PBS) when the Tg was tailored close to body temperature by adjusting the comonomer concentrations of MA to MMA. The optimal composition, 29MA-co-MMA-co-PEGDMA, exhibited a toughness several orders of magnitude higher than other compositions and had an elastic modulus (100MPa) that aligned closely with many orthopaedic soft tissues [164]. However, the effects of long term exposure to PBS on the toughness of these materials have yet to be determined. Because it is desired that the implant maintain its function for years, the mechanical properties, including toughness, must be maintained throughout this period. Many studies have evaluated how moisture affects the mechanical properties of polymers after 24hrs to 1 week exposure to moisture [54, 164-165], but few studies have examined the effects of long term exposure to water over many months on the toughness of photopolymerizable networks [81, 166-167].

Thus, the primary objective of this study was to evaluate how immersion time in PBS affects the toughness of MA-co-MMA-co-PEGDMA networks containing various concentrations of MA. The tensile mechanical properties were determined by performing tensile strain-to-failure testing after soaking in PBS for different amounts of time (1 day up to 9 months). In addition, the Tg and PBS content were assessed in order to determine if time-dependent changes in toughness are related to changes in Tg or PBS absorption. From this study, PBS absorption is shown to affect network toughness in a manner that differs from short term conditions and that a polymer with suitable toughness initially in

PBS can eventually lose its toughness after long term exposure. These results have ramifications on the toughening of materials considered in this study (MA-co-MMA-co-PEGDMA) and possibly other acrylate systems being considered for biomedical applications such as in-situ cured acrylates [18, 20, 29] or shape memory polymers acrylates [10, 41].

5.2 Materials and Methods

5.2.1 Materials

Methyl methacrylate (MMA), methyl acrylate (MA), dodecanediol dimethacrylate (DDDA) and poly(ethylene glycol) dimethacrylate (PEGDMA) with a molecular weight of M_n=750 were obtained from Sigma-Aldrich and used as received. 2,2 dimethoxy 2-phenylacetophenone (DMPA) was used as the photoinitiator and was purchased from Sigma-Aldrich as well. Ultra high molecular weight polyethylene (UHMWPE) was obtained in 1mm thick sheets from McMaster-Carr, Inc (Atlanta, GA). The chemical structures of the monomers are shown in Figure 5.1.

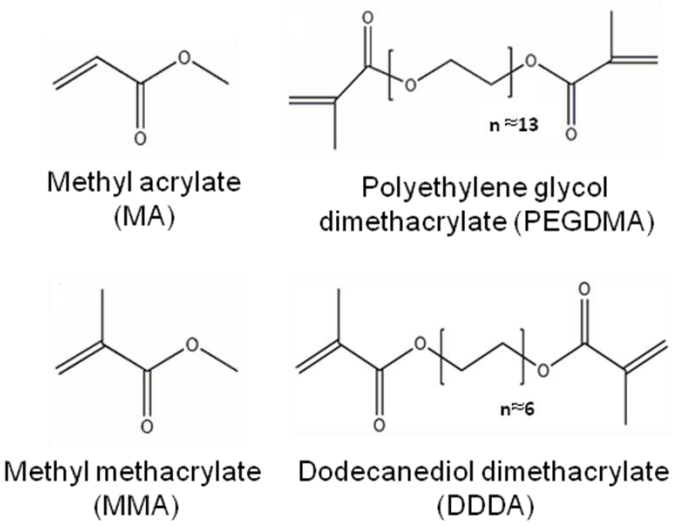

Figure 5.1. Chemical structure of monomers incorporated into the networks.

5.2.2 Synthesis

MA-co-MMA-co-PEGDMA solutions were prepared by combining ratios of MA and MMA by weight percentage with 10wt.% PEGDMA and 1wt.% DMPA. Four compositions with varying MA concentrations were used for further testing. A MA-co-MMA-co-5%DDDA network consisting of 50%MA and 45%MMA (50MA) was created in the same manner. Each solution was mixed manually in a glass vial and injected between two Rain-X coated glass slides using a glass pipette. Slides were separated with two 1mm glass spacers. To prevent leakage of the MA-co-MMA-co-PEGDMA solution, all four sides of the slides were taped. The samples were placed in a UV chamber (Model CL-1000L Ultraviolet Crosslinker; λ=365nm; energy=2000x100$\mu J/cm^2$) for 30 minutes.

5.2.3 Characterization

Test samples of each composition were incubated in phosphate buffered saline (PBS; Sigma-Aldrich) at either room temperature or 37°C for up to 9 months and then subjected to the following regime at various time points.

Tensile Testing

To determine the networks' stress strain behavior, polymer sheets were laser cut into ASTM D638 Type IV dogbones and strained to failure in tension mode at a strain rate of 5% strain/sec using a MTS Insight 2 with a 2kN load cell. Before testing, the edges were sanded to remove any defects from the laser and the width and thickness in the gauge section were measured using digital calipers. All tests, except for dry, were performed in an environmental chamber filled with PBS heated to 37°C. Samples were

allowed to equilibrate to the testing temperature for 10 minutes before initiating the test. Only samples that broke in their gauge length were used for property calculations. Toughness was calculated as the area under the stress-strain curve in units of MJ/m^3. Elastic modulus was calculated as the slope of the initial linear portion of the stress strain curve for each test (n=4).

Differential Scanning Calorimetry

The Tg of each network was determined by performing differential scanning calorimetry (DSC; TA Instruments Q100, Newcastle, DE) under a nitrogen environment. Samples were weighed on a balance (average sample mass between 10-15mg) prior to testing. Samples were cooled to -80°C and subsequently heated to 200°C at a constant rate of 5°C/min. The glass transition temperature was denoted as a second order endothermic transition, a step change on the DSC curve. Average Tg and standard deviation were calculated for each composition at each time point (n=3).

PBS Absorption

To evaluate the equilibrium swelling behavior of each network, 5mm x 20mm samples were soaked in PBS and their mass was measured at each time point (W_W). Each sample was dried in a vacuum (-15 in. Hg) at 40°C for 24 hours and the mass was measured again (W_D). Water content (W_f) was calculated according to the formula:

$$W_f = \frac{W_w - W_D}{W_D} \times 100$$

Average values and standard deviation were calculated for each composition (n=4).

5.3 Results

5.3.1 Stress-Strain Behavior

Representative stress-strain curves for each composition at select time points are displayed in Figure 5.2. The stress-strain behavior of MA-co-MMA-co-PEGDMA networks was affected by the time exposed to PBS in a manner dependent on the copolymer composition. For 18MA shown in Figure 5.2a, one day immersion in PBS resulted in a change in behavior from brittle to ductile, corresponding to decreased ultimate tensile stresses and elastic modulus but increased failure strains. Past one day in PBS, failure strains declined and elastic modulus increased as immersion time increased, mimicking the stress-strain behavior observed under dry conditions. In Figure 5.2b, 29MA experiences a progressive decrease in modulus and ultimate stress from 40MPa to 20MPa and increase in failure strain from 20% to 250% as immersion time increased to 7 days. Beyond 7 days in PBS, the stress-strain behavior remains stabilized until the 9 month time point where average failure strains decreased from 260% to 160% and average elastic moduli increased from 170MPa to 260MPa. Similarly, 36MA networks experienced a decrease in ultimate stresses from 18MPa to 5MPa and elastic modulus from 500MPa to 15MPa and increase in failure strains from 140% to 380% when exposed to PBS for 7 days (Figure 5.2c). However, unlike 29MA, there was no change in stress-strain behavior at longer time points in PBS. In Figure 5.2d, the stress-strain behavior of 72MA changed from a viscoelastic to rubbery state after 1 day in PBS corresponding to a decrease in elastic modulus from 1.5MPa to 1MPa and failure strain from 250% to 100%. After the initial 24 hours in PBS, no additional changes in stress-strain behavior were observed for 72MA at longer time points in PBS.

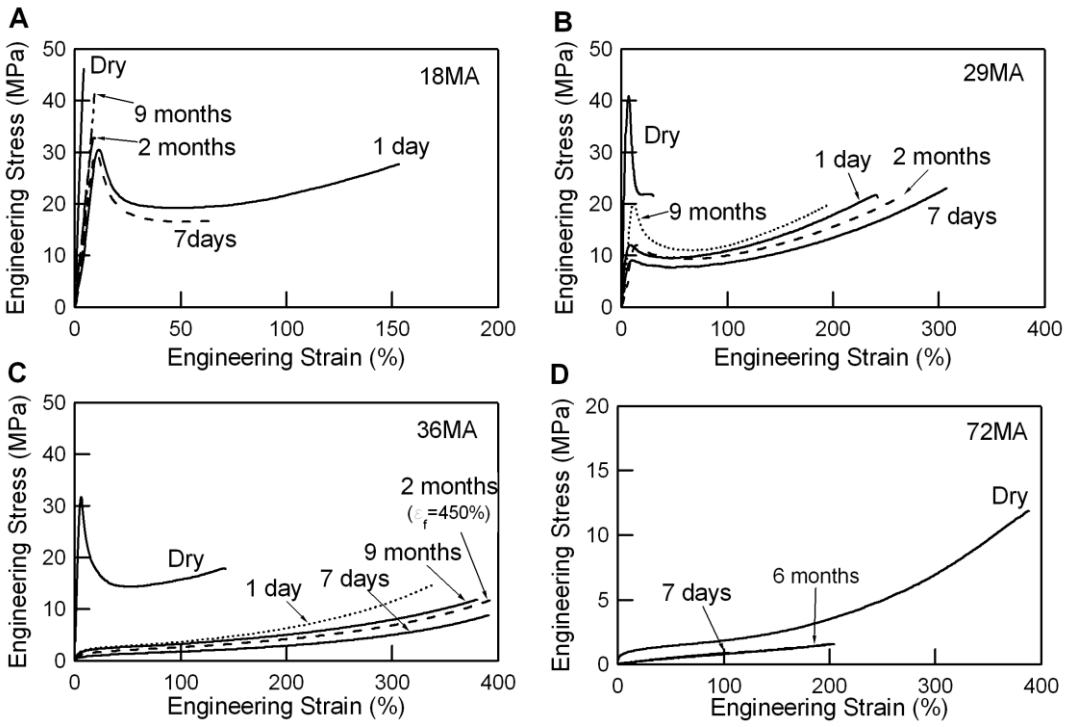

Figure 5.2. Effect of immersion time in PBS on the stress-strain behavior of (A) 18MA, (B) 29MA, (C), 36MA, and (D) 72MA. Each graph shows representative stress-strain curves for each composition tested at each time point.

5.3.2 Toughness

Mean toughness (± standard deviation) values as a function of time for each composition are displayed in Figure 5.3. UHMWPE is included in both figures for comparative purposes. The toughness of UHMWPE progressively increased with immersion time up to 6 months in PBS, but then abruptly decreased from 80MJ/m^3 to 30MJ/m^3 at 9 months. In Figure 5.3a, it can be seen that 29MA exhibits significantly higher toughness than 18MA after longer time spans in PBS, but lower toughness compared with UHMWPE, although not significant. Specifically, the toughness of 18MA increased with initial exposure to PBS but gradually decreased with longer exposure to PBS. On the other hand, toughness of 29MA increased after the initial 24 hours in PBS

and remained relatively stable around 35-40MJ/m^3 for up to 9 months in solution. In Figure 5.3b, the toughness of 36MA did not change with immersion time in PBS after the first 24 hours, but remained around 20-25MJ/m^3. A similar relationship with immersion time was observed for 72MA, although toughness values were less compared with that for 36MA.

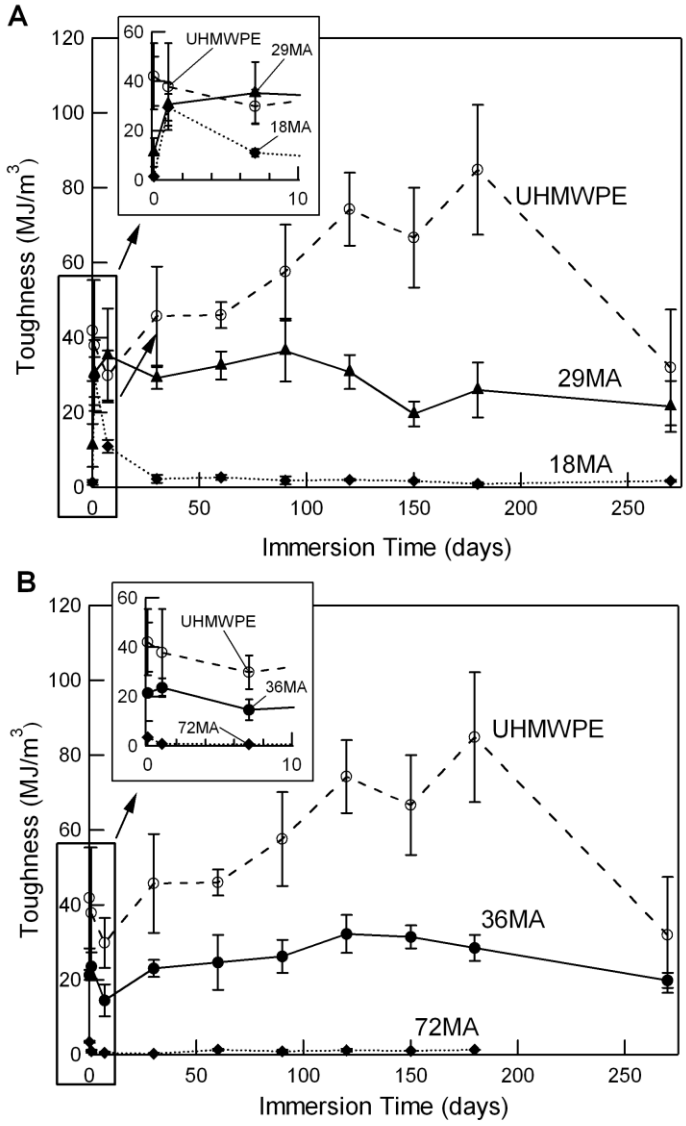

Figure 5.3. Effect of immersion time on the toughness of (A) 18MA and 29MA and (B) 36MA and 72MA networks tested at 37°C. UHMWPE is included on both graphs for comparative purposes.

5.3.3 Glass Transition Behavior

Differential scanning calorimetry (DSC) was performed to determine any relationships between the stress-strain behavior in PBS and Tg. The mean Tg's as a function of immersion time in PBS are shown in Figure 5.4. For all compositions, 1 day exposure to PBS resulted in a significant decrease in Tg compared with dry conditions. However, the effect of PBS on Tg varied with composition at later time points. For example, the Tg of 18MA significantly increased from 43°C at 1 day to 51°C at 9 months in PBS, close to its initial dry Tg. Similarly, the Tg of 29MA also significantly increased from 40°C to 45°C after 9 months immersion in PBS. For 36MA, Tg continued to decrease up to 2 months in PBS from its initial dry value (48°C) but then gradually increased at 3, 4, and 5 months to 40°C before decreasing to 30°C at 9 months. 72MA did not exhibit any significant change in Tg beyond the initial decrease at 1 day.

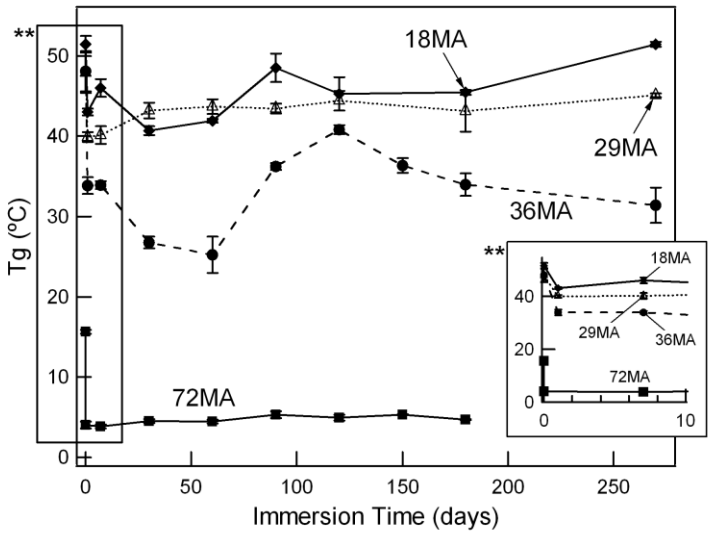

Figure 5.4. Effect of immersion time on the Tg of MA-co-MMA-co-PEGDMA networks. The inset shows the average Tg values at early time points up to 7 days.

5.3.4 PBS Absorption

The water content of each network as a function of immersion time is shown in Figure 5.5. In order to ascertain how the MA concentration affected the diffusive behavior of PBS into the network, PBS content was measured at 1-6, 12, and 24hrs and the average water content as a function of time is shown for each composition in Figure 5.5a.72MA exhibited the highest PBS absorption while 18MA had the lowest PBS content after 24hrs. Fickian diffusion was determined by fitting data at early time points within the first 24 hours to the following equation [168]:

$$\frac{W_t}{W_\infty} = kt^\alpha$$

where W_t represents the mass of PBS sorbed at time t, W_∞ represents the mass of PBS sorbed at equilibrium, and k and α are system parameters. An α of 0.5 indicates fickian diffusion. Except for 72MA, the diffusion of PBS into the MA-MMA networks displayed a non-Fickian behavior. The average water content after longer time spans in PBS (i.e. months) is illustrated in Figure 5.5b. Standard deviation bars were removed for clarity purposes, but were within +/-0.5wt.% for all data points. After 1 week, little change in water content was observed at later time points in PBS with water contents falling around 1.5-3.0 wt.% for all compositions. Degradation was also measured at all time points and mass loss was less than 2% for all networks (data not shown) at 9 months indicating that water molecules were not hydrolyzing significant portions of the network.

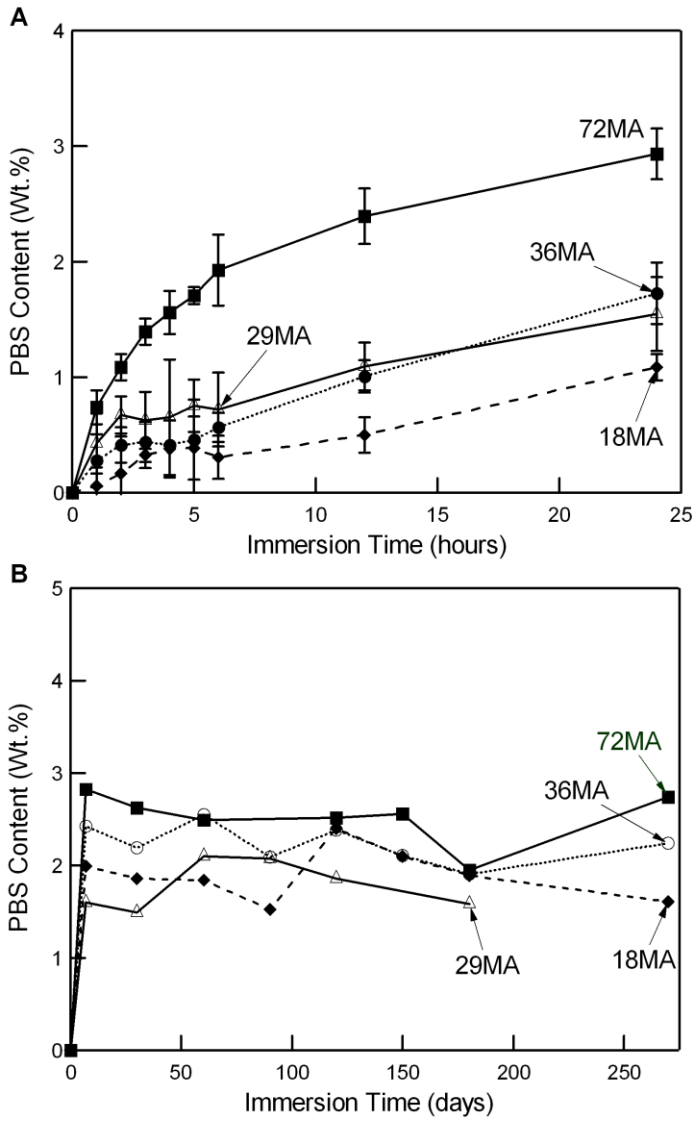

Figure 5.5. Effect of MA concentration on the PBS absorption into the network (A) for the first 24 hours in PBS and (B) after 9 months in PBS.

5.3.5 Effect of Increasing Hydrophobicity

To determine whether the effect of PBS on the mechanical properties of MA-MMA networks was affected by changing hydrophobicity, an MA-co-MMA network crosslinked with DDDA (instead of PEGDMA) was subjected to the same regime of testing after immersion in PBS. To minimize changes in network structure, a 5 wt.%

DDDA concentration was selected such that the network would possess the same crosslinking density as the MA-co-MMA-co-PEGDMA networks. Crosslinking density was determined by performing dynamic mechanical analysis and measuring the storage modulus (E_r) 20°C above Tg (data not shown). In this rubbery regime, Flory's theory relates crosslinking density to E_r by:

$$E_r = \frac{3\rho RT}{M_C}$$

where ρ is the polymer density, R is the universal gas constant, T is temperature (K), and Mc is the molecular weight between crosslinks.

In addition, the specific MA:MMA ratio, 50:45, was selected such that the network Tg aligned closely with 36MA in order to foster a direct comparison between PBS content and the change in toughness over time, independent of the initial viscoelastic state. In Figure 5.6a, it can be seen that PBS content is reduced in 50MA-DDDA compared with 36MA, an effect that does not change with immersion time up to 9 months. The effect of immersion time in PBS on the Tg of each network is shown in Figure 5.6b. Although the Tg of 50MA-DDDA is about 5°C higher than 36MA, both networks display the same change in Tg with immersion time with an initial decrease within the first 24 hours followed by a continual decrease to 2 months and then an increase close to the original dry Tg through 4 months. While the Tg of 36MA continues to decrease as time increases to 9 months, the Tg of 50MA-DDDA remains constant up to 9 months. Figure 5.6c illustrates the effect of immersion time in PBS on the stress-strain behavior. Similar to 36MA (Figure 5.2c), the largest change is observed within the first 24hrs from a ductile to viscoelastic behavior corresponding to decreased modulus and increased failure strains. This behavior continues up to 7 days. After 2 months, the

behavior of 50MA-DDDA reverts back to that at 24hrs and is not further affected by immersion time through 9 months. As seen in Figure 5.6d, this change in stress-strain behavior over time does not correlate to any significant change in toughness over months' time scale in PBS. At 9 months, the mean toughness of 50MA is greater than that for 36MA and similar to UHMWPE.

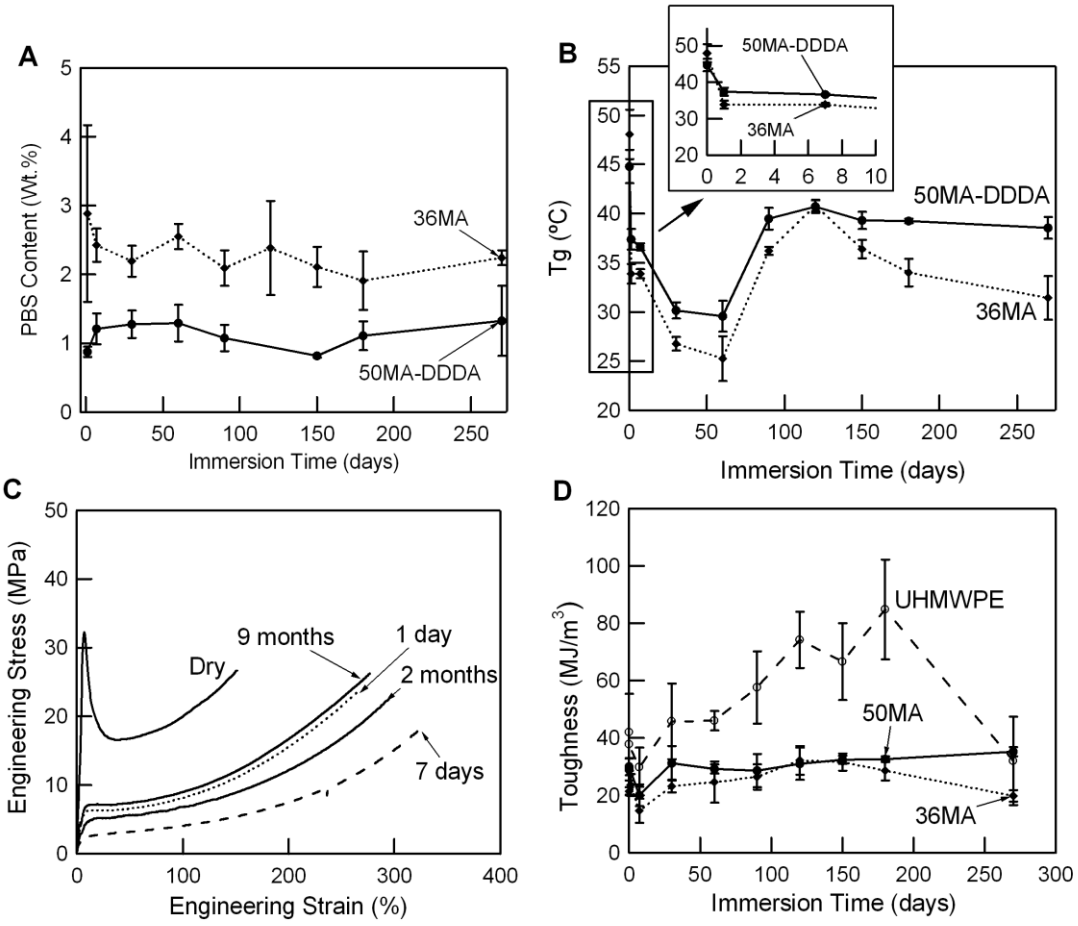

Figure 5.6. Effect of adding a hydrophobic crosslinker (DDDA) on the properties of MA-MMA networks. (A) PBS content, (B) Tg, (C) stress-strain behavior, and (D) toughness as a function of immersion time are shown for 50MA-DDDA in comparison with 36MA. p values<0.05 for 50MA-DDDA vs. 36MA at 9 months for PBS content and Tg.

5.3.6 Effect of Immersion Temperature

To determine if the effect of immersion time on toughness would be affected by temperature, samples were soaked in PBS at 37°C to simulate implantation temperature for up to 2 months. The effect of immersion time on the toughness of 29MA, 36MA, and 50MA-DDDA incubated in PBS at room temperature (23°C) and 37°C are displayed in Figure 5.7. For 29MA and 36MA, average toughness increased after 24 hours when samples were immersed at 37°C versus 23°C, but then significantly decreased below that of samples soaked at 23°C after 1 month immersion. In contrast, 50MA-DDDA exhibited a lower toughness after immersion at 37°C compared with the toughness at 23°C after 24h and maintained this level of toughness at later time points up to 2 months.

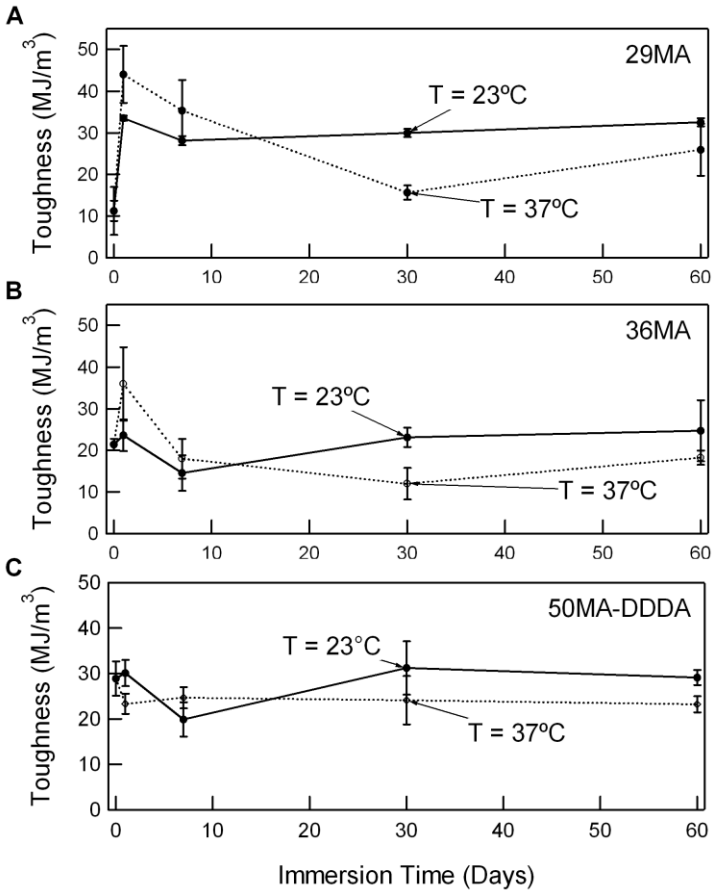

Figure 5.7. Toughness as a function of immersion time for (A) 29MA, (B) 36MA, and (C) 50MA incubated in PBS at temperatures (T) of 23°C and 37°C. Student's t-test was performed to determine statistical significance between values assessed at room temperature and body temperature at each time point for each composition. $p<0.05$ for 29MA at 1 and 30days and 36MA at 30days.

To elucidate mechanisms by which toughness was affected by incubation temperature, Tg and water content were measured for samples soaked for various amounts of time in PBS. As seen in Figure 5.8, the Tg of 29MA decreased significantly more upon exposure to PBS when the incubation temperature was increased to 37°C, an effect that remains up to 2 months in PBS. Similarly after 7 days, 36MA and 50MA-DDDA experienced a larger decrease in Tg upon initial immersion when incubation temperature increased; however after 2 months immersion, Tg for both materials was

higher when incubated at 37°C versus 23°C. Increasing incubation temperature also affected the PBS content for 29MA (Figure 5.9a) after 7 days immersion by almost doubling the water content at all time points up to 2 months immersion. This effect was not observed for 36MA and 50MA (Figures 5.9b and 5.9c) at all time points up to 2 months in PBS.

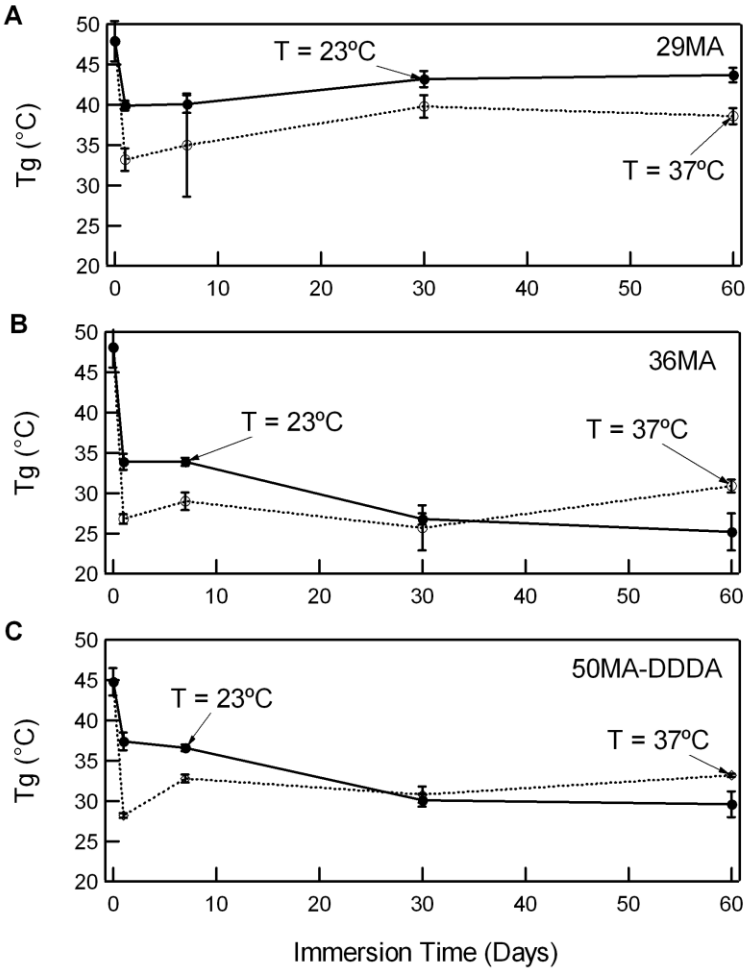

Figure 5.8. Tg as a function of immersion time for (A) 29MA, (B) 36MA, and (C) 50MA incubated in PBS at temperatures (T) of 23°C and 37°C. Student's t-test was performed to determine statistical significance between values assessed at room temperature and body temperature at each time point for each composition. $p<0.05$ at all time points except 29MA at 7 days, 36MA at 30 days, and 50MA-DDDA at 60 days.

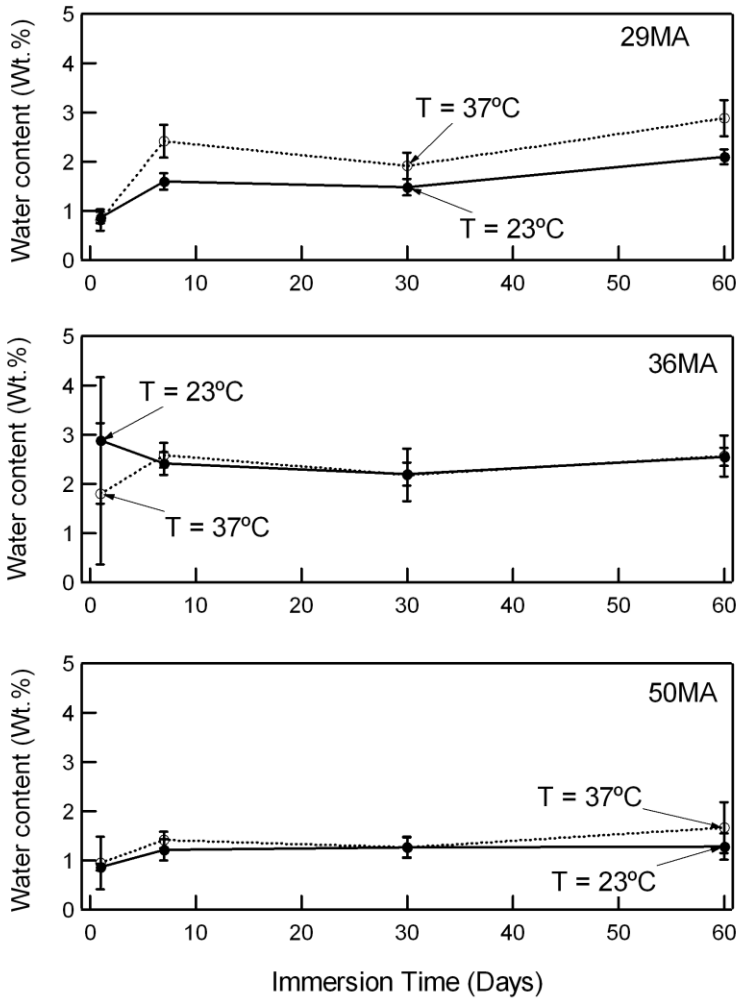

Figure 5.9. Water content as a function of immersion time for (A) 29MA, (B) 36MA, and (C) 50MA incubated in PBS at temperatures (T) of 23°C and 37°C. Student's t-test was performed to determine statistical significance between values assessed at room temperature and body temperature at each time point for each composition. $p<0.05$ for 29MA at 7 days and 60 days.

5.4 Discussion

A key criterion of many biomedical implant materials is their ability to maintain their physiological function for long time spans in the body. For implants that specifically serve a mechanical function, the mechanical properties of the material, including toughness, must not significantly degrade over long time scales in a physiological environment. Previous studies have reported on how water absorption affects mechanical

properties, but these studies have focused on glassy polymers [54, 81, 165, 167, 169] or on rubbery hydrogels that possess inherently poor mechanical properties [82]. Because it is known that toughness can be enhanced by designing a network whose Tg is just above the testing temperature, it is important to gain an understanding of how immersion time affects the relationship between Tg and toughness of polymer networks as well as ascertain whether the network toughness optimized using this approach can be maintained long term in PBS.

The MA-co-MMA-co-PEGDMA network was chosen for this study as a model system due to its previously reported tailorability of mechanical properties by varying the weight ratio of MA to MMA [164]. Specifically, adding more MA to the network results in a decrease in Tg causing a precipitous change in mechanical properties from glassy to ductile to rubbery with increasing MA concentration, with toughness reaching a maximum in the composition whose Tg is slightly above the testing temperature (i.e. body temperature). The compositions used in this study were selected based on their specific thermomechanical properties. For example under dry conditions, 18MA exhibits a Tg well above testing temperature and thus exhibits glassy, brittle behavior. With a Tg just above testing temperature, 29MA exhibits ductile tensile behavior under dry conditions maintaining adequate strength and modulus while also deforming to large strains providing good toughness. On the other hand, 36MA has a Tg at testing temperature and thus, possesses relatively viscoelastic behavior characterized by slight yielding, large strains, and in some cases strain hardening. Finally, 72MA has a Tg well below the testing temperature and thus exhibits rubbery behavior by having a low modulus and toughness. By comparing the effects of immersion time on the mechanical

properties of each composition, relationships between polymer viscoelasticity, water absorption, and toughness can be examined.

Examining the water content, Tg, and toughness for each composition as a function of immersion time (Figures 5.3, 5.4, and 5.5), it can be suggested that PBS absorption affects the mechanical properties of MA-MMA-PEGDMA networks in a biphasic manner. In the initial phase of absorption (less than 7 days), the Tg of each composition decreases to an extent governed by the amount of PBS absorbed into the network (Figure 5.4). This decrease in Tg with PBS absorption has been previously shown in other acrylate-based networks and is attributed to water molecules disrupting secondary intermolecular bonding to form their own hydrogen bonds with polar groups such as ester and ethylene glycol groups within the network [35, 82, 164]. Consequently, the PBS-induced reduction in Tg causes the stress-strain behavior of each network to change by experiencing a decrease in tensile strength and modulus, and an increase in failure strain, commensurate with the shift in Tg relative to a fixed testing temperature (Figure 5.2).

It has previously been suggested that network toughness will reach a maxima when Tg aligns with body temperature, and thus when Tg decreases due to PBS absorption, toughness will either increase or decrease depending upon the location of Tg in PBS in relation to body temperature [162]. From Figures 5.3 and 5.4, the results of this study further support this idea. For example, both 18MA and 29MA have a dry Tg above testing temperature but when PBS is absorbed, Tg is reduced closer to testing temperature, thus causing toughness to increase after 24hrs in PBS. On the other hand, 36MA initially has a Tg about 5°C above 37°C and exhibits a decrease in Tg to below

testing temperature at 7 days causing toughness to moderately decrease. 72MA has a Tg well below testing temperature and experiences the largest change in Tg, but because toughness is already low for this network there is no significant change in toughness with PBS absorption.

Considering the stress-strain behavior and Tg's of each composition at later time points in PBS (i.e. monthly time scale), the PBS absorption continues to affect the mechanical properties in a manner that does not follow the relationship between Tg and stress-strain behavior outlined above, but rather is dependent on the viscoelastic or relaxation state of the copolymer after 24hrs immersion in PBS. For example, after 1 month in PBS, 18MA, a glassy network, experiences an increase in modulus and decrease in failure strains indicative of the material reverting back to its behavior pre-immersion (Figure 5.2a). This change in stress-strain behavior results in an order of magnitude decrease in toughness that continues to decline with longer immersion time in PBS. Interestingly, this initial reversion to a brittle state is accompanied by an increase in Tg but no change in PBS content after one month suggesting that mechanisms other than a change in PBS content are affecting the polymer mechanics. For 29MA (Figure 5.2b), the stress-strain behavior as a function of immersion time follows a similar trend as 18MA via increasing modulus and decreasing in failure strains as immersion time increases, but this effect does not become evident until after 6 months in PBS.

These changes in mechanical properties over time for the 18MA and eventually 29MA copolymers can be attributed to a combination of the water diffusion kinetics and molecular relaxation dynamics of the polymer-PBS system. Since the MA-co-MMA networks are mostly hydrophobic, water diffusion is driven partially by the formation of

hydrogen bonds with water-binding sites in the network [164], but is mostly affected by factors such as chain mobility and the amount of free volume present [88, 170]. This is made evident by the non-fickian diffusion behavior observed for these two compositions during initial PBS absorption (Figure 5.2a), a characteristic of most glassy polymers that have limited chain mobility [88]. Previous studies have shown that chain mobility increases and free volume decreases as temperature approaches Tg [171]. Thus, the lower Tg of the 29MA network compared with 18MA suggests that chain mobility in 29MA is increased compared with 18MA providing less initial free volume in the network for water molecules to inhabit. Thus if the chains are rigid, the water molecules absorbed into the network are challenged to find any binding sites on the polymer and instead will cluster into microvoids causing segmental chain rearrangements [172]. As water molecules accumulate in these voids, microcrazes are created that can lead to a loss of extensibility and pre-mature fracture during deformation as is observed with the 18MA and, to a lesser extent, 29MA compositions [169].

In addition, because these materials were immersed for long time spans in solution, changes in mechanical properties could also be caused by physical ageing effects. In general, physical ageing causes a decrease in chain mobility and specific volume due to a relaxation of the polymer chains over time resulting in an increase in Tg, but this effect is mitigated as the ageing temperature (room temperature in this study) approaches Tg [173]. The decreased failure strains and increased modulus of 18MA in combination with the upward trend of Tg with immersion time reflect similar findings from these previous studies (Figure 5.2a). Furthermore, because 29MA exhibits a Tg closer to the immersion temperature, the ageing rate is much slower compared with

18MA, thus potentially requiring more time for the chains to relax and the water molecules to form clusters in the microvoids. In fact, the upward trend in Tg at 9 months for 29MA suggests that longer exposure to PBS could potentially result in a further decrease in toughness.

In contrast, 36MA maintains its toughness after 9 months immersion in solution corresponding to a slight increase in modulus but no significant change in failure strain. Unlike 18MA and 29MA, 36MA possesses a Tg less than 10°C from immersion temperature after the initial 24hours in PBS and thus is in a more viscoelastic state having increased chain mobility. Looking at how Tg evolves with immersion time, there is interestingly a decrease in Tg at 1 and 2 months but a subsequent increase in Tg at later time points (Figure 5.4). This increase in Tg after 3 months could be attributed to the Tg reaching close to the immersion temperature causing a conformational rearrangement in the presence of PBS due to changes in chain flexibility that drives Tg on an increasing trend. Because the Tg of this composition hovers around the testing temperature, the associated high chain mobility allows for extensive chain deformation in the presence of water molecules without crazing occurring. This behavior drastically differs from 18MA and 29MA and suggests that tough networks whose Tg falls close to immersion temperature will have sustained toughness over long time spans in solution even if they do not have maximal toughness initially. Because 72MA is in its rubbery state having a Tg below 37°C upon initial PBS absorption, the mechanical properties are not further altered after the initial change due to the decline in Tg at 1 day. Thus, although the extra chain mobility helps to accommodate PBS storage in the 36MA sample, the completely

rubbery 72MA composition has overly free chain mobility and thus no inherent toughness once PBS penetrates the network.

To further discern whether the effect of immersion time on network toughness is determined by the total water content or Tg, a second copolymer network was created substituting the PEGDMA crosslinker with a more hydrophobic crosslinker, DDDA. DDDA has a similar hydrophobic structure as MMA and MA which reduces the amount of PBS absorption compared with the MA-co-MMA-co-PEGDMA networks (Figure 5.6a). The 50MA-DDDA network exhibits an initial Tg similar to 36MA and like 36MA, experiences the least change in stress-strain behavior beyond the initial change with exposure to PBS, and consequently, little change in toughness after 9 months immersion in PBS (Figures 5.6c and 5.6d). These findings further indicate that the viscoelastic state of the polymer, dictated by its Tg in relation to the environmental temperature, governs how water absorption affects long term mechanical properties rather than the total water content in the network, at least in low swelling networks. Interestingly, the overall toughness of 50MA-DDDA compared with 36MA is higher, almost equivalent to UHMWPE at 9 months. One possible explanation for this occurrence could be that the addition of DDDA allows for more hydrophobic bonding between pendant groups on the monomers [174] thus providing better overall strength during deformation, an effect that would not be inhibited but actually enhanced by the presence of PBS [35].

Under *in vivo* conditions, implant materials are exposed to moist conditions at body temperature during implantation. Therefore, samples of 29MA, 36MA, and 50MA-DDDA were also tested after exposure to PBS at 37°C, versus room temperature, to ascertain any temperature-dependent changes in toughness with immersion time. As seen

in Figures 5.7, 5.8, and 5.9, temperature influences the relationship between PBS absorption and toughness in a manner that is dependent on composition. The increased toughness of 29MA at 37°C versus 23°C after 24h immersion can be attributed to a larger reduction in Tg when networks are soaked at elevated temperatures allowing the temperature that which peak toughness occurs closer to the testing temperature. Increasing temperature causes chain flexibility and free volume in the network to increase allowing more PBS to enter the network that will reduce the Tg to a greater extent compared with lower temperatures [35], thus causing a shift in toughness [162]. This effect is also observed in 36MA but not in 50MA-DDDA suggesting that the role of incubation temperature on immersion time-dependent changes in network toughness is determined by the network hydrophilicity rather than its initial viscoelastic state.

This study demonstrates that MA-co-MMA networks, given the right composition and resulting glass transition behavior, can have enhanced long-term toughness. It is also important to note that these relationships between toughness, immersion time, Tg, and PBS content can possibly be extended to other relevant polymer systems, including photocured and degradable materials where improving toughness, without losing degradability, has proven challenging to date [175-176]. Based on the results of this study, MA-co-MMA-co-DDDA networks have the potential to serve as implant materials for load-bearing biomedical applications given the stability of mechanical properties after 9 months exposure in PBS. Depending on the specific application, the modulus can also be tuned to match that of surrounding tissue without compromising toughness [164]. These materials can also be programmed to exhibit shape memory properties or photopolymerized *in situ* allowing them to be implanted in a minimally invasive manner.

However, to further verify these materials' efficacy under *in vivo* loading environments, extensive testing involving more complex loading regimes and cellular biocompatibility are necessary.

5.5. Conclusion

The long term stability of mechanical properties, specifically toughness, of MA-co-MMA networks was evaluated in the presence of PBS in an effort to determine whether these acrylate-based materials could be exposed to physiological conditions for long implantation times. It was shown that copolymer networks in a glassy state experience a stiffening effect and loss of extensibility after several months in PBS that is linked with a gradual increase in Tg and significant decrease in toughness while networks whose Tg fall close to the testing temperature maintain their mechanical properties up to 9 months in PBS. The addition of a hydrophobic crosslinker (DDDA) reduced water content, thus further improving the long term toughness of MA-co-MMA networks. One network, 50MA-co-MMA-co-5DDDA, was shown to have comparable toughness to UHMWPE at 9 months and could thus be an appropriate material for high load-bearing biomedical applications. These results provide insight into strategies for improving the long term toughness of not only photopolymerizable (meth)acrylate networks but other polymer-based material platforms that are implemented in load0bearing biomedical applications.

CHAPTER 6

EFFECT OF CHEMISTRY AND STIFFNESS OF (METH)ACRYLATE NETWORKS ON *IN VITRO* OSTEOBLAST RESPONSE

6.1. Introduction

Understanding the interaction between cells and an implant material is of great importance in ensuring the implant's effectiveness. Many studies have examined how various material surfaces affect the osteoblast response and peri-implant bone formation [11, 91, 104-105, 107-109, 112, 114, 116, 177]. These studies indicate that implants are more likely to osseointegrate with surrounding bone when cells cultured *in vitro* on the material surface form a cuboidal morphology, exhibit elevated levels of differentiation markers including alkaline phosphatase specific activity and osteocalcin, and produce more osteogenic factors. Materials with these properties have improved bone to implant contact and increased pullout strength when tested *in vivo* [91, 127-128].

In order to understand how materials affect bone formation, it is important to determine how specific surface characteristics including the surface wettability, topography, and stiffness mediate the osteoblast response. For example, wettability,

*Modified from
Smith KE, Hyzy SL, Sunwoo M, Gall K, Schwartz Z, and Boyan BD. The dependence of the osteoblast response to (meth)acrylate networks on chemical structure and stiffness. *Biomaterials*, 2010; 31(24): 6131-6141.

as measured by the contact angle between water droplets and the surface, affects both cell attachment and proliferation [103] by changing the surface presentation of extracellular matrix proteins to which cells bind. On hydrophilic metal oxide surfaces, human osteoblast-like MG63 cells exhibit a differentiated phenotype and also secrete factors that create an osteogenic microenvironment [105]. Increasing surface roughness also promotes osteoblast attachment and differentiation in a manner dependent on the size scale of the topographical features [91, 107-110]. For instance, MG63 cells become more differentiated on titanium with micron scale roughness in comparison to smooth or sub-micron scale rough surfaces [111].

Several studies have reported that cell attachment, proliferation, and differentiation are all modulated by the substrate rigidity to a degree dependent upon the substrate stiffness in relation to the stiffness of the native tissue [11, 113-117]. In other words, cells will mimic their *in vivo* behavior more when they are cultured on substrates whose rigidity matches that of that cell type's native tissue matrix. Kong et al. have proposed that this modulated osteoblast response relates to the cells' ability to more efficiently generate force through their cytoskeleton in response to the larger resistance induced by the rigid substrate [113], and that these generated traction forces will alter the assembly of intracellular machinery that drives its ability to enter the cell cycle or differentiate [115]. These findings suggest that the mechanical microenvironment can have implications on developing therapies to promote bone formation and osseointegration.

Despite these advancements, it has proven challenging to independently vary the stiffness of the substrate without drastically changing chemistry or functionalizing the

surface with bioactive molecules [11, 114, 116]. For most studies, polyacrylamide substrates crosslinked with different concentrations of bis-acrylamide were produced to attain surfaces with various moduli [11, 116], but it has been shown that osteoblasts can alter their morphology in response to changes in network structure, suggesting that network chemistry, independent of wettability, could be a potential regulator in the overall cell response [9]. To overcome the chemistry effect, polymer substrates are coated with extracellular matrix ligands, usually either collagen or arginine-glycine-aspartic acid (RGD) peptides [11, 114], but this approach does not represent how actual polymer implant surfaces affect the osteoblast response. Also, the relationship between matrix elasticity and cell response has mostly been reported on substrates with moduli less than 1MPa; however most orthopaedic polymer implants possess moduli in the megaPascal to gigaPascal range. In one instance, the effect of moduli ranging between 100-500MPa was indirectly studied using bone marrow stromal cells on a biodegradable polymer network, but no significant difference in cell number, alkaline phosphatase activity, or osteopontin expression was observed, potentially due to the complex trade-offs of chemistry, degradation and substrate mechanics [177]. Thus, a copolymer system with a modulus that is tunable over several orders of magnitude with little change in chemistry would be useful to study the relationship between polymer properties and cell response.

Due to their easily tailorable properties, (meth)acrylate networks serve as excellent model systems to evaluate how certain polymer chemistries and material properties affect the osteogenic response. In this present study, the first objective was to measure the local surface modulus of cortical and trabecular human bone both in mineralized and demineralized states to determine the mechanical environment

osteoblasts sense during different stages of remodeling. Based upon the determined moduli, a copolymer system comprised of two PEG-based crosslinkers, poly(ethylene glycol) dimethacrylate (PEGDMA) and diethylene glycol dimethacrylate (DEGDMA) was designed with an elastic modulus that could be adjusted by varying the ratio of the two crosslinkers while still presenting the same surface chemistry. To further decouple the effects of chemistry and stiffness, a second copolymer network comprised of 2-hydroxyethyl methacrylate (2HEMA) and PEGDMA with various molecular weights was also used to test different chemical compositions while maintaining a range of moduli similar to the PEGDMA-co-DEGDMA networks. The response of MG63 osteoblast-like cells on each surface was evaluated by assessing morphology, cell number, and the production of certain osteogenic markers. Within this study, we present the first results showing that surface chemistry has a greater effect on osteoblast differentiation *in vitro* than surface stiffness even when stiffness is varied over two orders of magnitude.

6.2 Materials and Methods

6.2.1 Materials

Diethylene glycol dimethacrylate (DEGDMA), poly(ethylene glycol) dimethacrylate (PEGDMA; Mn~550 or 750), and 2-hydroxyethyl methacrylate (2HEMA) monomers were obtained from Sigma-Aldrich (St. Louis, MO) and used as received. 2,2-dimethoxy-2-phenylacetophenone (DMPA, Sigma Aldrich) was used as the photoinitiator.

6.2.2 Nanoindentation of Bone

Human trabecular and cortical (both periosteal and endosteal) bone were taken from donor femurs and tibias, courtesy of Musculoskeletal Transplant Foundation (Edison, NJ). The condyles were cut into 3mm thick trabecular sheets, then after all the surrounding cortical tissue was removed, cut to 2cm x 2cm trabecular wafers. The shafts were cleaned and cut to 2cm rings, and the rings with flat sides were used to make the 2cm x 2cm x 1cm cortical wafers. The wafers were cleaned with a combination of antibiotics, surfactant, and ethanol and then washed with deionized (DI) water. To demineralize the bone matrix, the wafers were soaked in 0.6N hydrochloric acid for 5 minutes. Both mineralized and demineralized wafers were rinsed in DI water, soaked in ethanol, dried, and stored at -70°C prior to shipping. Upon receipt, the wafers were stored at 5°C prior to use. The surface elastic moduli were determined by performing nanoindentation using a 130μm diameter spherical ruby tip on a NanoIndenter XP (MTS Systems Corporation, Eden Prairie, MN). The displacement of the tip into the surface was recorded as a function of tip load. Using Hertz' theory for the contact of a sphere into an elastic half space [26], model load vs. displacement curves were created from the following equation:

$$\delta = (\frac{3}{4E^*})^2 \frac{P^2}{R}$$

where P is the applied tip load, δ is the displacement into the surface, R is the tip radius, and E^* is the reduced modulus as determined by:

$$\frac{1}{E^*} = \frac{\left(1-\nu^2\right)}{E} + \frac{\left(1-\nu'^2\right)}{E'}$$

where v and v' are the Poisson's ratios and E and E' are the elastic moduli of the specimen surface and indenter tip, respectively. To determine the elastic modulus from the experimental load versus displacement curves, E values of the predicted curve were adjusted until the experimental data fit the predicted curve in the unloading region. Two wafers from each bone region were indented with the average modulus value calculated from at least 10 indents for each bone specimen.

6.2.3 Network Synthesis

Monomer solutions were formulated by combining various weight ratios of PEGDMA (Mn~750) and DEGDMA with 0.2 wt.% DMPA. The elastic modulus of the copolymer system was adjusted by varying the weight ratio of PEGDMA to DEGDMA. Three compositions (by weight %) were selected based on their determined moduli values: (1) 10%PEGDMA:90%DEGDMA (10PEG), (2) 50%PEGDMA:50%DEGDMA (50PEG), and (3) 90%PEGDMA:10%DEGDMA (90PEG). Each solution was mixed manually in a glass vial, filtered through 5μm filter paper under vacuum, and injected using a glass pipette between two glass slides separated with two glass spacers (thickness = 1mm). The sheets were placed in a UV chamber (UVP, Model CL-1000L Ultraviolet Crosslinker, Upland, CA; λ=365nm; energy=2000x100μJ/cm^2) for 10 minutes. Discs were laser-cut from the polymerized sheets to a diameter such that the disc of each composition would swell to fill the bottom of a well in a 24-well cell culture plate when incubated in cell culture media. All discs were post-cured in an oven at 90°C for 90 minutes and boiled in distilled water for 30 minutes to remove excess monomer. Discs were then sterilized by autoclaving at 121°C for 15 minutes.

To prepare the 2HEMA-co-PEGDMA surfaces, sheets were photopolymerized using the same procedure as the PEGDMA-co-DEGDMA copolymers using glass slides coated with poly(dimethylsiloxane) (PDMS; Dow Corning Sylgard 184; Midland, MI) to enhance release. Three compositions with the appropriate moduli were selected for the *in vitro* cell experiments (by weight %): (1) 65%HEMA:35%DEGDMA (65HEMA), (2) 80%2HEMA:20%PEGDMA (Mn~550) (80HEMA), and (3) 98%2HEMA:2%PEGDMA (Mn~750) (98HEMA). After laser cutting and sanding the edges, the discs were post-cured for 90 minutes at 90 °C and then soaked in distilled water for 3 days to remove excess monomer. Because these materials were unable to maintain their structural integrity during autoclaving, discs for these compositions were sterilized by UV light (λ=254nm) for 90 minutes.

6.2.4 Surface Characterization

Surface wettability was determined by performing contact angle measurements using the sessile drop method on a Ramé-hart goniometer (Mountain Lakes, NJ). A 3μL drop of deionized water was dropped onto the disc surface, and the contact angle between the side of the drop and polymer surface was measured using a camera and DROPimage CA software (Mountain Lakes, NJ). Three measurements of the left and right contact angle were taken on three separate discs of each composition.

Elemental analysis was performed by x-ray photoelectron spectroscopy (XPS) on a SSX-100spectrometer (Surface Science Laboratories, Mountain View, CA) under high vacuum ($3<10^{-8}$ Torr) using Al-Kα radiation (1486.6eV) and a pass energy of 50eV. Charge buildup on the polymer surfaces was neutralized by an electron flood gun at

3mV. To further correct for charging effects, the binding energies were offset such that the C1 peak was assigned to the binding energy of 284.6eV. Survey scans were obtained in the 0-1000eV range using 1 eV/step and 10 scans/time. Peak assignments and their corresponding area were determined using ESCA software (Service Physics; Bend, OR). Three scans were performed on three separate discs for each composition.

Fourier transform infrared (FTIR) spectroscopy in attenuated total reflectance (ATR) mode was performed to assess the chemical bonding present on the surface and compare the differences in the amounts of key chemical groups among the different copolymer systems. Spectra were obtained on discs using a Bruker Optics Tensor Spectrometer (Billerica, MA) with a KBr crystal. Ten scans were obtained on each sample at a 1Hz frequency and peak wavenumbers were determined using OMNIC software (Thermo Electron Corporation, Madison, WI). Three spectra were obtained for three separate discs for each composition.

To evaluate the surface roughness, atomic force microscopy (AFM) was performed using a Pacific Nanotechnology Nano-R AFM (Irvine, CA) in close-contact mode. Each sample was scanned using a scan size of 25x25μm at 0.5Hz frequency and a resolution of 512 scan lines. Average roughness (R_a) was calculated for each scan using the Pacific Nano Software (Irvine, CA). Three scans were performed on three separate discs for each copolymer system.

Surface elastic modulus was determined by performing nanoindentation using the same loading regime described above for bone. To simulate cell culture conditions, samples were soaked in phosphate buffered saline (PBS) prior to performing nanoindentation and placed on a sample mount immersed in PBS-soaked absorbent foam

to maintain hydration during indentation as illustrated in Figure 6.1 [178]. Previous testing (data not shown) suggested that the elastic modulus of a polymer changed with time when immersed in water. Thus, the elastic modulus was determined for all compositions after immersion in PBS for 24h or 7 days. Moduli values were determined from the load versus displacement curves using the method described above for the bone and the average elastic moduli was determined from at least 10 indents measured on at least three discs.

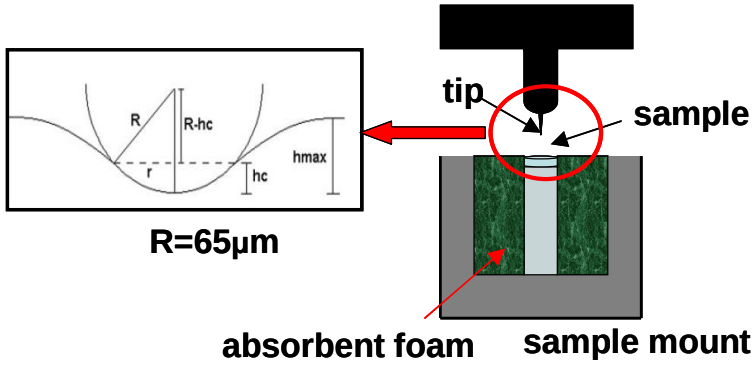

Figure 6.1. Testing setup for nanoindenting the polymer discs while submersed in PBS.

6.2.5 Cell Culture

Human MG63 osteoblast-like cells (ATCC, Manassas, VA) were cultured in Dulbecco's modification of Eagle's medium (DMEM, Cellgro, Manassas, VA), 10% fetal bovine serum (Hyclone, Waltham, MA), and 1% penicillin-streptomycin (Invitrogen, Carlsbad, CA) at 37°C, 5% CO_2, and 100% humidity. Polymer discs were soaked in media for 24h prior to plating in order to allow the discs to swell to fit the bottom of the culture well. To overcome the buoyancy of the polymer discs, CellCrown polymer inserts (Scaffdex, Finland) were used to anchor the disks. Cells were plated either on tissue

culture polystyrene (TCPS) or polymer discs at a density of 20,000 cells/cm^2 and cultured until cells reached confluence on TCPS, about 5-7 days.

6.2.6 Analysis of Cell Response

At confluence, fresh media were added to the cultures and cells were incubated for 24h prior to harvesting. At harvest, the conditioned media were collected from each well. Cells were released from the surfaces using two sequential trypsinizations to ensure all cells were collected. Cell number was determined using a Beckman Coulter Z1 particle counter (Fullerton, CA). Cells were lysed and alkaline phosphatase specific activity was measured as the release of *p*-nitrophenol from *p*-nitrophenylphosphate at pH 10.2 as previously described [179] and normalized to total protein (Pierce BCA Protein Assay, Thermo Scientific, Waltham, MA). Osteocalcin was measured in the conditioned media using a commercially available radioimmunoassay kit (Human Osteocalcin RIA Kit, Biomedical Technologies, Inc., Stoughton, MA) as previously described [108]. The amount of osteoprotegerin (OPG), vascular endothelial growth factor (VEGF), and total transforming growth factor- β1 (TGF-β1) released by the cells was determined by performing an enzyme-linked immunosorbent assay (ELISA) of the conditioned media (DuoSet ELISA kits, R&D Systems, Inc., Minneapolis, MN) as previously described [180-181].

To determine if cell morphology was affected by copolymer composition, cells cultured on the copolymer surfaces were examined by scanning electron microscopy (SEM). Cells were plated as described and cultured for 24h or to confluency. At each time point, the media were removed and the samples rinsed three times with PBS to remove the excess media. Samples were fixed with Karnovsky's fixative (Electron

Microscopy Sciences, Hatfield, PA) for 24h at room temperature. After fixation, the samples were freeze-dried for 48h. Samples were coated with a thin layer of gold and imaged using a Zeiss Ultra60 SEM with an SE2 detector (Carl Zeiss SMT Inc., Peabody, MA).

6.2.6 Statistical Analysis

Six experiments were performed using the PEGDMA-co-DEGDMA surfaces. For each experiment, data represent mean ± SEM of six independent cultures. Data were analyzed by performing an analysis of variance, and, when statistical differences were found, a Student's t-test for multiple comparisons using Bonferroni's modification was used. P values<0.05 were considered significant. To compare the relative levels with TCPS, each independent culture of 6 total per variable was normalized by the average of the TCPS control for each experiment resulting in a treatment/control ratio for each variable in a given experiment. The data shown represent the mean ± SEM of the treatment/control ratios for the six separate experiments (cell number and alkaline phosphatase specific activity) or four separate experiments (osteocalcin, OPG, VEGF-A, TGF-β1). Data were compared by the Wilcoxon rank sum test. Data presented from the 2HEMA-based surfaces are from one of two independent experiments, each with comparable results. Data are the mean ± SEM of six independent cultures and show absolute values rather than treatment/control ratios. Data were analyzed by performing an analysis of variance, and, when statistical differences were found, a Student's t-test for multiple comparisons using Bonferroni's modification was used. P values<0.05 were considered significant.

6.3 Results

6.3.1 Nanoindentation of Human Bone

The average elastic moduli values of all bone specimens are listed in Table 6.1. As would be expected, the moduli of demineralized cortical and trabecular bone decreased relative to fully mineralized bone by almost an order of magnitude, and mineralized cortical bone (periosteal or endosteal) had higher moduli compared with trabecular bone.

Table 6.1: Average elastic moduli values for human bone measured by nanoindentation.

Bone Region	E (MPa)	
	Mineralized	**Demineralized**
Cortical Periosteum	9905 ± 1763	871 ± 218*
Cortical Endosteum	11500 ± 1656	2364 ± 588*#
Trabecular	365 ± 223#^	92.7 ± 74.9*#^

*p<0.05 vs. mineralized for that region; #p<0.05 vs. cortical periosteum; ^p<0.05 vs. cortical endosteum

In order to identify any similarities in the nanomechanical loading behavior of bone compared with the copolymers, representative load vs. displacement curves from the unloading regime are illustrated for each type of bone and copolymer in Figure 6.2. The load versus displacement behavior of 10PEG fell in between the measured moduli of the demineralized cortical periosteum and trabecular bone while the behaviors of 65HEMA and 50PEG were similar to the demineralized and mineralized trabecular bone. The other three copolymers had smaller moduli compared to the measured values of any of the bone types tested.

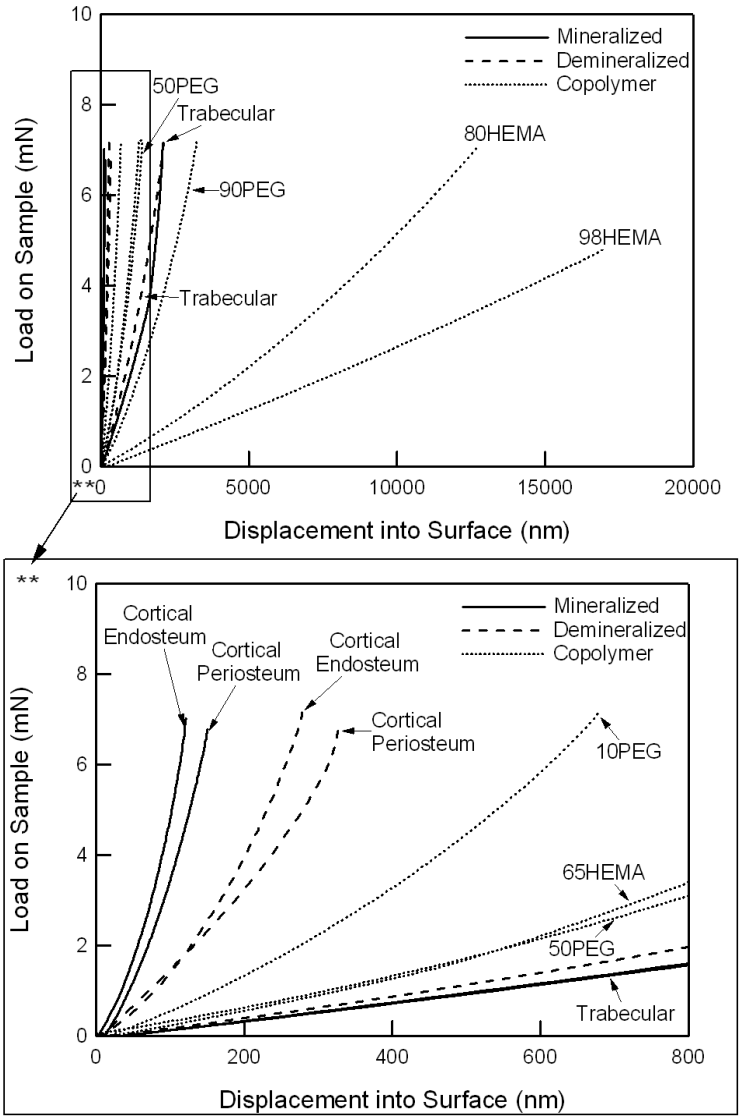

Figure 6.2. Representative load versus displacement curves of bone wafers using nanoindentation. The copolymer networks tested in this study are included for comparative purposes. Calculated elastic moduli for each bone type, region, and degree of mineralization are listed in Table 6.1.

6.3.2 Polymer Surface Characterization

The average surface roughness, contact angle, and elastic modulus values for all six copolymer surfaces are shown in Table 6.2. Average roughness (R_a) was below 70nm for all copolymer surfaces. There was no significant difference in contact angle between each PEGDMA-DEGDMA or 2HEMA-PEGDMA surface with TCPS (82.0± 6.4°).

50PEG was moderately more hydrophilic compared with the other surfaces having a significantly lower contact angle compared with 90PEG, 65HEMA, 80HEMA, and 98HEMA. The elastic moduli of the PEGDMA-DEGDMA copolymers varied over several orders of magnitude and decreased as the weight fraction of PEGDMA increased. Similarly, moduli values for the three 2HEMA-PEGDMA compositions varied over several orders of magnitude, but fell within the same range as the PEGDMA-DEGDMA copolymers. When nanoindentation was performed after one day or one week immersion in PBS, slight decreases in moduli were observed between the two time points; however, there was no significant difference in the moduli of each copolymer composition after one day or one week soaking.

Table 6.2: PEGDMA-DEGDMA and 2HEMA-PEGDMA/DEGDMA compositions and their corresponding contact angle, average roughness (R_a), and surface elastic modulus (E_s) after soaking for 24h and 7 days in PBS.

Substrate	**Composition Wt.%**	**Contact Angle (°)**	**R_a (nm)**	**E_s: 24h (MPa)****	**E_s: 1 week (MPa)****
TCPS	Tissue culture polystyrene	82.0 ± 6.5*		2150 ± 100	2150 ± 100
10PEG	10%PEGDMA750 90%DEGDMA	73.1 ± 4.6	12.8 ± 9.7	851 ± 223	507 ± 120
50PEG	50%PEGDMA750 50%DEGDMA	63.1 ± 7.5	5.4 ± 2.3	355 ± 63	311 ± 26
90PEG	90%PEGDMA750 10%DEGDMA	81.9 ± 5.8*	26.2 ± 8.7	67.9 ± 5.5	63.6 ± 2.0
65HEMA	65%2HEMA 35%DEGDMA	78.4 ± 5.4*	60.3 ± 22.8	609 ± 70	582 ± 103
80HEMA	80%2HEMA 20%PEGDMA550	80.2 ± 4.9*	18.7 ± 2.5* #	8.74 ± 1.2	8.80 ± 1.8
98HEMA	98%2HEMA 2%PEGDMA750	84.5 ± 2.7*	7.5 ± 1.8	5.55 ± 1.9	5.6 ± 2.0

*$p<0.05$ vs. 50PEG; #$p<0.05$ vs. 65HEMA; **E_s values for different compositions are statistically significant ($p<0.05$) except 10PEG vs. 65HEMA.

The percent elemental compositions obtained by XPS are listed in Table 6.3. Peaks corresponding to C and O were detected on all copolymer surfaces at a elemental ratio (C:O) of around 7:3, as would be expected given the chemical structures of the incorporated monomers. There was no significant difference in composition amongst the six copolymer surfaces.

Table 6.3: Percent elemental composition of PEGDMA-DEGDMA and 2HEMA-PEGDMA/DEGDMA copolymers using XPS.

Copolymer Composition	%C	%O
10PEG	69.2 ± 1.7	30.9 ± 1.7
50PEG	73.1 ± 0.1	27.0 ± 0.1
90PEG	73.3 ± 0.9	26.8 ± 0.9
65HEMA	72.8 ± 5.0	27.2 ± 5.0
80HEMA	70.3 ± 5.1	29.8 ± 5.1
98HEMA	74.8 ±1.0	25.2 ± 1.0

Representative FTIR-ATR spectra for the PEGDMA-DEGDMA and 2HEMA-PEGDMA copolymers are shown in Figure 6.3a and 6.2b, respectively. For the PEGDMA-DEGDMA copolymers, key chemical groups including the $–CH_3$ or $–CH_2$, O-C=O, and C-O-C can be identified by peaks at 2800-3000cm^{-1}, 1750cm^{-1}, and 1140cm^{-1} wavenumbers, respectively. As more PEGDMA was added, the intensity of the peak at 2800 cm^{-1} increased due to the increased surface presentation of $–CH_2$ in the ethylene glycol groups. An increased surface presentation of PEG was also evident by a right shift in frequency of the C-O-C peak. Looking at the spectra for 2HEMA-PEGDMA copolymers, a different chemical profile was observed, specifically with a peak appearing around 3200-3450cm^{-1} due to the addition of –OH side groups presented on the surface.

The intensity of this peak increased as more 2HEMA was added to the system. A biphasic peak around 1000-1150cm^{-1} became more distinct as the 2HEMA concentration increased due to the dual presentation of C-O in both the 2HEMA and PEGDMA monomers.

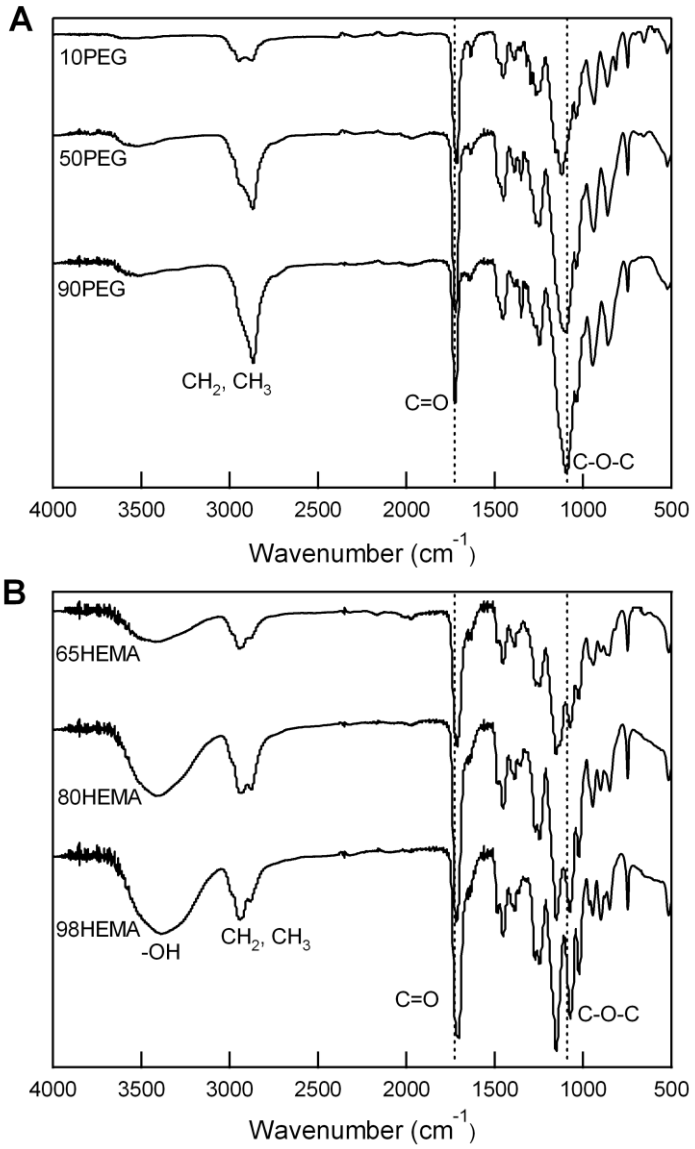

Figure 6.3. FTIR-ATR spectra of (A) PEGDMA-co-DEGDMA and (B) 2HEMA-PEGDMA/DEGDMA surfaces. Peaks corresponding to key chemical components of the networks are indicated. Dotted lines represent the wavenumber corresponding to the C=O and C-O-C peaks for 90PEG. It can be observed that these peak wavenumbers shift for the other copolymer systems relative to the 90PEG.

6.3.3 Cellular Morphology

Substrate-dependent differences in cell morphology were observed on the PEGDMA-DEGDMA copolymers using scanning electron microscopy. Cells were able to attach on all surfaces by 24h in culture. In general, MG63 cells on 10PEG were elongated and exhibited spindle-like shapes about 5-10μm diameter and over 40μm long (Figure 6.4a). Conversely, cells on 50PEG were more flat and spread on the surface with multiple extensions stretching over 10μm (Figure 6.4b). The fewest number of cells were observed on 90PEG with the majority of cells on the surface forming a polygonal shape around 10-20μm in diameter (Figure 6.4c).

MG63s also attached by 24h in culture on the 2HEMA-PEGDMA copolymers, exhibiting variable morphologies depending on the copolymer composition. Cells on 65HEMA exhibited mostly an elongated, spindle-like shape (Figure 6.4d) similar to that observed on the 10PEG surfaces (Figure 6.4a). A range of morphologies from flat and spread to round and cuboidal was observed on both the 80HEMA and 98HEMA compositions (Figure 6.4e and 6.4f, respectively), but more cells were seen attached on 98HEMA and 65HEMA than 80HEMA.

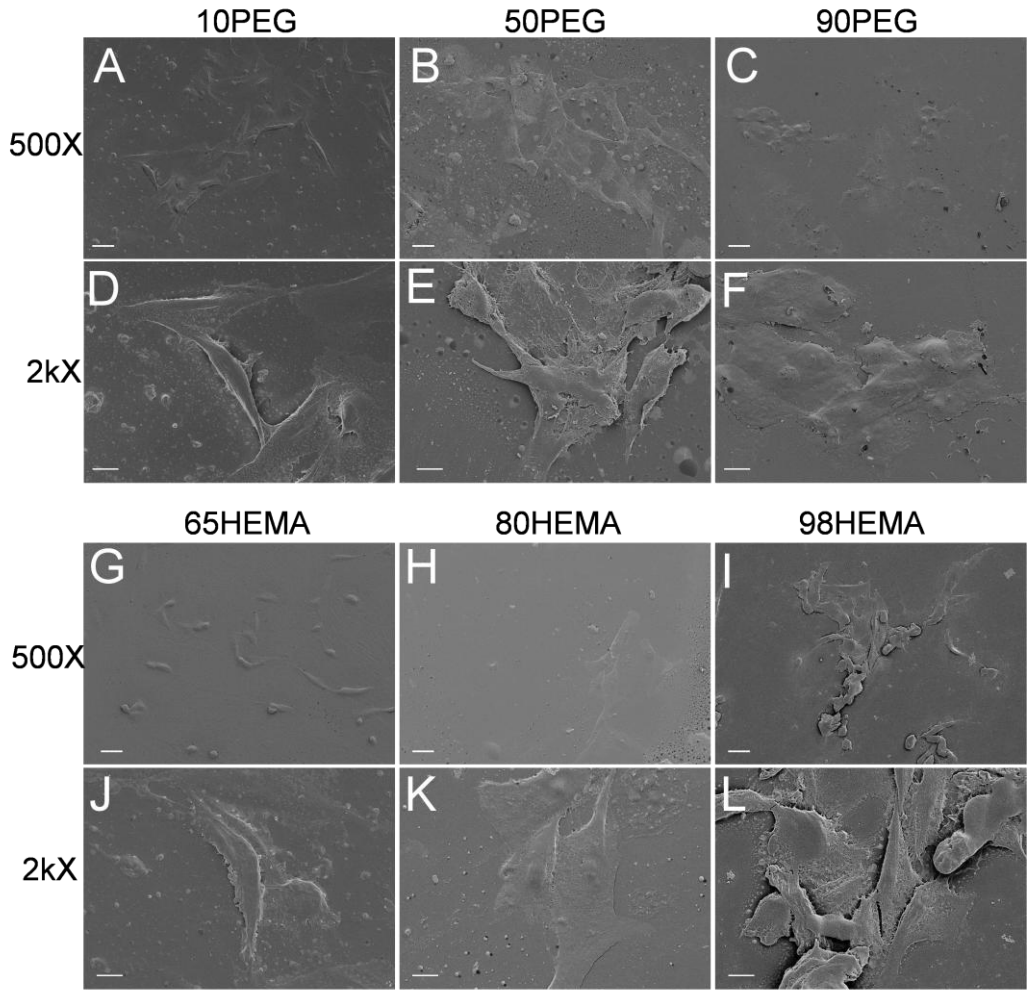

Figure 6.4. Scanning electron micrographs of MG63 cells after 24h in culture on 10PEG, 50PEG, and 90PEG (A-F) and 65HEMA, 80HEMA, and 98HEMA (G-L) at 500X (A-C and G-I) and 2kX (D-F and J-L) magnifications. Scale bar represents 40μm and 10μm for 500X and 2kX images, respectively.

6.3.4 Cellular Response

Mean +/- SEM data from one experiment using the PEG-DEG surfaces is shown in Figure 6.5. Because the levels measured on the PEG-DEG surfaces varied in comparison to TCPS with each experiment, the mean of the ratios representing treatment versus control (TCPS) from each experiment were compared and these results were used to draw conclusions on the cell response to these surfaces (Figure 6.6). The data from

each experiment can be found in Appendix B. Cell number for the PEGDMA-DEGDMA copolymers was sensitive to copolymer composition and stiffness (Figure 6.6a). Compared to TCPS, cell number was reduced 3-fold on the PEGDMA-DEGDMA surfaces. Cell numbers were at least two-fold higher on 50PEG and 90PEG surfaces than on 10PEG surfaces, the stiffest surface with the highest cell number observed on 50PEG, the medium stiffness surface.

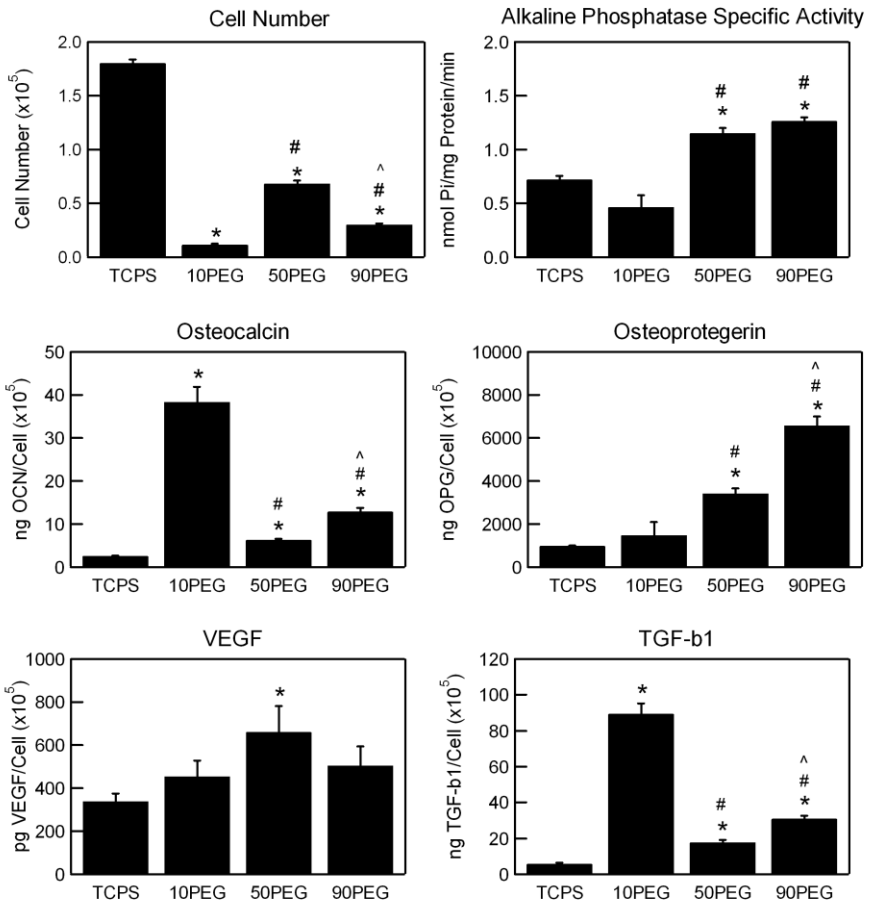

Figure 6.5. Effect of copolymer composition and stiffness on MG63 cell response. Data represent mean +/- SEM from one of 6 individual experiments.

Osteoblast differentiation was also affected by the surface chemistry and stiffness. Compared with TCPS, the PEGDMA-DEGDMA copolymers had a variable effect on alkaline phosphatase specific activity with activities increasing slightly on the less stiff 50PEG and 90PEG surfaces, but decreasing by 30% on the most stiff 10PEG (Figure 6.6b). Like cell number, the alkaline phosphatase specific activity increased at least 2-fold on 50PEG and 90PEG with respect to 10PEG. A three-fold increase in osteocalcin levels in the conditioned media of cells grown on the copolymer surfaces was observed compared to TCPS (Figure 6.6c). Osteocalcin levels were also affected by polymer stiffness, decreasing by at least 60% on 50PEG and 90PEG compared with 10PEG. The osteocalcin levels of cells on 50PEG, the moderately stiff surface, were significantly reduced compared with both 10PEG and 90PEG. The production of local regulatory factors was also sensitive to copolymer composition. OPG levels increased 4-fold on the 10PEG and 50PEG surfaces and at least 6-fold on 90PEG (Figure 6.6d). In contrast, both VEGF-A and TGF-β1 levels were higher on 10PEG surfaces than on 50PEG and 90PEG (Figure 6.6e and 6.6f).

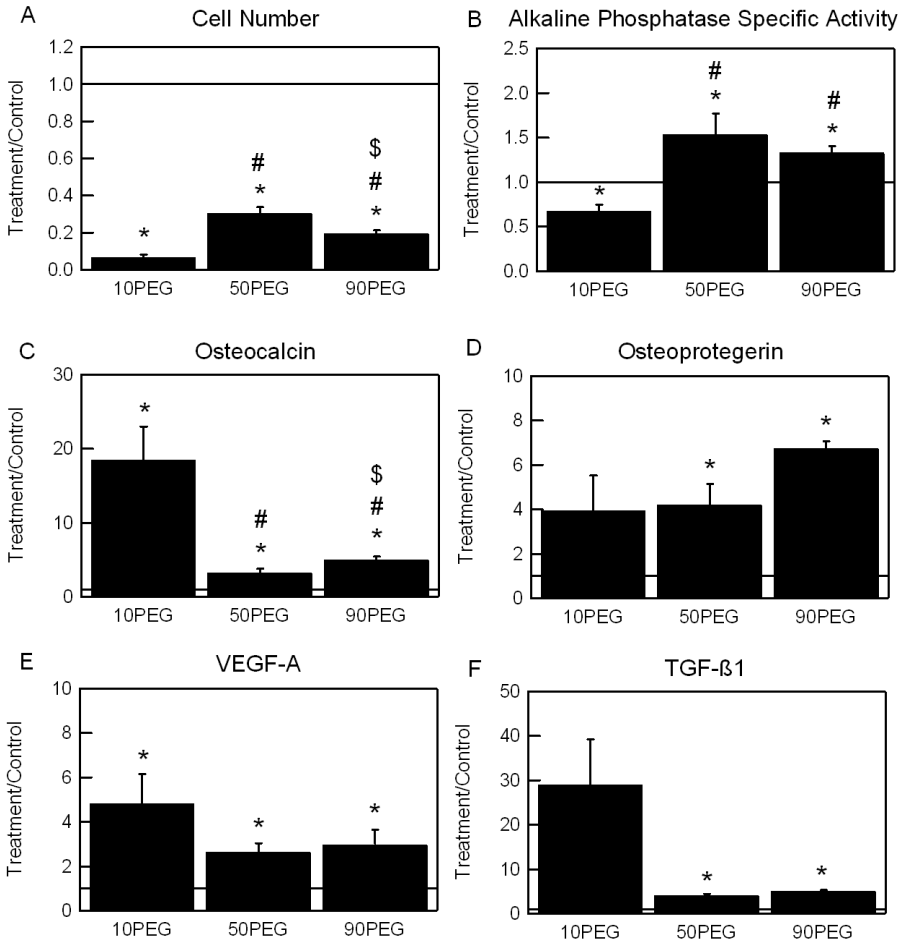

Figure 6.6. Effect of composition and stiffness on the differentiation of MG63 cells. Cells were cultured on tissue culture polystyrene (TCPS) or the copolymer surfaces with various weight ratios of PEGDMA to DEGDMA: 90%PEGDMA (90PEG), 50%PEGDMA (50PEG), and 10%PEGDMA (10PEG). At confluence (A) cell number, (B) alkaline phosphatase specific activity, (C) osteocalcin, (D) OPG, (E) VEGF-A, and (F) total TGF-β1 levels were measured. Data is the ratio of polymer surfaces to TCPS control for at least four independent experiments.*$p<0.05$, polymer surface vs. TCPS; #$p<0.05$, polymer surface vs. 10PEG; \$$p<0.05$, 90PEG vs. 50PEG.

The MG63 cell response on the 2HEMA-PEGDMA surfaces was affected by copolymer composition in a different manner compared with the PEGDMA-DEGDMA copolymers. To effectively compare the changes in cell response between the two copolymer systems, 90PEG was included in these experiments because its surface modulus was within the same order of magnitude of 80HEMA. Cell number was affected

by both the copolymer composition and stiffness (Figure 6.7a), reducing by 50% on the 65HEMA and 98HEMA surfaces and 75% on the 80HEMA in comparison with TCPS. Compared with 90PEG, cell number was increased 2-fold on 65HEMA and 98HEMA surfaces, but there was no significant difference in cell number between 80HEMA and 90PEG.

Osteoblast differentiation was affected by copolymer composition. Similar to the results described above for the PEGDMA-DEGDMA surfaces, alkaline phosphatase specific activity and osteocalcin levels increased on 90PEG compared with TCPS (Figure 6.7b and 6.7c). Comparing the 2HEMA-based surfaces with TCPS, alkaline phosphatase specific activities were reduced 50% on the moderately stiff and least stiff surfaces (80HEMA and 98HEMA, respectively). Activities also decreased on the three 2HEMA-PEGDMA copolymers compared with 90PEG. In contrast, osteocalcin levels on 80HEMA and 98HEMA surfaces were elevated at least 2-fold from the levels detected on TCPS, but no there was no difference between 65HEMA and TCPS. The levels on the 2HEMA-based surfaces were reduced by at least 50% compared with the levels on 90PEG. Surface stiffness did not affect osteocalcin production using the 2HEMA compositions.

The production of local regulatory factors was also regulated by copolymer composition. Both OPG and VEGF-A levels were again significantly increased on the 90PEG in comparison to TCPS (Figure 6.7d and 6.7e). OPG levels increased at least three fold on the three 2HEMA copolymers compared with TCPS, but there was no difference amongst the three compositions. Compared with 90PEG, OPG levels were reduced by at least 50% on 65HEMA and 98HEMA, but were not significantly different

on 80HEMA. There was no significant change in VEGF levels between the 2HEMA copolymers, but levels were 60% lower on all three 2HEMA-PEGDMA compositions in comparison to 90PEG. TGF-β1 was also evaluated on the 2HEMA-PEGDMA compositions, but no detectable levels were observed.

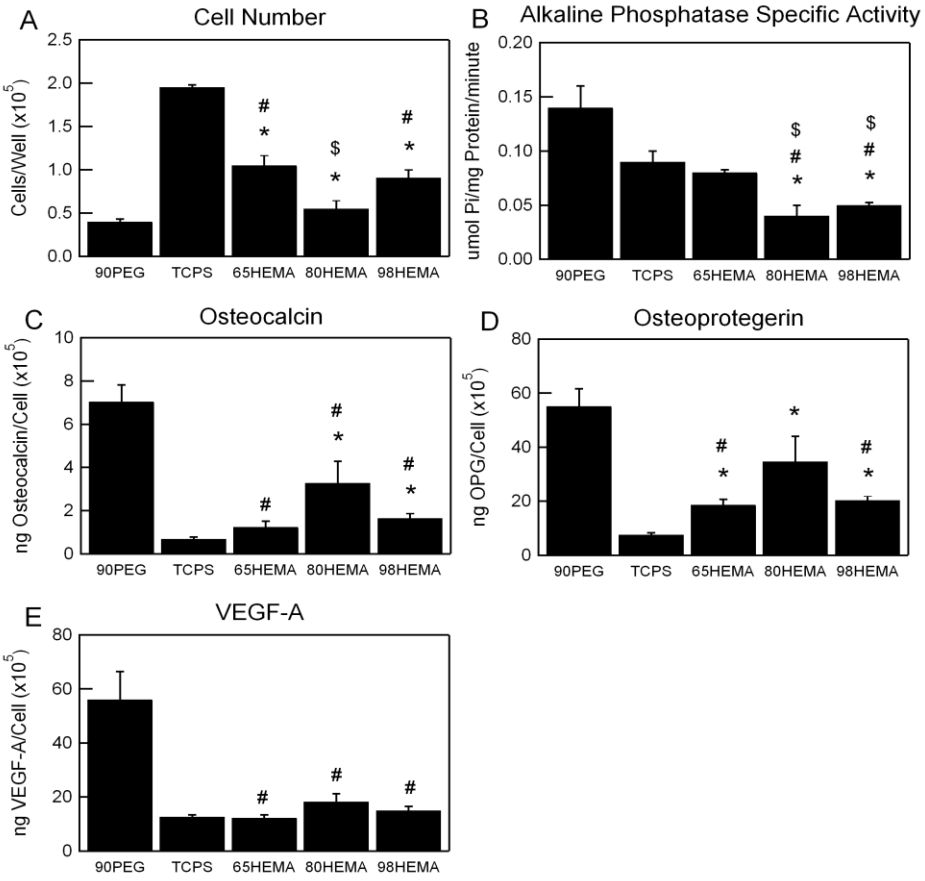

Figure 6.7. Effect of composition and stiffness on the differentiation of MG63 cells. Cells were cultured on either tissue culture polystyrene (TCPS) or the copolymer surfaces (65HEMA, 80HEMA, and 98HEMA) with similar stiffness values to PEGDMA-DEGDMA materials. 90PEG was included as a positive control for the PEGDMA-DEGDMA surfaces. At confluence, (A) cell number, (B) alkaline phosphatase specific activity, (C) osteocalcin, (D) OPG, (E) VEGF-A, and (F) total TGF-β1 levels were measured. *$p<0.05$, HEMA copolymer surface vs. TCPS; #$p<0.05$, HEMA copolymer surface vs. 90PEG; ‡$p<0.05$, 80HEMA or 98HEMA vs. 65HEMA.

6.4 Discussion

The results of this study demonstrate that bone stiffness on the micro-scale varies amongst the different structural components and mineralized states. The surface modulus of different bone components and mineralized state has been measured previously [31-32], but to the best of our knowledge, this is the first study comparing the elastic surface moduli of the cortical periosteal, endosteal surfaces of cortical and trabecular bone, both in mineralized and demineralized states. As would be expected, the elastic modulus of cortical bone was significantly higher than trabecular bone. This result can be attributed to the structural differences between the components in that cortical bone is a dense, compact tissue, whereas trabecular bone is more porous consisting of mostly strut-like trabeculae. The decrease in modulus for demineralized bone compared with mineralized bone for all regions occurs because the demineralized tissue is deplete of the mineral content known to give bone its rigidity. Interestingly, there was no difference in modulus between the periosteal and endosteal bone surfaces when mineralized, but the average modulus of the periosteal bone was significantly lower than the endosteal bone after demineralization.

In this study, it was hypothesized that the osteoblast response was affected by copolymer stiffness in a manner related to the rigidity the cells experience within the native tissue. The results of this study demonstrate that MG63 cells respond in a differential manner to both polymer stiffness and chemistry. The two copolymer systems, PEGDMA-DEGDMA and 2HEMA-PEGDMA, were designed to exhibit specific mechanical properties and chemical features. In the PEGDMA-DEGDMA copolymer system, the same chemical features (the PEG and acrylate groups) were presented on the

surface regardless of composition, but in varying concentrations. For example because PEGDMA (Mn~750) has more PEG repeating units compared with DEGDMA, the addition of PEGDMA to the material allowed for more surface presentation of ethylene glycol units while keeping the concentration of oxygen and carbon atoms constant and a lower crosslinking density compared with compositions with higher DEGDMA content (i.e., 90PEG vs. 10PEG). By systematically varying the PEGDMA to DEGDMA ratio, the surface modulus was effectively tailored over several orders of magnitude. With the 2HEMA-PEGDMA system, the hydroxyl groups in the 2HEMA structure created a different interfacial chemistry compared with the PEGDMA-DEGDMA copolymers. Adding more PEGDMA to the 2HEMA network resulted in less hydroxyl groups on the surface, lower crosslink density, and subsequently lower surface modulus. The range of surface moduli attained by changing the monomer ratio (PEGDMA:DEGDMA or PEGDMA:2HEMA) were within the same orders of magnitude for the two copolymer systems, thus allowing for distinct comparisons between the effects of copolymer chemistry on the cell response when stiffness is controlled. As observed in the results and to be discussed below, the effect of surface stiffness on the cell response was not comparable between the two copolymer systems indicating that the base chemical structure serves as the primary mediator of the osteoblast response while the effect of surface modulus differs with surface chemistry.

On both copolymer systems, the low cell numbers suggest that cell attachment or proliferation was not well supported on these surfaces. This result agrees well with previous findings showing that cell number is decreased on PEG and HEMA-presenting surfaces compared with TCPS [33-34]. Cell attachment and adhesion are usually

dependent upon the surface wettability, which is controlled by hydrophilicity and roughness. Despite having a significantly lower contact angle, 50PEG surfaces promoted the highest cell number amongst the three PEGDMA-DEGDMA copolymers suggesting that cell number was affected by surface features other than wettability. These findings are consistent with previous studies reporting that contact angle is not always a suitable measure of wettability on copolymer surfaces or an accurate way to predict degree of cell attachment due to the inherent heterogeneity of the network structure [35]. Considering that the contact angles were similar for all 2HEMA-PEGDMA surfaces, the increased cell numbers on 65HEMA and 98HEMA compared with 80HEMA further suggests that other surface effects possibly including stiffness could affect cell attachment and/or proliferation. Because proliferation and cell viability were not directly measured, it is difficult to ascertain whether the increased cell number on 50PEG and 80HEMA is the result of increased cell attachment or proliferation or decreased viability. From the SEM images, it is apparent that cells adhered to all copolymer surfaces after 24h in culture, but the number of cells attaching is variable on composition. Although surface wettability did not differ, it is also possible that protein adsorption was altered in a manner dependent on copolymer composition that resulted in key osteoblast binding proteins to be present in active conformations. The effect of polymer chemistry on protein adsorption has been detailed elsewhere [36].

On the PEGDMA-DEGDMA surfaces, MG63 cells grown on the stiffest surface (10PEG) exhibited characteristics corresponding to a more mature osteoblast phenotype. Alkaline phosphatase specific activity and osteocalcin production are both well-studied differentiation markers for osteoblasts [37]. In general, alkaline phosphatase specific

activity increases during the early stages of osteoblast differentiation, but then decreases over time as differentiation progresses and mineral deposition begins to occur. In contrast, osteocalcin levels are low during the early stages of differentiation and then increase and plateau as the cell reaches a mature osteoblast phenotype. Thus in this present study, the reduced alkaline phosphatase specific activity in combination with elevated osteocalcin levels on the PEGDMA-DEGDMA surfaces indicate that MG63 cells are more differentiated on these surfaces compared with cells grown on TCPS. Considering that differentiated osteoblasts will cease to proliferate, the reduced cell numbers observed on these surfaces further supports this hypothesis and agrees with previous studies showing that PLL-*g*-PEG coating on rough titanium can promote an osteogenic response from MG63 cells [33].

By comparing the cell numbers and osteocalcin levels produced on the 2HEMA-PEGDMA surfaces with 90PEG, it can be suggested that cells reach a more differentiated phenotype on the PEGDMA-DEGDMA surfaces than on the 2HEMA-PEGDMA surfaces. Interestingly, changing the 2HEMA concentration did not statistically affect osteoblast differentiation within the context of this copolymer system. This result contrasts with what is observed on the PEGDMA-DEGDMA surfaces where cell differentiation was increased the most on 10PEG, the stiffest surface, indicating that cells were preferentially responding to changes in copolymer chemistry versus changes in surface stiffness. Considering that contact angle and average roughness measurements were essentially similar amongst all copolymer compositions, this differential response signifies that osteoblast differentiation is primarily affected by copolymer chemistry in a manner that is not dependent on surface wettability and roughness.

Copolymer chemistry and stiffness may affect osseointegration through mechanisms involving changes in the production of local osteogenic factors. The results of this study indicate that both OPG and TGF-β1 production are modulated by the copolymer chemistry. OPG is produced by osteoblasts and acts as a decoy receptor by binding with RANKL to suppress osteoclastogenesis and regulate the bone remodeling cycle [38]. TGF-β1 is a growth factor that stimulates extracellular matrix formation and is believed to mediate OPG production [15]. It is produced in a latent form by osteoblasts and then stored in the extracellular matrix until it becomes activated [39]. In previous studies, fully differentiated osteoblasts exhibited elevated levels of OPG and TGF-β1 when cultured on microrough titanium surfaces [29, 40]. The elevated OPG and TGF-β1 production from MG63 cells cultured on the PEGDMA-DEGDMA surfaces further support the contention that MG63 cells are in a more differentiated state on these copolymer surfaces compared with TCPS by synthesizing mediators that enhance the osteogenic microenvironment. However, MG63 cells appear to produce more OPG on the less stiff surface (90PEG) while TGF-β1 levels are elevated more on the stiffest surface suggesting that the effects of copolymer stiffness mediate OPG and TGF-β1 production through different pathways. The reduced OPG levels on the 2HEMA-PEGDMA surfaces compared with 90PEG further indicates that the copolymer chemistry regulates osteoblast differentiation in a manner that affects osteogenic factor production.

Interestingly, the increased OPG production on 80HEMA compared with 65HEMA and 98HEMA also mirrors the change in OPG production with copolymer stiffness observed on the PEGDMA-DEGDMA copolymer (90PEG vs. 10PEG and 50PEG). It has been suggested that cells mimic their *in vivo* behavior on synthetic

matrices when the matrix stiffness matches the rigidity of the native tissue [3, 18]. In bone, the stiffness of the tissue is changing as bone is continuously remodeling itself. During the initial stages of bone formation, osteoblasts are beginning to lay down osteoid, which consists mostly of collagen and other matrix proteins and has a reported modulus of 27kPa [3]. As the matrix begins to mineralize during latter stages of bone formation, the stiffness increases to between 1 and 30GPa depending on the bone type, cortical or trabecular and degree of mineralization [31-32, 41]. In the present study, the moduli of 90PEG and 80HEMA represent the mechanical environment during early stages of bone development when the extracellular matrix is beginning to mineralize. During early osteogenesis, it is important that osteoclast activity is reduced so that bone resorption is repressed and enough of the matrix is deposited. The increased OPG production on the 90PEG and 80HEMA suggest that softer copolymer substrates, within the 10-70MPa range, will inhibit bone resorption by preventing osteoclast activation. Conversely on stiffer substrates such as 10PEG that mechanically mimic mature, mineralized bone, OPG production is reduced, potentially allowing osteoclasts to become activated and initiate bone resorption.

Besides modulating the ability of MG63 cells to promote bone formation versus resorption, copolymer chemistry and stiffness can also potentially regulate other processes that accompany bone formation. VEGF-A is an important angiogenic factor that osteoblasts produce to promote blood vessel formation within newly formed bone matrix [42]. Previous studies have suggested that VEGF-A production in pre-osteoblasts signifies the latter stages of osteoblast differentiation [43]. Within this current study, the elevated VEGF-A levels on the PEGDMA-DEGDMA surfaces compared with TCPS

further indicate that cells cultured on these surfaces exhibit characteristics of mature osteoblasts, and the extent of VEGF-A production by MG63 cells on these surfaces is mediated by stiffness. However, there was no significant difference in VEGF-A production on the 2HEMA-PEGDMA copolymers compared with TCPS. Considering the reduced osteocalcin and OPG levels observed on the 2HEMA-PEGDMA copolymers in comparison with 90PEG, it can be suggested that cells on these surfaces have not fully differentiated and thus are not readily producing key functional proteins characteristic of mature osteoblasts.

This study illustrates the importance of surface chemistry in evaluating the cell response on polymer surfaces. Comparing the two copolymer systems investigated, the PEGDMA-DEGDMA copolymer overall better promoted osteoblast differentiation compared with 2HEMA-PEGDMA. This result is significant as PEGDMA and 2HEMA are both common biocompatible polymers used in many implants and tissue engineering applications, but their osteogenic potential has never been compared. Previous studies have shown that cell attachment and spreading does not differ when osteoblasts are cultured on both PEG and HEMA surfaces [34]. These findings are supported by the SEM images shown in this study indicating that the copolymer chemistry affects osteoblast behavior through mechanisms other than attachment and adhesion, possibly by changing the conformation of adsorbed matrix proteins and causing certain extracellular membrane receptors including integrins to be differentially expressed. Several studies have documented how protein adsorption and subsequently cell attachment are altered by the addition of 2HEMA [36], but this effect has not been fully correlated to changes in osteoblast differentiation. Looking at the structure of each network, the PEGDMA-

DEGDMA copolymers were more highly crosslinked than the 2HEMA-PEGDMA compositions, a structural characteristic that could affect protein adsorption and cell binding on the surface leading to changes in intracellular signaling. This hypothesis is supported by a previous study showing that osteoblast attachment is affected by changes in the molecular weight between crosslinks in a degradable acrylate-based network [20], although there is no prior evidence that this leads to altered cell differentiation potential.

Previous studies have shown that the extracellular matrix rigidity within the kPa range can influence the cell morphology, proliferation, and differentiation of MC3T3-E1 cells [3, 5, 18]. To the best of our knowledge, this is the first study examining the effect of stiffness within the MPa range on the MG63 cell response. For the PEGDMA-DEGDMA system, it is apparent that MG63 cells differentiate and begin to create an osteogenic microenvironment at a faster rate on the stiffest surface (in the 100 MPa range), but the response of MG63s on the 2HEMA-PEGDMA surfaces suggests that a lower stiffness material around 10MPa will better promote osteogenesis. These results challenge whether MG63 cells can sense their mechanical environment at this rigidity. If cells do alter their function in response to the surface stiffness, then this effect is dependent on the copolymer chemistry presented. Thus when selecting a copolymer surface to interface with bone, osseointegration can be potentially optimized by first selecting the appropriate surface chemistry, PEG in this present study, and then the appropriate stiffness of the copolymer. These relationships will be addressed further with respect to tailorable tough, structurally similar networks.

6.5 Conclusions

This study demonstrates that osteoblast differentiation is mediated by the copolymer chemistry and that PEG-based acrylate chemistries support osteoblast differentiation better than 2HEMA-based networks. Specifically, cell numbers were decreased and osteocalcin, OPG, and VEGF-A levels were elevated on the PEGDMA-DEGDMA surfaces versus 2HEMA-PEGDMA surfaces. In order to study the effect of various surface properties on the cell response, polymer networks are typically used because their surface properties can be easily tailored by varying the chemical structure. These results emphasize the importance of minimizing changes in surface chemistry when evaluating the role of surface stiffness. Further studies will examine potential cellular mechanisms creating the differential response to copolymer composition and stiffness. A better understanding of these cell-polymer interactions will facilitate the development of orthopedic polymer materials that will better promote osseointegration.

CHAPTER 7

CONCLUSIONS

This research highlights several approaches that can be used to develop tough photopolymerizable (meth)acrylate networks that elicit an appropriate biological response. Copolymer networks were created to test their mechanical properties in tandem with evaluating their *in vitro* effect on immature osteoblasts in order to foster direct comparisons between the mechanical properties and biological response in relation to copolymer network structure. A central issue throughout this work was the role of PBS absorption on the material properties, including toughness. Several structure-property relationships of (meth)acrylate networks were established in the presence of PBS that could serve as design tools for developing novel polymeric materials for orthopaedic applications, in particular for spinal disc repair where the mechanical loading conditions are some of the most strenuous *in vivo*. Of note, it was demonstrated that combining two linear monomers with a crosslinker to form ternary networks enables the systematic tailoring of several material properties by (1) varying crosslinker concentration and (2) varying the ratio of the two linear monomers. Studying the properties of ternary networks as a function of monomer concentration thus facilitated the development of key relationships between network structure, toughness and environmental conditions. Some of these relationships are summarized below:

1. Network toughness is maximized when Tg is aligned with testing temperature (i.e. body temperature) by changing the concentrations of two monomers with opposing individual Tgs.

2. Toughness can be maximized in the presence of aqueous solutions by tailoring the copolymer composition such that the Tg in PBS decreases close to body temperature.
3. Long term stability of mechanical properties is best achieved in materials whose Tg falls at or below body temperature where the segmental vibrations are at a maximum allowing for easy transport of water molecules through the polymer chains during deformation.
4. The inclusion of structurally-similar hydrophobic monomers in the network provides increased strength and strain-hardening in the presence of PBS due to the cooperative intermolecular hydrophobic bonding that limits the number of water-polymer interactions.
5. The ability to promote an osteogenic response on (meth)acrylate networks relies on incorporating the appropriate chemistry, in particular PEG groups into the network.
6. The ability to tailor the osteogenic response on ternary (meth)acrylate copolymer networks is limited by the heterogeneity and random presentation of chemical groups inherent to photopolymerized copolymer networks.

Toughness: A Measure of Material Durability?

Although implant materials must meet a variety of mechanical property criteria, toughness was chosen as the central focus of this research due to its positive correlation with other mechanical properties including strength, deformability, and wear resistance [153]. In addition, those polymers that have found success clinically appear to possess

high toughness in comparison to many biological tissues, further emphasizing the importance of developing novel tough polymer-based biomaterials (Figure 2.6). Because toughness reflects the total amount of energy required to break the material, a tough material will exhibit high strength and/or large failure strains. What is important to remember is that this same correlation does not exist between elastic modulus and toughness suggesting that materials deemed "tough" can possess a broad range of moduli. For example, in Chapter 4 tough (meth)acrylate networks possessed moduli between 10-500MPa, a range that encompasses the moduli of many load-bearing tissues including tendon and the disc annulus [60-61]. Expanding this moduli envelope might be limiting with (meth)acrylate networks, but could be achieved by incorporating or adopting alternative polymer systems such as double networks or interpenetrating polymer networks [182-184].

Much debate has centered on whether the inherent toughness of materials is related to other complex mechanical properties related associated with durability including fracture toughness, fatigue and wear resistance. It is certainly recognized that fracture toughness is crucial in implant materials in ensuring that small defects created during loading do not propagate and lead to catastrophic failure. Because fracture toughness relates to a material's ability to prevent crack propagation whereas inherent toughness concerns more of the ability to prevent defect formation and ultimate failure, these two properties do not necessarily follow the same structure-property relationships in polymers. In the broad scope of materials, general trends between fracture toughness and inherent toughness are evident when comparing metals that typically exhibit excellent fracture and inherent toughness versus polymers which traditionally are known

for low fracture toughness despite sometimes exhibiting high inherent toughness. It was not the intent of this work to neither determine any correlation between these two properties nor insinuate that an inherently "tough" material will exhibit excellent fracture or impact toughness. Future studies exploring the behavior of the tough copolymer networks developed in this study (namely, MA-co-MMA-co-DDDA) under fatigue and wear conditions would aid in verifying if ultimate durability can be achieved using the approaches discussed above.

Toughness in Relation Tg: Alternative Perspectives

Looking at the principles outlined above, a common element becomes evident with each relationship: the glass transition temperature. In fact, it can be suggested that Tg is the thread that intertwines the relationships between mechanical properties, water absorption, and network structure for (meth)acrylate networks. By adjusting Tg, a range of mechanical properties can be achieved, and the extent to which water interacts with the polymer chains can be controlled by changing chain mobility associated with the viscoelastic state of the polymer. The fact that toughness is enhanced in this glass transition region is not too unsurprising given the characteristic molecular behavior inherent in this regime. Having optimal toughness at Tg offers additional advantages for those polymers that undergo the shape memory effect by ensuring that the polymers remain durable during activation when implanted. As illustrated though in Chapter 4, this Tg-temperature approach does have its limitations mostly due to the mechanical properties of (meth)acrylate networks being dependent on strain rate in a manner related to the time-temperature superposition principle. Mitigating strain rate effects, perhaps by

broadening the thermal transition region, could serve as an objective of future studies. Broader thermal transitions can usually be achieved by increasing the crosslinking density and or heterogeneity in the network by including gradient copolymer moieties or phase-separated copolymer blends [185].

Although the Tg-temperature approach greatly improves mechanical properties, toughness cannot be fully optimized without considering certain factors relating to network chemistry that provide even higher toughness at this Tg-temperature peak. Interestingly, many of the "tough" chemistries identified in this work did not exhibit the characteristic chemical structures deemed tough by previous theories. Specifically, Wu showed an inverse relationship between Flory's characteristic ratio and polymer chain toughness for homopolymers [186]. However, tailoring specific material properties often requires combining multiple monomers to form copolymer networks where intermolecular secondary bonding and monomer affinities become important. Within this work, both 2HEMA and MMA-based networks displayed this effect through the formation of hydrogen bonding and hydrophobic interactions, respectively, although this effect is negated for 2HEMA once the material is exposed to PBS. In regards to ternary networks, combining two linear monomers with similar pendant chemistries would be necessary to produce strong intermolecular bonds. For example, both 2HEMA and BMA have the potential to form strong intermolecular bonds amongst their own linear chains, but when the two are copolymerized, their unlike chemistries (polar vs. nonpolar) minimize these interactions. Crosslink density can also determine the extent to which network toughness can be tailored through monomer chemistry. Specifically it has been shown that lower crosslink densities, with Er<10MPa, are required for the monomer

chemistry to affect network toughness [34]. These previous findings also coincide with the fact that crosslinking concentration must also be kept low in order to maintain large failure strains as well as achieve a broad range of stiffnesses in order to mimic the mechanical behavior of many orthopaedic soft tissue including annulus fibrosis tissue.

Photopolymerizable (meth)acrylate networks were the primary copolymer systems evaluated in this research, but it is plausible and certainly worth investigating whether the toughness of other copolymer networks could be improved by using the Tg-toughness approach. For instance, biodegradable polymers could potentially benefit from having enhanced toughness in order to limit the extent to which the mechanical properties decline during the degradation process. Creating tough biodegradable materials is often complicated by the trade-offs between tailoring the mechanical properties and degradation rate, but using the Tg-toughness approach could facilitate the independent tailoring of toughness and degradation rate, possibly by incorporating high-Tg degradable components such as polylactide [187].

Additionally, although the final network selected, MA-co-MMA-co-DDDA, ultimately contained little PBS content, it can also be suggested that a tough network consisting of polar, water-binding, chemistries can be designed using the Tg-temperature approach if the extent by which Tg drops due to changes in water content is distinctly controlled. Even if Tg cannot be aligned precisely with body temperature, bringing network Tg closer to body temperature even moderately would reduce the brittle behavior of glassy polymers or increase the strength and failure strains for rubbery polymers as the Tg's of the network approach the sides of the temperature-toughness peak (Chapter 3 Figure 3.15).

Other possible ways to further improve material durability include developing photopolymerizable composites that contain a polymer matrix toughened by the Tg-toughness approach filled with an additional component that provides for specific enhanced mechanical properties. In fact, a composite material appears the most logical from a biomimetic perspective given that most biological tissues including bone and intervertebral disc tissue are composite materials themselves. Fillers or fiber reinforcements can serve to increase the strength, improve ductility, or adjust the modulus within either a high- or low-modulus polymer matrix depending on the desired application. For example, fiber-reinforced polymers that consist of a low-modulus matrix can exhibit low moduli, characteristic of many soft tissues, AND high strength. To mitigate poor creep and fatigue properties, fiber-reinforced UHMWPE has proven useful in total knee replacements [188]. However, some challenges exist in designing photopolymerizable polymer composites including using fillers that do not affect the photopolymerization reaction and that can remain homogenously mixed during curing. The clinical application of *in situ*-formed fiber-reinforced PMMA bone cement has previously been thwarted by problems associated with the former issue [188].

Tailoring the Osteogenic Potential

The ability to promote a favorable *in vitro* osteogenic response was also demonstrated on (meth)acrylate copolymer systems with MG63 cells producing a more differentiated phenotype in response to specific monomer chemistries. The regulation of cell response through material chemistry has been extensively studied, but yet only recently has the fine control of the osteogenic response, beyond attachment and

proliferation, through surface chemistry been successfully demonstrated [189-190]. Using the surface properties to stimulate a warranted cell response eliminates the need to deliver growth factors and other drugs to implant sites as a means to facilitate tissue growth. Because load-bearing implant materials should mimic the compliance of adjacent tissue (i.e. bone for this application), the effect of substrate stiffness on osteoblast function and bone formation is critical to understand from a materials selection perspective. More studies are being reported detailing the mechanisms by which cells "mechano"-sense their environment and, in particular, how substrate stiffness affects this response. In this current work, MG63 cells reached a more differentiated phenotype on stiff PEG-based networks than their softer counterparts. Considering this effect of copolymer stiffness was not repeatable on 2HEMA-based surfaces, it is unclear whether this response was due to the stiffer environment (~1GPa) or some of the microscopic changes in structure due to increased crosslink density.

The relationship between Tg and mechanical properties also enabled the design of a copolymer system that could be used to study the effect of stiffness on cell attachment and differentiation. By using a ternary network with two structurally similar linear monomers, a range of moduli over several orders of magnitude was achieved without drastically altering the chemistry. For polymers that undergo their transition from glassy to rubbery upon implantation via shape memory activation, determining whether bone development is affected by the thermomechanical state of the polymer is critical if these materials are to be used as orthopaedic fixation applications as previously described [10]. From the work presented in Appendix A, it is somewhat surprising that MG63 cells appear insensitive to this viscoelastic regime of the networks because it could be

speculated that the increased vibrational motions would alter protein adsorption onto the surface and the presentation of binding sites, although this effect has never been reported. However, the ability to tailor Tg without changing cellular compatibility enables ternary copolymer networks to be used in various applications that require materials to be in a glassy, ductile or rubbery state. Furthermore although copolymer stiffness was identified as a secondary mediator of osteoblast differentiation within this current study, a proposed mechanism and the precise control was difficult to achieve on the chemistry-controlled ternary (meth)acrylate networks as discussed in Appendix A.

One potential drawback to the utility of these networks as bone-interfacing implant materials is the limited cell attachment observed on these surfaces. Although cell attachment and proliferation were not independently studied, it is apparent from SEM images taken after 24h culture that these materials do not initially provide a favorable surface for cells to bind; however, those cells that do attach are able to reach a mature osteoblast phenotype within 5 days in cultures. Low cell attachment to (meth)acrylate surfaces could inhibit proper bone-to-implant contact *in vivo.* Based from previous studies reporting that osseointegration was achieved around implant surfaces despite decreased cell numbers, it would be of use to assess the degree of cell attachment required to ensure appropriate bone-to-implant contact and whether the low cell numbers observed within this work translates to decreased cell attachment *in vivo.*

Assessing Clinical Applicability

Photopolymerizable materials have the potential to serve as vehicles to deliver cells to an injury site by encapsulating the cells with the monomer solution and then

curing the polymer *in situ*. The polymer network would prevent cells from migrating from the injury site and protect the cells from the harsh surrounding environment as the cells produce new extracellular matrix. This last characteristic is particularly important for spinal repair applications as both large abnormal mechanical loads and harsh biochemical attack found in degenerated tissue have been shown to reduce the cell viability and function [6]. Because these polymers can be formed within the body, they can replace tissues or fill defect sites that have irregular shapes, an attribute that can allow for a minimally invasive insertion.

Using the principles outlined above, one photopolymerizable network, MA-co-MMA-co-DDDA, has been identified as a candidate material for spinal repair applications. At the appropriate MA to MMA ratio, this network maintains an elastic modulus around 50-100MPa and failure strains around 250-300% for up to 9 months in PBS with toughness values comparable to UHMWPE and surpassing both bone and intervertebral disc tissue (both annulus and nucleus pulposus). By varying the MA to MMA ratio, some tailoring of the elastic modulus without compromising toughness can be achieved to meet the compliance requirements of various tissues (i.e. bone vs. annular tissue). Initial *in vitro* cellular results indicate that this material also supports the attachment and differentiation of pre-osteoblast cells although the ability to enhance the differentiation potential of pre-osteoblast cells has yet to be achieved. Although this work identifies compositions that meet the preliminary mechanical and biological criteria, the eventual clinical application of these materials relies on tackling some of the limitations that have been discussed above as well as identifying how some of the proposed tough materials function in more clinically relevant mechanical and biological environments.

The next appropriate step is to design and test implant prototypes under conditions particularly relevant to the spine. In this regard, it is important to consider that the photopolymerization reaction is dependent on sample geometry with rates of bond conversion being dependent on sample thickness (greater than 1mm). Photopolymerizing prototypes might prove challenging using many current molding techniques and thus, other means of UV-curing, such as mask projection micro-stereolithography [191] and radiation crosslinking [192] should be exlpored. In order to determine if the enhanced toughness of these networks translates to improved durability under more complex loading regimes, future studies will examine their mechanical behavior under compression, torsion and/or cyclic and wear fatigue in the presence of solution. It is also imperative to evaluate the biomechanical response of these materials under loading conditions inherent specifically to the spine using a rotational disc simulator.

Further steps to be taken in regard to implementing these tough photopolymerizable compositions as implant materials would be to evaluate their *in vivo* mechanical performance as well as how these materials affect peri-implant bone formation. Under *in vivo* conditions, a more complex cascade of physiological events occur in response to the presence of an implant material, including the induction of the foreign body reaction and fibrous tissue formation, that are involved in the post-implantation tissue repair process. Although the *in vitro* MG63 cell culture model proves useful in gaining an initial assessment of the biocompatibility of the copolymer networks for bone-interfacing technologies, it is certainly an oversimplification as many distinct cell populations including mesenchymal stem cells as well as macrophage-like cells and vascular-related cells (i.e. endothelial) are known to migrate to the implant surface. Thus, the presence of

multiple cell types can also greatly impact the ability to promote bone formation around the implant material through cell-cell interactions and the production of extracellular molecules specific to that tissue type. In particular within this current research, the exact mechanism between the copolymer surface and osteogenic response remained somewhat elusive, particularly on the ternary MA-MMA-PEGDMA networks. Therefore, evaluating the *in vivo* biological response of those deemed "tough" compositions might provide more accurate and certainly relevant assessment of tissue-material interactions. First, the biocompatibility in terms of inflammation and fibrous capsule formation would need to be investigated through subcutaneous implantations in small animal models. The biological response and ability to promote bone formation in the spinal region would subsequently be the subject of further studies.

Other areas of investigation regarding the *in vivo* implementation of photopolymerizable networks pertain to determining the appropriate delivery or implantation technique. Although photopolymerizable materials are hailed for their ability to be cured *in situ,* if certain toughness-enhancing monomers that are known to be cytotoxic in their unreacted form are included in the composition, the material must then be pre-formed and delivered to the implant site in another manner, such as using shape memory capabilities. With regards to the copolymer compositions proposed in Chapter 5, the presence of MA, which has reported cytotoxicity [32], certainly makes *in situ* polymerization unfeasible. In addition, the variability of the MG63 osteoblast response to MA-co-MMA-co-PEGDMA networks (Appendix A) calls into question whether these materials can consistently promote favorable tissue formation *in vivo.* It was suggested that this variability was due to the inherent random formation of the copolymer network

that is associated with the photopolymerization reaction. Despite these possibilities, the insight gained on toughening mechanisms can still be applied to other copolymer systems with known osteo-compatibility.

In summary, the ability to independently tailor network toughness in the presence of solution using cytocompatible copolymer networks has been demonstrated as a novel approach to develop more durable polymer implant materials. Furthermore, the relationships between network structure, mechanical behavior, and biological response established in this work will facilitate the design of tough, biocompatible photopolymerizable networks for load-bearing applications, particularly for spinal disc repair. In a broad sense, the results presented will contribute to the growing field of biomaterials by better defining the interrelationships between polymer chemistry, mechanics, and bone biology.

APPENDIX A

MG63 CELL RESPONSE TO THE SURFACE PROPERTIES OF TAILORABLE TOUGH PHOTOPOLYMERIZABLE MA-CO-MMA NETWORKS

A.1 Introduction

The design of materials for use in orthopaedic implants or devices, specifically for spinal repair, has proven challenging because they must have suitable mechanical properties to withstand complex loading regimes as well as promote tissue growth and integration. Previous studies have explored the biocompatibility of acrylate-based materials in regards to how these materials support cell attachment. In these studies, properties such as wettability, chemistry, roughness, and stiffness have all been shown to modulate the cell response. The effect of surface chemistry is usually tied to changing the surface energy or wettability that mediates protein adsorption and the presentation of cell-binding sites on the proteins. More recently, the effects of substrate stiffness on cell differentiation have been explored using various copolymer systems, including acrylate-based networks [114, 117, 124, 177]. Results reported in Chapter 6 showed that copolymer chemistry has a stronger effect on osteoblast differentiation *in vitro* than surface stiffness. Specifically, MG63 cells were able to differentiate at a faster rate on PEG-based surfaces versus 2HEMA based surfaces in a manner independent of surface wettability and stiffness.

In Chapter 4, a photopolymerizable network consisting of methyl methacrylate (MMA) and methyl acrylate (MA) crosslinked with either poly(ethylene glycol) dimethacrylate (PEGDMA) or dodecanediol dimethacrylate (DDDA) was proposed as a

candidate material for orthopaedic applications where it is important that the implant material be readily deformable, yet have excellent toughness such that it maintains its function for long time spans *in vivo* [164]. By adjusting the MA concentration in the network, the Tg and subsequently, the mechanical properties of this system can be tailored to exhibit specific mechanical behavior from rigid and brittle to soft and rubbery. In particular, a several orders of magnitude variation in elastic modulus that can be achieved suggesting this material can be used for a range of load-bearing biomedical applications.

Although both PMMA-based and PEGDMA-based materials have been shown to be biocompatible and are already used clinically, the osteogenic response to these polymers photopolymerized into a copolymer network with the addition of MA has yet to be examined. The objective of this study was to evaluate how changing the copolymer composition, and thus copolymer stiffness, in combination with changing certain polymerization parameters affected the *in vitro* response of MG63 human pre-osteoblast cells. Several compositions were synthesized with varying amounts of MA to achieve a broad range of Tg's and consequently, elastic moduli. The cell response was evaluated by examining cell number, morphology, and the production of certain osteogenic factors. The results of this study provide evidence that MA-co-MMA-co-PEGDMA networks can promote osteoblast differentiation under certain conditions.

A.2 Materials and Methods

A.2.1 Materials

Methyl acrylate (MA), Methyl methacrylate (MMA), polyethylene glycol dimethacrylate (PEGDMA; Mn~750) were obtained from Sigma-Aldrich (St. Louis, MO) and used as received. 2,2-dimethoxy-2-phenylacetophenone (DMPA, Sigma Aldrich) was used as the photoinitiator. The chemical structures of the monomers are shown in Figure 5.1 in Chapter 5.

A.2.2 Network Synthesis and Disc Preparation

Monomer solutions were formulated by combining various weight ratios of MA and MMA with 10wt.% PEGDMA and 1 wt.% DMPA. The elastic modulus of the copolymer system was adjusted by varying the weight ratio of MA to MMA. Four compositions (by weight %) were selected based on their determined elastic moduli values: (1) 18%MA 72%MMA 10%PEGDMA (18MA), (2) 29%MA 61%MMA 10%PEGDMA (29MA), (3) 40%%MA 50%MMA 10%PEGDMA (40%MA), and 72%MA 18%MMA 10%PEGDMA (72MA). Each solution was mixed manually in a glass vial and injected using a glass pipette between two glass slides separated with two glass spacers (thickness = 1mm or 1.5mm). The sheets were placed in a UV chamber (UVP, Model CL-1000L Ultraviolet Crosslinker, Upland, CA; λ=365nm; energy=2000x100$\mu J/cm^2$) for 35 minutes. Discs were laser-cut from the polymerized sheets to a diameter such that the disc of each composition would swell to fill the bottom of a well in a 24-well cell culture plate when incubated in media. All discs were post-

cured in an oven at 90°C for 90 minutes and immersed in distilled water for 3 days to remove excess monomer. Discs were then UV sterilized for 90 minutes.

A.2.3 Thermomechanical Characterization

The glass transition temperature (Tg) of each network was determined by performing differential scanning calorimetry (DSC; TA Instruments Q100, Newcastle, DE) under a nitrogen environment. Samples were weighed on a balance (average sample mass between 10-15mg) and then cooled to -80°C and subsequently heated to 200°C at a constant rate of 5°C/min. Tg was denoted as the mid-point of the second order transition on the heating scan. Samples of each composition were soaked in phosphate buffered saline (PBS; Sigma Aldrich) for 24h prior to testing. Before testing, each sample was removed from the solution and patted dry with a paper towel to remove excess moisture. Average Tg and standard deviation were calculated for each composition (n=3).

Dynamic mechanical analysis (DMA) was performed on each copolymer composition using a TA Instruments DMA Q800. Samples were cut into 20mm x 5mm rectangular samples, and the edges were sanded to remove any microdefects. Samples were cooled to -75°C and then heated to 200°C at a rate of 5°C/min. Tests were performed in tension mode at a frequency of 1Hz with 0.1kN preload force, 0.2% strain rate, and 150% force track (n=2).

Elastic modulus was determined by performing tensile strain-to-failure testing on a MTS Insight 2 using a 2kN load cell. Samples were lasercut into ASTM D638 Type IV dogbones. Because polymer mechanical properties are highly temperature and moisture-dependent, all tests were conducted in a PBS bath at 37°C. To simulate *in vitro* culture

conditions, samples were soaked for 24h prior to testing. The elastic modulus was calculated as the slope the linear portion of the stress-strain curve (n=4).

A.2.4 Surface Characterization

Surface wettability was determined by performing contact angle measurements using the sessile drop method on a Ramé-hart goniometer (Mountain Lakes, NJ). A 3µL drop of deionized water was dropped onto the disc surface, and the contact angle between the side of the drop and polymer surface was measured using a camera and DROPimage CA software (Mountain Lakes, NJ) (n=3).

Elemental analysis was performed by x-ray photoelectron spectroscopy (XPS) on a Thermo K-alpha XPS (Thermo Scientific; Waltham, MA) under high vacuum ($3<10^{-8}$ Torr) using Al-Kα radiation (1486.6eV) and a pass energy of 50eV. Charge buildup on the polymer surfaces was neutralized by an electron flood gun at 3mV. Survey scans were obtained in the 0-1000eV range using 1 eV/step. High resolution scans were performed using 0.065 eV/step. Peak assignments and their corresponding area were determined using Avantage software (Thermo Fisher Scientific; Waltham, MA). Three scans were performed on two separate discs for each composition.

Fourier transform infrared (FTIR) spectroscopy in attenuated total reflectance (ATR) mode was performed to assess the chemical bonding present on the surface and compare the differences in the amounts of key chemical groups amongst the different copolymer systems. Spectra were obtained on discs using a Bruker Optics Tensor Spectrometer (Billerica, MA) with a KBr crystal. 32 scans were obtained on each sample at a 1Hz frequency and peak wavenumbers were determined using OMNIC software

(Thermo Electron Corporation, Madison, WI). Three spectra were obtained for three separate discs for each composition.

A.2.5 Cell Culture

Human MG63 osteoblast-like cells (ATCC, Manassas, VA) were cultured in Dulbecco's modification of Eagle's medium (DMEM, Cellgro, Manassas, VA), 10% fetal bovine serum (Hyclone, Waltham, MA), and 1% penicillin-streptomycin (Invitrogen, Carlsbad, CA) at 37°C, 5% CO_2, and 100% humidity. Polymer discs were soaked in media for 24h prior to plating in order to allow the discs to swell to fit the bottom of the culture well. To overcome the buoyancy of the polymer discs, CellCrown polymer inserts (Scaffdex, Finland) were used to anchor the disks. Cells were plated either on tissue culture polystyrene (TCPS) or polymer discs at a density of 10,000 cells/cm^2 and cultured until cells reached confluence on TCPS, about 5-7 days.

A.2.6 Analysis of Cell Response

At confluence, fresh media were added to the cultures, and cells were incubated for 24h prior to harvesting. At harvest, the conditioned media were collected from each well. Cells were released from the surfaces using two sequential trypsinizations to ensure all cells were collected. Cell number was determined using a Beckman Coulter Z1 particle counter (Fullerton, CA). Cells were lysed and alkaline phosphatase specific activity was measured as the release of *p*-nitrophenol from *p*-nitrophenylphosphate at pH 10.2 as previously described [179] and normalized to total protein (Pierce BCA Protein Assay, Thermo Scientific, Waltham, MA). Osteocalcin was measured in the conditioned

media using a commercially available radioimmunoassay kit (Human Osteocalcin RIA Kit, Biomedical Technologies, Inc., Stoughton, MA) as previously described [108]. The amount of osteoprotegerin (OPG), vascular endothelial growth factor (VEGF), and total transforming growth factor- β1 (TGF-β1) released by the cells was determined by performing an enzyme-linked immunosorbent assay (ELISA) of the conditioned media (DuoSet ELISA kits, R&D Systems, Inc., Minneapolis, MN) as previously described [180-181].

A.2.6 Statistical Analysis

Data presented are from one of two independent experiments, each with comparable results. Data are the mean ± SEM of six independent cultures. Data were analyzed by performing an analysis of variance, and, when statistical differences were found, a Student's t-test for multiple comparisons using Bonferroni's modification was used. P values<0.05 were considered significant.

A.3 Results

A.3.1 Thermomechanical Characterization

The thermomechanical behavior of MA-co-MMA-co-PEGDMA networks with varying MA concentrations is shown in Figure A.1. The glass transition region of each network can be identified as the region where the material undergoes a several orders of magnitude drop in modulus. The temperature span of this region decreases as more MA is added to the network. However by design, the rubbery modulus (1-2MPa) is not

affected by MA concentration indicating that crosslink density is the same in all copolymer formulations.

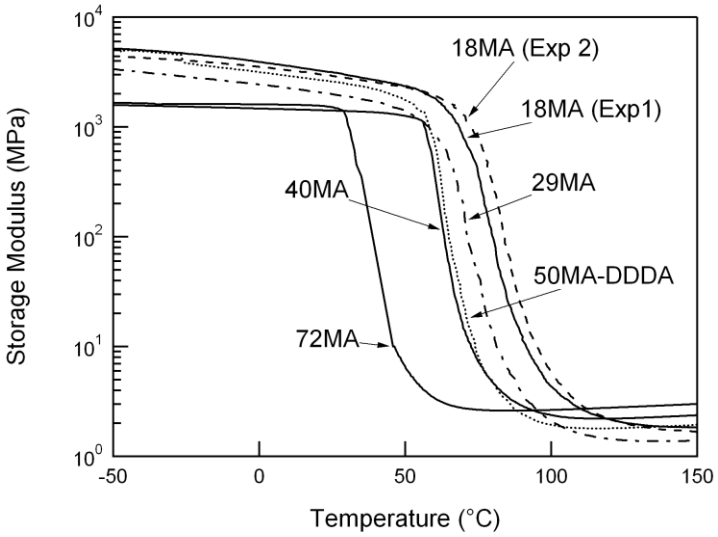

Figure A.1. Representative DMA curves showing storage modulus as a function of temperature for the MA-MMA networks tested in this study.

The mean elastic moduli and Tg (as determined by DSC) of each network are listed in Table A.1. The elastic moduli measured at 37°C in PBS varied over several orders of magnitude and decreased with increasing MA concentration. Similarly, Tg (as determined by DSC) decreased with increasing MA concentration. All modulus and Tg measurements were repeated for each new batch of copolymer synthesized for Studies 1-3 with no change difference in Tg or E values observed (data not shown).

Table A.1. Mean values for Tg, contact angle, and elastic modulus for each copolymer.

Name	Tg (°C)	Contact Angle (°)		E (MPa)*
		Exp 1	Exp 2	
TCPS		82.0±6.5		2150±100
18MA	43.0	75.9 ± 7.9	65.7 ± 14.2	309.9 ± 6.5
29MA	40	74.5 ± 10.7	83.53 ± 5.7	223.7 ± 31.5
40MA	25	89.4 ± 5.9	79.7 ± 5.5	4.7 ± 1.0
72MA	4.0	86.9 ± 5.0	90.9 ± 12.5	0.8 ± 0.1

*$p<0.05$ for all copolymers vs. TCPS and each copolymer

A.3.2. Surface Chemical Characterization

Average contact angle measurements for each copolymer are shown in Table A.1. There was no significant difference in contact angle between the different copolymers and TCPS. There was no significant difference in contact angle between compositions synthesized on 1mm and 1.5mm substrates except for 40MA.

Representative FTIR-ATR spectra for each copolymer are shown in Figure A.2. The presence of several characteristic chemical groups including the O-C=O, C-O-C, CH_2 o r CH_3 can be identified from peaks at 1750cm^{-1}, 1140cm^{-1}, and 2800-3000cm^{-1} wavenumbers, respectively. The absence of a peak at 1690cm^{-1} indicates full conversion of C=C double bonds within the network. Looking more closely at the collection of peaks at 2800-3000cm^{-1}, a shift in actual peak wavenumber is observed amongst the different compositions. Specifically, the peaks corresponding to the alpha-CH3 groups present in MMA monomer (but absent in MA) decreases in intensity as MA concentration increases. A decrease in peak intensity with increasing MA content is also observed in

the peak at 1200 cm^{-1}. Representative spectra for the 72MA surfaces made with both the 1mm and 1.5 mm thick glass substrates are included. No difference in peak wavenumber or intensity was observed between the two batches of surfaces. Although not shown for clarity purposes, a similar result was seen for the other MA-MMA copolymers as well.

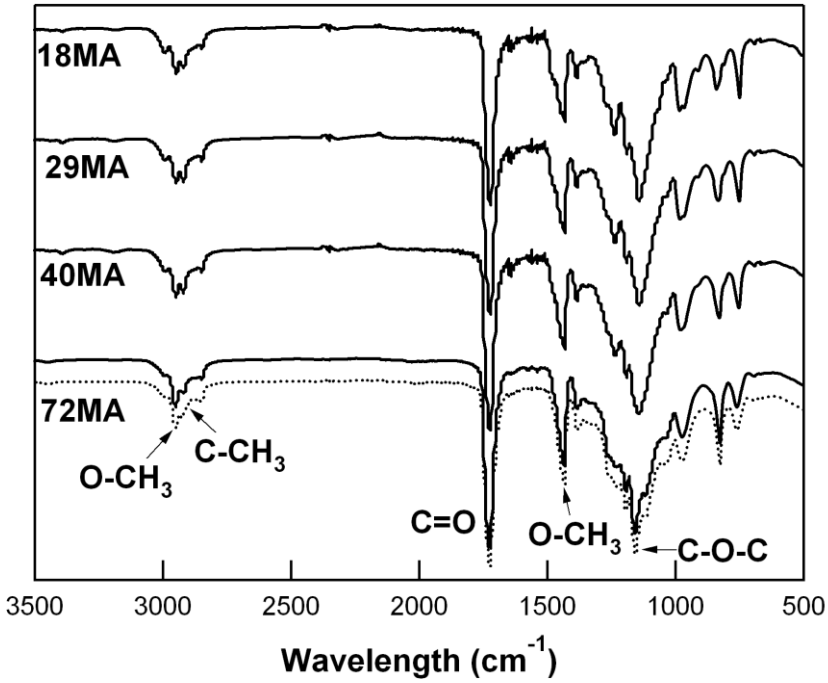

Figure A.2. Representative FTIR-ATR spectra showing key chemical peaks for each copolymer. Spectra of 72MA are shown from samples polymerized on both 1mm and 1.5mm thick glass substrates.

Elemental compositions determined through XPS for each copolymer are shown in Table A.2. The atomic percentages of C and O on the surface were not affected by MA concentration, but instead varied for each batch, although these changes were not significant, with about 70-90% carbon measured on the surface, nearly equivalent to calculated theoretical values. The percent composition of specific carbon-bonded groups were determined by performing high resolution scans and peak-fitting the C1s peak. Three peaks occurring at 284.5eV, 286eV, and 288eV were deconvoluted from the

primary C1s peak corresponding to the C-C, C-O-C, and O-C=O chemical groups found in all three monomers (Table A.2). Similar to the elemental concentrations, from Figure A.3, the peak areas corresponding to C-O-C and O-C=O groups on 18MA surfaces varies with each new batch of copolymer synthesized for cell study 1, 2, and 3. In general, the concentration of C-C groups on the surface was higher compared with what would be theoretically predicted based on the mole percentage of each monomer included (54-48%) while the percentage of C-O-C was less than expected (26-29%).

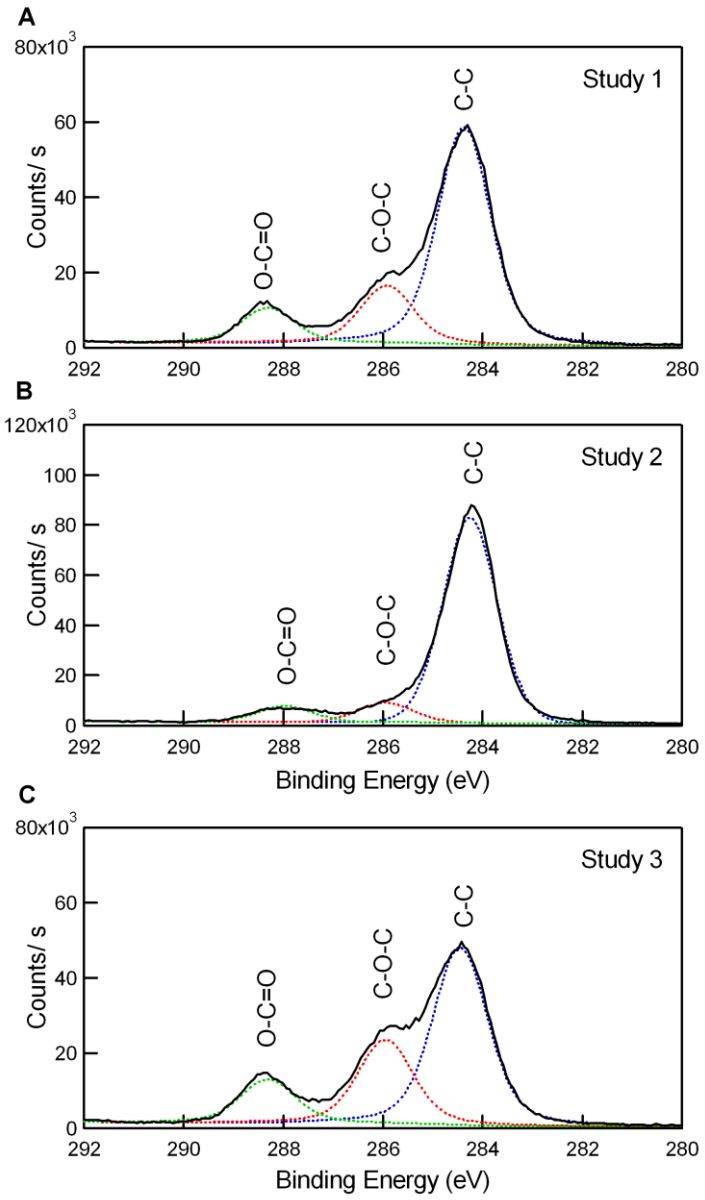

Figure A.3. Representative high resolution XPS scans of C1s peak for 18MA showing the deconvoluted peaks corresponding to specific chemical structures in the network. One scan is presented from study (a) 1 (1mm thick substrate), (b) 2 (1.5mm thick substrate), and (c) 3 (1.5mm thick substrate) showing the change in chemical group compositions for each batch of new copolymer made.

Table A.2. XPS elemental compositions (both survey and high resolution) for MA-co-MMA-co-PEGDMA networks.

Name	Substrate thickness	Atomic % C	Atomic % O	% C-C	% O-C=O	% C-O-C
	1 mm	78.5	21.4	70.2	11.3	18.5
18MA	1.5 mm	82.6	17.4	90.8	3.3	15.9
	1.5 mm	73.0	26.8	57.8	7.2	27.3
	1mm	81.6	18.4	79.1	4.7	16.1
29MA	1.5 mm	85.5	14.5	85.6	7.2	7.2
	1.5 mm	76.6	23.4	65.1	12.0	22.8
	1mm	79.3	20.7	73.6	9.6	16.8
40MA	1.5 mm	83.8	16.2	79.9	9.4	10.7
	1.5 mm	73.4	26.6	57.7	16.6	25.7
	1 mm	79.4	20.6	69.2	10.5	20.2
72MA	1.5 mm	77.3	22.7	70.4	11.1	18.4
	1.5 mm	80.6	19.4	74.3	10.8	14.9

A.3.3 MG63 Cell Response

Comparing the MG63 response on the MA-MMA-PEGDMA surfaces, cell number and differentiation were sensitive to the copolymer stiffness in a manner dependent upon the specific experiment (Figures A.4, A.5, and A.6). For copolymers polymerized on 1mm thick glass, cell number was reduced by 50% on the MA-MMA copolymer surfaces compared to TCPS. Comparing the different MA-MMA compositions, cell number increased by 50% on the 40MA (4.7 MPa) surface and 25% on the 72MA (0.8 MPa) surface compared with both 18MA and 29MA. Osteoblast differentiation and the production of certain osteogenic factors were also affected by copolymer stiffness. As seen in Figure A.4b, there is no significant difference in alkaline specific activity between the MA-MMA surfaces and TCPS, but 29MA, 40MA, and

72MA exhibited 30% less cells compared with 18MA. In contrast, osteocalcin production increased as stiffness increased with levels on the stiffest surface (18MA) 2-fold higher compared with TCPS. On the copolymers synthesized on 1mm thick glass, osteoprotegerin (OPG) levels increased at least by 50% on all MA compositions compared with TCPS with 29MA having the highest levels of OPG

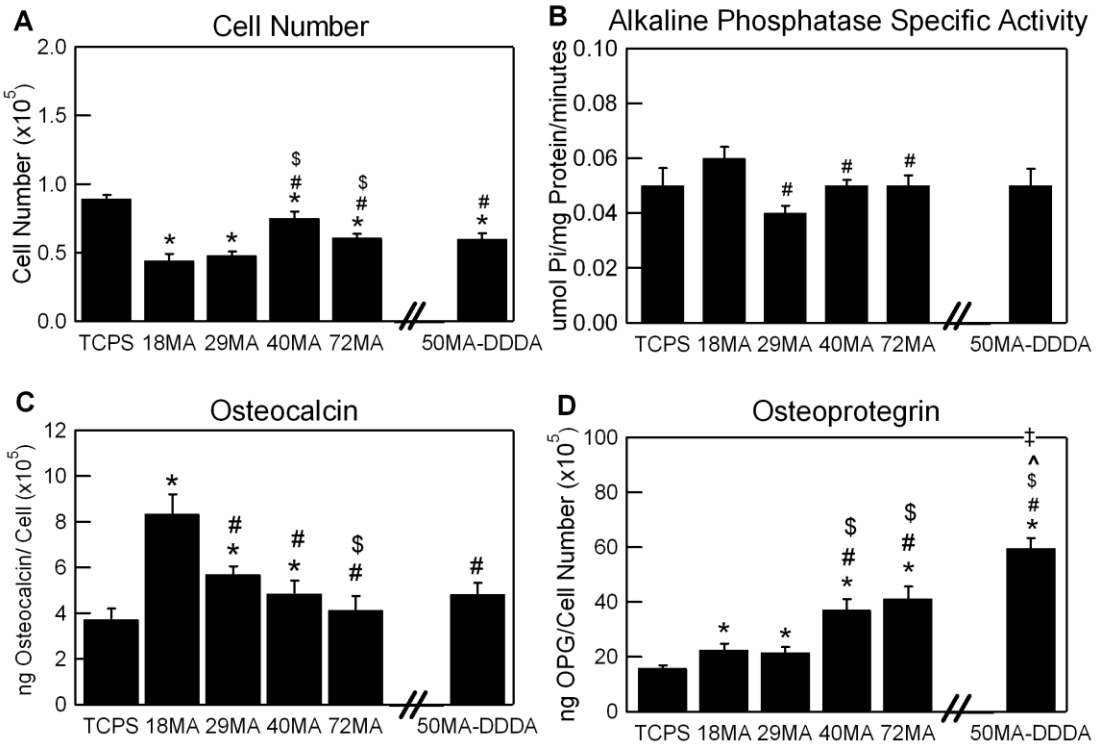

Figure A.4. Effect of composition and stiffness on differentiation of MG63 cells polymerized through 1mm thick substrate. Cells were cultured on tissue culture polystyrene (TCPS) or the copolymer surfaces and at confluence, (A) cell number, (B) alkaline phosphatase specific activity, (C) osteocalcin, and (D) OPG were measured .*p<0.05, polymer surface vs. TCPS; #p<0.05, polymer surface vs. 18MA; $p<0.05, polymer surface vs. 29MA; ^polymer surface vs. 40MA; ‡polymer surface vs. 72MA.

Cell number and differentiation were affected by MA-MMA surfaces polymerized on 1.5mm thick substrates in a different manner compared with those on 1mm thick substrates (Figure A.5). On the copolymers synthesized on the 1.5mm thick

glass, cell number decreased as copolymer stiffness decreased with an almost 50% reduction on the least stiff surface (72MA) compared with TCPS. There was no significant difference between the stiffer surfaces (18MA and 29MA) compared with TCPS. Osteoblast differentiation was also affected by UV intensity and copolymer stiffness. There was no significant difference in alkaline phosphatase specific activity compared with TCPS except for 72MA which, like cell number on this surface, exhibited about a 50% reduction in activity compared with TCPS. In contrast, cells on the 72MA surface produced the highest levels of osteocalcin, almost 4-fold higher compared with TCPS. Comparing the different copolymers within this group, osteocalcin increased with decreasing stiffness. The production of local regulatory factors was also sensitive to substrate thickness and copolymer stiffness. OPG production increased as copolymer stiffness decreased with cells on 72MA exhibiting a two-fold increase in OPG compared with TCPS.

To determine if these results were repeatable, a fresh set of copolymer discs was synthesized on 1.5mm thick substrates, and the MG63 cell response to the copolymer stiffness was evaluated (Figure A.6). Similar to the first experiment, cell number decreased as copolymer stiffness decreased exhibiting a 30% and 50% reduction compared with TCPS (Figure A.5 vs. Figure A.6). The effect of copolymer stiffness on OPG production was consistent for the two experiments with OPG levels increasing as copolymer stiffness decreased. However, both the effect of copolymer stiffness on alkaline phosphatase specific activity and osteocalcin production were not consistent between the two experiments. Specifically, in the second experiment, alkaline phosphatase specific activity was significantly higher by at least 30% on the MA

copolymers compared with TCPS with the most activity occurring on 40MA. No significant difference in osteocalcin production was observed between the MA copolymers and TCPS.

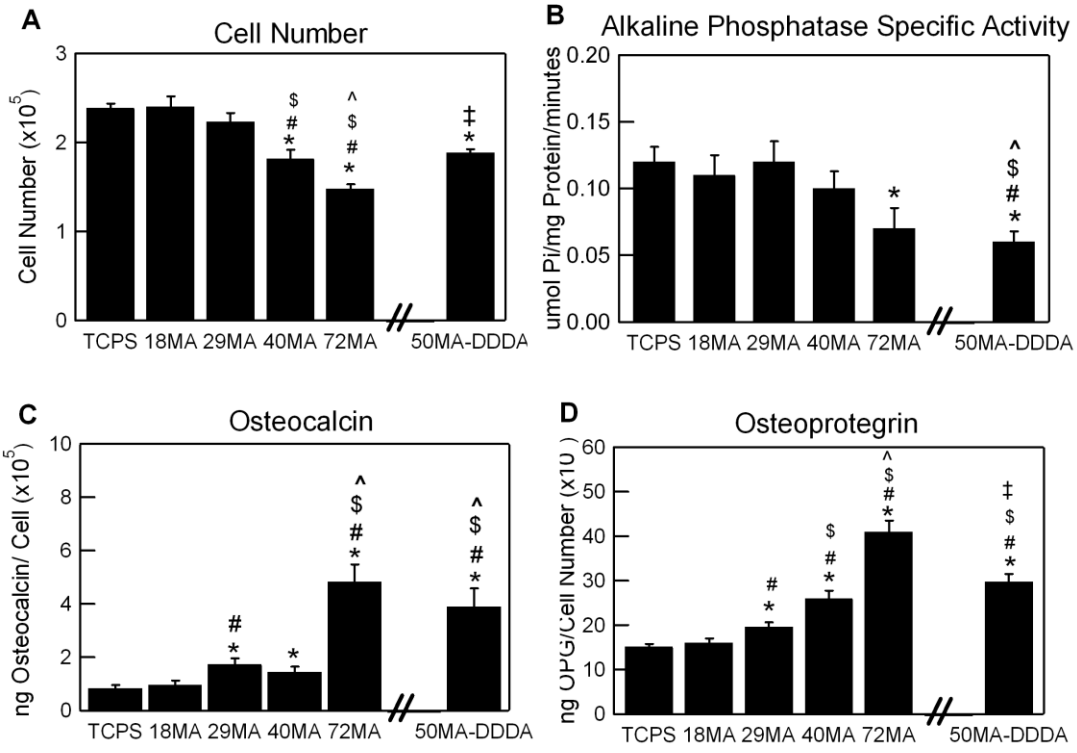

Figure A.5 Effect of composition and stiffness on differentiation of MG63 cells on surfaces polymerized through 1.5mm thick substrate. Cells were cultured on tissue culture polystyrene (TCPS) or the copolymer surfaces and at confluence, (A) cell number, (B) alkaline phosphatase specific activity, (C) osteocalcin, and (D) OPG were measured .*p<0.05, polymer surface vs. TCPS; #p<0.05, polymer surface vs. 18MA; $p<0.05, polymer surface vs. 29MA; ^polymer surface vs. 40MA; ‡polymer surface vs. 72MA.

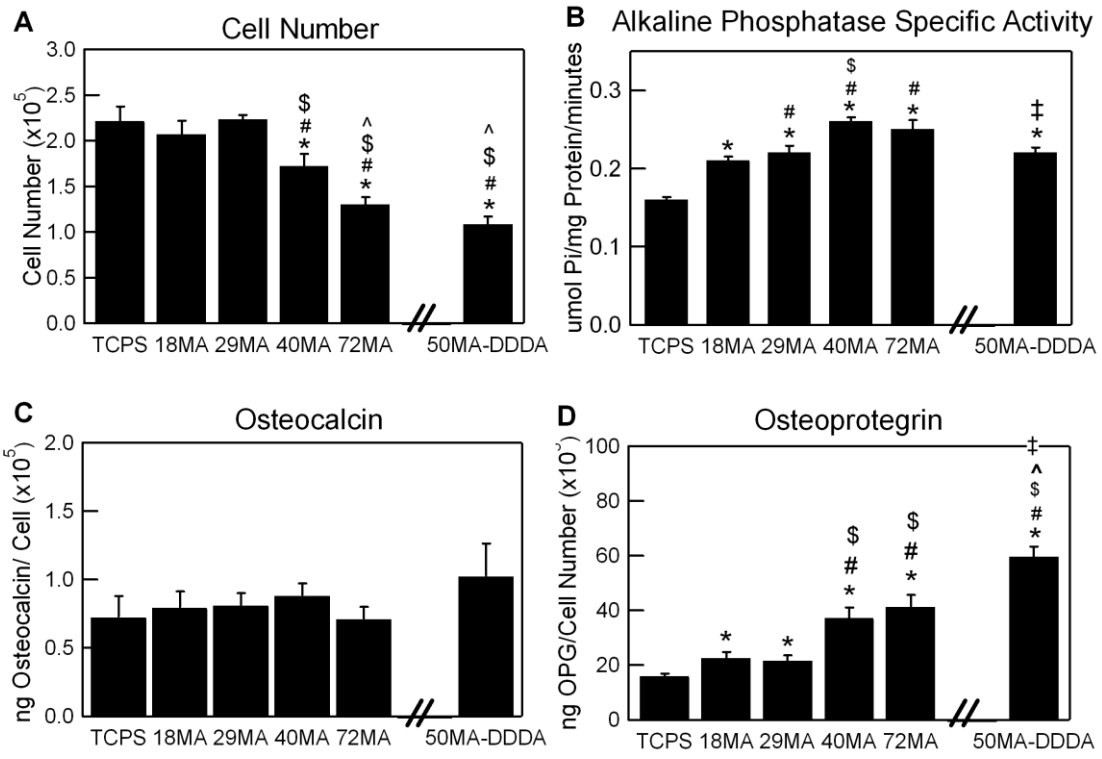

Figure A.6. Effect of composition and stiffness on differentiation of MG63 cells on surfaces polymerized through 1.5mm thick substrate (Experiment 2). Cells were cultured on tissue culture polystyrene (TCPS) or the copolymer surfaces and at confluence (A) cell number, (B) alkaline phosphatase specific activity, (C) osteocalcin, and (D) OPG were measured .*$p<0.05$, polymer surface vs. TCPS; #$p<0.05$, polymer surface vs. 18MA; \$$p<0.05$, polymer surface vs. 29MA; ^polymer surface vs. 40MA; ‡polymer surface vs. 72MA.

Similar to the MA-MMA-PEGDMA surfaces, the cell response on 50MA-DDDA surfaces differed for each individual experiment (Figures A.4 vs. A.5 vs. Figure A.6). When polymerized on 1mm thick glass, cell number, alkaline phosphatase specific activity, and osteocalcin production were not significantly different compared to TCPS while OPG levels were elevated 3-fold. When comparing the response of 50MA-DDDA to 40MA, a PEGDMA-crosslinked copolymer whose stiffness is similar to 50MA-DDDA, there was no difference in the cell response except for 2-fold higher OPG levels on 50MA-DDDA. Similarly, cells cultured in the first experiment using 1.5mm thick

glass on 50MA-DDDA exhibited a reduced cell number by 25%, decreased alkaline phosphatase specific activity, and increase in both osteocalcin and OPG levels compared with TCPS. These results were repeatable in the second experiment except there was no significant difference in osteocalcin levels between 50MA-DDDA and TCPS.

A.4 Discussion

Because osteoblasts are anchorage-dependent cells, they readily respond to physical and chemical stimuli in the ECM or on a synthetic surface. Previous studies have demonstrated the dependence of substrate stiffness on regulating the osteogenic potential of cells [97, 117], but a major limitation with these studies is that stiffness is usually altered by changing the chemical structure of the network such as increasing crosslinking density or coating with adhesion peptides such as arginine-glycine-aspartic acid (RGD) residues. To date, it has proven challenging to distinguish between the effects of copolymer mechanics and the corresponding chemical structural changes, making the actual mechanism by which cell differentiation is regulated through copolymer surfaces unclear. The results of this current study demonstrate that the effect of copolymer stiffness of MA-MMA copolymers on osteoblast differentiation is dependent upon properties of the photopolymerization process in manner that related to the inherent heterogeneity of the network formation.

MA-MMA based photopolymerizable networks have been identified as potential orthopaedic implant materials due to their enhanced toughness after long term exposure to physiological solution. Their mechanical properties, including modulus and toughness, can be tailored by adjusting Tg through varying the weight ratio of MA to MMA without

changing crosslinking density, as made evident from the DMA curves (Figure A.1). The MA-MMA copolymers selected for this study displayed a broad range of thermomechanical behaviors at 37°C from glassy (18MA) to ductile (29MA) to viscoelastic (40MA) to rubbery (72MA) allowing for a several orders of magnitude difference in stiffness.

In general for all three experiments, MG63 cells cultured on MA-MMA surfaces exhibited characteristics corresponding to a mature osteoblast phenotype. In comparison to TCPS, MA-MMA copolymers supported similar or less cell number. Although there was no significant difference in wettability as measured by contact angle between the copolymer surfaces and TCPS, the presence of PEG groups (C-O-C) on the surface has been shown to reduce cell attachment. Alkaline phosphatase specific activity and osteocalcin production are both well-studied differentiation markers for osteoblasts [92]. In general, alkaline phosphatase specific activity increases during the early stages of osteoblast differentiation, but then decreases over time as differentiation progresses and mineral deposition begins to occur. In contrast, osteocalcin levels are low during the early stages of differentiation and then increase and plateau as the cell reaches a mature osteoblast phenotype. Thus in this present study, the increased or similar levels of osteocalcin exhibited by cells on the MA-MMA copolymers compared with TCPS indicate that the cells are able to differentiate on these surfaces. OPG is produced by osteoblasts and acts as a decoy receptor by binding with RANKL to suppress osteoclastogenesis and regulate the bone remodeling cycle [193]. In previous studies, fully differentiated osteoblasts exhibited elevated levels of OPG in combination with increased osteocalcin production when cultured on microrough titanium surfaces [180,

194]. Once again in general, a similar result is seen on MA-MMA surfaces indicating that these copolymers affect the production of important osteogenic factors. A similar result showing elevated levels of both OCN and OPG has been observed on microrough titanium surfaces which also exhibited excellent bone-material contact and improved pullout strength *in vivo*. Thus, the results presented within this study suggest that MA-MMA copolymers are able to support osteoblast attachment and differentiation, an important characteristic of bone-interfacing implant materials.

In Chapter 5, an MA-MMA network crosslinked with DDDA was identified as a candidate material that could sustain excellent toughness for long durations in PBS. To further evaluate its ability to perform as an orthopaedic implant material in a bone-interfacing setting, the MG63 cell response was evaluated and compared with TCPS and the PEGDMA-crosslinked MA-MMA copolymers. Similar to the MA-MMA-PEGDMA copolymers, the ability of MG63 cells to differentiate on the 50MA-DDDA surface varied with each individual experiment, but promoted a similar level of cell attachment with each experiment. The comparable results on the 50MA-DDDA copolymer with the PEGDMA-crosslinked networks indicate that changing the crosslinker chemistry will not significantly affect the MG63 cell response. Considering the low crosslinking concentration in the network, it would thus be expected that this change in crosslinking chemistry does not affect protein adsorption and cell binding. The general elevated levels of both osteocalcin and OPG on this surface indicate that 50MA-DDDA materials are able to support osteoblast differentiation.

However, the effect of copolymer stiffness on the MG63 cell response on MA-MMA copolymers is somewhat unclear. For instance, cell number decreased and

osteocalcin production of MG63 cells increased with increasing copolymer stiffness when copolymer networks were polymerized on 1mm thick substrates but in contrast, cell number increased and osteocalcin levels decreased with copolymer stiffness when the copolymers were polymerized on 1.5mm thick substrates. Even when substrate thickness remained constant, the relationship between MA copolymer composition and osteocalcin production differed, but cell number and OPG production remained consistent between the two experiments (Figure A.5 vs. Figure A.6). This change in osteocalcin production in response to copolymer stiffness on surfaces synthesized on 1mm and 1.5mm thick glass signifies that the substrate thickness is affecting the material surface in a manner that the cells can sense.

Photopolymerizable copolymers are formed by mixing various ratios of monomers in the presence of a photoinitiator and then exposing the mixture to UV light while the solution is fixated in between two substrates or encompassed in a mold. Previous studies have reported that the intensity of UV light is affected by the substrate thickness and composition [27, 195-196]. Specifically according to the Beer-Lambert Law, UV intensity decreases as substrate thickness increase causing the polymerization rate to slow and monomers that are usually less reactive to convert their bonds at a similar rate as more reactive monomers resulting in changes in network formation. If the sample is thick enough, a gradient in polymerization rate with depth occurs resulting in structural heterogeneities between the surface and bulk of the material, often altering other material properties [36]. Thus, a possible explanation for the differential cell response could be that changing the substrate thickness altered the polymerization reaction causing changes in the surface network structure. From the DMA and DSC

performed in this study, changing the substrate thickness does not affect the bulk material properties, including Tg and elastic modulus, of the MA-MMA networks or the overall surface wettability suggesting that any alterations in network formation due to changes in UV intensity are specific to the surface in a manner independent of altering surface energy.

It has previously been shown that the cell response is affected not only by chemistry on the surface but also by the presentation of specific chemical groups and any intermolecular bonding that may occur in a manner related to changing the conformation of proteins that serve as primary cell adhesion molecules [31, 106, 197-198]. Thus, it was hypothesized that changes in the presentation of certain chemical groups on the surface due to a decrease in UV intensity affected the MG63 cell response to MA-MMA surfaces. Because no initial change in surface chemistry was observed in the FTIR-ATR spectra, high resolution XPS was performed to evaluate the concentration of chemical groups found on the monomers incorporated into the network. The higher surface concentration of C-C bonds on the surface compared with what would be theoretically predicted provides evidence that the copolymer network structure found on the surface is not indicative of the bulk network structure. Although only trace amounts of Si related to the Rain-X used on the glass were found (less than 1%), it is possible that the hydrophobic nature of the substrate surface initiated the aggregation of C-C backbone and alpha-methyl groups on the surface while the carboxyl and methyl terminal ends of MA and MMA and PEGDMA monomers remained buried in the bulk of the material. This effect has been observed in other polymers synthesized on silicone.

To distinguish whether the altered MG63 cell response to copolymer stiffness was specific to changing substrate thickness rather than creating a fresh set of copolymers through a new reaction, a second experiment was performed on surfaces synthesized separately on 1.5 mm thick glass substrates. Comparing the results from these two experiments (Figures A.5 and A.6), it is evident that MG63 cell differentiation in response to copolymer stiffness, as noted by changes in osteocalcin production, varies with each new batch of copolymers tested. Photopolymerization reactions involving the mixing of multiple monomers produce random amorphous networks that often contain localized microregions of certain chemical constituents [106]. Although it would be expected that these microregions would be spatially averaged over the area of one sample disc (15mm in diameter), the variability in the presentation of chemical groups on the surface for each new set of copolymer surfaces in combination with the higher concentrations of C-C groups than theoretically predicted indicates that the photopolymerization of three-component networks results in heterogeneic surfaces that exhibit variable chemical groups on the surface with each new polymerization, despite incorporating the same weight ratios of monomers. This variability in the surface presentation of chemical groups independent of the total concentrations of carbon and oxygen atoms, affects how MG63 cells differentiate on MA-co-MMA-co-PEGDMA surfaces. Interestingly, the effect of copolymer stiffness on cell number did not change between these two experiments, but was only influenced by changing substrate thickness suggesting that these subtle changes in chemistry might not affect the ability of the cells to bind to the copolymer, but instead influence the presentation of ECM proteins that provide important signals to initiate osteoblast differentiation.

An advantage of photopolymerizable networks is their ability to be formed into complex geometries using a variety of molding and lithography techniques. In many of these methods, the polymer solution is injected into a transparent mold such as silicone or glass and then exposed to UV light. Within this study, we have shown that MG63 cells are sensitive to the copolymerization reaction of MA-MMA networks in a manner potentially related to the substrate thickness and polymerization reaction. If these materials were to be implemented in implant devices, their ability to favorably promote tissue integration could be affected by the implant geometry in relation to overall thickness. In addition, the MG63 response to MA-MMA surfaces is batch-dependent suggesting that in order to get a complete understanding of copolymer-cell interactions, several studies using multiple batches of material must be performed. These findings must be taken into consideration when examining *in vitro* cellular responses to photopolymerizable networks containing multiple monomers.

A.5 Conclusions

The response of MG63 cells to MA-co-MMA-co-PEGDMA networks was assessed to determine if copolymer stiffness and the copolymerization process affected the cells reaching a mature osteoblast phenotype. Significant variations in the surface presentation of chemical groups from batch to batch of materials affected the differentiation potential of MG63 cells in response to copolymer stiffness. Interestingly, the bulk material properties did not change with each new batch indicating the sensitivity of MG63 cells to the specific chemical surface presentation. In general, these materials promoted osteoblast maturation to a greater extent compared with TCPS that in

combination with their excellent mechanical properties suggests their potential use for bone-interfacing applications.

APPENDIX B

PROTOCOLS

B.1 Cell Harvest Protocol and Determining Cell Number

1. Turn on water bath and thaw trypsin/warm harvest media (DMEM+10%FBS).

2. Turn on and flush cell counter (Place vial with saline into counter Hit **Function)** and then **Fill System)** and turn on centrifuge so it has time to cool.

3. Label test tubes for storage of cell lysates and conditioned media while harvest materials thaw.

4. Pull cell culture inserts off of surfaces to make easier to remove media (but keep plugged in wells).

5. Remove media from each well of confluent experimentally treated cells grown in 24-well plate and place in individually labeled centrifuge tubes.

6. Wash cells twice with 1mL per well of DMEM (Cellgro Corporation). Pipette towards side of well and not directly on surfaces.

7. To initialize release from surfaces, incubate cells with 1mL of 0.25% Trypsin (Gibco) for 10 minutes at 37°C.

8. After incubation, shake the plate gently and the released cells should begin to be seen. Pipette contents from each well into labeled 13x100mm test tubes (pipette up/down to get evenly mixed sample).

9. Add 1mL of full media to each test tube to stop the trypsin reaction.

10. Remove inserts and then add another 500uL 0.25% Trypsin to each well again and incubate at 37°C for 10 minutes. (The second trypsinization is very important to get all the cells released from the surfaces).

11. Repeat Step 8. Add 500uL of full media into each well, flush each well by pipetting the full media up and down and then transfer contents to corresponding tubes.

12. Vortex tubes to make sure pellet stays in solution and does not stick on the side wall of the test tubes.

13. Centrifuge tubes at 3200rpm, 4°C for 15 minutes in a tabletop centrifuge. Meanwhile, fill counting vials with 10mL of 0.9% NaCl (9g NaCl per 1 Liter Ultrapure Water).

14. Discard supernatant (do not remove pellet!) and resuspend pellet with 500uL 0.9% NaCl taken from individual counter vials.

15. Pipette up and down to break up pellet and transfer all of tubes' contents into counting vials containing remaining 9.5mL 0.9%NaCl.

16. Count cells using Coulter Counter:
    a. Flush counter with saline.
    b. Go to **Function** and make sure particle size is 9.5um to 22.5um (for MG63s).
    c. Place each vial containing cells in counter and hit **Setup** and **Start/Stop**.
    d. Flush counter with saline between each group.
    e. If counter gets clogged (look in upper window), Hit **Function** and **Flush Aperture**.
    f. After finished counting, place vial with blue contents in counter and turn off.

17. After counting, pour samples from counting vials back into test tubes and spin the samples at 3200rpm at 4°C for 15minutes in tabletop centrifuge. (Pour entire contents of counting vials into test tube.)

18. Discard the supernatant and resuspend pellet with 500uL 0.05% Triton X-100 (500uL Triton X-100 per 1 Liter Ultrapure Water). Store in -20°C freezer.

19. Thaw samples at room temperature and sonicate at amplitude of 60 for 4 seconds before protein and alkaline phosphatase specific activity assays.

B.2 Protocol for Preparing Cells on Polymer Surfaces for SEM Analysis

1. Materials

    a. Phosphate Buffered Saline
    b. Karnovsky's fixative (EMS):
        - 16%paraformaldehyde solution
        - 50% gluteraldehyde (EM Grade)
        - 0.2M sodium phosphate buffer
        - Distilled Water

2. Method

    a. Add 1mL of media to polymer discs in 24-well culture plate for 24hrs.

    b. Aspirate media from wells. Plate 20,000 cells/well onto each disc and incubate for 24hrs.

    c. After 24hrs, aspirate media. Add 1mL PBS to each well to rinse out residual media (Repeat twice).

d. Add 1mL Karnovsky's fixative to each well and incubate for overnight at room temperature.

e. Remove fixative and rinse three times with PBS.

f. Immediately place discs (still in cell culture plate) in freeze dryer (Labconco Freezone; 0.1mbar, -50C) for up to 3 days. Check every 24hrs to evaluate polymer shrinkage.

g. Immediately mount discs to SEM sample studs and sputter coat in gold.

h. Store samples under vacuum prior to performing SEM

B.3. Assay for Alkaline Phosphatase Specific Activity (adapted from [199]

1. Materials/Reagents — Concentrations
   a. 2-amino-2methyl-1-propanol (AMP) (Sigma Aldrich) 1.5M balanced to pH = 10.25 — 7.54mL/50mL
   b. P-nitrophenyl phosphate (pnPP) Sigma Aldrich) — 371.14mg/50mL
   c. Magnesium Chloride ($MgCl_2$) (Sigma Aldrich) — 51mg/25mL
   d. Sodium Hydroxide (NaOH) (Sigma Aldrich — 2g/50mL
   e. p-nitrophenyl Standard (pNP) — 1 part stock with 9 parts ultra pure water

2. Procedure
   a. Thaw cell lysates of samples and sonicate for 10s. While samples are thawing, label test tubes #1-9.
   b. Add buffer solution (1:1:1 ratio of AMP+pnPP+ $MgCl_2$)
   c. Vortex tubes then pipette 100uL of each standard into rows A-C of the corresponding number in a 96-well plate.
   d. Add 100uL of NaOH to all wells of standard and read on microplate reader at 405nm.
   e. Save standard as visual reference of color change during sample incubation.
   f. Vortex samples thoroughly. Pipette 50uL of each sample into a 96-well plate.
   g. Add 50uL of buffer solution into all sample wells.

h. Incubate at 37C for up to 90 minutes. During incubation, watch for color change to a light yellow. Remove samples when color change is seen majority of wells. Record total incubation time.
i. Immediately add 100uL of NaOH into all sample wells.
j. Read on microplate reader at 405nm.

APPENDIX C

SUPPLEMENTAL RESULTS OF MG63 CELL RESPONSE TO MA-MMA COPOLYMER SURFACES

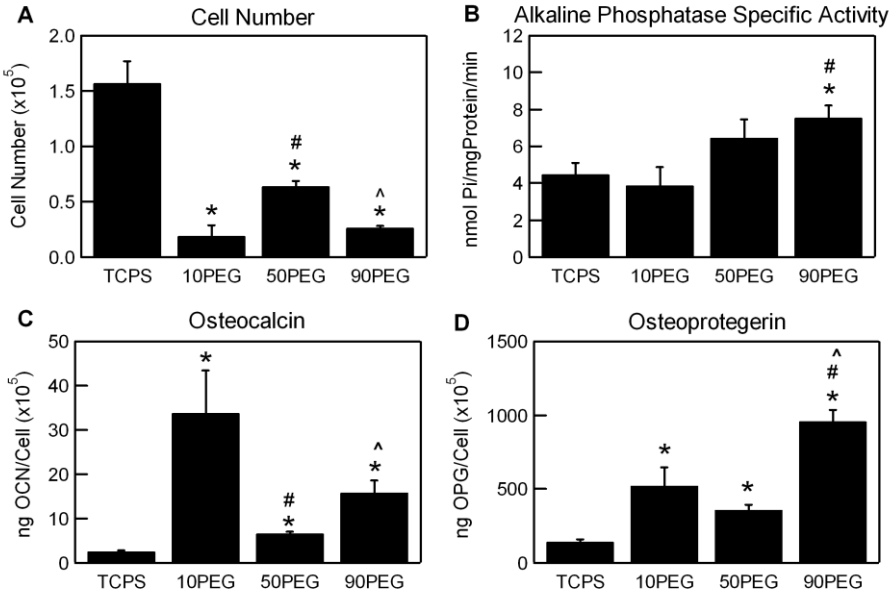

Figure C.1. The effect of copolymer composition on (A) cell number, (B) alkaline phosphatase specific activity, (C) osteocalcin, and (D) osteoprotegerin production. Data are mean +/-SEM from experiment 1.

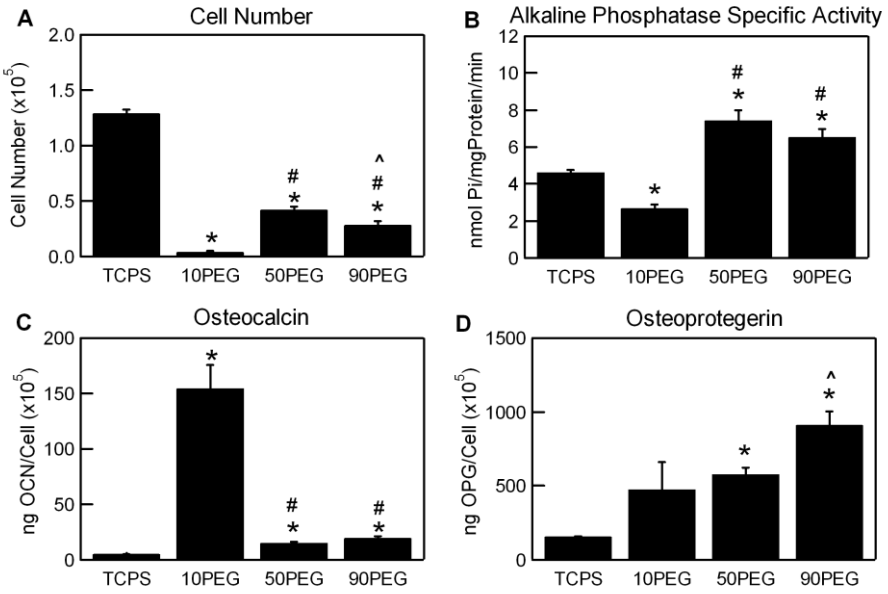

Figure C.2. The effect of copolymer composition on (A) cell number, (B) alkaline phosphatase specific activity, (C) osteocalcin, and (D) osteoprotegerin production. Data are mean +/-SEM from experiment 2.

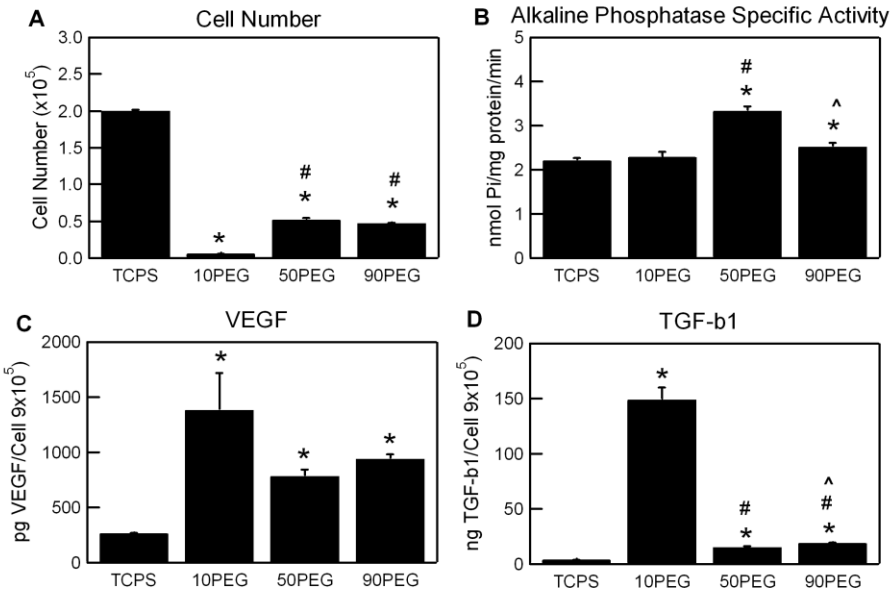

Figure C.3 The effect of copolymer composition on (A) cell number, (B) alkaline phosphatase specific activity, (C) VEGF-A, and (D) TGF- β1 production. Data are mean +/-SEM from experiment 3.

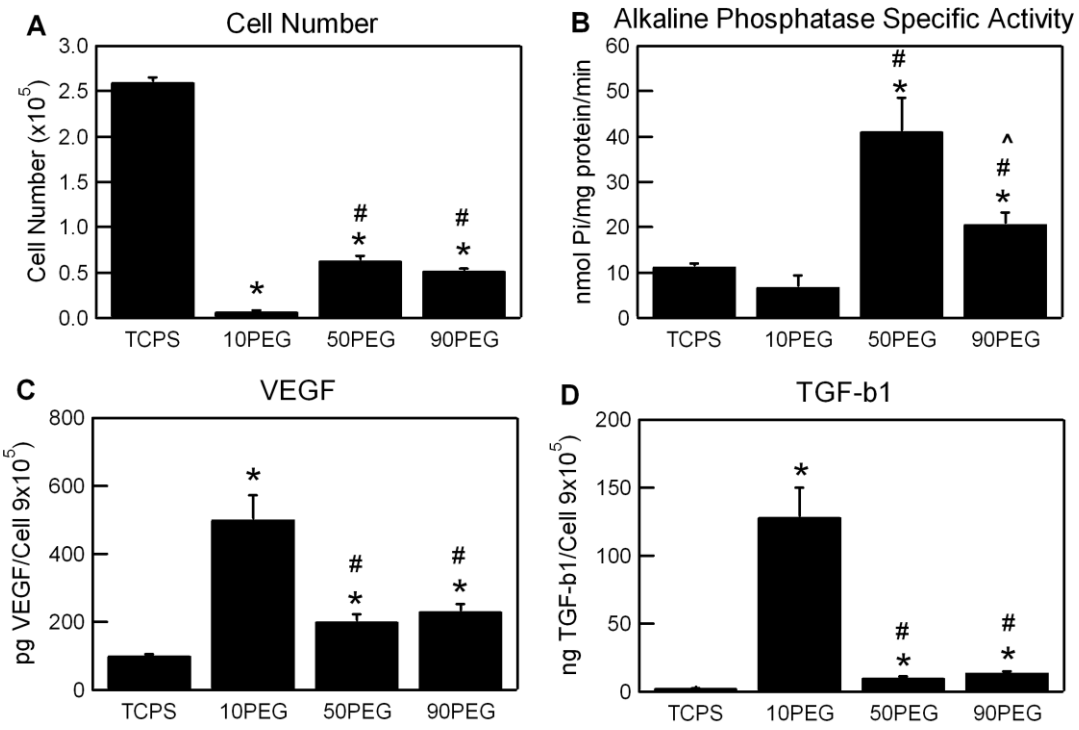

Figure C.4. The effect of copolymer composition on (A) cell number, (B) alkaline phosphatase specific activity, (C) VEGF-A, and (D) TGF- β1 production. Data are mean +/-SEM from experiment 4.

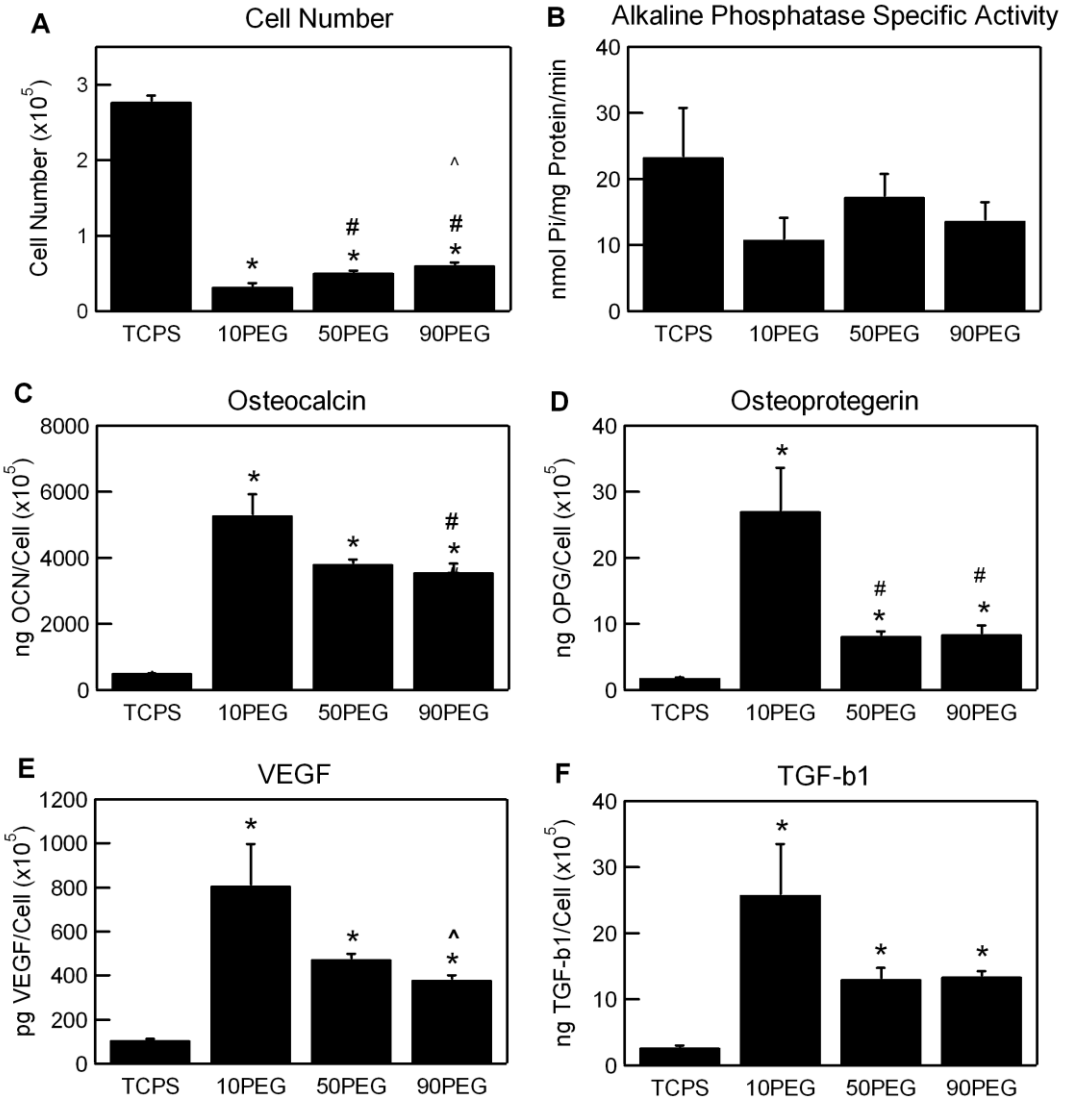

Figure C.5. The effect of copolymer composition on (A) cell number, (B) alkaline phosphatase specific activity, (C) osteocalcin, (D) osteoprotegerin, (E) VEGF-A, and (F) TGF- β1 production. Data are mean +/-SEM from experiment 5.

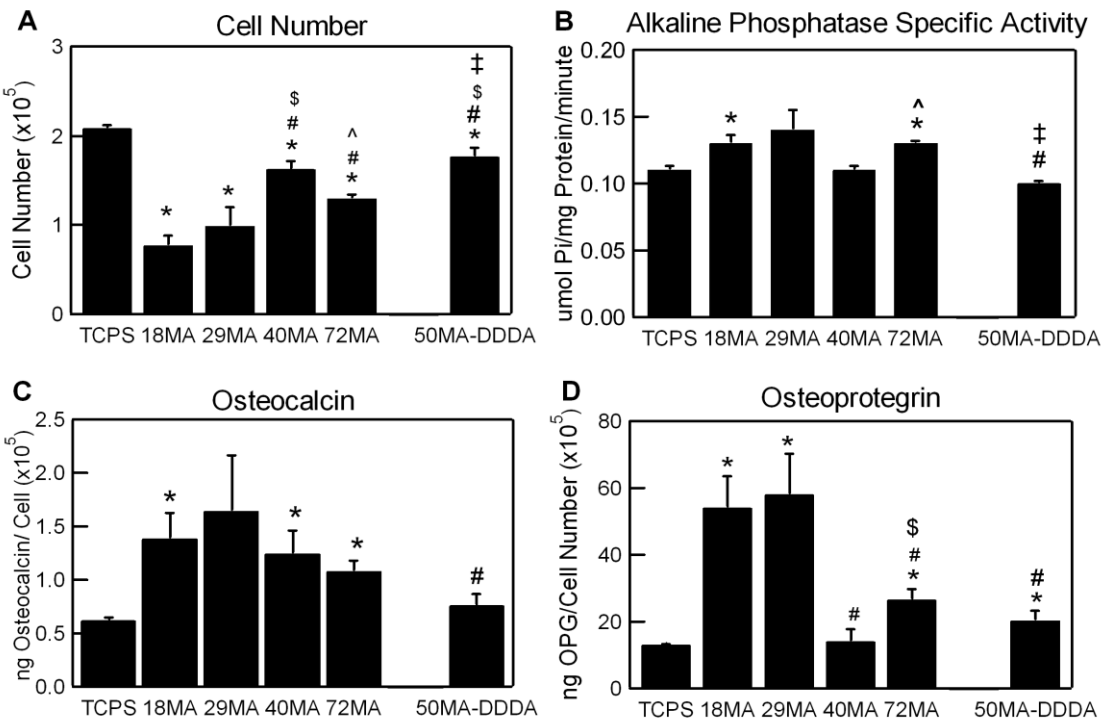

Figure C.6: Effect of composition and stiffness on differentiation of MG63 cells polymerized through 1mm thick substrate (Repeat for Figure A.4). Cells were cultured on tissue culture polystyrene (TCPS) or the copolymer surfaces and at confluence (A) cell number, (B) alkaline phosphatase specific activity, (C) osteocalcin, and (D) OPG were measured .*p<0.05, polymer surface vs. TCPS; #p<0.05, polymer surface vs. 18MA; $p<0.05, polymer surface vs. 29MA; ^polymer surface vs. 40MA; ‡polymer surface vs. 72MA.

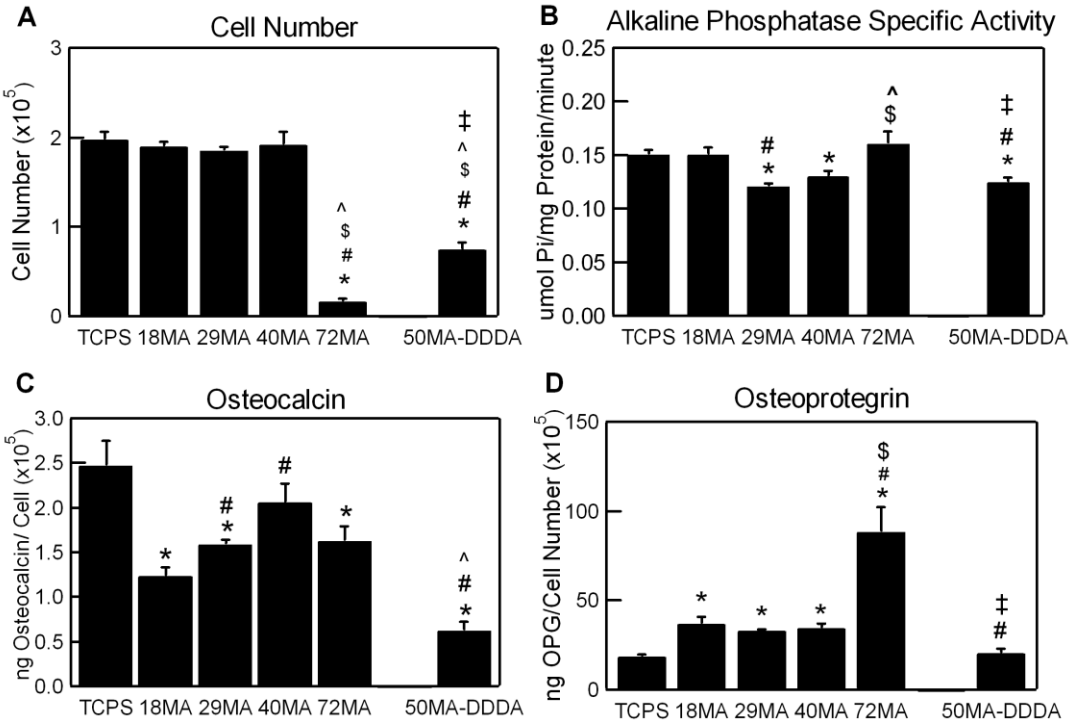

Figure C.7: Effect of composition and stiffness of MA-MMA copolymers on differentiation of MG63 cells polymerized through 1.5mm thick substrate (1 of three experiments performed on independently synthesized materials). Cells were cultured on tissue culture polystyrene (TCPS) or the copolymer surfaces and at confluence (A) cell number, (B) alkaline phosphatase specific activity, (C) osteocalcin, and (D) OPG were measured .*$p<0.05$, polymer surface vs. TCPS; #$p<0.05$, polymer surface vs. 18MA; \$$p<0.05$, polymer surface vs. 29MA; ^polymer surface vs. 40MA; ‡polymer surface vs. 72MA.

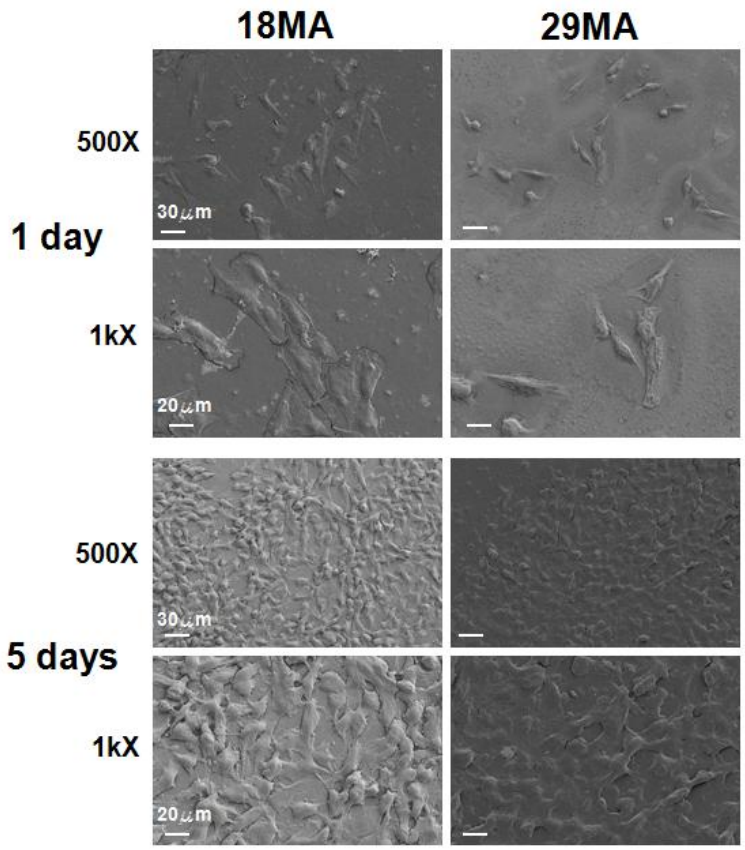

Figure C.8. Scanning electron micrographs of MG63 cells after 24h and 5 days in culture on 18MA and 29MA surfaces synthesized on 1.5mm substrates at 500X and 1kX magnifications.

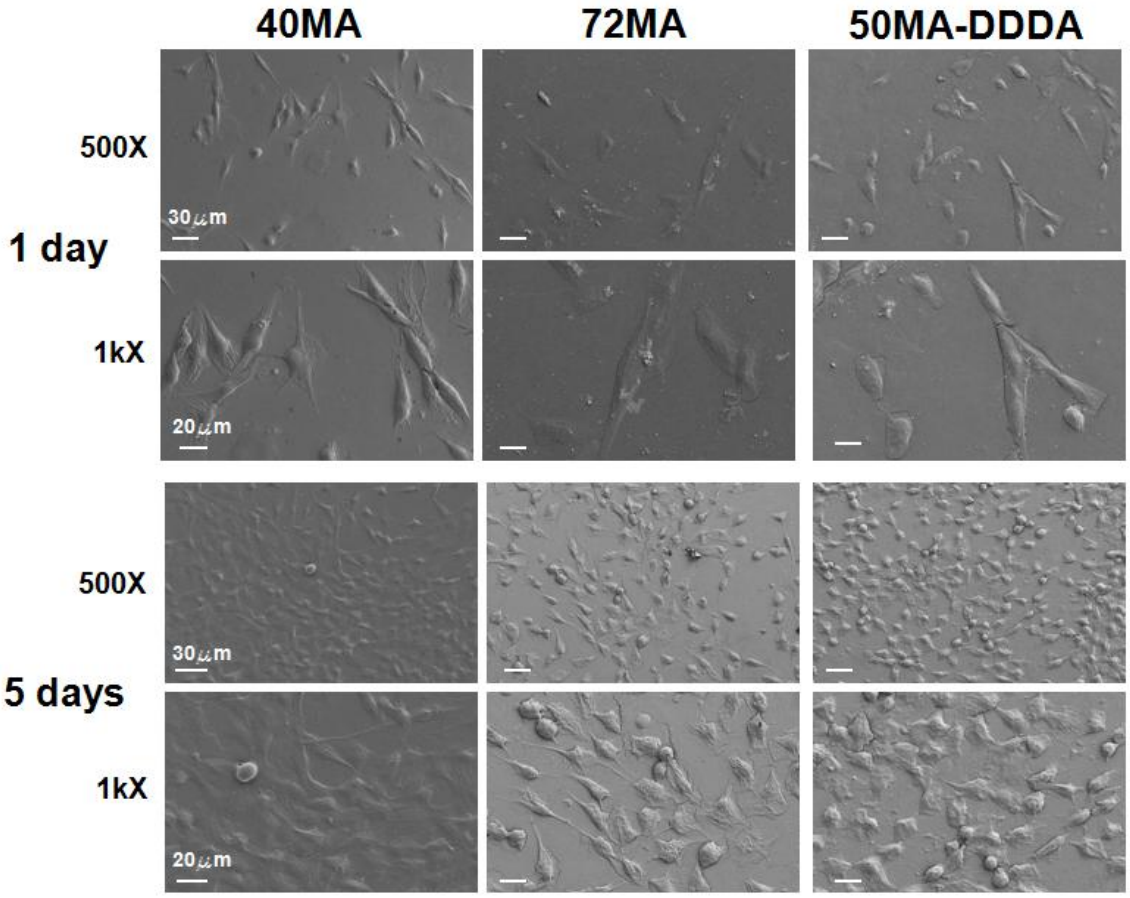

Figure C.9. Scanning electron micrographs of MG63 cells after 24h and 5 days in culture on 40MA, 72MA, and 50MA-DDDA surfaces synthesized on 1.5mm substrates at 500X and 1kX magnifications.

APPENDIX D

EFFECT OF IMMERSION FLUID ON TOUGHNESS OF MA-CO-MMA-CO-PEGDMA NETWORKS

PBS has been the primary fluid chosen to investigate the effects of physiological media on toughness because of its similarity to water, of which its effects on polymer properties has already been extensively reported. Due to the long testing times associated with some of the tensile strain-to-failure testing, samples needed to be immersed in the solution throughout the duration of the test to ensure the absorbed PBS did not evaporate. Thus using the equipment available, PBS was the only physiological media that would not cause corrosion to the fixtures and equipment. However, it is important to understand if some of the same structure-property relationships established in the previous chapter still hold up in other physiologically-relevant fluids. Thus, the fluid content, Tg, and toughness was assessed in 29MA-co-MMA-co-PEGDMA after immersion in fetal bovine serum (FBS), Dulbecco's Modified Eagle's Medium (DMEM), and PBS (pH=6.0). FBS was adopted to simulate the blood serum proteins that are present *in vivo* and that are known to attack materials upon implantation. DMEM represented the conditions found in *in vitro* cell culture experiments similar to those carried out in Chapter 6. When a material is initially implanted into the body, inflammation occurs around the implant site and some of the resultant proteins and factors produced during the inflammatory process create an acidic environment. Therefore to simulate the aqueous environment under inflammatory conditions, samples were tested in PBS with a pH=6.0, the pH reported in tissue during inflammation. Samples of 29%MA-co-MMA-co-10%PEGDMA were

immersed in each fluid for 1 week and then subjected to tensile strain-to-failure testing, differential scanning calorimetry, and swelling measurements as described in the Methods section of Chapter 4. The results, shown below in Figure C.1, C.2, C.3, and C.4, demonstrate that the type of physiological fluid does not affect the toughness and thermal transition behavior of photopolymerizable MA-co-MMA networks.

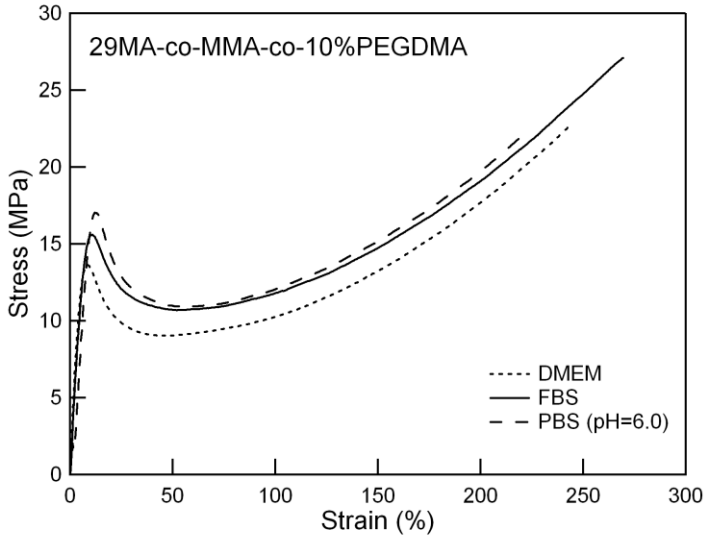

Figure D.1. Representative stress-strain behavior of 29MA-co-MMA-co-PEGDMA after 1 week immersion in each physiological fluid.

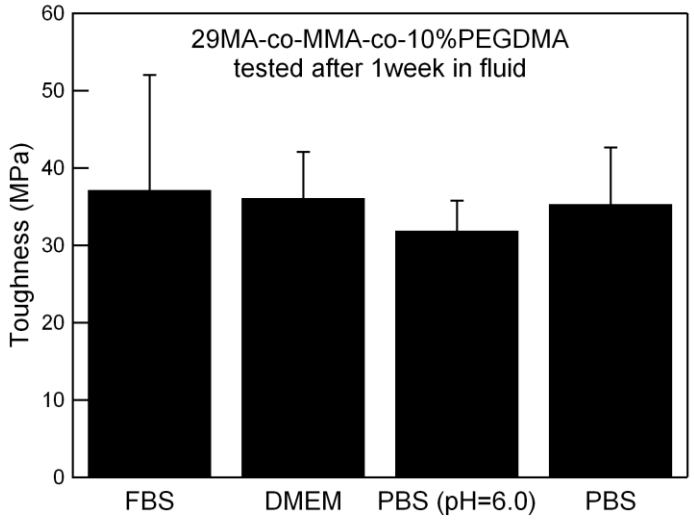

Figure D.2. Mean toughness values for 29MA-co-MMA-co-PEGDMA after 1 week immersion in each physiological fluid. There is no significant difference between any of the fluids tested (n=4).

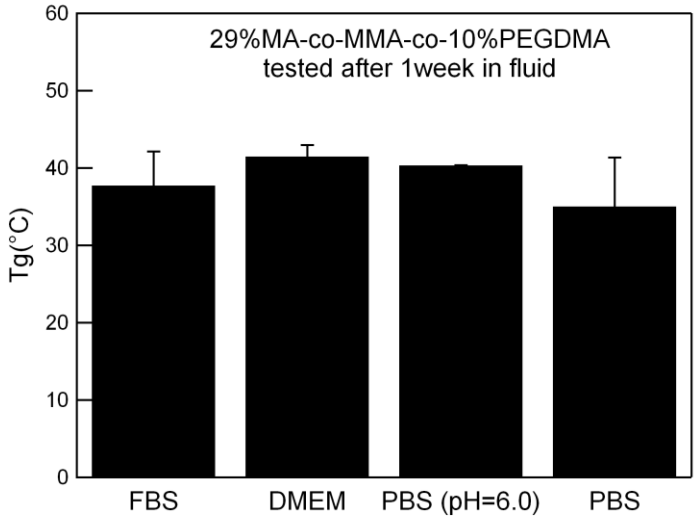

Figure D.3. Mean Tg values for 29MA-co-MMA-co-PEGDMA after 1 week immersion in each physiological fluid. There is no significant difference between any of the fluids tested (n=3).

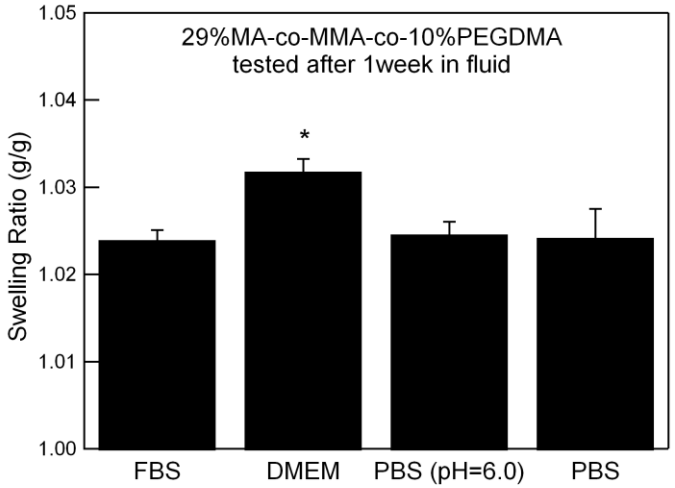

Figure D.4. Mean swelling ratios for 29MA-co-MMA-co-PEGDMA after 1 week fluid. The swelling ratio of DMEM was significantly higher compared with FBS and PBS (pH=6.0) (n=4).

REFERENCES

[1] Katz JN. Lumbar disc disorders and low-back pain: Socioeconomic factors and consequences. Journal of Bone and Joint Surgery-American Volume 2006;88A:21-24.

[2] Goins ML, Wimberley DW, Yuan PS, Fitzhenry LN, Vaccaro AR. Nucleus pulposus replacement: an emerging technology. The Spine Journal 2005;5:317S-324S.

[3] Lee CK, Goel VK. Artificial disc prosthesis: design concepts and criteria. The Spine Journal 2004;4:209S-218S.

[4] Gloria A, Causa F, De Santis R, Netti PA, Ambrosio L. Dynamic-mechanical properties of a novel composite intervertebral disc prosthesis. Journal of Materials Science-Materials in Medicine 2007;18(11):2159-2165.

[5] Mercuri D, Leone G, Barbucci R, Favaloro R, Facchini A, Signori F, et al. An artificial disc: chemical and biomechanical analysis. Macromolecular Symposia 2008;266(1):74-80.

[6] Urban JPG, Roberts S. Degeneration of the intervertebral disc. Arthritis Research & Therapy 2003;5(3):120-130.

[7] Nguyen KT, West JL. Photopolymerizable hydrogels for tissue engineering applications. Biomaterials 2002;23(22):4307-4314.

[8] Elisseeff J, Anseth K, Sims D, McIntosh W, Randolph M, Langer R. Transdermal photopolymerization for minimally invasive implantation. Proceedings of the National Academy of Sciences of the United States of America 1999;96(6):3104-3107.

[9] Brey DM, Erickson I, Burdick JA. Influence of macromer molecular weight and chemistry on poly(beta-amino ester) network properties and initial cell interactions. J Biomed Mater Res A 2008;85A(3):731-741.

[10] Yakacki CM, Shandas R, Safranski D, Ortega AM, Sassaman K, Gall K. Strong, tailored, biocompatible shape-memory polymer networks. Adv Funct Mater 2008;18(16):2428-2435.

[11] Engler AJ, Sen S, Sweeney HL, Discher DE. Matrix elasticity directs stem cell lineage specification. Cell 2006;126(4):677-689.

[12] Wong JY, Leach JB, Brown XQ. Balance of chemistry, topography, and mechanics at the cell-biomaterial interface: Issues and challenges for assessing the

role of substrate mechanics on cell response. Surface Science 2004;570(1-2):119-133.

[13] Schmid H, Michel B. Siloxane polymers for high-resolution, high-accuracy soft lithography. Macromolecules 2000;33(8):3042-3049.

[14] Odom TW, Love JC, Wolfe DB, Paul KE, Whitesides GM. Improved pattern transfer in soft lithography using composite stamps. Langmuir 2002;18(13):5314-5320.

[15] Yu TY, Ober CK. Methods for the topographical patterning and patterned surface modification of hydrogels based on hydroxyethyl methacrylate. Biomacromolecules 2003;4(5):1126-1131.

[16] Decker C. UV-curing chemistry -past, present, and future Journal of Coatings Technology 1987;59(751):97-106.

[17] Anseth K, Metters A, Bryant S, Martens P, Elisseeff J, Bowman C. In situ forming degradable networks and their application in tissue engineering and drug delivery. J Controlled Release 2002;78(1-3):199-209.

[18] Burkoth AK, Anseth KS. A review of photocrosslinked polyanhydrides: in situ forming degradable networks. Biomaterials 2000;21(23):2395-2404.

[19] Nuttelman CR, Henry SM, Anseth KS. Synthesis and characterization of photocrosslinkable, degradable poly(vinyl alcohol)-based tissue engineering scaffolds. Biomaterials 2002;23(17):3617-3626.

[20] Poshusta AK, Anseth KS. Photopolymerized biomaterials for application in the temporomandibular joint. Cells Tissues Organs 2001;169(3):272-278.

[21] Gall K, Yakacki CM, Liu Y, Shandas R, Willett N, Anseth KS. Thermomechanics of the shape memory effect in polymers for biomedical applications. J Biomed Mater Res, Part A 2005;73A:339-348.

[22] Yakacki CM, Shandas R, Safranski D, Ortega AM, Sassaman K, Gall K. Strong, Tailored, Biocompatible Shape-Memory Polymer Networks. Adv Funct Mater 2008;18:1-8.

[23] Hillwest JL, Chowdhury SM, Dunn RC, Hubbell JA. Efficacy of a resorbably hydrogel barrier, oxidized regenerated cellulose, and hyaluronic-acid in the prevention of ovarian adhesions in a rabbit model Fertility and Sterility 1994;62(3):630-634.

[24] Hillwest JL, Chowdhury SM, Slepian MJ, Hubbell JA. Inhibition of thrombosis and intimal thickening by in-situ photopolymerization of thin hydrogel-barriers.

Proceedings of the National Academy of Sciences of the United States of America 1994;91(13):5967-5971.

[25] Peppas NA, Keys KB, Torres-Lugo M, Lowman AM. Poly(ethylene glycol)-containing hydrogels in drug delivery. Journal of Controlled Release 1999;62(1-2):81-87.

[26] Baroli B. Photopolymerization of biomaterials: issues and potentialities in drug delivery, tissue engineering, and cell encapsulation applications. Journal of Chemical Technology and Biotechnology 2006;81(4):491-499.

[27] Goodner MD, Bowman CN. Modeling and experimental investigation of light intensity and initiator effects on solvent-free photopolymerizations. . In: Long TE, Hunt MO, editors. Solvent-free polymerizations and processesL Minimization of conventional organic solvents. Washington D.C.: American Chemical Society; 1998. p. 220-231.

[28] Lovell LG, Lu H, Elliott JE, Stansbury JW, Bowman CN. The effect of cure rate on the mechanical properties of dental resins. Dental Materials 2001;17(6):504-511.

[29] Burdick JA, Peterson AJ, Anseth KS. Conversion and temperature profiles during the photoinitiated polymerization of thick orthopaedic biomaterials. Biomaterials 2001;22(13):1779-1786.

[30] Geurtsen W, Leyhausen G. Chemical-biological interactions of the resin monomer triethyleneglycol-dimethacrylate (TEGDMA). Journal of Dental Research 2001;80(12):2046-2050.

[31] Schuster M, Turecek C, Kaiser B, Stampfl J, Liska R, Varga F. Evaluation of biocompatible photopolymers I: Photoreactivity and mechanical properties of reactive diluents. Journal of Macromolecular Science Part a-Pure and Applied Chemistry 2007;44(4-6):547-557.

[32] Yoshii E. Cytotoxic effects of acrylates and methacrylates: Relationships of monomer structures and cytotoxicity. Journal of Biomedical Materials Research 1997;37(4):517-524.

[33] Ortega AM, Kasprzak SE, Yakacki CM, Diani J, Greenberg AR, Gall K. Structure-property relationships in photopolymerizable polymer networks: Effect of composition on the crosslinked structure and resulting thermomechanical properties of a (meth)acrylate-based system. Journal of Applied Polymer Science 2008;110(3):1559-1572.

[34] Safranski DL, Gall K. Effect of chemical structure and crosslinking density on the thermo-mechanical properties and toughness of (meth)acrylate shape memory polymer networks. Polymer 2008;49(20):4446-4455.

[35] Corkhill PH, Jolly AM, Ng CO, Tighe BJ. Synthetic Hydrogels .1. Hydroxyalkyl acrylate and methacrylate copolymers - water-binding studies. . Polymer 1987;28(10):1758-1766.

[36] Goodner MD, Bowman CN. Development of a comprehensive free radical photopolymerization model incorporating heat and mass transfer effects in thick films. Chemical Engineering Science 2002;57(5):887-900.

[37] Barnes A, Corkhill PH, Tighe BJ. Synthetic hydrogels .3. Hydroxyalkyl acrylate and methacrylate copolymers - surface and mechanical properties. Polymer 1988;29(12):2191-2202.

[38] Fox TG, Loshaek S. Influence of molecular weight and degree of crosslinking on t he specific volume and glass temperature of polymers. Journal of Polymer Science 1955;15:371-390.

[39] Gibbs JH, DiMarzio EA. Nature of the glass transition and the glassy state. The Journal of Chemical Physics 1958;28(1):373-383.

[40] Fitzgerald ER, Ferry JD. Method for determining the dynamic mechanical behavior of gels and solids at audio-frequencies - comparison of mechanical and electrical properties. Journal of Colloid Science 1953;8(1):1-34.

[41] Gall K, Yakacki CM, Liu YP, Shandas R, Willett N, Anseth KS. Thermomechanics of the shape memory effect in polymers for biomedical applications. J Biomed Mater Res A 2005;73A(3):339-348.

[42] Lustig SR, Caruthers JM, Peppas NA. Dynamic mechanical properties of polymer-fluid systems: characterization of poly(2-hydroxyethyl methacrylate) and poly(2-hydroxyethyl methacrylate-co-methyl methacrylate) hydrogels. Polymer 1991;32(18):3340-3353.

[43] Shen MC, Strong JD, Matusik FJ. The effect of hydrogen bonds on the dynamic mechanical properties of glassy polymethacylated from 77dK. Journal of Macromolecular Science Part B 1967;1(1):15-27.

[44] Kannurpatti AR, Anseth JW, Bowman CN. A study of the evolution of mechanical properties and structural heterogeneity of polymer networks formed by photopolymerizations of multifunctional (meth)acrylates. Polymer 1998;39(12):2507-2513.

[45] Couchman PR, Karaz PE. A classical thermodynamic discussion of the effect of composition on glass transition temperatures. Macromolecules 1978;11(1):117-119.

[46] Gordon M, Taylor JS. Ideal copolymers and the second-order transitions of synthetic rubbers. i. non-crystalline copolymers. Journal of Applied Chemistry 1952;2(9):493-500.

[47] Feldstein MM. Peculiarities of glass transition temperature relation to the composition of poly(N-vinyl pyrrolidone) blends with short chain poly(ethylene glycol). Polymer 2001;42(18):7719-7726.

[48] Fox TG. Influence of diluent and copolymer composition on the glass transition temperature of a polymer system. Bulletin of the American Physical Society 1956;1:123.

[49] Burfield DR, Lim K. Differential scanning calorimetry analysis of natural rubber and related polyisoprenes. Measurement of the glass transition temperature. Macromolecules 1982;16(1170-1175).

[50] Lambert A. Glass transition measurements on polystyrene by differential scanning calorimetry. Polymer 1969;10(5):319-&.

[51] Rault J, Lucas A, Neffati R, Pradas MM. Thermal transitions in hydrogels of poly(ethyl acrylate) poly(hydroxyethyl acrylate) interpenetrating networks. Macromolecules 1997;30(25):7866-7873.

[52] Kim SJ, Lee CK, Kim SI. Characterization of the water state of hyaluronic acid and poly(vinyl alcohol) interpenetrating polymer networks. J Appl Polym Sci 2004;92(3):1467-1472.

[53] Hatakeyama T, Nakamura K, Hatakeyama H. Determination of bound water-content in polymers by DTA, DSC, and TG. Thermochimica Acta 1988;123:153-161.

[54] Yang B, Huang WM, Li C, Li L. Effects of moisture on the thermomechanical properties of a polyurethane shape memory polymer. Polymer 2006;47(4):1348-1356.

[55] Liu C, Qin H, Mather PT. Review of progress in shape-memory polymers. Journal of Materials Chemistry 2007;17(16):1543-1558.

[56] Anseth K, Bowman CN, Brannon-Peppas L. Mechanical Properties of Hydrogels and their Experimental Determination. Biomaterials 1996;17(17):1647-1657.

[57] Lustig SR, Caruthers JM, Peppas NA. Dynamical mechanical properties of polymer fluid systems- characterization of poly(2-hydroxyethylmethacrylate) and poly (2-hydroxyethyl methacrylate-co-methyl methacrylate) hydrogels Polymer 1991;32(18):3340-3353.

[58] Wu SH. Control of Intrinsic Brittleness and Toughness of Polymers and Blends by Chemical Structure-A Review Polym Int 1992;29(3):229-247.

[59] Ebara S, Iatridis JC, Setton LA, Foster RJ, Mow VC, Weidenbaum M. Tensile properties of nondegenerate human lumbar anulus fibrosus. Spine 1996;21(4):452-461.

[60] Mow VC, Ratcliffe A, Poole AR. Cartilage and diarthrodial joints as paradigms for hierarchical materials and structures. Biomaterials 1992;13:67-97.

[61] Zhu D, Gu GS, Wu W, Gong H, Zhu WM, Jiang T. Micro-structure and mechanical properties of annulus fibrosus of the L4-5 and L5-S1 intervertebral discs. . Clinical Biomechancs 2008;23:S74-S82.

[62] Bevill G, Farhamand F, Keaveny TM. Heterogeneity of yield strain in low-density versus high-density human trabecular bone. J Biomech 2009;42(13):2165-2170.

[63] Chan YL, Ngan AHW, King NM. Use of focused ion beam milling for investigating the mechanical properties of biological tissues: A study of human primary molars. J Mech Behav Biomed Mater 2009;2(4):375-383.

[64] DiSilvestro MR, Zhu QL, Suh JKF. Biphasic poroviscoelastic simulation of the unconfined compression of articular cartilage: II - Effect of variable strain rates. J Biomech Eng-Trans ASME 2001;123(2):198-200.

[65] Edwards C, Marks R. Evaluation of biomechanical properties of human skin. Clin Dermat 13(4):375-380.

[66] Jantarat J, Palamara JEA, Lindner C, Messer HH. Time-dependent properties of human root dentin. Dent Mater 2002;18(6):486-493.

[67] Kotha SP, Guzelsu N. Tensile damage and its effects on cortical bone. J Biomech 2003;36(11):1683-1689.

[68] Mow VC, Ratcliffe A, Poole AR. Cartilage and diarthrodial joints as paradigms for hierarchical materials and structures. Biomaterials 1992;13(2):67-97.

[69] Wang XD, Nyman JS. A novel approach to assess post-yield energy dissipation of bone in tension. J Biomech 2007;40(3):674-677.

[70] Zhu D, Gu GS, Wu W, Gong H, Zhu WM, Jiang T, et al. Micro-structure and mechanical properties of annulus fibrous of the L4-5 and L5-S1 intervertebral discs. Clin Biomech 2008;23:S74-S82.

[71] Averett RD, Realff ML, Michielsen S, Neu RW. Mechanical behavior of nylon 66 fibers under monotonic and cyclic loading. Compos Sci Tech 2006;66(11-12):1671-1681.

[72] Puskas JE, Chen YH, editors. Biomedical application of commercial polymers and novel polyisobutylene-based thermoplastic elastomers for soft tissue replacement, 2004.

[73] Biomaterials Science: An Introduction to Materials in Medicine. Ranter BD, Hoffman AS, Schoen FJ, Lemons JE, editors. London: Elsevier Press; 2004.

[74] Abraham GA, Frontini PM, Cuadrado TR. Physical and mechanical behavior of sterilized biomedical segmented polyurethanes. J Appl Polym Sci 1997;65(6):1193-1203.

[75] Maglio G, Migliozzi A, Palumbo R, Immirzi B, Volpe MG. Compatibilized poly(epsilon-caprolactone)/poly(L-lactide) blends for biomedical uses. Macromol Rapid Commun 1999;20(4):236-238.

[76] Semba T, Kitagawa K, Ishiaku US, Hamada H. The effect of crosslinking on the mechanical properties of polylactic acid/polycaprolactone blends. J Appl Polym Sci 2006;101(3):1816-1825.

[77] Alberola ND, Mele P, Bas C. Tensile mechanical properties of PEEK films over a wide range of strain rates .2. J Appl Polym Sci 1997;64(6):1053-1059.

[78] Matsushige K, Radcliffe SV, Baer E. Pressure and Temperature Effects on Brittle-to-Ductile Transition in PS and PMMA J Appl Polym Sci 1976;20(7):1853-1866.

[79] Tobolsky A, Shen M. The effect of hydrogen bonds on the viscoelastic properties of amorphous polymers networks. J Phys Chem 1963;67(9):1886-1891.

[80] Senyurt AF, Wei HY, Hoyle CE, Piland SG, Gould TE. Ternary thiol-ene/acrylate photopolymers: Effect of acrylate structure on mechanical properties. Macromolecules 2007;40(14):4901-4909.

[81] Hamouda AMS. The influence of humidity on the deformation and fracture behaviour of PMMA. J Mater Process Technol 2002;124(1-2):238-243.

[82] Barnes A, Corkhill PH, Tighe BJ. Synthetis hydrogels 3. Hydroxyalkyl acrylate and methacrylate copolymers - surface and mechanical properties. . Polymer 1988;29(12):2191-2202.

[83] Corkhill PH, Jolly AM, Ng CO, Tighe BJ. Synthetic hydrogels .1. Hydroxyl acrylate and methacrylate copolymers - Water binding-studies. Polymer 1987;28(10):1758-1766.

[84] Yang B, Huang WM, Li C, Lee CM, Li L. On the enects of moisture in a polyurethane shape memory polymer. Smart Materials & Structures 2004;13(1):191-195.

[85] Hofer K, Mayer E, Johari GP. Glass liquid transitions of water and ethylene-glycol solution in poly(2-hydroxyethyl methacrylate) hydrogel. Journal of Physical Chemistry 1990;94(6):2689-2696.

[86] Nakamura K, Hatakeyama T, Hatakeyama H. Relationship between hydrogen-bonding and bound water in polyhydroxystyrene derivatives. Polymer 1983;24(7):871-876.

[87] Singh TRR, McCarron PA, Woolfson AD, Donnelly RF. Investigation of swelling and network parameters of poly(ethylene glycol)-crosslinked poly(methyl vinyl ether-co-maleic acid) hydrogels. European Polymer Journal 2009;45(4):1239-1249.

[88] Pogany GA. Anomalous diffusion of water in glassy polymers. Polymer 1976;17:690-694.

[89] Tanaka Y, Osada Y. Novel Hydrogels with excellent mechanical performance. Progress in Polymer Science 2005;30:1-9.

[90] Yong, Qiu KP. Superporous IPN hydrogels having enhanced mechanical properties. AAPS PharmSciTech 2003;4(4):406-412.

[91] Schwartz Z, Raz P, Zhao G, Barak Y, Tauber M, Yao H, et al. Effect of Micrometer-Scale Roughness of the Surface of Ti6Al4V Pedicle Screws in Vitro and in Vivo. J Bone Joint Surg-Am Vol 2008;90A(11):2485-2498.

[92] Lian JB, Stein GS. Concepts of Osteoblast Growth and Differentiation: Basis for Modulation of Bone Cell Development and Tissue Formation. Crit Rev Oral Biol Med 1992;3(3):269-305.

[93] Owen TA, Aronow M, Shalhoub V, Barone LM, Wilming L, Tassinari MS, et al. Progressive Development of the Rat Osteoblast Phenotype In Vitro- Reciprocal Relationships in Expression of Genes Associated with Osteoblast Proliferation and Differentiation During Formation of Bone Extracellular Matrix Journal of Cellular Physiology 1990;143(3):420-430.

[94] Schwartz Z, Lohmann CH, Sisk M, Cochran DL, Sylvia VL, Simpson J, et al. Local factor production by MG63 osteoblast-like cells in response to surface roughness and 1,25-(OH)(2)D-3 is mediated via protein kinase C- and protein kinase A-dependent pathways. Biomaterials 2001;22(7):731-741.

[95] Lossdorfer S, Schwartz Z, Wang L, Lohmann CH, Turner JD, Wieland M, et al. Microrough implant surface topographies increase osteogenesis by reducing osteoclast formation and activity. Journal of Biomedical Materials Research Part A 2004;70A(3):361-369.

[96] Boyan BD, Lossdorfer S, Wang L, Zhao G, Lohmann CH, Cochran DL, et al. Osteoblasts generate an osteogenic microenvironment when grown on surfaces with rough microtopographies. European Cells and Materials 2003;6:22-27.

[97] Khatiwala CB, Peyton SR, Metzke M, Putnam AJ. The regulation of osteogenesis by ECM rigidity in MC3T3-E1 cells requires MAPK activation. Journal of Cellular Physiology 2007;211(3):661-672.

[98] Glossop JR, Cartmell SH. Differential Gene Expression of Integrins Alpha 2 and Beta 8 in Human Mesenchymal Stem Cells Exposed to Fluid Flow. Cellular and Molecular Bioengineering 2009;2(4):544-553.

[99] Lee DY, Yeh CR, Chang SF, Lee PL, Chien S, Cheng CK, et al. Integrin-mediated expression of bone formation-related genes in osteoblast-like cells in response to fluid shear stress: Roles of extracellular matrix, Shc, and mitogen-activated protein kinase. Journal of Bone and Mineral Research 2008;23(7):1140-1149.

[100] Pavalko FM, Chen NX, Turner CH, Burr DB, Atkinson S, Hsieh YF, et al. Fluid shear-induced mechanical signaling in MC3T3-E1 osteoblasts requires cytoskeleton-integrin interactions. Am J Physiol-Cell Physiol 1998;275(6):C1591-C1601.

[101] Olivares-Navarrete R, Raz P, Zhao G, Chen J, Wieland M, Cochran DL, et al. Integrin alpha 2 beta 1 plays a critical role in osteoblast response to micron-scale surface structure and surface energy of titanium substrates. Proceedings of the National Academy of Sciences of the United States of America 2008;105(41):15767-15772.

[102] Keselowsky BG, Collard DM, Garcia AJ. Surface chemistry modulates focal adhesion composition and signaling through changes in integrin binding. Biomaterials 2004;25(28):5947-5954.

[103] Redey SA, Nardin M, Bernache-Assolant D, Rey C, Delannoy P, Sedel L, et al. Behavior of human osteoblastic cells on stoichiometric hydroxyapatite and type A carbonate apatite: Role of surface energy. J Biomed Mater Res 2000;50(3):353-364.

[104] Adden N, Hoffmann A, Gross G, Windhagen H, Thorey F, Menzel H. Screening of photochemically grafted polymer films for compatibility with osteogenic precursor cells. J Biomater Sci, Polym Ed 2007;18(3):303-316.

[105] Zhao G, Schwartz Z, Wieland M, Rupp F, Geis-Gerstorfer J, Cochran DL, et al. High surface energy enhances cell response to titanium substrate microstructure. J Biomed Mater Res A 2005;74A(1):49-58.

[106] Meredith JC, Sormana JL, Keselowsky BG, Garcia AJ, Tona A, Karim A, et al. Combinatorial characterization of cell interactions with polymer surfaces. Journal of Biomedical Materials Research Part A 2003;66A(3):483-490.

[107] Boyan BD, Lohmann CH, Dean DD, Sylvia VL, Cochran DL, Schwartz Z. Mechanisms involved in osteoblast response to implant surface morphology. Annu Rev Mater Res 2001;31:357-371.

[108] Lincks J, Boyan BD, Blanchard CR, Lohmann CH, Liu Y, Cochran DL, et al. Response of MG63 osteoblast-like cells to titanium and titanium alloy is dependent on surface roughness and composition. Biomaterials 1998;19(23):2219-2232.

[109] Zinger O, Zhao G, Schwartz Z, Simpson J, Wieland M, Landolt D, et al. Differential regulation of osteoblasts by substrate microstructural features. Biomaterials 2005;26(14):1837-1847.

[110] Schwartz Z, Olivares-Navarrete R, Wieland M, Cochran DL, Boyan BD. Mechanisms regulating increased production of osteoprotegerin by osteoblasts cultured on microstructured titanium surfaces. Biomaterials 2009;30(20):3390-3396.

[111] Zhao G, Zinger O, Schwartz Z, Wieland M, Landolt D, Boyan BD. Osteoblast-like cells are sensitive to submicron-scale surface structure. Clin Oral Implants Res 2006;17(3):258-264.

[112] Lee SJ, Choi JS, Park KS, Khang G, Lee YM, Lee HB. Response of MG63 osteoblast-like cells onto polycarbonate membrane surfaces with different micropore sizes. Biomaterials 2004;25(19):4699-4707.

[113] Bischofs IB, Schwarz US. Cell organization in soft media due to active mechanosensing. Proc Natl Acad Sci USA 2003;100(16):9274-9279.

[114] Khatiwala CB, Peyton SR, Metzke M, Putnam AJ. The regulation of osteogenesis by ECM rigidity in MC3T3-E1 cells requires MAPK activation. J Cell Physiol 2007;211(3):661-672.

[115] Kong HJ, Polte TR, Alsberg E, Mooney DJ. FRET measurements of cell-traction forces and nano-scale clustering of adhesion ligands varied by substrate stiffness. Proc Natl Acad Sci USA 2005;102(12):4300-4305.

[116] Pelham RJ, Wang YL. Cell locomotion and focal adhesions are regulated by substrate flexibility. Proc Natl Acad Sci USA 1997;94(25):13661-13665.

[117] Peyton SR, Ghajar CM, Khatiwala CB, Putnam AJ. The emergence of ECM mechanics and cytoskeletal tension as important regulators of cell function. Cell Biochem Biophys 2007;47(2):300-320.

[118] Burdick JA, Anseth KS. Photoencapsulation of osteoblasts in injectable RGD-modified PEG hydrogels for bone tissue engineering. Biomaterials 2002;23(22):4315-4323.

[119] Hillwest JL, Chowdhury SM, Dunn RC, Hubbell JA. Efficacy of a resorbably hydrogel barrier, oxidized regenerated cellulose, and hyaluronic-acid in the prevention of ovarian adhesions in a rabbit model. Fertility and Sterility 1994;62(3):630-634.

[120] Lawrence WH, Purcell WP, Autian J, Bass GE. Use of mathematical models in study of structure-toxicity trlationships of dental compounds .1. Esters of acrylic and methacrylic acids. Journal of Dental Research 1972;51(2):526-&.

[121] Timmer MD, Ambrose CG, Mikos AG. Evaluation of thermal- and photo-crosslinked biodegradable poly(propylene fumarate)-based networks. J Biomed Mater Res, Part A 2003;66A(4):811-818.

[122] Adden N, Hoffmann A, Gross G, Windhagen H, Thorey F, Menzel H. Screening of photochemically grafted polymer films for compatibility with osteogenic precursor cells. Journal of Biomaterials Science-Polymer Edition 2007;18(3):303-316.

[123] Thorey F, Witte F, Nellesen J, Griep-Raming N, Menzel H, Gross G, et al. Improved osseointegration of titanium implants after surface coating with polymers in a rabbit model. Orthopade 2005;34(11):1112-+.

[124] Chatterjee K, Lin-Gibson S, Wallace WE, Parekh SH, Lee YJ, Cicerone MT, et al. The efffect of 3D hydrogel scaffold modulus on osteoblast differentiation and mineralization revealed by combinatorial screening. Biomaterials 2010;31(19):5051-5062.

[125] Wang DA, Williams CG, Li QA, Sharma B, Elisseeff JH. Synthesis and characterization of a novel degradable phosphate-containing hydrogel. Biomaterials 2003;24(22):3969-3980.

[126] Zhao G, Raines AL, Wieland M, Schwartz Z, Boyan BD. Requirement for both micron- and submicron scale structure for synergistic responses of osteoblasts to substrate surface energy and topography. Biomaterials 2007;28(18):2821-2829.

[127] Buser D, Schenk RK, Steinemann S, Fiorellini JP, Fox CH, Stich H. Influence of surface characteristics on bone integration of titanium implants - a histomorphometric study in miniature pigs. J Biomed Mater Res 1991;25(7):889-902.

[128] Li DH, Ferguson SJ, Beutler T, Cochran DL, Sittig C, Hirt HP, et al. Biomechanical comparison of the sandblasted and acid-etched and the machined and acid-etched titanium surface for dental implants. J Biomed Mater Res 2002;60(2):325-332.

[129] Gloria A, Causa F, De Santis R, Netti PA, Ambrosio L, editors. Dynamic-mechanical properties of a novel composite intervertebral disc prosthesis2007: Springer.

[130] Lendlein A, Kelch S. Shape-memory polymers as stimuli-sensitive implant materials. Clin Hemorheol Microcirc 2005;32(2):105-116.

[131] Yakacki CM, Shandas R, Lanning C, Rech B, Eckstein A, Gall K. Unconstrained recovery characterization of shape-memory polymer networks for cardiovascular applications. Biomaterials 2007;28(14):2255-2263.

[132] Smith TL. Deformation and Failure of Plastics and Elastomers. Polym Eng Sci 1965:270-279.

[133] Smith TL. Ultimate Tensile Properties of Elastomers. I. Characterization by a time and Temperature Independent Failure Envelope. J Polym Sci, Part A 1963;1:3597-3615.

[134] Smith TL. Ultimate Tensile Properties of Elastomers. III. Dependence of the Failure Envelope on Crosslink Density. Proc Fourth Inter Congr Rheology, Part 2 1965:525.

[135] Clayden NJ. H-2 NMR spin relaxation study of the molecular dynamics in poly(oxy-1,4-phenyleneoxy-1,4-phenylenecarbonyl-1,4-phenylene) (PEEK). Polymer 2000;41(3):1167-1174.

[136] Chivers RA, Moore DR. The effect of molecular weight and crystallinity on the mechanical properties of injection moulded poly(aryl-ether-ether-ketone) resin. Polymer 1994;35(1):110-116.

[137] Xia Lou CvC. Mechanical characteristics of poly(2-hydroxethyl methacrylate) hydrogels crosslinked with various difunctional compounds. Polym Int 2001;50:319-325.

[138] Cook WD, Delatyck.O. Relaxations in the transition region of crosslinked polyesters .2. Glass-transition. J Polym Sci, Part B: Polymer Physics 1974;12(9):1925-1937.

[139] Peppas NAe. Hydrogels in Medicine and Pharmacy, Volume 1: Fundamentals. CRC Press, Inc, Boca Raton, Fl 1986;(Ch. 2):28-29.

[140] Abraham GA, Frontini PM, Cuadrado TR. Molding of biomedical segmented polyurethane delamination events and stretching behavior. J Appl Polym Sci 1998;69(11):2159-2167.

[141] Fang LM, Leng Y, Gao P. Processing and mechanical properties of HA/UHMWPE nanocomposites. Biomaterials 2006;27(20):3701-3707.

[142] Vigolo B, Penicaud A, Coulon C, Sauder C, Pailler R, Journet C, et al. Macroscopic fibers and ribbons of oriented carbon nanotubes. Science 2000;290(5495):1331-1334.

[143] Vincent PI. The Tough-Brittle Transition in Thermoplastics Polymer 1960;1(4):425-444.

[144] Monnerie L, Halary JL, Kausch HH. Deformation, yield and fracture of amorphous polymers: Relation to the secondary transitions. Intrinsic Molecular Mobility and Toughness of Polymers I2005. p. 215-364.

[145] Ortega AM, Kasprzak S, Yakacki CM, Greenberg AR, Gall K. Structure-Property Relationships in Photopolymerizable Polymer Networks: Composition and crosslinking effects on the structure and thermomechanical properties of a model (meth)acrylate system. J Appl Polym Sci 2007;in review.

[146] Kong HJ, Wong E, Mooney DJ. Independent control of rigidity and toughness of polymeric hydrogels. Macromolecules 2003;36(12):4582-4588.

[147] Temenoff JS, Athanasiou KA, LeBaron RG, Mikos AG. Effect of poly(ethylene glycol) molecular weight on tensile and swelling properties of oligo(poly(ethylene glycol) fumarate) hydrogels for cartilage tissue engineering. J Biomed Mat Res 2002;59(3):429-437.

[148] Bolon DA, Lucas GM, Olson DR, Webb KK. Effect of Humidity and Elevated-temperatures on Physical Properties of UV-cured Polymers. J Appl Polym Sci 1980;25(4):543-553.

[149] Hamouda AMS. The influence of humidity on the deformation and fracture behaviour of PMMA. J Mater Process Tech 2002;124(1-2):238-243.

[150] Shen J, Chen CC, Sauer JA. Effects of Sorbed Water on Properties of Low and High Molecular-Weight PMMA.1. Deformation and Fracture Behavior. Polymer 1985;26(4):511-518.

[151] Yang B, Huang WM, Li C, Lee CM, Li L. On the enects of moisture in a polyurethane shape memory polymer. Smart Mat Struct 2004;13(1):191-195.

[152] Bobyn JD, Mortimer ES, Glassman AH, Engh CA, Miller JE, Brooks CE. Producing and avoiding stress shielding - laboratory and clinical observations of noncemented total hip-arthroplasty. Clinical Orthopaedics and Related Research 1992;274:79-96.

[153] Briscoe B. Wear of polymers: an essay on fundamental aspects. . Tribology International 1981;14(4):231-243.

[154] Bobyn JD, Mortimer ES, Glassman AH, Engh CA, Miller JE, Brooks CE. Producing and avaoiding stress shielding - laboratory and clinical observations of noncemented total hip-arthroplasty Clinical Orthopaedics and Related Research 1992;(274):79-96.

[155] Gall K, Yakacki CM, Liu YP, Shandas R, Willett N, Anseth KS. Thermomechanics of the shape memory effect in polymers for biomedical applications. Journal of Biomedical Materials Research Part A 2005;73A(3):339-348.

[156] Yakacki CM, Shandas R, Safranski D, Ortega AM, Sassaman K, Gall K. Strong, tailored, biocompatible shape-memory polymer networks. Advanced Functional Materials 2008;18(16):2428-2435.

[157] Elisseeff J. Injectable cartilage tissue engineering. Expert Opinion on Biological Therapy 2004;4(12):1849-1859.

[158] Peter SJ, Nolley JA, Widmer MS, Merwin JE, Yaszemski MJ, Yasko AW, et al. In vitro degradation of a poly(propylene fumarate)/beta-tricalcium phosphate composite orthopaedic scaffold. Tissue Engineering 1997;3(2):207-215.

[159] Briscoe B. Wear of polymers: an essay on fundamental aspects. Tribol Int 1981;14(4):231-243.

[160] Beatty MW, Swartz ML, Moore BK, Phillips RW, Roberts TA. Effect of cross-linking agent content, monomer functionality, and repeat unit chemistry on properties of unfilled resins J Biomed Mater Res 1993;27(3):403-413.

[161] Leinfelder KF. New developments in resin restorative systems. J Am Dent Assoc 1997;128(5):573-581.

[162] Smith KE, Temenoff JS, Gall K. On the Toughness of Photopolymerizable (Meth)Acrylate Networks for Biomedical Applications. J Appl Polym Sci 2009;114(5):2711-2722.

[163] Drummond JL. Degradation, fatigue, and failure of resin dental composite materials. J Dent Res 2008;87(8):710-719.

[164] Smith KE, Parks SS, Hyjek MA, Downey SE, Gall K. The effect of the glass transition temperature on the toughness of photopolymerizable (meth)acrylate networks under physiological conditions. Polymer 2009;50(21):5112-5123.

[165] Sideridou I, Tserki V, Papanastasiou G. Study of water sorption, solubility and modulus of elasticity of light-cured dimethacrylate-based dental resins. Biomaterials 2003;24(4):655-665.

[166] Boubakri A, Elleuch K, Guermazi N, Ayedi HF. Investigations on hygrothermal aging of thermoplastic polyurethane material. Mater Des 2009;30(10):3958-3965.

[167] Rivera-Torres F, Vera-Graziano R. Effects of water on the long-term properties of Bis-GMA and Silylated-(Bis-GMA) polymers. J Appl Polym Sci 2008;107(2):1169-1178.

[168] Brazel CS, Peppas NA. Mechanisms of solute and drug transport in relaxing, swellable, hydrophilic glassy polymers. Polymer 1999;40(12):3383-3398.

[169] Arnold JC. The effects of diffusion on environmental stress crack initiation in PMMA. Journal of Materials Science 1998;33(21):5193-5204.

[170] Unemori M, Matsuya Y, Matsuya S, Akashi A, Akamine A. Water absorption of poly(methyl methacrylate) containing 4-methacryloxyethyl trimellitic anhydride. Biomaterials 2003;24(8):1381-1387.

[171] Aronhime MT, Peng X, Gillham JK, Small RD. Effect of Time-temperature path of cure on the water-absorption of high Tg epoxy resins J Appl Polym Sci 1986;32(2):3589-3626.

[172] Perrin FX, Nguyen MH, Vernet JL. Water transport in epoxy-aliphatic amine networks - Influence of curing cycles. Eur Polym J 2009;45(5):1524-1534.

[173] Hu Y, Rogunova M, Topolkaraev V, Hiltner A, Baer E. Aging of poly(lactide)/poly(ethylene glycol) blends. Part 1. Poly(lactide) with low stereoregularity. Polymer 2003;44(19):5701-5710.

[174] Refojo MF, Yasuda H. Hydrogels from 2-hydroxyethyl methacrylate and propylene glycol monoacrylate H. J Appl Polym Sci 1965;9(7):2425-&.

[175] Robertson ML, Chang KH, Gramlich WM, Hillmyer MA. Toughening of Polylactide with Polymerized Soybean Oil. Macromolecules 2010;43(4):1807-1814.

[176] Cha C, Kohmon RE, Kong H. Biodegradable Polymer Crosslinker: Independent Control of Stiffness, Toughness, and Hydrogel Degradation Rate. Adv Funct Mater 2009;19(19):3056-3062.

[177] Kavlock KD, Pechar TW, Hollinger JO, Guelcher SA, Goldstein AS. Synthesis and characterization of segmented poly(esterurethane urea) elastomers for bone tissue engineering. Acta Biomater 2007;3(4):475-484.

[178] Ebenstein DM, Pruitt LA. Nanoindentation of soft hydrated materials for application to vascular tissues. J Biomed Mater Res A 2004;69A(2):222-232.

[179] Martin JY, Schwartz Z, Hummert TW, Schraub DM, Simpson J, Lankford J, et al. Effect of titanium surface-roughness on proliferation, differentiation, and protein-synthesis of human osteoblast-like cells (MG63s) J Biomed Mater Res 1995;29(3):389-401.

[180] Lossdorfer S, Schwartz Z, Wang L, Lohmann CH, Turner JD, Wieland M, et al. Microrough implant surface topographies increase osteogenesis by reducing osteoclast formation and activity. J Biomed Mater Res, Part A 2004;70A(3):361-369.

[181] Kieswetter K, Schwartz Z, Hummert TW, Cochran DL, Simpson J, Dean DD, et al. Surface roughness modulates the local production of growth factors and cytokines by osteoblast-like MG-63 cells. J Biomed Mater Res 1996;32(1):55-63.

[182] Myung D, Koh WU, Ko JM, Hu Y, Carrasco M, Noolandi J, et al. Biomimetic strain hardening in interpenetrating polymer network hydrogels. Polymer 2007;48(18):5376-5387.

[183] Myung D, Waters D, Wiseman M, Duhamel PE, Noolandi J, Ta CN, et al. Progress in the development of interpenetrating polymer network hydrogels. Polymers for Advanced Technologies 2008;19(6):647-657.

[184] Tominaga T, Osada Y, Gong JP. Structural Approaches on the Toughness in Double Network Hydrogels: Springer Netherlands; 2009.

[185] Wong CLH, Kim J, Torkelson JM. Breadth of glass transition temperature in styrene/acrylic acid block, random, a unusual sequence distribution and gradient copolymers: Distribution effects. Journal of Polymer Science Part B-Polymer Physics 2007;45(20):2842-2849.

[186] Wu SH. Control of intrinsic brittleness and toughness of polymers and blends by chemical-structure - A review. Polymer International 1992;29(3):229-247.

[187] Safranski DL, Lesniewski MA, Caspersen BS, Uriarte VM, Gall K. The effect of chemistry on the polymerization, thermo-mechanical properties and degradation rate of poly([beta]-amino ester) networks. Polymer 2010;51(14):3130-3138.

[188] Ramakrishna S, Mayer J, Wintermantel E, Leong KW. Biomedical applications of polymer-composite materials: a review. Composites Science and Technology 2001;61(9):1189-1224.

[189] Petrie TA, Reyes CD, Burns KL, Garcia AJ. Simple application of fibronectin-mimetic coating enhances osseointegration of titanium implants. J Cell Mol Med 2009;13(8B):2602-2612.

[190] Petrie TA, Stanley BT, Garcia AJ. Micropatterned surfaces with controlled ligand tethering. Journal of Biomedical Materials Research Part A 2009;90A(3):755-765.

[191] Jariwala AS, Ding F, Zhao X, Rosen DW, editors. A Process Planning Method for Thin Film Mask Projection Micro-sterelithography. ASME 2009 International Design Engineering Technical Conferences & Computers and Information in Engineering Conference; 2009 Aug 30; San Diego, CA.

[192] Ware T, Voit W, Gall K. Effects of sensitizer length on radiation crosslinked shape-memory polymers. Radiation Physics and Chemistry 2010;79(4):446-453.

[193] Khosla S. Minireview: The OPG/RANKL/RANK system. Endocrinology 2001;142(12):5050-5055.

[194] Bonewald LF, Schwartz Z, Swain LD, Ramirez V, Poser J, Boyan BD. Stimulation of plasma-membrane and matrix vesicle enzyme-activity by transforming growth factor-beta in osteosarcoma cell-cultures. Journal of Cellular Physiology 1990;145(2):200-206.

[195] Petitjean S, Ghitti G, Jerome R, Teyssie P, Marien J, Riga J, et al. Investigation of the surface activity of a poly(styrene-b-dimethylsiloxane) copolymer blended within a polystyrene matrix. Macromolecules 1994;27(15):4127-4133.

[196] Neo WK, Chan-Park MB, Gao JX, Dong L. Effects of silicone acrylate on morphology, kinetics, and surface composition of photopolymerized acrylate mixtures. Langmuir 2004;20(25):11073-11083.

[197] James K, Levene H, Parsons JR, Kohn J. Small changes in polymer chemistry have a large effect on the bone-implant interface: evaluation of a series of degradable tyrosine-derived polycarbonates in bone defects. Biomaterials 1999;20(23-24):2203-2212.

[198] Garcia AJ, Vega MD, Boettiger D. Modulation of cell proliferation and differentiation through substrate-dependent changes in fibronectin conformation. Molecular Biology of the Cell 1999;10(3):785-798.

[199] Bretaudiere JP, Spillman T. Alkaline phosphatases. In: Bergmeyer HV, editor. Methods of Enzymatic Analysis. Weinheim, Germany.

VITA

KATHRYN ELIZABETH SMITH

Kathryn was born in Houston, TX and resided there until she was ten years old, long enough to develop a deep love for tex-mex food and the Dallas Cowboys. She spent part of her childhood living in Madison, MS and then Concord, NC. After her freshman year in high school, she returned to Madison, MS where she graduated from Madison Central High School in 2002. Thinking that medical school was in her future, she attended Mississippi State University and obtained a B.S. in biological engineering and a minor in mathematics. During her tenure at State, Kathryn spent much of her time with her sorority, Delta Gamma, working out, attending football games, and participating in various service and engineering societies. During her junior year when medical school aspirations had begun to wane, Kathryn stumbled upon a research opportunity with Dr. James Warnock evaluating the effect of cyclic strain on the expression of pro-inflammatory genes in aortic valve cells. It was during this time when Kathryn realized her true passion lay in developing new therapies to treat debilitating diseases or injuries. She began graduate school at Georgia Tech in August 2006 in pursuit of her doctorate in bioengineering under the mentorship of Ken Gall and Barbara Boyan. When not spending numerous hours in the lab, she enjoys running, reading, and drinking wine.